

DEVELOPMENT OF A NONLINEAR QUADRILATERAL LAYERED
MEMBRANE ELEMENT WITH DRILLING DEGREES OF FREEDOM AND A
NONLINEAR QUADRILATERAL THIN FLAT LAYERED SHELL ELEMENT
FOR THE MODELING OF REINFORCED CONCRETE WALLS

by

Fabian Rojas Barrales

A Dissertation Presented to the
FACULTY OF THE USC GRADUATE SCHOOL
UNIVERSITY OF SOUTHERN CALIFORNIA
In Partial Fulfillment of the
Requirements for the Degree
DOCTOR OF PHILOSOPHY
(CIVIL ENGINEERING)

August 2012

Copyright 2012

Fabian Rojas Barrales

Dedication

to my parents, wife and daughter.

Acknowledgements

I would like to express my gratitude and deep appreciation to my advisor, Professor James C. Anderson, for his invaluable help, guidance, encouragement, patience and support during this project. My sincerely appreciations and thanks also goes to Professor L. Carter Wellford for his time and willingness to answer my questions about nonlinear finite element and his constant encouragement and comments during this project. My sincerely thanks also goes to Professor Anders Carlson, who reviewed this dissertation carefully and offered important comments.

A special word of gratitude and thanks also goes to Dr. Farzad Naeim for serving as member of my qualifying exam committee, and for his encouragement during my studies of PhD.

Sincerely thanks are given to my friend Francisco Ortega for the support, encouragement and fruitful discussions and conversations during these years. Also, I would like to thanks to my friend and fellow graduate student Miguel Hernandez Garcia. Special word of gratitude is extended to my friends in Chile and in the US.

I would like to express my gratitude to all those who have given me emotional support and encouragement: to my brothers, Alejandro and Christian, to my parents-in-law, Luis

and Carmen, and my family. In special, I would like to express my gratitude and admiration to my loving parents, German and Monica, for their love, support, encouragement that has allowed me to fulfill my goals during my hole life.

Finally, I would like to express my gratitude and love to my wife and daughter, Carolina and Sofia, for their love, generosity, encouragement, support, and assistance. I will be eternally indebted to my wife for being always by my side during this journey.

Table of Contents

Dedication	ii
Acknowledgements	iii
List of Tables	vii
List of Figures	viii
Abstract	xiii
Chapter 1 Introduction	1
1.1 Background and Motivation	1
1.2 Objectives and Scope	4
Chapter 2 Review of Literature of Reinforced Concrete Wall Element Models	7
2.1 Macroscopic Models	9
2.1.1 Equivalent Beam Models	9
2.1.2 Truss Type Model	11
2.1.3 Combined Model	12
2.1.4 Fiber - Base Model	12
2.2 Microscopic Models	15
2.2.1 Membrane Elements	16
2.2.2 Shell Elements	18
2.2.3 Brick Elements	20
2.3 Summary	22
Chapter 3 Finite Element Formulation	24
3.1 Quadrilateral Layered Membrane Element with Rotational DOF Formulation	27
3.1.1 Blended Displacement Interpolation	35
3.2 Quadrilateral Thin Flat Layered Shell Formulation	45
3.2.1 Discrete Kirchhoff quadrilateral Element (DKQ) Interpolation . . .	55
3.3 Summary	63

Chapter 4 Material Constitutive Models	65
4.1 Constitutive Model for Concrete	68
4.1.1 Review of Literature	68
4.1.1.1 Orthotropic Model for Concrete	71
4.1.2 Formulation of the Concrete Constitutive Model	80
4.1.2.1 Uniaxial Concrete Models using Thorenfeldt Curve	87
4.1.2.2 Uniaxial Concrete Model using a Simplified Chang-Mander Model	91
4.1.2.3 Biaxial Strength Coefficients	96
4.2 Constitutive Model for Steel	99
4.2.1 Uniaxial Mild Steel Bar Embedded in Concrete Model	103
4.2.2 Uniaxial Menegotto and Pinto Steel Model	106
4.3 Summary	108
Chapter 5 Finite Element Implementation	111
5.1 Object-Oriented Approaches for Finite Elements	114
5.2 Finite Elements Toolbox for MATLAB	120
5.2.1 Review of Finite Element Toolbox for MATLAB	121
5.2.2 Proposed Object-Oriented Finite Elements Toolbox for MATLAB	123
5.3 Incremental Iterative Solution Algorithm	132
5.3.1 Load-Control Iterative Algorithm	134
5.3.2 Displacement-Control Iterative Algorithm	136
5.3.3 Convergence Criteria	139
5.4 Summary	141
Chapter 6 Evaluation and Verification of Analytical Results	143
6.1 Monotonic Loading	144
6.1.1 Reinforced Concrete Shear Wall - Cervenka and Gerstle	144
6.1.2 Reinforced Concrete Walls - Lefas, Kotsovos and Ambraseys	151
6.2 Reversal or Cyclic Loading	167
6.2.1 Reinforced Concrete Rectangular Wall - Thomsen and Wallace	173
6.2.2 Reinforced Concrete Wall with T-Shaped Cross Section - Thomsen and Wallace	180
6.3 Summary	188
Chapter 7 Summary and Conclusions	191
7.1 Future work and Recommendations	199
References	201
Appendix A Tensor Transformation	213
A.1 Strain Transformation	213
A.1.1 Principal Direction of Strains	215
A.2 Stress Transformation	217

List of Tables

6.1	Properties of the Renforcement Steel Bars	153
6.2	Properties of the Wall Specimens	154
6.3	Properties of the Renforcement Steel Bars	169

List of Figures

3.1	In-Plane Stresses	27
3.2	A typical rectangular layered membrane section	31
3.3	Element develop by Xia et al. [151] in 2009	34
3.4	Blended Interpolation for the Horizontal Displacement	37
3.5	Blended interpolation for the vertical displacement	39
3.6	Distorted Blended element	43
3.7	Factors to determinate variation with respect to the true rotation $\Omega = \frac{1}{2} \left(\frac{\partial v}{\partial x} - \frac{\partial u}{\partial y} \right)$	44
3.8	Shell Element definitions	45
3.9	Sign Convention for local resulting of stress for the Shell Element	49
3.10	A typical rectangular layered shell section	50
3.11	Discrete Kirchhoff Quadrilateral Element	56
4.1	Uniaxial behavior of concrete	66
4.2	Variation of the stress in the Concrete and Steel bars between cracks	67
4.3	Principal Direction of Strain	83
4.4	Constitutive Model for Concrete in Compression using Thorenfeldt base curve	88
4.5	Constitutive Model for Concrete in Tension using the Belarbi and Hsu [16] equation	89

4.6	Hysteretic Rules for the Concrete Model	90
4.7	Compression Envelope Curves of the Simplified Chang-Mander Concrete Model	92
4.8	Tension Envelope Curves of the Simplified Chang-Mander Concrete Model .	94
4.9	Hysteretic rules for the Simplified Chang-Mander Concrete Model proposed by Waugh [147] in 2009	96
4.10	Compression Softening Effect	97
4.11	Steel Layer Orientation	101
4.12	Stress-Strain relation of embedded steel bar in concrete and bare steel Bar .	102
4.13	Constitutive Model for Embedded Steel Bars Model	104
4.14	Constitutive Model for Menegotto and Pinto Steel model	106
5.1	Main Abstractions in OpenSees [82] Framework	117
5.2	Class Diagram Notation used in MATLAB [62]	124
5.3	MATLAB's Class Definition structure	125
5.4	Main Abstractions in the proposed Toolbox	126
5.5	Model abstraction in the proposed Toolbox	127
5.6	Analysis abstraction in the proposed Toolbox	129
5.7	Model response recorder abstractions in the proposed Toolbox	131
5.8	Model Graphics abstractions in the proposed Toolbox [92]	132
5.9	Full Newton-Raphson with Load-Control Iterative Algorithm	134
6.1	Geometry and Reinforcement Details of the RC Shear Panel W2	145
6.2	Analytical Model of the RC Shear Panel W2	147
6.3	Deformation of the Analytical Model of the RC Shear Panel W2 at $P \approx 114$ [KN] (Scale Factor of 10)	147

6.4	Load-Deformation of the Response of the RC Shear Panel W2	148
6.5	Load-Deformation of the Response of the RC Shear Panel W2 with the plane stress concrete model with Thorenfeldt's curve and the smeared steel model using the uniaxial mild steel bar embedded in concrete model and a quadrilateral layered membrane element without drilling degrees of freedom	149
6.6	Strains and Stresses in the Model of the RC Shear Panel W2 at $P \approx 114$ [KN]	149
6.7	Crack Patterns observed in the RC Shear Panel W2 at $P \approx 114$ [KN]	150
6.8	Geometry and Reinforcement Details of Type-I and Type-II Walls tested by Lefas et al. [80] in 1990	152
6.9	Schematic of Testing Setting used by Lefas et al. [80] in 1990	155
6.10	Analytical Model for Type-I and Type-II Walls	156
6.11	Load-Displacement Curve of Analytical Model with the plane stress concrete model with Thorenfeldt's curve and the smeared steel model using the uniaxial mild steel bar embedded in concrete model versus Experiment Results for Type-I Walls	157
6.12	Load-Displacement Curve of Analytical Model with the plane stress concrete model with Thorenfeldt's curve and the smeared steel model using the uniaxial Menegotto-Pinto steel model versus Experiment Results for Type-I Walls	158
6.13	Load-Displacement Curve of Analytical Model with the plane stress concrete model with Chang-Mander Model and the smeared steel model using the uniaxial mild steel bar embedded in concrete model versus Experiment Results for Type-I Walls	159
6.14	Load-Displacement Curve of Analytical Model with the plane stress concrete model with Thorenfeldt's curve and the smeared steel model using the uniaxial mild steel bar embedded in concrete modelversus Experiment Results for Type-I Walls and a quadrilateral layered membrane element without drilling degrees of freedom	160
6.15	Load-Displacement Curve of Analytical Model with the plane stress concrete model with Thorenfeldt's curve and the smeared steel model using the uniaxial mild steel bar embedded in concrete model versus Experiment Results for Type-II Walls	161

6.16 Load-Displacement Curve of Analytical Model with the plane stress concrete model with Thorenfeldt's curve and the smeared steel model using the uniaxial Menegotto-Pinto steel model versus Experiment Results for Type-II Walls	162
6.17 Deformation of the Analytical Model of the Type-I and Type-II Walls (Scale Factor of 10)	163
6.18 Crack Patterns observed in the Specimen SW12 of the Type-I wall at the end of the analysis vs the observed at the end of the experimental testing .	163
6.19 Strains and Stresses in the Model of the Specimen SW12 of the Type-I Wall at the maximum displacement	164
6.20 Crack Patterns observed in the Specimen SW24 of the Type-I wall at the end of the analysis vs the observed at the end of the experimental testing for the SW26 that represent the failure observed by Lefas et al. [80] in 1990 for the Type-II Walls	165
6.21 Strains and Stresses in the Model of the Specimen SW24 of the Type-II Wall at the maximum displacement	166
6.22 Three-Dimensional View of the Rectangular and T-Shaped Wall Specimen used by Thomsen and Wallace [132] in 1995	168
6.23 Schematic of Testing Setting used by Thomsen and Wallace [132] in 1995 .	170
6.24 Reinforcement Details for Specimen Wall RW1 used by Thomsen and Wallace [132] in 1995	174
6.25 Reinforcement Details for Specimen Wall RW2 used by Thomsen and Wallace [132] in 1995	174
6.26 Analytical Model for Rectangular Walls Specimens (RW)	175
6.27 Lateral Drift Procedure used by Thomsen and Wallace [132] in 1995 for Wall Specimens: RW1 and RW2	176
6.28 Load-Displacement Curve of Analytical Model with the plane stress concrete model with Thorenfeldt's curve vs Experiment Results for RW1	177
6.29 Load-Displacement Curve of Analytical Model with the plane stress concrete model with Thorenfeldt's curve vs Experiment Results for RW2	178

6.30 Deformation, Crack Pattern, Strain and Stress of the RW2 Analytical Model with the plane stress concrete model with Thorenfeldt's curve and the smeared steel model using the uniaxial Menegotto-Pinto steel model	179
6.31 Reinforcement Details for Specimen Wall TW1 used by Thomsen and Wallace [132] in 1995	181
6.32 Reinforcement Details for Specimen Wall TW2 used by Thomsen and Wallace [132] in 1995	182
6.33 Lateral Drift Procedure used by Thomsen and Wallace [132] in 1995 for Wall Specimens: TW1 and TW2	183
6.34 Analytical Model for T-Shaped Walls Specimens (TW)	184
6.35 Load-Displacement Curve of Analytical Model with the plane stress concrete model with Thorenfeldt's curve vs Experiment Results for TW1 . . .	185
6.36 Load-Displacement Curve of Analytical Model with the plane stress concrete model with Thorenfeldt's curve vs Experiment Results for TW2 . . .	186
6.37 Deformation, Crack Pattern, Strain and Stress of the TW2 Analytical Model with the plane stress concrete model with Thorenfeldt's curve and the smeared steel model using the uniaxial Menegotto-Pinto steel model . .	187

Abstract

The primary thrusts of this dissertation are to develop and test a new quadrilateral layered membrane element with drilling degrees of freedom (DOF) and a quadrilateral thin flat layered shell element for the nonlinear analysis of reinforced concrete walls. The drilling degrees of freedom refers to the incorporation of the in-plane rotation as a degree of freedom at each node of the element. The membrane element consists of a quadrilateral element with a total of 12 DOF, 3 per node, 2 displacements and 1 in-plane rotation, and uses a blended field interpolation for the displacements over the element. This formulation is an extension of the one developed by Xia et al. [151] in 2009. The shell element is created by the combination of the membrane element developed in this dissertation and a Discrete Kirchhoff Quadrilateral Element (DKQ, 12 DOF), formulated by Batoz and Tahar [11] 1982, to model the out of plane bending behavior of the element. The modeling of the section of the membrane and the shell element consists of a layered system of fully bonded, smeared steel reinforcement and smeared orthotropic concrete material with the rotating angle formulation. The layered section for the shell includes the coupling membrane and bending effects. These elements are implemented on a finite element framework using the object oriented programming language under MATLAB [62]. The framework or MATLAB toolbox for Finite Elements developed for this dissertation allows to incorporate, develop and test new elements, materials, sections and analysis algorithms in a easy and quick

manner. The proposed elements are evaluated using experimental results that are available in the literature. It is shown that the new elements are in excellent agreement with the experimental results for the different load configuration, monotonic and cyclic loading, and they are able to predict the failure modes for the different wall configurations analyzed in this dissertation.

Chapter 1

Introduction

1.1 Background and Motivation

Reinforced Concrete Walls are a fundamental part of the lateral resisting force systems against the lateral forces of earthquake and wind loads in tall and mid-rise multi-story buildings. In addition, in some cases, the walls are also used to carry the vertical loads produced by both, dead and live loads over the buildings. Wall and wall-frame systems provide the necessary strength and stiffness to satisfy the demands produced by strong ground motions and have exhibited a good performance in recent earthquakes with rare occurrences of complete collapse of these structures. For this reason and also for the small lateral drift that is developed by this system, it has also been employed for tall buildings.

The design and modeling of reinforced concrete wall elements has been an extensive area of research. This is not only due to the complex behavior of the material, but also due to the behavior of the wall as a structural element. The behavior of these walls change depending on the different possible configuration (sizes, shape), and disposition of the different components of the walls (reinforcement, aggregate size, confining of the concrete), and also their location as part of the structural system. This has been shown in past

research the studies of Paulay and Priestley [114], and Panagiotou [108]. Different types of models have been studied, using micro and macro elements, to try to represent the different characteristics of the reinforced concrete walls. These studies include concrete loss of stiffness after cracking, open and closing of cracks, tension-stiffening of the concrete, bond-slip between the reinforcing steel and concrete, influence of confinement on the maximum capacity of the concrete, and yielding and hardening of the steel.

Currently, the nonlinear modeling of the behavior of a wall structure is done with analytical models that assume only in-plane behavior, such as multi-component-in-parallel-model or multi-vertical-line-element model ([103, 144, 144]), membrane elements (Modified Compression Theory by Palermo and Vecchio [106] or Softened Membrane Model by Hsu and Zhu [58]). Commonly for 3D structures the elements have the bending and membrane action decoupled. These models tend to show good agreement with experimental data that typically considers isolated elements, whereas, the behavior of the actual walls are configuration dependent. However, a more complex behavior for structural walls have been observed in the wall buildings during the Chile Earthquake February 27, 2010. It is clearly indicated that when wall elements are interconnected forming Tee or Channel walls or even more complex configurations when are combined with beams and slabs, the out-of-plane behavior begins to play a role in the overall behavior of the structures due to the complex interrelation of the different elements. This behavior is described by the reports of the Reconnaissance team of the Los Angeles Tall Building Structural Design Council ([22, 99, 120, 154]) and the ERRI Reconnaissance team,[98] after the Chile Earthquake. This behavior is not captured by the previous simplified models that do not easily allow direct connection to the walls and other elements like beams or walls in other directions.

Nevertheless, the current standard for modeling the elastic behavior of reinforced concrete wall systems is done with the shell element that combines a membrane element with a plate element. Therefore, allowing the model to have the in-plane and out-of-plane behavior of the elements and also the analysis of the interrelation of the different components. For nonlinear analysis this type of element that includes in-plane and out-of-plane behavior has been left aside because they were considered very computationally expensive. With the recent advancements in computer capability and the use of frameworks such as OpenSees [82], it becomes of interest to explore these types of elements for the modeling of the complex behavior of wall structures.

Two main areas that need to be considered to be able to model Reinforced Concrete Walls using finite elements are the development of an element that represents specifically the behavior of the wall structures, and a nonlinear constitutive material model that represent the concrete and reinforcing steel bars in the walls [157]. The development of the specific element for wall, in this dissertation, is dealing by the use of a blended field interpolation for the displacement. This allows the use of an element with drilling degrees of freedom for the analysis two dimensional wall structures. Moreover, this will allow the element to have the capability to connect directly with beams because the element have rotations DOF, at difference of the typically membrane elements proposed before. In addition, for 3D structures the coupling of the membrane action (in-plane) and plate action (out-plane) by the combination of the membrane element proposed here with a plate element is considered using the Discrete Kirchhoff Quadrilateral Element (DKQ) formulated by Batoz and Tahar [11] , and the use of a layered section. For the nonlinear

constitutive material, a smeared crack rotating angle concrete model with tangent stiffness matrix formulation is used.

1.2 Objectives and Scope

The objectives of this dissertation are to develop and test a new nonlinear quadrilateral layered membrane element with drilling degrees of freedom and a nonlinear quadrilateral thin flat layered shell element. This element incorporates the coupling of in-plane flexural, axial and shear behavior for single wall models using membrane elements, and the flexural, axial and shear behavior of complex 3D, reinforced concrete wall systems using the proposed layered shell element. The drilling degrees of freedom refers to the incorporation of a degree of freedom that represent the rotation in the plane of the element. The modeling of the section by the membrane and shell element consists of a layered system that is fully bonded between the layers. The constitutive material used at each layer corresponds to a smeared crack orthotropic rotating angle concrete material with a tangent stiffness matrix formulation. In addition, it is developed in a finite element framework using the object oriented programing language under MATLAB, to implement the elements formulated in this dissertation.

In Chapter 2, a brief literature review of the current nonlinear element used to model wall structures will be presented.

In Chapter 3, the theory that will be used to implement the layered membrane and shell element will be studied and discussed. The quadrilateral membrane element will be formed by the use of a blended field interpolation for the displacement with 12-DOF (3-DOF at each node, two displacements and a rotational degree of freedom). This formulation is

an extension of the formulation developed by Xia et al. [151] in 2009. Meanwhile, the quadrilateral shell element will be formed by the combination of the membrane element formulated in this dissertation and a 4-node 12-DOF quadrilateral plate bending element, the Discrete Kirchhoff Quadrilateral Element (DKQ) formulated by Batoz and Tahar [11]. The modeling of the section for the membrane and shell element will consist of a layered system, that is fully bonded. In addition, the section model includes the coupled membrane and bending effects for the shell element.

In Chapter 4, the constitutive material that will be used for the implementation of the smeared steel reinforcement and orthotropic concrete material with the rotating angle and tangent stiffness formulation for the modeling of the in plane behavior of each layer is presented. This constitutive material is based on the fundamental principals of mechanics of materials, satisfying stress equilibrium and strain compatibility, using an average stress and strain. In addition, the parameters used to account for the softening, enhancement or damage of the concrete under multi-axial load states (biaxial compression, tension-compression, cycling loads) are reviewed.

In Chapter 5, a brief review of the current object oriented frameworks for finite elements, and the theory selected and diagrams of the developed finite element framework using the object oriented programing language under MATLAB are presented. In addition, the solution algorithm implemented in the framework that will be used to solve the pushover and cycling models is also discussed.

In Chapter 6, the evaluation and verification of the proposed membrane and shell element is presented. For this the analytical results obtained with the proposed elements

are compared to experimental results available in the literature for monotonic and cyclic loading.

In Chapter 7, a summary of the work performed during this dissertation and suggestions for future research are presented.

Chapter 2

Review of Literature of Reinforced Concrete Wall Element Models

Wall elements are effective in providing resistance and stiffness to lateral loads produced by wind and earthquake. Wall structures are typically used alone for mid and low rise buildings to control the lateral strength demands and deformation requirements, in parallel with frame systems in mid to high rise buildings. This is because the core wall helps to control the lateral shearing deformation (inter-story drift). Although, the construction and design of walls using current codes is a relatively simple procedure, the wall elements behave differently depending of their configuration (size wall, height/length ratio, steel reinforcement), under multi loading conditions. This implies that the behavior of the walls depends upon the interrelation and coupling of the combination of flexural, shear, and axial deformation over their cross section at different levels. In addition, complex mechanisms such as the rigid body rotation for the bond slippage of the reinforcement at the bottom, effects of the confinement, dowel action for the reinforcement, cracking, aggregate interlock, creep, tension stiffening also modify the behavior of the walls. This has been shown by different researchers ([20, 41, 103, 114]).

For Example, walls used in mid to high rise buildings exhibit mainly a flexural behavior, with the deformation concentrated at the level of larger moment, typically near to the ground level. This failure is characterized by horizontal cracks at the edges of the wall. Instead, in low rise buildings where the walls behave primarily in shear, diagonal cracks are produced. However, this main behavior occurs typically in isolated walls, once the walls are combined with other elements or other walls in the building the behavior can change producing different failures such as pure compression with crushing of the walls, combination of failure between flexural and shear, where the failure is produced before reaching the maximum capacity of the wall in pure flexural or pure shear behavior is attained. Due to this complex behavior of the wall a large amount of research and experiments have been developed in the past decades, with the idea of providing enough data to represent the walls and develop analytical models that can accurately predict the behavior and important material characteristics of these walls, such as concrete stiffening, cracking, bond slippage and neutral axial migration.

The analytical model can be separated into two groups: macroscopic models and microscopic models based on finite element models [144]. The macroscopic models are based on predicting the overall behavior of a wall element with the use of simplified assumptions and idealizations [144]. This is done typically by lumping a system of springs where each spring has an independent hysteretic curve that represents a part of the behavior of the wall. To model more complex structures, these macro models are typically stacked one over the other, using the assumption that each element is one floor. These models are simple and efficient to understand and incorporate in structural nonlinear programs. However, in some cases they are difficult to use due to the amount of coefficients necessary

to calculate from experimental results. These models also tend to be problem based [144], which mean only work for certain cases. Instead, the microscopic model are based on a more theoretical background of material mechanics, in which the structure is divided into a series of elements, and over each element the respective constitutive representation of the reinforced concrete material is imposed in a stress-strain space or other possible mixed representation and the equilibrium equation are satisfied in a average sense with a integration over each finite element. These models provide a better definition of the local response, and a more refined representation of the response of the wall structures and tend to be not problem specific, which is important to be able to represent a variety of problem with the same procedure. However, their principal drawbacks are that these elements sometimes rely in the definition of the constitutive laws which tend to be very difficult to implement in nonlinear finite element programs, and also they are very computational costly ([41, 103, 144])

To continue, a brief review of the different analytical models (macroscopic and microscopic models) that have been used to model wall elements will be presented.

2.1 Macroscopic Models

2.1.1 Equivalent Beam Models

A simple approach to model the nonlinear behavior of a wall element is the use of a line element (beam or beam-column model). If this approach is used to model a building, the line is located at the center line of the wall and it is connected to the rest of the structure by rigid links. In early models, the line element was modeled using an elastic beam with

concentrated plastic hinges. These hinges were represented by nonlinear rotational springs, located at the end of the elastic beam [144]. Different types of hysteretic rules can be used for the moment-rotation relationship of each nonlinear spring. In addition, the inclusion of another nonlinear rotational spring at the end of the rigid link can be used to take into account the fixed-end rotation at any connection interface [144].

Some modification has been done to this model to incorporate other behavior observed on the walls, Takayanagi and Schnobrich [129] in 1976, introduced additional inelastic shear-based rotational springs at the end of each line to model shear deformation, and Soleimani et al. [127] in 1979 incorporated spreading inelastic behavior by using a representation of multiply springs in the beam element. Keshavarzian and Schnobrich [71] incorporate an axial load effect and variation of the inelastic zone, Otani et al. [104] in 1985 and Roufaeil and Meyer [121] incorporate the bond slippage effects, and Ariatizabal-Ochoa [6] in 1983 incorporated additional inelastic shear behavior. In addition, it has also been tried to use representations of spread plasticity over the length developed for beam-column elements with force formulation and a fiber section formulation for walls like the work done by Martinelli and Filippou [89] in 2009.

The principal drawback of this type of model is the fact that it cannot model some interaction effects in the connection of the wall with other elements, and also the shifting of the neutral axis of the wall section, except for the fiber section formulation. The rotation of the wall due to bond slip effects cannot be reproduced because this model assumes that the rotation occurs at the centroidal axis of the wall ([41, 103, 144]).

2.1.2 Truss Type Model

Another approach to model the wall is the use of a truss analogy. This means, to represent the wall as a equivalent truss structure [144]. In this model the structure is represented as a series of inelastic truss elements that only resist tension and compression loads. Commonly in this model the concrete is represented by the elements that are subjected to compression and the steel or some kind of steel-concrete combination is represented by the elements in tension, in an effort to capture the mechanical behavior of the wall. Hiraishi [52] in 1983 used this representation with non-prismatic elasto-plastic truss members to analyze the behavior of the walls used in a tests conducted in the US-Japan Cooperative Research Program. This non-prismatical truss member was used to account for the variation of the stress along the height of the boundary elements. In this representation, two vertical edge elements where used to resist the moment over the wall, the diagonal element used to carry the shear loads, and the horizontal elements to complete the truss analogy. This model agreed with the experimental data which was used to compare the element. Panagiotou et al. [109] in 2012 used this approach to model the behavior of RC walls under cycling loads. The model proposed by Panagiotou et al. [109] including tension stiffening in the horizontal direction, takes into consideration the mesh size effect for the concrete constitutive material model, and instead of using a single truss or panel per wall, the model is subdivided in a minimum of nine sub panels. This new variation of a truss model approach agreed with the experimental data.

Some of the difficulties of this model are the definition of the truss members and their mechanical properties, which are represented by hysteric rules and also selection of the equivalent truss system, which depend of the crack patterns during the load history [144].

This type of analogy is currently used to study and design deep beams (strut and tie model).

2.1.3 Combined Model

In 1997, Eimani [41] proposed a macro model in which the wall is discretized in a series of subelements. The elastic part of the wall is represented by an elastic panel element, that is used to represent the in plane behavior. The cracked segment or plastic zone is assembled by a series of inelastic springs. Each spring in the element is derived from the known material behavior. This was done for the purpose of eliminating part of the complete dependency of the experimental data to defined the spring hysteretic rules and plastic crack area. The crack area was assembled by two system of springs at each edge, that work to account for axial and flexural load. Meanwhile, the web of the wall is represented by a non-prismatic beam-type element to enforce the coupling of shear and flexural deformation using a flexibility matrix approach. Each of the spring systems at the edge were represented by two subsets of springs; one subset was a single spring which represents the inelastic behavior of the concrete, and the other subset of springs consist of two springs working in series to account for the bond-slipage and non linear effect of the steel.

2.1.4 Fiber - Base Model

This type of element are characterized by the combination of several axial, shear, and rotational springs working together; some in parallel and others in series to represent the global response of the reinforced concrete wall element. One of the first attempt for this

type of element was the Three-Vertical-Line (TVL) proposed by Kabeyesawa et al. [66] in 1982 , this model was based on the results of experiments done on a 7 story, wall building test case. The TVL element consists of two axial springs located at the boundary of the wall, and a central spring system, connected together to an infinitely rigid beam at the top and bottom. The central spring system consists of a horizontal, a vertical and a rotational spring concentrated at the base of the wall. The rotational and horizontal spring are modeled with an origin-oriented-hysteresis model, and the axial spring is represented with an axial-stiffness hysteretic model. This model produced an improved representation of some of the key features of the wall elements, and showed good agreement with the experimental data. However, it is difficult to implement because the use of complex and experimental based hysteretic rules that in the majority of the cases are peculiar to the problem being considered. Also it does not account for the coupling between flexural, axial and shear behavior [103].

This model was later modified by Vulcano and Bertero [144] in 1987, changing the complicated axial-stiffness, hysteretic rule in the TVL by a simple idealization of two axial element working in series. The top spring represent the axial stiffness of the part of the boundary element in which the bond is still active, and the bottom part consist of two spring working in series one representing the steel (bilinear model) and the other the concrete (compression behavior only) to represent the behavior of the cracked wall where the bond has vanished. The lambda value in the figure was adjusted to account for the extent of bond deterioration, meaning the separation between cracked and uncracked concrete. It also includes shear degradation. This new model is known as the TVLM (TVL Modified). This model can represent yield hardening, concrete cracking, degradation

of bond between concrete and steel, but continues lacking the coupling behavior of the moment-axial and shear effects.

The model was further modified in 1987 by Charney [28], and by Vulcano et al. [145] in 1988. These new modifications were done by simply replacing the rotational center spring by a series of axial linear element through the length of the transverse cross section. With this modification, the model is able to incorporate the coupling axial-flexural effect, and better represent the migration of the neutral axis over the cross section, Also, it included a better representation for the hysteretic rules for the axial elements, and for the steel. This model known as the Multi-Vertical-Line Element Model (MVL Model or MVLM) showed good agreement with the test data, but still lacked the coupling between flexural and shear components, and also presented the same problem as the TVLM, which is sensitivity to the non-dimensional lambda factor. In 1990, Fajfar and Fischinger [43] proposed further modifications to the system of springs in the TVLM.

Kabeyasawa and Milev [65] in 1997 proposed a variation of the TVL , by replacing the center system of springs by a panel element, in order to get a better prediction of the behavior of the reinforced concrete wall to reversed cycling and monotonic loads, and to account for some coupling between the shear and axial component. The element showed overall good agreement with the experimental data but the contribution of deformation for the flexural and shear component showed some error relative to the experimental results, and still lacks the capability of accounting for the coupling behavior of shear and flexure.

After a series of experiments conducted to investigate the interaction and coupling between flexural and shear deformation on slender RC walls by Massone and Wallace [91] in 2004, it was shown that the flexural yielding affect and the shear deformation in

slender walls are dominated by bending. In an attempt to include this behavior and the shear-flexural coupling Orakcal et al. [103] in 2006 and Massone [90] in 2006, modified the Multi-Vertical-Linear element. The modification consisted of replacing the uncoupled central spring for a series of vertical springs (uniaxial elements) over the cross section of the wall, which means, that each fiber or axial element is represented as a reinforced concrete panel with in-plane behavior. For the constitutive law of the panel, it used a rotating angle concrete model based on the rotating angle softened-truss model (RA-STM) proposed by Pang and Hsu [110] in 1995 with a more refined concrete constitutive stress-strain model, which was calibrated with the experimental data from Massone and Wallace [91] in 2004. This model resulted in a reasonably good agreement with the experimental data for slender walls but it underestimated the shear deformations and overestimated the flexural behavior on the walls. However, the error in results of the model vs experimental results increased for squat walls, where the shear behavior is predominant.

Xiaolei et al. [152] extended the MVL element model to account for 3D effects when used in the modeling of I T or L type of Walls. The model increased the number of axial elements to account for the variation of strain on the flange of the I T or L walls and also additional horizontal springs are used in each direction of the element to include shear in both directions.

2.2 Microscopic Models

The microscopic models are based on the finite element method (FEM), and theory of continuum mechanics. In this methodology the wall elements are divided into simpler elements which are interconnected by their nodal points, and the element mechanical

response is represented by equations that are a function of a finite number of degrees of freedom (DOF) at each node. The finite element method has been applied to the representation of the nonlinear behavior of wall systems since the method was formulated. However, in the early days the FEM was limited to represent the behavior of isolated walls because of the increase in the computational cost when modeling more complex wall structures, as mentioned by Vulcano and Bertero [144]

The microscopic model for reinforced concrete walls can be grouped into three main categories group: membrane elements that are used for 2D models and shell and 3D solid brick elements for 3D models. The principal difference between the models proposed through the years within the three different groups are the use of different material constitutive representations that define the stress-strain relation of the concrete and the reinforcing steel bars inside of each element. The principal constitutive laws for modeling the behavior of reinforced concrete structures can be classified as non-linear material models, fracture mechanics models, orthotropic models, plasticity model, hypo-elastic materials models, microplane models and nonlocal continuum mechanics models [7, 157]. A more detailed review of these constitutive laws will be presented in Chapter 4. In the following section a brief review of the microscopic model will be presented.

2.2.1 Membrane Elements

This type of model is characterized by the representation of the wall by plane membrane elements. This element only has in-plane behavior, that can be represented by a plane stress behavior, typically with two DOF per node (2 displacements). This type of model is typically used for two types of representation to incorporate the steel inside of the wall.

One assumes the steel as a smeared material which means distributed homogenously over the area of the element in the direction of the bars. The second approach is using a truss type element to represent the steel bar, the main drawbacks of this second representation is that the mesh of the element needs to coincide with the position of the bar in the wall and the need of elaborate connecting elements between the bar and the membrane element to account for bond slippage, if it is considered. One of the first of these elements to be used in FEM formulation for the representation of the nonlinear behavior of a shear panel was Cervenka and Gerstle (1970, 1971, 1972) [29]. Cervenka [24] used a quad element with four nodes and two DOF per node (one horizontal and one vertical displacement), with a Mises Yield condition for modeling the concrete. Since this time different researchers have used this type of element or variation with a larger number of nodes in the elements (higher element), but with only two DOF per node. The main difference is the constitutive material laws used in the analysis for the representation of the reinforced concrete. Commonly, the constitutive laws used to model the material behavior are non-linear material models, fracture mechanics models, orthotropic models, plasticity models, hypo-elastic material models, microplane models and nonlocal continuum mechanics models. [7, 157].

Between all the constitutive laws used to represent the concrete in the plane stress condition, the orthotropic models are one of the more widely used by many researchers to represent reinforced concrete structures like walls [157]. Some of this model are: Darwin and Pecknold [39] (1977), Cervenka [25] (1985), Vecchio and Collins [140] (1986), Izumo et al. [64] (1991), Shin et al. [124] (1991), Bolander and Wight [21] (1991), Hsu [54] (1991), Belarbi and Hsu [17] (1995), Pang and Hsu [110] (1995), Pang and Hsu [111] (1996), Ayoub and Filippou [7] (1998), Vecchio [137] (2000), Vecchio [138] (2001), Palermo and Vecchio

[106] (2003) , Foster and Marti [49] (2003), Mansour and Hsu [86] (2005), Mansour and Hsu [87] (2005), Zhong [157] (2005). For other types of constitutive laws good references are the reviews done by Chen [29] and Maekawa et al. [84]. This type of model generally give good results when compared with the experimental data. However this type of model has the drawback that the element can not be easily used in combination with beams for the fact that only 2 displacement degrees of freedom are used at the nodes, and no rotation is allowed.

Kwan [76] in 1993 and Kwan and Cheung [77] in 1994 used a variation of the model develop by Sisodiya and Cheung [125] in 1971 initially for bridge analysis, and also used by Cheung [30] in 1983, in an attempt to incorporate a rotational degree of freedom to the membrane element for the analysis of reinforced concrete walls. This model was used to ensure compatibility between the walls and the beams that are connected together. The initial model was represented by a bilinear representation for the vertical deformation in the plane element and a cubic representation in "y" and a linear function in "x" for the horizontal displacement. The variation included by Kwan was done by assuming a constant horizontal displacement at each level through the cross section of the element. This model is found to be helpful for modeling the analyses of shear-core wall buildings, but it has a major drawback in that it returns only the average of the bending moment within the elements and it overestimates the shear stress.

2.2.2 Shell Elements

Another type of representation is the shell element, which combines in-plane and out-plane behavior of the wall. This is one of the most complete representations, because it

can represent the interrelation of the wall elements with the different components of the building. Not many of this type of the element has been developed with the principal purpose of analysis of reinforced concrete walls, principally because for single walls, the out of plane behavior of the wall can be neglected, and the increase of more DOF in the element make it more computational expensive. However, for the modeling of realistic interrelation of walls with the beams and the slabs, it is necessary to incorporate out of plane behavior.

Typical FEM programs like ABAQUS [51] or ADINA [3] have already implemented some shell elements, and commonly assign a nonlinear material property that is available in the program, such as plasticity laws or damage cracking material used to model soils, or some simple concrete material property that could represent the nonlinear reinforced concrete behavior over the structure.

Only a few attempts of specific shell elements to model reinforced concrete wall or slabs have been developed. From these efforts the principal approach for the modeling of RC with shell elements is with the use of layers, as has been done by Oñate [101] in 1992, Polak and Vecchio [115] in 1993, Miao et al. [95] in 2006, Zhang et al. [155] in 2007, Zhang et al. [156] in 2007. In this approach the wall section is divided into layers that represent the different components of the wall, such as unconfined concrete (cover), reinforced steel bars and the confined concrete, over the thickness. Each layer is assumed to behave in a plane stress state, and the same type of material constitutive laws used for membrane elements can be used for the layered shell element.

Oñate [101] in 1992 presented a formulation for the layered shell elements that can be applied to different types of structures. This shell was based on flat elements assembled

with the combination of a membrane with two DOF per node (using bilinear displacement interpolation), and a plate element based on Reissner-Mindlin thick plate theory. The material was assumed to be smeared concrete and smeared steel. For the concrete it was used as a damage constitutive model. In addition a modification of the shear strain definition was used to avoid shear locking. This element gave good agreement with experimental results, however, it lacks the in-plane rotation.

Polak and Vecchio [116] developed a shell layered element with the use of a 9-node Heterosis type degenerate, isoparametric element with 42 dof in total that included shear deformation. For materials, the authors used the modified compression field theory (MCFT) formulate by Vecchio and Collins [140] in 1986. They used a reduced integration for the shear strain energy term to obtain a satisfactory result for thin shells. This element agreed with the experimental data and could represent the simple bending and membrane problems. The principal problem of this element was the number of DOF needed to be used, and also the lack of a in-plane rotational DOF.

Miao et al. [95] in 2006, developed a shell element that used a smeared approach for the steel reinforcement and a microplane model developed by Bazant for the concrete. This study concluded that the multi-layer shell element can correctly simulate the coupled in-plane and out-of-plane bending failure of tall walls and the coupled in-plane bending-shear failure of short walls.

2.2.3 Brick Elements

This type of model is characterized by the representation of the walls by 3D solid brick elements, with 3 DOF per node (displacements in the principal directions). This type of

model is principally used for the study of simple and isolated walls because of the computational cost and the complexity to generate the model. Typically for this approach the steel is represented as truss-type elements that are simply connected to the brick element at the node positions. For this reason the mesh of this structures tends to be very complex, unless an embedded constraint is used to connect the line element with the solid element. Commonly, for the representation of the concrete, the plasticity material or orthotropic material models are used, and the researchers use more robust and sophisticated FEM programs like ABAQUS [51] or ADINA [3].

Some examples of this approach to represent the behavior of wall structures can be found in the literature, like the work done by Khatri [72] in 1998. In this study the software program ADINA [3] was used to model the nonlinear behavior of a 14 story building, with an 8-node solid "brick" element to model the concrete and a truss-type element to represent the steel. For the material: a Von-Mises constitutive law for the steel and a concrete material model already implemented in ADINA was used.

A more recent study using this type of approach was done by Gulec et al. [70] in 2009, in this study the authors used ABAQUS [51] to model squat RC walls and compared the results with the experimental tests. The steel was considered fully bonded with the concrete, and used the embedded elements constraint found in ABAQUS [51]. Also an elasto-plastic hysteresis rule with isotropic hardening was used for the steel. The concrete used the Concrete Damaged Plasticity constitutive law already implemented inside of the FEM program in conjunction with the brick element. During this study it was concluded that the behavior of the walls was significantly affected by the dilatation angle that controls

the volumetric component of the plastic strain, and the results were sufficiently accurate to represent the experimental data.

This type of representation commonly gives good agreement with the experimental data and allows a more inside view of the phenomena happening in the concrete. Also, it allows directly to account for the coupling of the different deformations in the structure because they are based on continuum mechanics equation. The main difficulty of this approach is in the complexity of the definition of the constitutive laws due to the number of factors required. In addition, the difficulty to define the mesh of the structures, and the required computational time that needs to be used to perform the analysis.

2.3 Summary

In this chapter the standard models used to study the nonlinear behavior of shear wall structures have been reviewed. For simplicity and computational cost the macro models stand out. However, this tends to be limited to the cases or problems from which the experimental data was used to create the model. In addition, they typically do not take into account the coupling effect of the different deformations, or multi-load cases. Also, these models are difficult to be used to study the interrelation of walls with other elements in buildings.

The other type of model, the microscopic model, presents a more theoretical background and tends to be more flexible to model different structures. Among the microscopic models, the membrane element with the use of smeared orthotropic constitutive material laws is the most common for modeling 2D structures. However, they only include the

in-plane effects over the walls, and typically use only two degrees of freedom per node, and due to this are difficult to connect with other elements like beams.

In the case of 3D structures regarding the two types of representation, the solid brick elements have the problem of computational cost and the level of difficulty to create the wall structure model. Instead, the shell elements allow model the complete interrelation of simple and complex wall structures and buildings. It is seen that layered shell elements should be the best option to model walls. The shell element has the advantage of incorporating the interrelation of all the different elements in a building in a simple but robust manner, and also incorporate all the coupling effects of the deformations inside each wall, thus allowing it to model complex behaviors of wall structures and buildings.

Chapter 3

Finite Element Formulation

Wall structures, like wall buildings, nuclear reactors, water tanks and shell roofs are commonly used in civil engineering. However the designers typically simplify the structures or assume elastic materials, and use techniques like the Finite Element Method (FEM) to analyze the structure and predict the structural response under different load conditions. Unfortunately, for the analysis of nonlinear, complex reinforced concrete wall structures, the typical approach is represented by two options. The first option is to use macroscopic elements like those presented in the last chapter or the implemented elements in Perform3D or SAP2000 [38] or to use models with membrane elements with only 2 DOF per node. But these models start to be difficult to used when the designer or engineer is trying to determine the interrelation inside of complex structures, due to the connection with slabs, beams and walls in different orientations, or when more refined meshes are required. The second option is used in FEM packages like ABAQUS [51] or ADINA [3] that have implemented some shell elements or 3D solid brick elements, and assign to these elements a nonlinear material available, such as plasticity laws or damage cracking

material used to model soils, or some simple concrete material available in this software that could represent the nonlinear reinforced concrete behavior over the structure.

The FEM has been used extensively in the analysis of wall or shell type reinforced concrete structures, mainly in the analysis of curved structures, slabs and shear panels (e.g Cervera et al. [26] in 1987, Polak and Vecchio [115] in 1993, Loo and Guan [81] in 1997, Ayoub and Filippou [7] in 1998 , Kim et al. [73] in 2005, Zhang et al. [155] in 2007, Zhang et al. [156] in 2007). The use of shell elements for the complete modeling of wall buildings for the analysis of nonlinear response of these structure has been excluded or ignored because the nonlinear multi axial material properties and the complex interface and interconnection of elements was typically ignored or treated in an approximate manner. However, with the computational capabilities available today, it is interesting to try to use these more robust elements to study the behavior of wall structures that can be modeled with shell elements.

The more frequently used elements to model shells are : flat shell elements, degenerated three-dimensional elements and curved shell elements. A large number of research has been done around these types of elements over the last decades with the motivation to develop efficient and simple shell elements [100]. Between these three types of elements, the flat shell elements are very attractive because they are simple but robust, and also have a low computational cost. In addition, flat shell elements have the ability to model the effects of stretching and bending behavior in building structures and folded shell structures. However, the poor performance of some flat shell elements to model RC structures is due to the exclusion of coupling between membrane and bending action, and the inadequate modeling of the membrane behavior. This is clearly pointed by Zhang et al. [156] in 2007,

when he expressed that an accurate and robust flat shell element should ideally have the following characteristics:

- a. *Membrane and bending effects must be included.*
- b. *Avoidance of possible singularity in the stiffness matrix.*
- c. *Nodes must have the usual 6-DOF.*
- d. *Freedom from locking for membrane and shear behavior.*
- e. *Application for non-linear material properties and large deformations.*

For this reason, it is necessary first to develop a quadrilateral membrane element with a rotational DOF at each node using a layered section formulation, that satisfies that the rotational DOF is the strain representation of the true rotation $\left(\Omega = \frac{1}{2} \left(\frac{\partial v}{\partial x} - \frac{\partial u}{\partial y} \right)\right)$, which allows the connection of beams and other element directly to the membrane and shell element without any extra difficulty. The formulation for the quadrilateral membrane element is an extension of the formulation developed by Xia et al. [151] in 2009. This new quadrilateral membrane element will be used as the base to develop the formulation of the quadrilateral layered shell element, for the in-plane behavior of the shell. The Discrete Kirchhoff Quadrilateral Element (DKQ) formulated by Batoz and Tahar [11] in 1982 will be used to model out-of-plane bending of the shell. The modeling of the section of the membrane and shell element consists of a layered system that is fully bonded between the layers. It also includes the coupled membrane and bending effects for the shell element.

In the next section of this chapter, the finite element formulation for the quadrilateral layered membrane and the quadrilateral layered shell adopted in this study and also the displacement interpolation used for the elements are studied and reviewed.

3.1 Quadrilateral Layered Membrane Element with Rotational DOF Formulation

Membranes are in a state of plane stress, in which only in-plane behavior is considered, this means $\sigma_z = \tau_{zx} = \tau_{zy} = 0$, Fig. 3.1. The finite element formulation for this type of elements using a displacement-based approach is well known and can be found in any book of finite elements. Typically the formulation for this type of element is developed from the concept of virtual work, and is used to determinate the stiffness matrix and the resisting force of the plane element, which are necessary to implement the element in a nonlinear finite element framework. This section shows the derivation of the displacement-based finite element method (stiffness matrix, and resisting force) for plane stress elements under small strains. For this a combination of the formulations presented in Bathe [9] (1996), Cook et al. [35] (2002), and Chen [29] (2007) are used with additional modifications to include the layered section.

The principle of virtual works for a membrane in plane stress state can be written as

$$\delta W_{internal} = \delta W_{external} \quad (3.1)$$

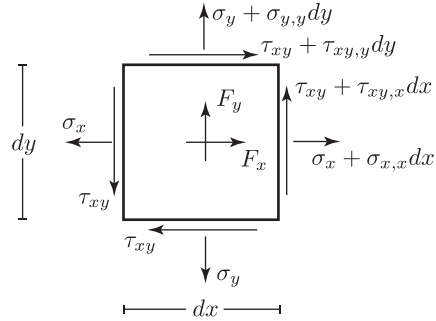


Figure 3.1: In-Plane Stresses

with the internal virtual work defined as:

$$\delta W_{internal} = \int_V \{\delta\varepsilon\}^T \{\sigma\} dV \quad (3.2)$$

where $\{\sigma\}$ is the vector of stresses in the membrane, and $\{\delta\varepsilon\}$ is the virtual vector of strains, which is produced by the virtual displacements $\{\delta u\}$.

With the external virtual work defined as:

$$\delta W_{external} = \int_V \{\delta u\}^T \{F_{body}\} dV + \int_A \{\delta u\}^T \{T\} dA + \int_S \{\delta u\}^T \{t_{edge}\} dS \quad (3.3)$$

where $\{F_{body}\}$ is the body force over the membrane, and $\{T\}$ the external forces over the surface of the membrane and $\{t_{edge}\}$ the external forces over the edge of the membrane

Now following the displacement-based approach for finite elements, the interpolation of the displacement (horizontal and vertical) over the element at the middle plane can be defined as:

$$\{u\} = \begin{Bmatrix} u \\ v \end{Bmatrix} = [\Psi(x, y)] \{U\} \quad (3.4)$$

where $[\Psi(x, y)]$ are the shape functions that represent the interpolation over the element and $\{U\}$ is the displacement of the degrees of freedom at each node. Since this formulation is using small strain theory, the kinematic or strain-displacement relationship is represented by:

$$\begin{Bmatrix} \varepsilon_x \\ \varepsilon_y \\ \gamma_{xy} \end{Bmatrix} = \begin{Bmatrix} \frac{\partial u}{\partial x} \\ \frac{\partial v}{\partial y} \\ \frac{\partial u}{\partial y} + \frac{\partial v}{\partial x} \end{Bmatrix} = \underbrace{\begin{bmatrix} \frac{\partial}{\partial x} & 0 \\ 0 & \frac{\partial}{\partial y} \\ \frac{\partial}{\partial y} & \frac{\partial}{\partial x} \end{bmatrix}}_{[\partial]} \begin{Bmatrix} u \\ v \end{Bmatrix} = \underbrace{\begin{bmatrix} 1 & 0 & 0 & 0 \\ 0 & 0 & 0 & 1 \\ 0 & 1 & 1 & 0 \end{bmatrix}}_{[A]} \begin{Bmatrix} \frac{\partial u}{\partial x} \\ \frac{\partial u}{\partial y} \\ \frac{\partial v}{\partial x} \\ \frac{\partial v}{\partial y} \end{Bmatrix} \quad (3.5)$$

Using Eq. 3.4 and Eq. 3.5 , the strain at each point over the element can be written as

$$\{\varepsilon\} = [B(x, y)] \{U\} \quad \text{where} \quad [B(x, y)] = [\partial] [\Psi(x, y)] \quad (3.6)$$

Replacing everything back in the virtual work for the membrane (Eq. 3.1), and including also initial stresses for the general case as proposed by Cook et al. [35] in 2002, the following is obtained:

$$\{\delta U\}^T \left(\underbrace{\int_V [\Psi]^T \{F_{body}\} dV + \int_A [\Psi]^T \{T\} dA + \int_S [\Psi]^T \{t_{edge}\} dS}_{F_{External}} - \underbrace{\int_V [B]^T \{\sigma\} dV - \int_V [B]^T \{\sigma_0\} dV}_{-R} \right) = 0 \quad (3.7)$$

where $F_{External}$ is the external force over the system, and R is the resistant internal force of the membrane that is a function of the displacement at the nodes.

Now, in order to implement this in a nonlinear material implementation, e.g. using Newton-Raphson method, it is necessary to determine two expressions, the tangent stiffness matrix and the resistant internal force of the membrane at each iteration. From virtual work, the residual equation for the system at each iteration is obtained as:

$$\text{Residual} (U^i) = F_{\text{external}} - R^i \quad (3.8)$$

Now linearize the $\text{Residual} (U^i + \Delta U^i)$ using a Taylor expansion, and excluding high order terms:

$$\text{Residual} (U^i + \Delta U^i) = \text{Residual} (U^i) + \frac{\partial \text{Residual} (U^i)}{\partial U} \Delta U^i \quad (3.9)$$

Performing the derivative over the *Residual* equation, and performing the integration over the thickness results in:

$$\begin{aligned} \frac{\partial \text{Residual} (U^i)}{\partial U} &= -\frac{\partial}{\partial U} \left(\int_V [B]^T \{\sigma\} dV \right) = -\int_V [B]^T \frac{\partial \{\sigma\}}{\partial \{U\}} dV \\ &= -\int_V [B]^T \frac{\partial \{\sigma\}}{\partial \{\varepsilon\}} [B] dV = -\int_A [B]^T \underbrace{\left(\int_{-\frac{t}{2}}^{\frac{t}{2}} \frac{\partial \{\sigma\}}{\partial \{\varepsilon\}} dz \right)}_{[D_{\text{tangent}}]} [B] dA \end{aligned} \quad (3.10)$$

Using this, the tangent stiffness of the membrane is defined as

$$K_t = \int_A [B]^T [D_{\text{tangent}}] [B] dA \quad (3.11)$$

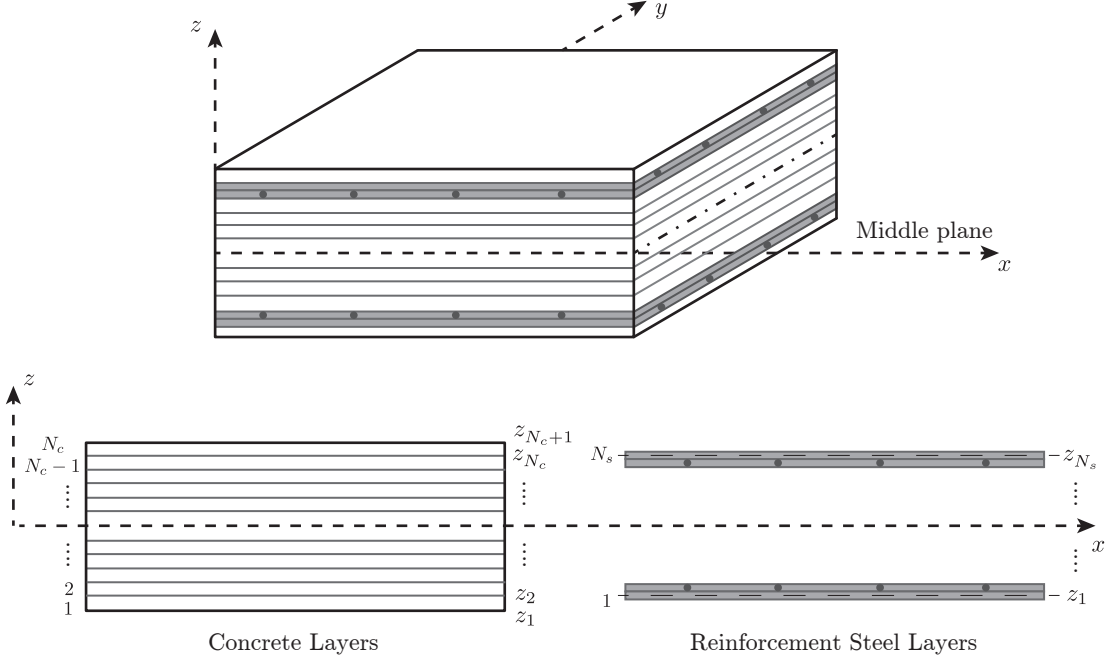


Figure 3.2: A typical rectangular layered membrane section

where the material tangent matrix $[D_{Tangent}]$, can be expressed in discrete manner using the expression applied by Zhang et al. [155] and Zhang et al. [156] in 2007, Fig. 3.2, to include concrete and steel layers over the thickness, but only for the membrane part:

$$[D_{Tangent}] = \int_{-\frac{t}{2}}^{\frac{t}{2}} [D] dz = \sum_{i=1}^{N_c} [D_{c_i}] (z_{i+1} - z_i) + \sum_{j=1}^{N_s} [D_{s_j}] t_{s_j} \quad (3.12)$$

where the matrices $[D_{c_i}]$ and $[D_{s_j}]$ are the plane stress material stiffness tangent of the i^{th} concrete layer and j^{th} steel layer, respectively. N_c and N_s are the number of layers of concrete and steel respectively, and z_i is the location of the top and bottom part of each layer. In addition, t_{s_j} is the thickness of the section for the j^{th} steel layer.

Defining the internal resisting force R for the membrane from Eq. 3.7, and performing the integration over the thickness the following is obtained, and assuming zero initial stress:

$$R = \int_A [B]^T \underbrace{\left(\int_{-\frac{t}{2}}^{\frac{t}{2}} \{\sigma\} dz \right)}_{\{\hat{\sigma}\}} dA = \int_A [B]^T \begin{Bmatrix} n_x \\ n_y \\ n_{xy} \end{Bmatrix} dA \quad (3.13)$$

where, the vector stress $\{\hat{\sigma}\}$ can also be calculated using a discrete manner as:

$$n_x = \int_{-\frac{t}{2}}^{\frac{t}{2}} \sigma_x dz = \sum_{i=1}^{Nc} \sigma_{x_i}^c (z_{i+1} - z_i) + \sum_{j=1}^{Ns} \sigma_{x_j}^s t_{s_j} \quad (3.14a)$$

$$n_y = \int_{-\frac{t}{2}}^{\frac{t}{2}} \sigma_y dz = \sum_{i=1}^{Nc} \sigma_{y_i}^c (z_{i+1} - z_i) + \sum_{j=1}^{Ns} \sigma_{y_j}^s t_{s_j} \quad (3.14b)$$

$$n_{xy} = \int_{-\frac{t}{2}}^{\frac{t}{2}} \tau_{xy} dz = \sum_{i=1}^{Nc} \tau_{xy_i}^c (z_{i+1} - z_i) + \sum_{j=1}^{Ns} \tau_{xy_j}^s t_{s_j} \quad (3.14c)$$

where $\{\sigma_i^c\}$ is the in-plane stresses at i^{th} concrete layer, and $\{\sigma_j^s\}$ is the in-plane stresses at j^{th} steel layer, and z_{i+1} and z_i are the locations of the top and bottom part of the i^{th} concrete layer, respectively.

Using the definition for the matrix tangent stiffness and the internal resisting force R , Eq. 3.9 is rewritten for the iteration procedure as:

$$K_t \Delta U^i = F_{external} - R^i \quad (3.15)$$

Despite the fact that the element formulation is straight forward, searching for an optimal representation of the membrane element that includes rotation as a degree of

freedom is still an area of constant research. These types of elements are very attractive, because they can be combined with a bending plate directly to form shell elements. Allman [4] in 1984 was the first to develop a simple triangular element with 3 DOF per node that produced good results. This element was based on a quadratic displacement with vertex connectors. In 1986, Cook [34] directly extended this formulation to be used in quadrilateral elements, however it was observed to produce shear locking for nearly incompressible materials and it also produced spurious modes. The spurious mode can be simply suppressed by fixing one of the rotational DOF of the model. MacNeal and Harder [83] in 1988, took the extended Allman-type element done by Cook and simplified it, to be able to add the element to a finite element program and also include some modifications like least square smoothing of the strains calculated from the displacement to improve the formulation. Although, this element is simple to formulate it has the drawback that the rotational DOF used to define the displacement interpolation is not the true rotation derived from mechanics $\Omega = \frac{1}{2} \left(\frac{\partial v}{\partial x} - \frac{\partial u}{\partial y} \right)$.

Following the Allman element type and its variations, other researchers have been successful in developing this type of quadrilateral element (e.g Bergan and Felippa [19] in 1985, Hughes and Brezzi [59] in 1989). However these approaches tend to be either very complex or to come from mixed formulations that make it difficult to be combined with bending elements. Ibrahimbegovic et al. [60] in 1990, used a variational approach to obtain the membrane element with rotational DOF. The element was based on an independent rotational field interpolation and an Allman type quadrilateral element for the displacement over the element. It was found that a penalty method appears to naturally ensure that the rotational DOF are the true rotation over the element.

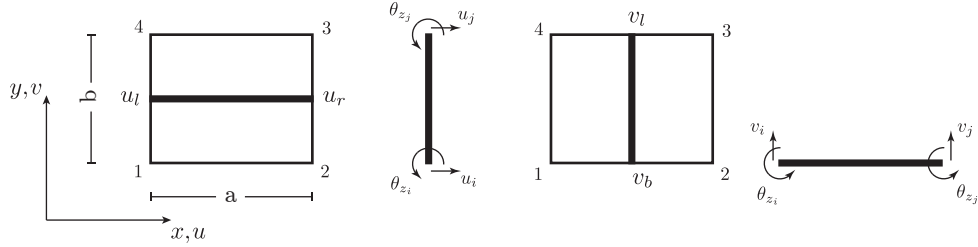


Figure 3.3: Element develop by Xia et al. [151] in 2009

Another option to develop an element with rotational degrees of freedom, is to use a combination of interpolation functions that satisfied the restraints of the element. In this case the restriction that needs to be satisfied is that the rotation degree of freedom returns the true rotation derived from mechanics $\Omega = \frac{1}{2} \left(\frac{\partial v}{\partial x} - \frac{\partial u}{\partial y} \right)$. Some elements using this approach have been proposed by Xia et al. [151] (2009), Sisodiya and Cheung [125] (1971), Abu Ghazaleh [1] (1966).

In 1966, Abu Ghazaleh [1] proposed a quadrilateral membrane type element with rotational degrees of freedom at each node, using a combination of cubic (beam type displacement and rotation interpolations) and linear interpolations (damping functions) for the horizontal and vertical displacement, and studied the accuracy of the proposed element. Sisodiya and Cheung [125] in 1971 used a bilinear representation for the vertical displacement and a cubic interpolation in y and a linear interpolation in x for the horizontal displacement. Sisodiya and Cheung [125] in 1971 used this interpolation to model panels and study bridges. It was later used by Kwan [76] in 1993 and by Kwan and Cheung [77] in 1994 with some simplifications to model walls. Xia et al. [151] in 2009, reported that Zeng in 1981 proposed a finite belt method that consisted of simple use of linear and cubic functions to represent the shape function on plates and some type of beams. Xia et al. [151] used this finite belt approach to develop a rectangular plane element with rotational

degrees of freedom, which is based on the same horizontal displacement as Sisodiya et al [125] in 1971, but for the vertical it used a cubic function in x and a linear interpolation in y , see Fig. 3.3, which is something similar to the approach proposed by Abu Ghazaleh [1] in (1966). With this selection of interpolation, the rotational DOF at each node represented the true rotation for small deformation. However, this representation was only present for rectangular elements.

In the next subsection, the displacement interpolation used to define the membrane with rotational degrees of freedom used in this dissertation will be presented. This new formulation is an extension of the formulation developed by Xia et al. [151] in 2009, to be used in a general finite element framework using natural coordinates. In addition, it will analyze the effect on the true rotation if the element is assumed to be different from rectangular.

3.1.1 Blended Displacement Interpolation

In this section, the extension of the 4 node rectangular element developed by Xia et al. [151] in 2009, using the finite belt method, see Fig. 3.3, to be used in a general finite element framework using natural coordinates is developed. The element proposed by Xia et al. [151] starts with a cubic interpolation in y and a linear interpolation in x for the horizontal displacement, and in the vertical displacement direction it uses a cubic interpolation in x and a linear interpolation in y .

To develop the element using natural coordinates, first it is necessary to represent the geometry of the element using natural coordinates, this is done with the bilinear representation:

$$X(\xi, \eta) = \sum_{i=1}^4 \psi_i(\xi, \eta) x_i \quad (3.16)$$

$$Y(\xi, \eta) = \sum_{i=1}^4 \psi_i(\xi, \eta) y_i \quad (3.17)$$

where x_i and y_i are the coordinates of the corner nodes and $\psi_i(\xi, \eta)$ are the shape functions, which are defined as:

$$\psi_i(\xi, \eta) = \frac{1}{4} (1 + \xi_i \xi) (1 + \eta_i \eta) \quad i = 1, 2, 3, 4 \quad (3.18)$$

where $\xi_i = \begin{bmatrix} -1 & 1 & 1 & -1 \end{bmatrix}$ and $\eta_i = \begin{bmatrix} -1 & -1 & 1 & 1 \end{bmatrix}$ for $i = 1, 2, 3, 4$ are the coordinates of the nodes in the natural coordinate system.

Using this, the relation between the derivatives in the two spaces (Jacobian $[J]$) can be calculated as:

$$\begin{Bmatrix} \frac{\partial}{\partial \xi} \\ \frac{\partial}{\partial \eta} \end{Bmatrix} = \underbrace{\begin{bmatrix} \frac{\partial X(\xi, \eta)}{\partial \xi} & \frac{\partial Y(\xi, \eta)}{\partial \xi} \\ \frac{\partial X(\xi, \eta)}{\partial \eta} & \frac{\partial Y(\xi, \eta)}{\partial \eta} \end{bmatrix}}_{[J]} \begin{Bmatrix} \frac{\partial}{\partial x} \\ \frac{\partial}{\partial y} \end{Bmatrix} \quad (3.19)$$

and

$$\begin{Bmatrix} \frac{\partial}{\partial x} \\ \frac{\partial}{\partial y} \end{Bmatrix} = \underbrace{\frac{1}{|J|} \begin{bmatrix} \frac{\partial Y(\xi, \eta)}{\partial \eta} & -\frac{\partial Y(\xi, \eta)}{\partial \xi} \\ -\frac{\partial X(\xi, \eta)}{\partial \eta} & \frac{\partial X(\xi, \eta)}{\partial \xi} \end{bmatrix}}_{[J]^{-1}} \begin{Bmatrix} \frac{\partial}{\partial \xi} \\ \frac{\partial}{\partial \eta} \end{Bmatrix} \quad (3.20)$$

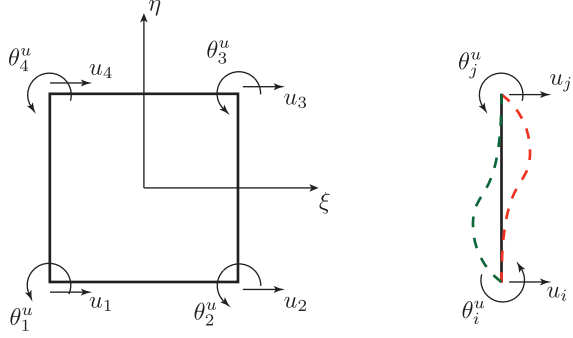


Figure 3.4: Blended Interpolation for the Horizontal Displacement

Now, it is possible to define the displacement interpolation or field interpolation using natural coordinates. First, an analysis of the field interpolation used to define the horizontal displacement u over the element is presented, see Fig. 3.4. This interpolation is assembled for the combination of a linear shape function in ξ :

$$M_1(\xi) = \frac{1}{2}(1 - \xi) \quad M_2(\xi) = \frac{1}{2}(1 + \xi) \quad (3.21)$$

and a cubic interpolation in η , for this is used for the hermitian interpolation:

$$N_1(\eta) = \frac{1}{2} - \frac{3}{4}\eta + \frac{\eta^3}{4} \quad (3.22)$$

$$N_2(\eta) = \frac{1}{4} - \frac{\eta}{4} - \frac{\eta^2}{4} + \frac{\eta^3}{4} \quad (3.23)$$

$$N_3(\eta) = \frac{1}{2} + \frac{3}{4}\eta - \frac{\eta^3}{4} \quad (3.24)$$

$$N_4(\eta) = -\frac{1}{4} - \frac{\eta}{4} + \frac{\eta^2}{4} + \frac{\eta^3}{4} \quad (3.25)$$

Now the displacement $u(\xi, \eta)$ can be written as:

$$u(\xi, \eta) = \begin{bmatrix} M_1(\xi) \\ M_2(\xi) \end{bmatrix}^T$$

$$\begin{bmatrix} N_1(\eta) & N_2(\eta) & 0 & 0 & 0 & 0 & N_3(\eta) & N_4(\eta) \\ 0 & 0 & N_1(\eta) & -N_2(\eta) & N_3(\eta) & -N_4(\eta) & 0 & 0 \end{bmatrix} \{U^u\} \quad (3.26)$$

or

$$u(\xi, \eta) = \begin{bmatrix} M_1(\xi) N_1(\eta) & -M_1(\xi) N_2(\eta) & M_2(\xi) N_1(\eta) & -M_2(\xi) N_2(\eta) \\ M_2(\xi) N_3(\eta) & -M_2(\xi) N_4(\eta) & M_1(\xi) N_3(\eta) & -M_1(\xi) N_4(\eta) \end{bmatrix} \{U^u\} \quad (3.27)$$

where

$$\{U^u\} = \left\{ u_1 \quad \theta_1^u \quad u_2 \quad \theta_2^u \quad u_3 \quad \theta_3^u \quad u_4 \quad \theta_4^u \right\}^T \quad (3.28)$$

Defining the rotation θ_i^u $i = 1, 2, 3, 4$ as function of the rotational DOF at each node as:

$$\theta_1^u = \frac{y_4 - y_1}{2} \theta_1 \quad (3.29a)$$

$$\theta_2^u = \frac{y_3 - y_2}{2} \theta_2 \quad (3.29b)$$

$$\theta_3^u = \frac{y_3 - y_2}{2} \theta_3 \quad (3.29c)$$

$$\theta_4^u = \frac{y_4 - y_1}{2} \theta_4 \quad (3.29d)$$

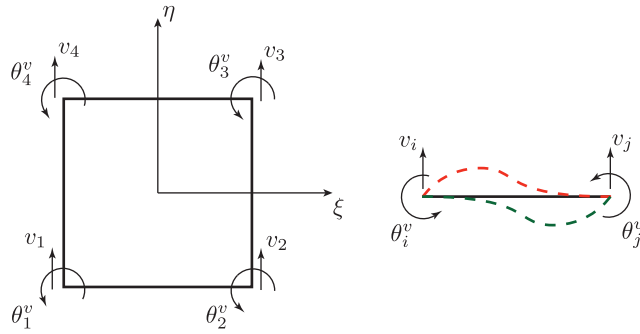


Figure 3.5: Blended interpolation for the vertical displacement

Now, the same procedure is used for the vertical field displacement (Fig. 3.5). This means, it is assembled for the combination of a linear shape function in η :

$$M_1(\eta) = \frac{1}{2}(1 - \eta) \quad M_2(\eta) = \frac{1}{2}(1 + \eta) \quad (3.30)$$

and a cubic interpolation in ξ , for this is used for the hermitian interpolation:

$$N_1(\xi) = \frac{1}{2} - \frac{3}{4}\xi + \frac{\xi^3}{4} \quad (3.31)$$

$$N_2(\xi) = \frac{1}{4} - \frac{\xi}{4} - \frac{\xi^2}{4} + \frac{\xi^3}{4} \quad (3.32)$$

$$N_3(\xi) = \frac{1}{2} + \frac{3}{4}\xi - \frac{\xi^3}{4} \quad (3.33)$$

$$N_4(\xi) = -\frac{1}{4} - \frac{\xi}{4} + \frac{\xi^2}{4} + \frac{\xi^3}{4} \quad (3.34)$$

Now the displacement $v(\xi, \eta)$ can be written as:

$$v(\xi, \eta) = \begin{bmatrix} M_1(\eta) \\ M_2(\eta) \end{bmatrix}^T$$

$$\begin{bmatrix} N_1(\xi) & N_2(\xi) & N_3(\xi) & N_4(\xi) & 0 & 0 & 0 & 0 \\ 0 & 0 & 0 & 0 & N_3(\xi) & N_4(\xi) & N_1(\xi) & N_2(\xi) \end{bmatrix} \{U^v\} \quad (3.35)$$

or

$$v(\xi, \eta) = \begin{bmatrix} M_1(\eta)N_1(\xi) & M_1(\eta)N_2(\xi) & M_1(\eta)N_3(\xi) & M_1(\eta)N_4(\xi) \\ M_2(\eta)N_3(\xi) & M_2(\eta)N_4(\xi) & M_2(\eta)N_1(\xi) & M_2(\eta)N_2(\xi) \end{bmatrix} \{U^v\} \quad (3.36)$$

where

$$\{U^v\} = \left\{ v_1 \quad \theta_1^v \quad v_2 \quad \theta_2^v \quad v_3 \quad \theta_3^v \quad v_4 \quad \theta_4^v \right\}^T \quad (3.37)$$

Define the rotation θ_i^v $i = 1, 2, 3, 4$ as function of the rotational DOF at each node as:

$$\theta_1^v = \frac{x_2 - x_1}{2}\theta_1 \quad (3.38a)$$

$$\theta_2^v = \frac{x_2 - x_1}{2}\theta_2 \quad (3.38b)$$

$$\theta_3^v = \frac{x_3 - x_4}{2}\theta_3 \quad (3.38c)$$

$$\theta_4^v = \frac{x_3 - x_4}{2}\theta_4 \quad (3.38d)$$

Now, assemble the u and v displacement to form the displacement interpolation for the element:

$$\begin{aligned} \begin{Bmatrix} u(\xi, \eta) \\ v(\xi, \eta) \end{Bmatrix} &= \begin{bmatrix} M_1(\xi) N_1(\eta) & 0 & -M_1(\xi) N_2(\eta) & 0 \\ 0 & M_1(\eta) N_1(\xi) & 0 & M_1(\eta) N_2(\xi) \\ M_2(\xi) N_1(\eta) & 0 & -M_2(\xi) N_2(\eta) & 0 \\ 0 & M_1(\eta) N_3(\xi) & 0 & M_1(\eta) N_3(\xi) \\ M_2(\xi) N_3(\eta) & 0 & -M_2(\xi) N_4(\eta) & 0 \\ 0 & M_2(\eta) N_3(\xi) & 0 & M_2(\eta) N_4(\xi) \\ M_1(\xi) N_3(\eta) & 0 & -M_1(\xi) N_4(\eta) & 0 \\ 0 & M_2(\eta) N_1(\xi) & 0 & M_2(\eta) N_2(\xi) \end{bmatrix} \\ \{U^{uv}\} &= \left[MN(\xi, \eta) \right] \{U^{uv}\} \end{aligned} \quad (3.39)$$

where

$$\{U^{uv}\} = \left\{ u_1 \ v_1 \ \theta_1^u \ \theta_1^v \ u_2 \ v_2 \ \theta_2^u \ \theta_2^v \ u_3 \ v_3 \ \theta_3^u \ \theta_3^v \ u_4 \ v_4 \ \theta_4^u \ \theta_4^v \right\}^T$$

However, the relation between the rotation is known and can be written in matrix form as:

$$\left\{ \begin{array}{l} u_1 \\ v_1 \\ \theta_1^u \\ \theta_1^v \\ u_2 \\ v_2 \\ \theta_2^u \\ \theta_2^v \\ u_3 \\ v_3 \\ \theta_3^u \\ \theta_3^v \\ u_4 \\ v_4 \\ \theta_4^u \\ \theta_4^v \end{array} \right\} = \underbrace{\left[\begin{array}{cccccccccccc} 1 & 0 & 0 & 0 & 0 & 0 & 0 & 0 & 0 & 0 & 0 & 0 & 0 \\ 0 & 1 & 0 & 0 & 0 & 0 & 0 & 0 & 0 & 0 & 0 & 0 & 0 \\ 0 & 0 & \frac{y_4-y_1}{2} & 0 & 0 & 0 & 0 & 0 & 0 & 0 & 0 & 0 & 0 \\ 0 & 0 & \frac{x_2-x_1}{2} & 0 & 0 & 0 & 0 & 0 & 0 & 0 & 0 & 0 & 0 \\ 0 & 0 & 0 & 1 & 0 & 0 & 0 & 0 & 0 & 0 & 0 & 0 & 0 \\ 0 & 0 & 0 & 0 & 1 & 0 & 0 & 0 & 0 & 0 & 0 & 0 & 0 \\ 0 & 0 & 0 & 0 & 0 & \frac{y_3-y_2}{2} & 0 & 0 & 0 & 0 & 0 & 0 & 0 \\ 0 & 0 & 0 & 0 & 0 & \frac{x_2-x_1}{2} & 0 & 0 & 0 & 0 & 0 & 0 & 0 \\ 0 & 0 & 0 & 0 & 0 & 0 & 1 & 0 & 0 & 0 & 0 & 0 & 0 \\ 0 & 0 & 0 & 0 & 0 & 0 & 0 & 1 & 0 & 0 & 0 & 0 & 0 \\ 0 & 0 & 0 & 0 & 0 & 0 & 0 & 0 & \frac{y_3-y_2}{2} & 0 & 0 & 0 & 0 \\ 0 & 0 & 0 & 0 & 0 & 0 & 0 & 0 & \frac{x_3-x_4}{2} & 0 & 0 & 0 & 0 \\ 0 & 0 & 0 & 0 & 0 & 0 & 0 & 0 & 0 & 1 & 0 & 0 & 0 \\ 0 & 0 & 0 & 0 & 0 & 0 & 0 & 0 & 0 & 0 & 1 & 0 & 0 \\ 0 & 0 & 0 & 0 & 0 & 0 & 0 & 0 & 0 & 0 & 0 & \frac{y_4-y_1}{2} & 0 \\ 0 & 0 & 0 & 0 & 0 & 0 & 0 & 0 & 0 & 0 & 0 & 0 & \frac{x_3-x_4}{2} \end{array} \right]}_{[Tr]} \left\{ \begin{array}{l} u_1 \\ v_1 \\ \theta_1 \\ u_2 \\ v_2 \\ \theta_2 \\ u_3 \\ v_3 \\ \theta_3 \\ u_4 \\ v_4 \\ \theta_4 \end{array} \right\} \quad (3.40)$$

which reduces the displacement to:

$$\left\{ \begin{array}{l} u(\xi, \eta) \\ v(\xi, \eta) \end{array} \right\} = \underbrace{\left[\begin{array}{c} MN(\xi, \eta) \\ \Psi(\xi, \eta) \end{array} \right] \left[Tr \right]}_{[\Psi(\xi, \eta)]} \{U\} = [\Psi(\xi, \eta)] \{U\} \quad (3.41)$$

where $[\Psi(\xi, \eta)]$ is the field interpolation function, and $\{U\}$ is the displacement at the nodes:

$$\{U\} = \left\{ u_1 \ v_1 \ \theta_1 \ u_2 \ v_2 \ \theta_2 \ u_3 \ v_3 \ \theta_3 \ u_4 \ v_4 \ \theta_4 \right\}^T \quad (3.42)$$

Now, it is possible to define the kinematic matrix $[B]$, in Eq. 3.6 as:

$$[B] = \begin{bmatrix} 1 & 0 & 0 & 0 \\ 0 & 0 & 0 & 1 \\ 0 & 1 & 1 & 0 \end{bmatrix} \begin{bmatrix} [J]^{-1} & [0] \\ [0] & [J]^{-1} \end{bmatrix} \begin{bmatrix} \frac{\partial MN_{1,i}}{\partial \xi} \\ \frac{\partial MN_{1,i}}{\partial \eta} \\ \frac{\partial MN_{2,i}}{\partial \xi} \\ \frac{\partial MN_{2,i}}{\partial \eta} \end{bmatrix} [Tr] \quad (3.43)$$

Using some algebraic manipulation, it is possible to define the true rotation for a distorted element defined by Fig. 3.6. For example the true rotation for the node 1 ($\Omega(-1, -1)$) is defined by the Eq. 3.44. If the element shape is rectangular, it is found that the rotation at the nodes are the true rotations $\Omega = \frac{1}{2} \left(\frac{\partial v}{\partial x} - \frac{\partial u}{\partial y} \right)$. However, if the

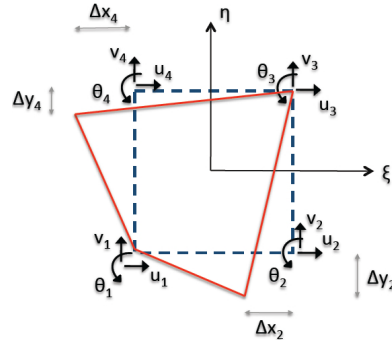


Figure 3.6: Distorted Blended element

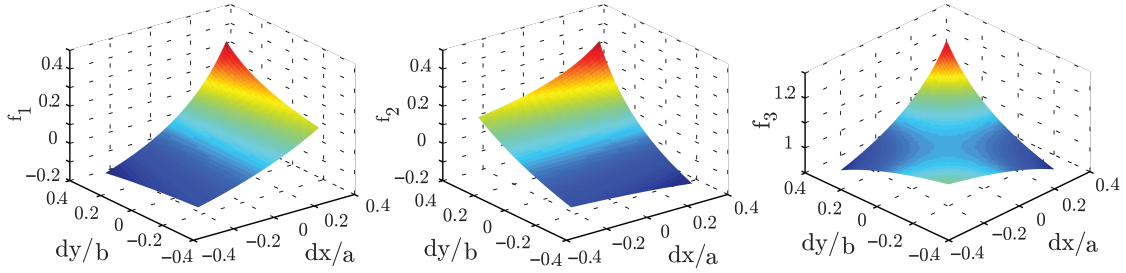


Figure 3.7: Factors to determinate variation with respect to the true rotation $\Omega = \frac{1}{2} \left(\frac{\partial v}{\partial x} - \frac{\partial u}{\partial y} \right)$

element shape is distorted, the rotation at the node and the true rotation start to diverge one from the other.

$$\begin{aligned}
 \Omega(-1, -1) &= \underbrace{\frac{\frac{dx_4}{a}}{2 \left(\frac{dx_2}{a} - \frac{dx_4}{a} \frac{dy_2}{b} + \frac{dx_2}{a} \frac{dy_4}{b} + \left(1 + \frac{dy_4}{b} \right) \right)}}_{f_1} \left(\frac{u_2 - u_1}{b} \right) \\
 &\quad + \underbrace{\frac{\frac{dy_2}{b}}{2 \left(\frac{dx_2}{a} - \frac{dx_4}{a} \frac{dy_2}{b} + \frac{dx_2}{a} \frac{dy_4}{b} + \left(1 + \frac{dy_4}{b} \right) \right)}}_{f_2} \left(\frac{v_1 - v_4}{a} \right) \\
 &\quad + \underbrace{\frac{\left(1 + \frac{dx_2}{a} \right) \left(1 + \frac{dy_4}{b} \right)}{\left(\frac{dx_2}{a} - \frac{dx_4}{a} \frac{dy_2}{b} + \frac{dx_2}{a} \frac{dy_4}{b} + \left(1 + \frac{dy_4}{b} \right) \right)}}_{f_3} \theta_1
 \end{aligned} \tag{3.44}$$

From the Fig. 3.7, it can be observed that the true rotation is similarly influenced by the three factors, with a rapid increase for highly distorted elements, around 40 percent of the dimension of the element. However, for small distorted elements it is observed that the factors f_1 , f_2 and f_3 have small variations and do not modify the true rotation much. But typically for wall structures, and in the test used in this dissertation, a meshing procedure is used that creates only rectangular elements without any distortion.

3.2 Quadrilateral Thin Flat Layered Shell Formulation

As a continuation, the formulation for a thin flat quadrilateral shell element for small deformation is presented. In addition, it is incorporated into the formulation for the use of a layered section for the shell element to account for the variation of material through the section. Similar to the quadrilateral layered membrane formulation, the finite element formulation for this type of element is developed from the concept of virtual work, and is used to determinate the stiffness matrix and the resisting force of the shell element, which are necessary to implement the element in a nonlinear finite element framework. A continuation is shown for the derivation of the displacement-based finite element method (stiffness matrix, and resisting force) for a thin flat shell element under small strains using a similar formulation presented before in combination with the formulation developed by Oñate [101] in 1992 with some modifications.

The principle of virtual works for shell element in the local coordinate system $x' - y'$ can be written as

$$\delta W_{internal} = \delta W_{external} \quad (3.45)$$

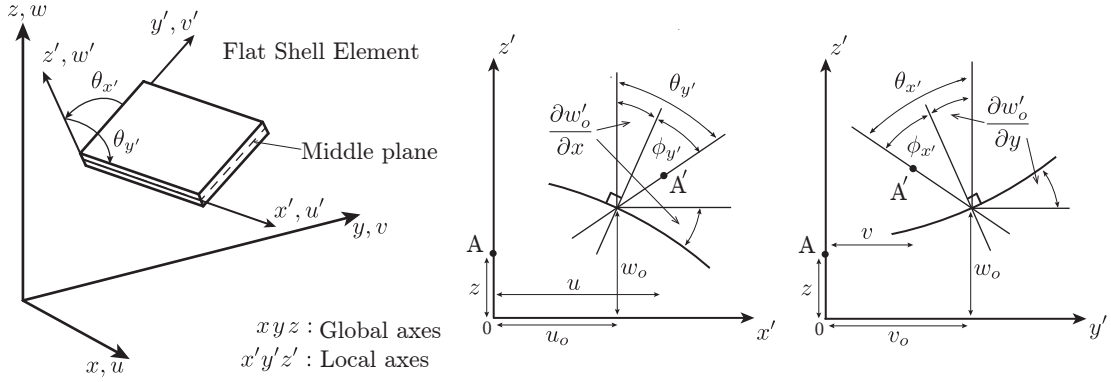


Figure 3.8: Shell Element definitions

with the internal virtual work defined as

$$\delta W_{internal} = \int_A \{\delta \hat{\varepsilon}'\}^T \{\hat{\sigma}'\} dA \quad (3.46)$$

where $\{\hat{\sigma}'\}$ is the vector of stresses in the shell, and $\{\delta \hat{\varepsilon}'\}$ is the virtual vector of strains, which are produced by the virtual displacements $\{\delta u'\}$ in the local coordinate system

and also with the external virtual work defined as

$$\delta W_{external} = \int_V \{\delta u'\}^T \{F_{body}\} dV + \int_A \{\delta u'\}^T \{T\} dA + \int_S \{\delta u'\}^T \{t_{edge}\} dS \quad (3.47)$$

where $\{F_{body}\}$ is the body force over the shell, $\{T\}$ is the external forces over the surface of the shell and $\{t_{edge}\}$ is the external forces over the edge of the shell.

Now following the displacement-based approach for finite elements, the interpolation of the displacement over the element at the middle plane of the section can be defined as:

$$\begin{aligned} u' (x', y', z') &= u'_m (x', y') + z' \theta_{y'} \\ v' (x', y', z') &= v'_m (x', y') - z' \theta_{x'} \\ w' (x', y', z') &= w'_b (x', y') \end{aligned} \quad (3.48)$$

where $u'_m (x', y')$ and $v'_m (x', y')$ are in-plane displacement (membrane displacements) and θ_x , θ_y and $w'_b (x', y')$ are the rotations out of plane and the transversal displacement (flexural component), respectively. Assuming that the shell is in a state of plane stresses ($\sigma_{z'} = 0$) over the thickness, it is possible to reduce the strain vector to:

$$\{\varepsilon'\} = \begin{Bmatrix} \varepsilon_{x'} \\ \varepsilon_{y'} \\ \gamma_{x'y'} \\ \dots \\ \gamma_{x'z'} \\ \gamma_{y'z'} \end{Bmatrix} = \begin{Bmatrix} \frac{\partial u'}{\partial x'} \\ \frac{\partial v'}{\partial y'} \\ \frac{\partial u'}{\partial y'} + \frac{\partial v'}{\partial x'} \\ \dots \\ \frac{\partial u'}{\partial z'} + \frac{\partial w'}{\partial x'} \\ \frac{\partial v'}{\partial z'} + \frac{\partial w'}{\partial y'} \end{Bmatrix} = \begin{Bmatrix} \frac{\partial u'_m}{\partial x'} \\ \frac{\partial v'_m}{\partial y'} \\ \frac{\partial u'_m}{\partial y'} + \frac{\partial v'_m}{\partial x'} \\ \dots \\ 0 \\ 0 \end{Bmatrix} + \begin{Bmatrix} z' \frac{\partial \theta_{y'}}{\partial x'} \\ -z' \frac{\partial \theta_{x'}}{\partial y'} \\ z' \left(\frac{\partial \theta_{y'}}{\partial y'} - \frac{\partial \theta_{x'}}{\partial x'} \right) \\ \dots \\ \frac{\partial w'_b}{\partial x'} + \theta_{y'} \\ \frac{\partial w'_b}{\partial y'} - \theta_{x'} \end{Bmatrix} \quad (3.49)$$

or rewritten as:

$$\{\varepsilon'\} = \begin{Bmatrix} \varepsilon'_m \\ \dots \\ 0 \end{Bmatrix} + \begin{Bmatrix} z' \varepsilon'_b \\ \dots \\ \varepsilon'_s \end{Bmatrix} \quad (3.50)$$

where:

$$\varepsilon'_m = \left[\frac{\partial u'_m}{\partial x'} \quad \frac{\partial v'_m}{\partial y'} \quad \frac{\partial u'_m}{\partial y'} + \frac{\partial v'_m}{\partial x'} \right]^T \quad (3.51a)$$

$$\varepsilon'_b = \left[\frac{\partial \theta_{y'}}{\partial x'} \quad -\frac{\partial \theta_{x'}}{\partial y'} \quad \left(\frac{\partial \theta_{y'}}{\partial y'} - \frac{\partial \theta_{x'}}{\partial x'} \right) \right]^T \quad (3.51b)$$

$$\varepsilon'_s = \left[\frac{\partial w'_b}{\partial x'} + \theta_{y'} \quad \frac{\partial w'_b}{\partial y'} - \theta_{x'} \right]^T \quad (3.51c)$$

However, for a thin shell the bending can be defined by the Kirchhoff theory, where the shearing strain (ε'_s) is neglected (≈ 0), which means, $-\frac{\partial w'_b}{\partial x'} = \theta_{y'}$ and $\frac{\partial w'_b}{\partial y'} = \theta_{x'}$, and the strain vector can be redefined as:

$$\{\varepsilon'\} = \begin{Bmatrix} \varepsilon_{x'} \\ \varepsilon_{y'} \\ \gamma_{x'y'} \end{Bmatrix} = \begin{Bmatrix} \varepsilon'_m \\ \varepsilon'_b \end{Bmatrix} + z' \begin{Bmatrix} \varepsilon'_b \end{Bmatrix} = \underbrace{\begin{bmatrix} 1 & 0 & 0 & z & 0 & 0 \\ 0 & 1 & 0 & 0 & z & 0 \\ 0 & 0 & 1 & 0 & 0 & z \end{bmatrix}}_{[A_t]} \underbrace{\begin{Bmatrix} \varepsilon'_m \\ \dots \\ \varepsilon'_b \end{Bmatrix}}_{\{\hat{\varepsilon}'\}} = [A_t] \{\hat{\varepsilon}'\} \quad (3.52)$$

where, ε'_m is the membrane strain at the middle plane of the shell, and ε'_b is the curvature of the shell due to bending at the middle plane of the shell which are defined as:

$$\varepsilon'_m = \left[\frac{\partial u'_m}{\partial x'} \quad \frac{\partial v'_m}{\partial y'} \quad \frac{\partial u'_m}{\partial y'} + \frac{\partial v'_m}{\partial x'} \right]^T \quad (3.53a)$$

$$\varepsilon'_b = \left[\frac{\partial \theta_{y'}}{\partial x'} \quad -\frac{\partial \theta_{x'}}{\partial y'} \quad \left(\frac{\partial \theta_{y'}}{\partial y'} - \frac{\partial \theta_{x'}}{\partial x'} \right) \right]^T = \left[-\frac{\partial^2 w'_b}{\partial x'^2} \quad -\frac{\partial^2 w'_b}{\partial y'^2} \quad -2 \frac{\partial^2 w'_b}{\partial x' \partial y'} \right]^T \quad (3.53b)$$

The stress vector ($\{\hat{\sigma}'\}$) for a thin shell element is defined as :

$$\{\hat{\sigma}'\} = \begin{Bmatrix} \hat{\sigma}'_m \\ \dots \\ \hat{\sigma}'_b \end{Bmatrix} = \begin{Bmatrix} n_{x'} \\ n_{y'} \\ n_{x'y'} \\ \dots \\ m_{x'} \\ m_{x'y'} \\ m_{x'y'} \end{Bmatrix} = \int_{-\frac{t}{2}}^{\frac{t}{2}} \begin{Bmatrix} \sigma_{x'} \\ \sigma_{y'} \\ \tau_{x'y'} \\ \dots \\ z' \sigma_{x'} \\ z' \sigma_{y'} \\ z' \tau_{x'y'} \end{Bmatrix} dz' = \int_{-\frac{t}{2}}^{\frac{t}{2}} [A_t]^T \begin{Bmatrix} \sigma_{x'} \\ \sigma_{y'} \\ \tau_{x'y'} \end{Bmatrix} dz' \quad (3.54)$$

with the sign convention as defined in the Fig. 3.9.

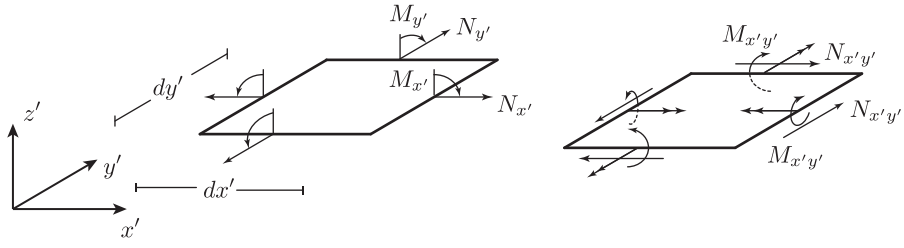


Figure 3.9: Sign Convention for local resulting of stress for the Shell Element

In addition, for the case of a layered section, the stress vector can be expressed in discrete manner using the expression applied by Zhang et al. [155] and Zhang et al. [156] in 2007, Fig. 3.10 to include concrete and steel layers over the thickness as:

$$n_{x'} = \int_{-\frac{t}{2}}^{\frac{t}{2}} \sigma'_x dz' = \sum_{i=1}^{N_c} \sigma_{x'_i}^c (z'_{i+1} - z'_i) + \sum_{j=1}^{N_s} \sigma_{x'_j}^s t_{s_j} \quad (3.55a)$$

$$n_{y'} = \int_{-\frac{t}{2}}^{\frac{t}{2}} \sigma'_y dz' = \sum_{i=1}^{N_c} \sigma_{y'_i}^c (z'_{i+1} - z'_i) + \sum_{j=1}^{N_s} \sigma_{y'_j}^s t_{s_j} \quad (3.55b)$$

$$n_{x'y'} = \int_{-\frac{t}{2}}^{\frac{t}{2}} \tau_{x'y'} dz' = \sum_{i=1}^{N_c} \tau_{x'y'_i}^c (z'_{i+1} - z'_i) + \sum_{j=1}^{N_s} \tau_{x'y'_j}^s t_{s_j} \quad (3.55c)$$

$$m_{x'} = \int_{-\frac{t}{2}}^{\frac{t}{2}} z' \sigma'_x dz' = \frac{1}{2} \sum_{i=1}^{N_c} \sigma_{x'_i}^c (z'_{i+1}^2 - z'_i^2) + \sum_{j=1}^{N_s} z'_j \sigma_{x'_j}^s t_{s_j} \quad (3.55d)$$

$$m_{y'} = \int_{-\frac{t}{2}}^{\frac{t}{2}} z' \sigma'_y dz' = \frac{1}{2} \sum_{i=1}^{N_c} \sigma_{y'_i}^c (z'_{i+1}^2 - z'_i^2) + \sum_{j=1}^{N_s} z'_j \sigma_{y'_j}^s t_{s_j} \quad (3.55e)$$

$$m_{x'y'} = \int_{-\frac{t}{2}}^{\frac{t}{2}} z' \tau_{x'y'} dz' = \frac{1}{2} \sum_{i=1}^{N_c} \tau_{x'y'_i}^c (z'_{i+1}^2 - z'_i^2) + \sum_{j=1}^{N_s} z'_j \tau_{x'y'_j}^s t_{s_j} \quad (3.55f)$$

where $\{\sigma_i^c\}$ is the in-plane stresses at i^{th} concrete layer, and $\{\sigma_j^s\}$ is the in-plane stresses at j^{th} steel layer, and z_{i+1} and z_i are the locations of the top and bottom part of i^{th} concrete layer, respectively, and z_j the middle position of the j^{th} steel layer. N_c and N_s

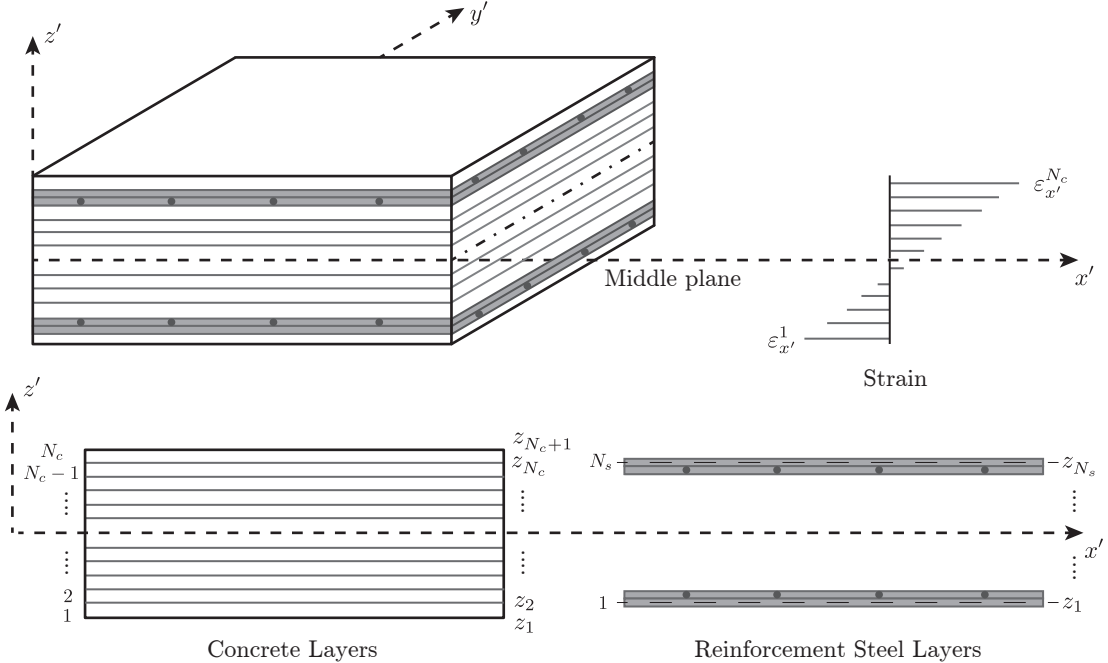


Figure 3.10: A typical rectangular layered shell section

are the number of layers of concrete and steel, respectively. In addition, t_{s_j} is the thickness of the section for the j^{th} steel layer.

A displacement interpolation over the element, for the membrane and bending, can be expressed as $\{u'\} = [\Psi(x', y')] \{U'\}$, where $[\Psi(x', y')]$ are the shape functions that define the interpolation for the membrane and bending and $\{U'\}$ are the displacements of the DOF at each node. The strain vector can be written as:

$$\{\hat{\varepsilon}'\} = \begin{Bmatrix} \varepsilon'_m \\ \dots \\ \varepsilon'_b \end{Bmatrix} = [B(x', y')] \{U'\} = \begin{Bmatrix} B_m(x', y') \\ \dots \\ B_b(x', y') \end{Bmatrix} \{U'\} \quad (3.56)$$

where $[B(x', y')]$ is the kinematic matrix that relates the strain and the displacement for the membrane ($[B_m(x', y')]$) and for the bending ($[B_b(x', y')]$).

Replacing everything back into the virtual work expression for the shell (Eq. 3.45), the following is obtained:

$$\{\delta U'\}^T \left(\underbrace{\int_V [\Psi]^T \{F_{body}\} dV + \int_A [\Psi]^T \{T\} dA + \int_S [\Psi]^T \{t_{edge}\} dS}_{F_{External}} - \underbrace{\int_A [B]^T \{\hat{\sigma}'\} dA}_{-R} \right) = 0 \quad (3.57)$$

where $F_{External}$ is the external force over the system, and R is the resistant internal force of the shell that is a function of the displacements at the nodes.

Now, implementing this in a nonlinear material implementation, e.g. using the Newton-Raphson method, it is necessary to determine two expressions, the tangent stiffness matrix and the resistant internal force of the shell at each iteration. The residual equation for the system at each iteration is obtained using virtual work.

$$Residual(U'^i) = F_{external} - R^i \quad (3.58)$$

Linearize the $Residual(U'^i + \Delta U'^i)$ using a taylor expansion, excluding higher order terms:

$$Residual(U'^i + \Delta U'^i) = Residual(U'^i) + \frac{\partial Residual(U'^i)}{\partial U'^i} \Delta U'^i \quad (3.59)$$

and performing the derivative over the *Residual* equation, this becomes:

$$\begin{aligned} \frac{\partial \text{Residual} (U'^i)}{\partial U'^i} &= -\frac{\partial}{\partial U'^i} \left(\int_A [B]^T \{\hat{\sigma}'\} dA \right) \\ &= - \int_A [B]^T \frac{\partial \{\hat{\sigma}'\}}{\partial \{U'^i\}} dA = - \int_A [B]^T \underbrace{\frac{\partial \{\hat{\sigma}'\}}{\partial \{\hat{\varepsilon}'\}}}_{[\hat{D}'_{tangent}]} [B] dA \end{aligned} \quad (3.60)$$

Using this, the stiffness tangent of the shell is defined as

$$K_t = \int_A [B]^T [\hat{D}'_{tangent}] [B] dA \quad (3.61)$$

where the section tangent matrix $[\hat{D}'_{tangent}]$, is defined as

$$\begin{aligned} [\hat{D}'_{tangent}] &= \int_{-\frac{t}{2}}^{\frac{t}{2}} [A_t]^T \frac{\partial \{\sigma'\}}{\partial \{\varepsilon'\}} [A_t] dz' \\ &= \int_{-\frac{t}{2}}^{\frac{t}{2}} \begin{bmatrix} [D'] & z' [D'] \\ z' [D'] & z'^2 [D'] \end{bmatrix} dz' = \begin{bmatrix} [\hat{D}'_m] & [\hat{D}'_{mb}] \\ [\hat{D}'_{mb}] & [\hat{D}'_b] \end{bmatrix} \end{aligned} \quad (3.62)$$

and $[D']$ is the plane stress material stiffness tangent, and $[\hat{D}'_m]$ is the stiffness tangent of the membrane portion, $[\hat{D}'_{mb}]$ is the stiffness tangent that relates the coupling between the membrane and bending, and $[\hat{D}'_b]$ is the stiffness tangent of the bending portion. In addition, $[\hat{D}'_{tangent}]$ can be formulated in discrete manner using the expression applied by

Zhang et al. [155] and Zhang et al. [156] in 2007, Fig. 3.10 to include concrete and steel layers over the thickness as:

$$[D'_m] = \int_{-\frac{t}{2}}^{\frac{t}{2}} [D'] dz' = \sum_{i=1}^{Nc} [D'_{ci}] (z'_{i+1} - z'_i) + \sum_{j=1}^{Ns} [D'_{sj}] t_{sj} \quad (3.63a)$$

$$[D'_b] = \int_{-\frac{t}{2}}^{\frac{t}{2}} z'^2 [D'] dz' = \frac{1}{3} \sum_{i=1}^{Nc} [D'_{ci}] (z'_{i+1}^3 - z_i^3) + \sum_{j=1}^{Ns} [D'_{sj}] t_{sj} z_j'^2 \quad (3.63b)$$

$$[D'_{mb}] = \int_{-\frac{t}{2}}^{\frac{t}{2}} z' [D'] dz' = \frac{1}{2} \sum_{i=1}^{Nc} [D'_{ci}] (z'_{i+1}^2 - z_i^2) + \sum_{j=1}^{Ns} [D'_{sj}] t_{sj} z'_j \quad (3.63c)$$

where the matrices $[D'_{ci}]$ and $[D'_{sj}]$ are the plane stress material tangent stiffness of the i^{th} concrete layer and j^{th} steel layer, respectively. Nc and Ns are the number of layers of concrete and steel, respectively, and z_{i+1} and z_i are the locations of the top and bottom part of the i^{th} layer, respectively. In addition, t_{sj} is the thickness of the section for the j^{th} steel layer.

Define the internal resisting force R for the shell, from Eq. 3.57 as:

$$R = \int_A [B]^T \{\hat{\sigma}'\} dA = \int_A [B]^T \left\{ \begin{array}{l} n_{x'} \\ n_{y'} \\ n_{x'y'} \\ \dots \\ m_{x'} \\ m_{x'y'} \\ m_{x'y'} \end{array} \right\} dA \quad (3.64)$$

where, the vector stress $\{\hat{\sigma}\}$ is defined by the Eq. 3.55.

Using the definition for the matrix tangent stiffness and the internal resisting force R , Eq. 3.59 is rewritten for the iteration procedure as:

$$K_t \Delta U'^i = F_{external} - R^i \quad (3.65)$$

The displacement interpolation for the membrane was already presented, the only missing piece in the formulation is the definition of the displacement interpolation and the Kinematic matrix ($[B_b(x', y')]$) for the bending behavior of the shell. Different theories can be used to define the bending behavior of a plate structure. The principal ones are Kirchhoff theory for thin plates, and the Mindlin-Reissner theory for moderately thick plates. In this dissertation only the Kirchhoff theory for thin plates will be presented.

The Kirchhoff thin plate theory is based on the following assumptions [128]:

- a. Straight lines normal to the midsurface remain straight after deformation.
- b. Straight lines normal to the mid-surface remain normal to the mid-surface after deformation.
- c. The thickness of the plate does not change during a deformation.

Different approaches have been used to define the field interpolation for the bending displacement. The direct one is the use of a polynomial representation. However, for the quadrilateral element with 12 DOF based on Kirchhoff theory an exact one cannot be found, because the polynomial representation is incomplete, and the slope at adjacent edges is discontinuous, but for rectangular elements the results are relatively good [128]. However, quadrilateral shapes do not work for all the cases. Some representations can

cause singularities in the stiffness matrix [11]. Hermitian interpolation are also used to represent the thin plate bending, but this representation lacks twist modes, and for this the convergence is not always guaranteed [128].

Other approaches use hybrid stress formulation, mixed formulation, or start from the Mindlin-Reissner theory and modify the element to satiesfied the Kirchhoff assumptions. One of the most successful and simple to implement is the so-called discrete Krichhoff technique, demostrated for quadrilateral element by Batoz and Tahar [11] in 1982. This element, known as the discrete Kirchhoff quadrilateral element (DKQ) , starts from an 8-node serendipity Mindlin-Reissner theory element and imposes that the Kirchhoff kinematical boundary conditions need to be satisfied at some points. This is done by explicitly coupling the rotation and vertical deformation by enforced zero transverse shear strain at certain locations, which produce a reduction to a 12 DOF element with four corner nodes [35]. This element gives excellent results for the analysis of thin plate elements and has been implemented in different FEM softwares.

In the next subsection, the theory used to formulated the displacement interpolation of the DKQ element will be presented.

3.2.1 Discrete Kirchhoff quadrilateral Element (DKQ) Interpolation

The DKQ was formulated by Batoz and Tahar [11], this formulation initially used independent interpolations for the deflection and the rotation out of plane in each direction, and afterwards introduces Kirchhoff hypothesis at discrete points over the edge of the element. This is done to relate the vertical displacements with the rotations. For the rotational DOF the 8-node serendipity isoparametric element [11] is used.

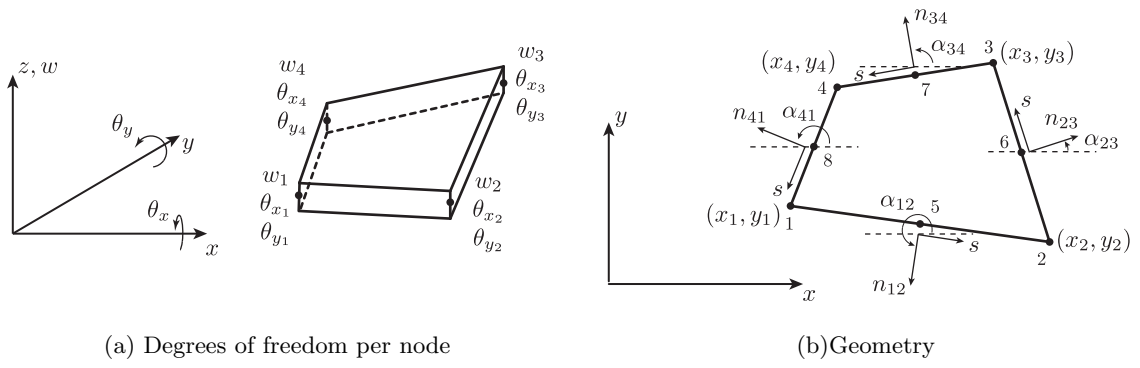


Figure 3.11: Discrete Kirchhoff Quadrilateral Element

The formulation presented here follows the formulation developed by Batoz and Tahar [11] in 1982. The rotational interpolation used is the 8-node serendipity element:

$$\beta_x(\xi, \eta) = \sum_{i=1}^8 \psi_i(\xi, \eta) \beta_{x_i} \quad (3.66)$$

$$\beta_y(\xi, \eta) = \sum_{i=1}^8 \psi_i(\xi, \eta) \beta_{y_i} \quad (3.67)$$

where:

$$\psi_i(\xi, \eta) = -\frac{1}{4} (1 + \xi_i \xi) (1 + \eta_i \eta) (1 - \xi_i \xi - \eta_i \eta) \quad i = 1, 2, 3, 4 \quad (3.68a)$$

$$\psi_k(\xi, \eta) = \frac{1}{2} (1 - \xi^2) (1 + \eta_k \eta) \quad k = 5, 7 \quad (3.68b)$$

$$\psi_k(\xi, \eta) = \frac{1}{2} (1 + \xi_k \xi) (1 - \eta^2) \quad k = 6, 8 \quad (3.68c)$$

and ξ_i and η_i are the natural coordinates of the nodes for the serendipity element.

The Kirchhoff assumptions are enforced at the nodes as follows:

a. at corner:

$$\begin{cases} \beta_{x_i} + \frac{\partial w}{\partial x}|_i \\ \beta_{y_i} + \frac{\partial w}{\partial y}|_i \end{cases} = \begin{cases} 0 \\ 0 \end{cases} \quad i = 1, 2, 3, 4 \quad (3.69)$$

b. at mid-nodes:

$$\beta_{s_k} + \frac{\partial w}{\partial s}\Big|_k = 0 \quad k = 5, 6, 7, 8 \quad (3.70)$$

It is assumed that the transversal displacement w along the edge is represented by a cubic interpolation ($w(s) = a_0 + a_1s + a_2s^2 + a_3s^3$) where the boundary conditions at the ends are the displacements, and its derivative with respect to s (rotations) are evaluated at the ends of the edges. Now, evaluating the variation of $w(s)$ with respect to s at the middle point of the edge, $s_k = \frac{L_{ij}}{2}$, where L_{ij} is defined in Eq. 3.73, is obtained:

$$\frac{\partial w}{\partial s}\Big|_k = -\frac{3}{2L_{ij}}(w_i - w_j) - \frac{1}{4} \left(\frac{\partial w}{\partial s}\Big|_i + \frac{\partial w}{\partial s}\Big|_j \right) \quad (3.71)$$

where $k = 5, 6, 7, 8$ with the relation for (k, i, j) as $(5, 1, 2), (6, 2, 3), (7, 3, 4), (8, 4, 1)$. And if it is assumed that the normal rotation to the edge is linear:

$$\beta_{n_k} = \frac{1}{2}(\beta_{n_i} + \beta_{n_j}) = -\frac{1}{2} \left(\frac{\partial w}{\partial n}\Big|_i + \frac{\partial w}{\partial n}\Big|_j \right) \quad (3.72)$$

where $k = 5, 6, 7, 8$ with the relation (k, i, j) as $(5, 1, 2), (6, 2, 3), (7, 3, 4), (8, 4, 1)$

A characteristic of this element is that no displacement interpolation is defined inside of the element [11]. Using the past assumptions it is indicated that the Kirchhoff hypotheses are satisfied over the entire boundary of the element, the transverse shear energy is neglected, and finally convergence to the theory of thin plates is retrieved.

Now, the following relations are needed to finish the transformation:

$$L_{ij} = \sqrt{x_{ij}^2 + y_{ij}^2} \quad (3.73a)$$

$$x_{ij} = x_i - x_j \quad \sin(\alpha_{ij}) = \frac{x_{ij}}{L_{ij}} \quad (3.73b)$$

$$y_{ij} = y_i - y_j \quad \cos(\alpha_{ij}) = -\frac{y_{ij}}{L_{ij}} \quad (3.73c)$$

$$\begin{Bmatrix} \beta_x \\ \beta_y \end{Bmatrix} = \begin{bmatrix} \cos(\alpha) & -\sin(\alpha) \\ \sin(\alpha) & \cos(\alpha) \end{bmatrix} \begin{Bmatrix} \beta_n \\ \beta_s \end{Bmatrix} \quad (3.74)$$

and using $\frac{\partial w}{\partial x}\Big|_i = -\theta_{yi}$ and $\frac{\partial w}{\partial y}\Big|_i = \theta_{xi}$, see Fig. 3.11, the following relation is obtained:

$$\begin{Bmatrix} \frac{\partial w}{\partial s} \\ \frac{\partial w}{\partial n} \end{Bmatrix} = \begin{bmatrix} \cos(\alpha) & \sin(\alpha) \\ \sin(\alpha) & -\cos(\alpha) \end{bmatrix} \begin{Bmatrix} \theta_x \\ \theta_y \end{Bmatrix} \quad (3.75)$$

Now, it is possible to construct the transformation from the 16-DOF to the 12-DOF plate element. The initial interpolation of β_x and β_y are:

$$\beta_x(\xi, \eta) = \sum_{i=1}^8 \psi_i(\xi, \eta) \beta_{x_i} = - \sum_{i=1}^4 \psi_i(\xi, \eta) \frac{\partial w}{\partial x}\Big|_i + \sum_{k=5}^8 \psi_k(\xi, \eta) \beta_{x_k} \quad (3.76)$$

$$\beta_y(\xi, \eta) = \sum_{i=1}^8 \psi_i(\xi, \eta) \beta_{y_i} = - \sum_{i=1}^4 \psi_i(\xi, \eta) \frac{\partial w}{\partial y} \Big|_i + \sum_{k=5}^8 \psi_k(\xi, \eta) \beta_{y_k} \quad (3.77)$$

using the Eq. 3.74 and Eq. 3.70 into Eq. 3.76 and Eq. 3.77:

$$\begin{aligned} \beta_x(\xi, \eta) &= - \sum_{i=1}^4 \psi_i(\xi, \eta) \frac{\partial w}{\partial x} \Big|_i + \sum_{k=5}^8 \psi_k(\xi, \eta) \left(\cos(\alpha_{ij}) \beta_{n_k} - \sin(\alpha_{ij}) \beta_{s_k} \right) \\ &= - \sum_{i=1}^4 \psi_i(\xi, \eta) \frac{\partial w}{\partial x} \Big|_i + \sum_{k=5}^8 \psi_k(\xi, \eta) \left(\cos(\alpha_{ij}) \beta_{n_k} + \sin(\alpha_{ij}) \frac{\partial w}{\partial s} \Big|_k \right) \end{aligned} \quad (3.78)$$

$$\begin{aligned} \beta_y(\xi, \eta) &= - \sum_{i=1}^4 \psi_i(\xi, \eta) \frac{\partial w}{\partial y} \Big|_i + \sum_{k=5}^8 \psi_k(\xi, \eta) \left(\sin(\alpha_{ij}) \beta_{n_k} + \cos(\alpha_{ij}) \beta_{s_k} \right) \\ &= - \sum_{i=1}^4 \psi_i(\xi, \eta) \frac{\partial w}{\partial y} \Big|_i + \sum_{k=5}^8 \psi_k(\xi, \eta) \left(\sin(\alpha_{ij}) \beta_{n_k} - \cos(\alpha_{ij}) \frac{\partial w}{\partial s} \Big|_k \right) \end{aligned} \quad (3.79)$$

and replacing Eq. 3.71 and Eq. 3.72 into Eq. 3.78 and Eq. 3.79:

$$\begin{aligned} \beta_x(\xi, \eta) &= - \sum_{i=1}^4 \psi_i(\xi, \eta) \frac{\partial w}{\partial x} \Big|_i - \frac{1}{2} \sum_{k=5}^8 \psi_k(\xi, \eta) \cos(\alpha_{ij}) \left(\frac{\partial w}{\partial n} \Big|_i + \frac{\partial w}{\partial n} \Big|_j \right) \\ &\quad - \sum_{k=5}^8 \psi_k(\xi, \eta) \sin(\alpha_{ij}) \left(\frac{3}{2L_{ij}} (w_i - w_j) + \frac{1}{4} \left(\frac{\partial w}{\partial s} \Big|_i + \frac{\partial w}{\partial s} \Big|_j \right) \right) \end{aligned} \quad (3.80)$$

$$\begin{aligned} \beta_y(\xi, \eta) &= - \sum_{i=1}^4 \psi_i(\xi, \eta) \frac{\partial w}{\partial y} \Big|_i - \frac{1}{2} \sum_{k=5}^8 \psi_k(\xi, \eta) \sin(\alpha_{ij}) \left(\frac{\partial w}{\partial n} \Big|_i + \frac{\partial w}{\partial n} \Big|_j \right) \\ &\quad + \sum_{k=5}^8 \psi_k(\xi, \eta) \cos(\alpha_{ij}) \left(\frac{3}{2L_{ij}} (w_i - w_j) + \frac{1}{4} \left(\frac{\partial w}{\partial s} \Big|_i + \frac{\partial w}{\partial s} \Big|_j \right) \right) \end{aligned} \quad (3.81)$$

And using the Eq. 3.75 and the relation $\frac{\partial w}{\partial x}\Big|_i = -\theta_{y_i}$ and $\frac{\partial w}{\partial y}\Big|_i = \theta_{x_i}$, ones obtains:

$$\begin{aligned} \beta_x(\xi, \eta) &= \sum_{i=1}^4 \psi_i(\xi, \eta) \theta_{y_i} - \frac{1}{2} \sum_{k=5}^8 \psi_k(\xi, \eta) \cos(\alpha_{ij}) \left(\sin(\alpha_{ij}) \theta_{x_i} - \cos(\alpha_{ij}) \theta_{y_i} \right. \\ &\quad \left. + \sin(\alpha_{ij}) \theta_{x_j} - \cos(\alpha_{ij}) \theta_{y_j} \right) - \sum_{k=5}^8 \psi_k(\xi, \eta) \sin(\alpha_{ij}) \left(\left(\frac{3}{2L_{ij}} (w_i - w_j) \right) \right. \\ &\quad \left. + \frac{1}{4} (\cos(\alpha_{ij}) \theta_{x_i} + \sin(\alpha_{ij}) \theta_{y_i} + \cos(\alpha_{ij}) \theta_{x_j} + \sin(\alpha_{ij}) \theta_{y_j}) \right) \end{aligned} \quad (3.82)$$

$$\begin{aligned} \beta_y(\xi, \eta) &= - \sum_{i=1}^4 \psi_i(\xi, \eta) \theta_{x_i} - \frac{1}{2} \sum_{k=5}^8 \psi_k(\xi, \eta) \sin(\alpha_{ij}) \left(\sin(\alpha_{ij}) \theta_{x_i} - \cos(\alpha_{ij}) \theta_{y_i} \right. \\ &\quad \left. + \sin(\alpha_{ij}) \theta_{x_j} - \cos(\alpha_{ij}) \theta_{y_j} \right) + \sum_{k=5}^8 \psi_k(\xi, \eta) \cos(\alpha_{ij}) \left(\left(\frac{3}{2L_{ij}} (w_i - w_j) \right) \right. \\ &\quad \left. + \frac{1}{4} (\cos(\alpha_{ij}) \theta_{x_i} + \sin(\alpha_{ij}) \theta_{y_i} + \cos(\alpha_{ij}) \theta_{x_j} + \sin(\alpha_{ij}) \theta_{y_j}) \right) \end{aligned} \quad (3.83)$$

Introducing the definition from Eq. 3.73, and reordering the parameters, the equations for β_x and β_y can be rewritten as:

$$\begin{aligned} \beta_x(\xi, \eta) &= \sum_{i=1}^4 \psi_i(\xi, \eta) \theta_{y_i} \\ &\quad + \sum_{k=5}^8 \psi_k(\xi, \eta) \left(a_k \frac{3}{2} (w_i - w_j) + b_k (\theta_{x_i} + \theta_{x_j}) - c_k (\theta_{y_i} + \theta_{y_j}) \right) \end{aligned} \quad (3.84)$$

$$\begin{aligned} \beta_y(\xi, \eta) &= - \sum_{i=1}^4 \psi_i(\xi, \eta) \theta_{x_i} \\ &\quad + \sum_{k=5}^8 \psi_k(\xi, \eta) \left(d_k \frac{3}{2} (w_i - w_j) + e_k (\theta_{x_i} + \theta_{x_j}) - b_k (\theta_{y_i} + \theta_{y_j}) \right) \end{aligned} \quad (3.85)$$

where

$$a_k = -\frac{x_{ij}}{L_{ij}^2} \quad (3.86a)$$

$$b_k = \frac{3}{4} \frac{x_{ij}y_{ij}}{L_{ij}^2} \quad (3.86b)$$

$$c_k = \frac{\left(\frac{1}{4}x_{ij}^2 - \frac{1}{2}y_{ij}^2\right)}{L_{ij}^2} \quad (3.86c)$$

$$d_k = -\frac{y_{ij}}{L_{ij}^2} \quad (3.86d)$$

$$e_k = \frac{\left(-\frac{1}{2}x_{ij}^2 + \frac{1}{4}y_{ij}^2\right)}{L_{ij}^2} \quad (3.86e)$$

and $k = 5, 6, 7, 8$ with the relation (k, i, j) as $(5, 1, 2), (6, 2, 3), (7, 3, 4), (8, 4, 1)$

This established the following relation in terms of the 3 DOF per node:

$$\beta_x(\xi, \eta) = [\Psi^x(\xi, \eta)] \{U\} \quad (3.87)$$

$$\beta_y(\xi, \eta) = [\Psi^y(\xi, \eta)] \{U\} \quad (3.88)$$

where:

$$\{U\} = \begin{Bmatrix} w_1 & \theta_{x_1} & \theta_{y_1} & \dots & w_4 & \theta_{x_4} & \theta_{y_4} \end{Bmatrix}^T \quad (3.89)$$

and

$$[\Psi^x(\xi, \eta)] = \begin{bmatrix} \Psi_1^x(\xi, \eta) & \dots & \Psi_{12}^x(\xi, \eta) \end{bmatrix} \quad (3.90)$$

$$[\Psi^y(\xi, \eta)] = \begin{bmatrix} \Psi_1^y(\xi, \eta) & \dots & \Psi_{12}^y(\xi, \eta) \end{bmatrix} \quad (3.91)$$

These are defined as:

$$\Psi_{3(i-1)+1}^x(\xi, \eta) = \frac{3}{2} (a_r \psi_r(\xi, \eta) - a_s \psi_s(\xi, \eta)) \quad (3.92a)$$

$$\Psi_{3(i-1)+2}^x(\xi, \eta) = b_r \psi_r(\xi, \eta) + b_s \psi_s(\xi, \eta) \quad (3.92b)$$

$$\Psi_{3(i-1)+3}^x(\xi, \eta) = \psi_i(\xi, \eta) - c_r \psi_r(\xi, \eta) - c_s \psi_s(\xi, \eta) \quad (3.92c)$$

$$\Psi_{3(i-1)+1}^y(\xi, \eta) = \frac{3}{2} (d_r \psi_r(\xi, \eta) - d_s \psi_s(\xi, \eta)) \quad (3.92d)$$

$$\Psi_{3(i-1)+2}^y(\xi, \eta) = -\psi_i(\xi, \eta) + e_r \psi_r(\xi, \eta) + e_s \psi_s(\xi, \eta) \quad (3.92e)$$

$$\Psi_{3(i-1)+3}^y(\xi, \eta) = -b_r \psi_r(\xi, \eta) - b_s \psi_s(\xi, \eta) \quad (3.92f)$$

and $i = 1, 2, 3, 4$ with the relation (i, r, s) as $(1, 5, 8), (2, 6, 5), (3, 7, 6), (4, 8, 7)$.

Using the relation established in Eq. 3.87 and Eq. 3.88, the relation of curvature of the plate and the displacements at the nodes can be determinate as:

$$\{\varepsilon_b\} = \begin{Bmatrix} \frac{\partial \theta_y}{\partial x} \\ -\frac{\partial \theta_x}{\partial y} \\ \left(\frac{\partial \theta_y}{\partial y} - \frac{\partial \theta_x}{\partial x} \right) \end{Bmatrix} = \begin{Bmatrix} \frac{\partial \beta_x}{\partial x} \\ \frac{\partial \beta_y}{\partial y} \\ \left(\frac{\partial \beta_x}{\partial y} + \frac{\partial \beta_y}{\partial x} \right) \end{Bmatrix} = \underbrace{\begin{bmatrix} 1 & 0 & 0 & 0 \\ 0 & 0 & 0 & 1 \\ 0 & 1 & 1 & 0 \end{bmatrix}}_{[A]} \begin{Bmatrix} \frac{\partial \beta_x}{\partial x} \\ \frac{\partial \beta_x}{\partial y} \\ \frac{\partial \beta_y}{\partial x} \\ \frac{\partial \beta_y}{\partial y} \end{Bmatrix} = [B_b(x, y)] \{U\} \quad (3.93)$$

where the matrix $[B_b]$, is the Kinematic matrix used in the Eq. 3.56, and this matrix can be defined as Eq. 3.94 using the inverse of the Jacobian that defines the transformation from the natural coordinate system where the serendipity element is defined and the local coordinate system of the element, like the Jacobian defined in Eq. 3.69:

$$[B_b] = [A] \begin{bmatrix} [J]^{-1} & [0] \\ [0] & [J]^{-1} \end{bmatrix} \begin{Bmatrix} \frac{\partial \beta_x}{\partial \xi} \\ \frac{\partial \beta_x}{\partial \eta} \\ \frac{\partial \beta_y}{\partial \xi} \\ \frac{\partial \beta_y}{\partial \eta} \end{Bmatrix} = \begin{bmatrix} 1 & 0 & 0 & 0 \\ 0 & 0 & 0 & 1 \\ 0 & 1 & 1 & 0 \end{bmatrix} \begin{bmatrix} [J]^{-1} & [0] \\ [0] & [J]^{-1} \end{bmatrix} \begin{Bmatrix} \frac{\partial \Psi_i^x}{\partial \xi} \\ \frac{\partial \Psi_i^x}{\partial \eta} \\ \frac{\partial \Psi_i^y}{\partial \xi} \\ \frac{\partial \Psi_i^y}{\partial \eta} \end{Bmatrix} \quad (3.94)$$

3.3 Summary

The FEM has been used extensively in the analysis of wall type reinforced concrete structures, including curved structures and slabs and shear panels (e.g Cervera et al [26] 1987, Polak et al. [115] 1993, Loo et al. 1997 [81], Ayoub et al. [7] in 1998 , Kim et al. [73] 2005 ,Zhang et al 2007 [155],Zhang et al 2007 [156]). However, the use of shell elements for the complete modeling of complex structures for the analysis of their nonlinear response has been ignored, due to the computational cost and also because the interaction of different interconnections inside of the structure has been neglected. But with the computational capabilities available today it is interesting to try to use these more robust elements to study the behavior of wall structures that can be modeled with shell elements for 3D or membrane elements that consider a rotational DOF at each node, known as drilling DOF, for 2D structures.

In this chapter, the extension of the 4-node membrane element with drilling degrees of freedom proposed by Xia et al. [151] to be used in a general nonlinear finite element framework with a natural coordinate system was reviewed, described and developed. Also described was the DKQ element formulated by Batoz and Tahar [11], to model plate bending elements. These two elements were combined to present the theoretical framework

to develop the formulation for a thin flat quadrilateral layered shell element with 24 DOF (6 DOF per node) which will be used to model the response of structural walls using the finite element method. These selected element models balance accuracy, simplicity and computational cost.

Chapter 4

Material Constitutive Models

Extensive research has been done to capture the behavior of concrete, and the steel bars inside of the concrete. The main characteristic of concrete is the formation of cracks, when it experiences difference states of stress. This characteristic makes it difficult to develop rational constitutive material models, since the cracks produce new stress-free surfaces or complex interlocking effects, which cause redistribution of stresses and changes in the stiffness of the material [118]. In addition, the nonlinear behavior of the concrete is dependent on the stress (tension or compression) in the direction of action, and also on the stresses in different directions (multi-axial effect). The response is also modified due to the degradation and deterioration of stiffness for the unloading and reloading in cyclic loadings. However, the concrete model in the plane stress state has to be able to at least include tension stiffening (residual average tension stress in the concrete post cracking), softening (reduction of the compression resistance of the concrete in one direction due to the tension strain in the perpendicular direction) [90], hysteretic behavior, enhancement due to biaxial compression, enhancement due to confinement (increasing of the concrete compression resistant due to confinement of the concrete with stirrups, cross ties and

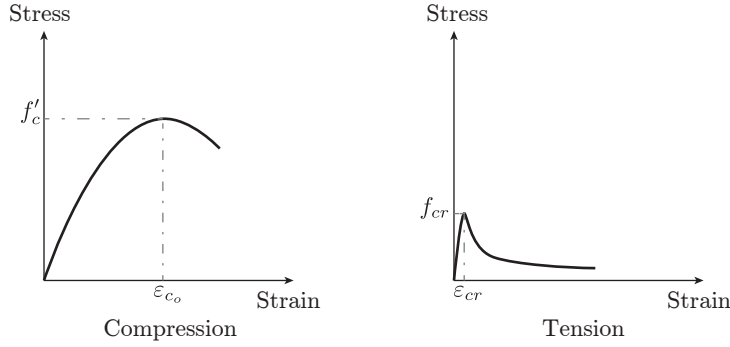


Figure 4.1: Uniaxial behavior of concrete

hoops), and degradation of the concrete (reduction of the compression resistance of the concrete under cyclic or reversal loads), which are key features that has been extensively research and mention in the literature, like in Vecchio and Collins [140] in 1986, Mander et al. [85] in 1986, Park [113] in 1994, Chen [29] in 2007 , Mansour and Hsu [87] in 2005, Powanusorn [118] in 2003.

Commonly, two different approaches can be taken to model concrete. One is a discrete crack approach in which every time that a crack in the analysis is formed, the model is updated at the crack. For example, in the finite element method a disassociation between the element where the crack appears is used to describe the crack. Although the discrete approach is more realistic, it is more complex and difficult to implement for the reason that an adaptive mesh must be considered, and a complex model needs to be considered to take into account the interlock at the cracks, and the other effects that happen at the cracks [118]. The other approach is the smeared crack approach which is based on the assumption that different cracks and variation of stress due to the crack over an area, can be modeled using the average stress-strain relation of concrete in that zone, and when a crack occurs the properties of the smeared material are modified to account for it, see

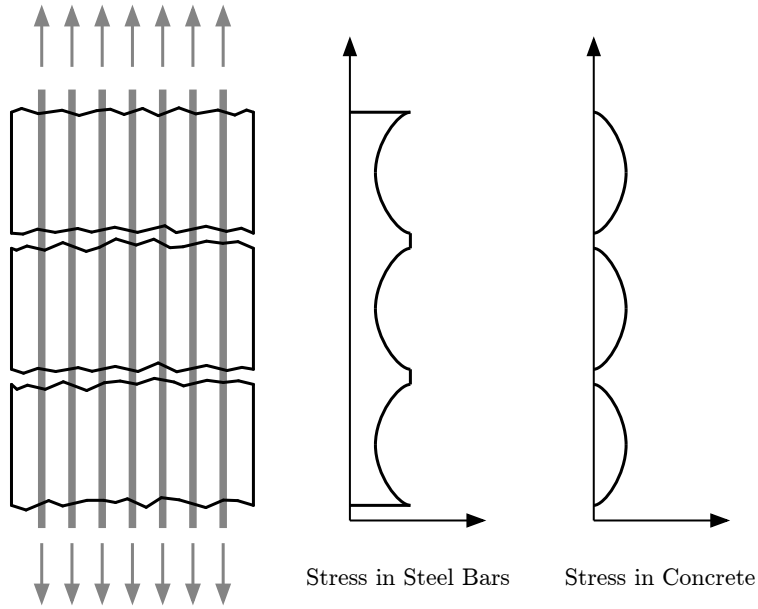


Figure 4.2: Variation of the stress in the Concrete and Steel bars between cracks

Fig. 4.2. The smeared approach is the current standard, because it is robust and efficiently captures the complex behavior of the concrete under different loadings.

In the case of reinforcing steel, a discrete and smeared approach can also be used. In the discrete approach the steel bars are modeled as linear element (truss members), that work only in the direction of the line element. However, this type of model in some cases produces a complex mesh in order to connect the elements that represent the concrete and the bar elements, and it also, needs some complex laws at the connection nodes to be able to model bond-slipage. In addition, the variations of stress over the bar that are produced in the bars embedded in the concrete are difficult to model. Instead, the smeared approach is based on the assumption that the steel bars are considered as a layer of homogenous material at certain positions inside the reinforced concrete element and the variation of stresses due to the crack over an area can be modeled using the average

stress-strain of steel in that zone, see Fig. 4.2. Commonly it is considered that the smeared steel works only in the direction of the bars, since the bars are typically in a uniaxial state of stress, and this allows the use of a uniaxial elasto-plastic constitutive model, including Bauschinger effects. However, other more complex models may be proposed for the steel to capture the degradation, the bond-slipage phenomenon that happens between the concrete and the steel, and the buckling of the longitudinal steel bars. This typically has been done by the use of factors or modification and inclusion of complex rules to the equations that define the steel model and account for the change of the response (Kunnath et al. [74]).

In this chapter, the different smeared constitutive models used for concrete are reviewed, and in particular the orthotropic models. Also, the smeared concrete model, which is used to represent the material law at each layer in the section on the elements for this study, is presented. In addition, the smeared steel model used to represent the behavior of the reinforcing steel embedded in concrete is reviewed.

4.1 Constitutive Model for Concrete

4.1.1 Review of Literature

The smeared models are very attractive because they allow the representation of the overall stiffness and strength characteristic of the cracked concrete without dealing directly with the principal difficulty of discrete concrete models such as crack width and crack spacing, since they use an average stress and strain representation [157]. The smeared concrete model can be classified depending on the hypothesis used to create the model. The

most common are the microplane model, non-local model, plasticity model, continuum damage model, endochronic model, nonlinear elastic model, and orthotropic model [118]. However, the plasticity and orthotropic models are the most commonly used and with more variations that have been developed by researchers. These different models were summarized by Powanusorn [118] in 2003. Also, in 1987, Willam et al. [149] provided a review of the issues of the smeared crack models, and analyses of the rotating crack, fixed crack and plasticity models. An overview of the models reviewed by Powanusorn [118] in 2003 is presented with additional information found in the literature.

The microplane model was developed by Bazant and Oh [13] in 1985. This model is based on the assumption that the material properties are represented by the relation of the components of stress and strain on planes of different orientation which represent the microstructure of the material. This relation is derived using the principle of virtual work to express that the stress at a particular point in the element is calculated as the volume average of traction vectors on all the microplanes [14]. After this first approach, Bazant et al. [14] in 1996, Bazant et al. [15] in 2000, and Bazant and Caner [12] in 2005 have been refining the model to be able to incorporate the cyclic behavior, softening and other key features of the concrete.

The nonlocal models are based on the assumption that the behavior of the strain-stress state at a point is not limited to the history of that point. This means, to represent the behavior of a point it is necessary to know the conditions of other points around the position of study. This approach is used because concrete are heterogeneous material, with complex interrelation between the different elements that conform to the microstructure of the concrete [118].

The plasticity models are typically based on plasticity theory, which tries to determine the response of the material by dividing the deformation into two parts, an elastic part and a plastic part. The behavior of the material is defined by a yield criterion, that is defined when a material starts to have plastic deformation, and a flow condition or plastic potential surface that defines the increment in plastic strain. This potential surface or flow rule can be associative or non-associative. The yield criteria used to represent concrete are the Mohr-Column, Drucker-Prager, Prandtl-Ruess (J2) and Willam-Warnke [29]. This type of material representation is typically used to model metal and soil. A thorough review of this type of model for concrete was done by Chen [29] in 1992 and republished in 2007. Some more new plasticity plastic-damage models to represent concrete directly are the work of Lee and Fenves [79] in 2001, that developed a plastic-damage model using the spectral decomposition form of the stress in a return-mapping formulation, and the model was compared against experimental data from a beam with an initial notch. Also, another new plasticity model is the plastic-damage model proposed by Cicekli et al. [31] in 2007, that used an anisotropic damage with two damage criteria (one for compression and one for tension) and a plasticity yield criterion. The model of Cicekli et al. [31] in 2007 also takes into consideration the recovery of stiffness by the opening and closing of cracks, and it was implemented in ABAQUS [51] using the user subroutine UMAT. The model returns good agreement with tests on plain concrete for uniaxial tests done by Karsan and Jirsa [67] in 1969 and biaxial tension and compression tests done by Kupfer et al. [75] in 1969. Also, other work was done by Wolf [150] in 2008 that proposed a plasticity model to directly take into account the effect of confinement in the concrete. This type of model is used to represent any type of loading case, but its drawbacks are: very computationally

costly, complex to implement, and generally requires a large number of constants. These constants need to be found from experimental data.

The nonlinear elastic material models are more simple and direct to use, because they try to represent the material behavior with elastic models. Two representations of this material are typically used: the hypoelastic and the hyperelastic material [29]. For the hyperelastic material, the representation is done in the total stress-strain relation proposed by Evans and Pister [42] in 1966. Instead, the hypoelastic model can be described in terms of the incremented strain-stress relation proposed by Truesdell [134] in 1955. This type of model is typically used to model only the static loading case.

The orthotropic concrete material models are based on the assumption made by Darwin and Pecknold [40] in 1974 and Darwin and Pecknold [39] in 1977. This assumption is that the behavior of the material in biaxial stress can be represented by an equivalent uniaxial strain-stress relation at the principal axis of orthotropy. Since then, many researchers have expanded and refined this model, and the equivalent uniaxial strain-stress relations to better represent the behavior of concrete and its key characteristics. In addition, it has been expanded to developed 3D representations of concrete material models, like the work done by Vecchio and Selby [142] in 1991.

4.1.1.1 Orthotropic Model for Concrete

Since Darwin and Pecknold [40] in 1974 and [39] 1977, many researchers have been using the assumption that the biaxial stress can be represented by an equivalent uniaxial strain-stress relation at the principal axis of orthotropy to represent the behavior of concrete. In this type of model, a subclassification between rotating angle or fixed angle models can

be defined. In the rotating angle model, the orthotropic direction of the material always follows the direction of the principal axis of stress or strain. This approach, which gives good results, has the problem that the contribution of concrete at the crack can not be predicted [157]. In the fixed angle, the axes of orthotropy follows the principal axis of stress until the first crack is formed, and at that moment the angle of the orthotropic direction is fixed. This method has the disadvantage that an empirical equation needs to be used to represent the concrete contribution (shear contribution " Vc ") at the crack angle. This type of model sometimes tends to overestimate the experimental data ([7, 36]).

The modeling of reinforced concrete material in biaxial stress using the orthotropic model has been in constant development. However, two different researcher groups, the group from the University of Toronto and the group from the University of Houston, have been constantly conducting analytical and experimental studies to develop the reinforced concrete constitutive models [118].

The models from the group at the University of Toronto are based on the smeared crack approach. The first attempt was done by Collins [32] in 1978, and Vecchio and Collins [139] in 1982, developing the Compression Field Theory (CFT), to represent monotonic loading. This model used the following assumptions:

- The principal directions of stress and strain are equal.
- The tension in the concrete after cracking can be neglected.
- The stress-strain relation can be represented by average stress-strain.
- The constitutive model for concrete in compression can be represented with a uniaxial model.

- Steel is considered as smeared and only acts in its orientation. The constitutive model used for steel was a perfectly elastic-plastic material (Bilinear).
- The Poisson ratio is neglected after cracking.

This model gave reasonably good results predicting the failure load, but it can not represent the shear stiffness of the experiment, and the deformation was overestimated. In 1986, Vecchio and Collins [140], after a large amount of experiment, refined the CFT and produced the Modified Compression Field Theory (MCFT). This modification was done by the incorporation of the tension behavior of the concrete after cracking, and the addition of a parameter to account for softening when concrete is submitted to compression-tension stresses in the principal axes of stress. In addition, a check for the crack is introduced, which uses an estimation of the crack width to predict the shear at the crack and verifies that the stress in the steel at the crack surface is not larger than the capacity of the bar passing the crack. In 1990, Vecchio [135] implemented the MCFT in a FEM code using a secant stiffness matrix approach. This modified model was able to predict the experimental data in an accurate manner. In 1991, Vecchio and Selby [142] extended the MCFT to a 3D representation of concrete and also changed the steel representation for a trilinear stress-strain relationship.

Vecchio [136] in 1992 suggested an additional modification to the (MCFT). In this refined model, a factor was introduced to account for the increase of the peak capacity of concrete for a state of biaxial compression load. Also, for this case the Poisson ratio was not neglected and a residual Poisson ratio was determinate. In 1993, Polak and Vecchio [115] extended the model to be used in shell elements with shear deformation. However,

the Poisson ratio was considered to be zero after cracking of the concrete, and a trilinear relation of stress-strain was used for this model.

In 2000 ([137]) and 2001 ([138]), Vecchio developed the Disturbed Stress Field Model (DSFM), which is a combination of a rotation crack and a fixed-crack model. This model is an extension of the MCFT [140], which differs from the MCFT in that the angle of the principal axis is rotated and the principal axis of strain and stress no longer coincide. For this reason improved treatment of the shear at the crack surface was used. The reason for this new model was to improve the modeling of panels with low shear reinforcing steel, or panels that have different amounts of reinforcing steel in each direction. This model was checked against the results of a series of RC panels testing in the University of Toronto and deep beams. Good agreement with the results were obtained. Typically no more than 10° of difference between the principal axis of stress and strain were obtained for the different cases of study.

Palermo [105] in 2002 and Palermo and Vecchio [106] 2003, and Palermo and Vecchio [107] 2004, expanded the MCFT to be used in cyclic loading cases. The element was based on the assumptions of the MCFT, and the DSFM which can be extended using the same method. The new model incorporated reloading and unloading curves, degradation in the reloading curve, and improvement in the plastic offset. Also, a Ramberg-Osgood formulation was included to describe the steel stress-strain behavior. This formulation also used a secant approach for the implementation. This new model was compared against experimental data done on squat walls, and slender walls, and showed good agreement with the experimental data. In 2007, Aquino and Erdem [5] implemented the MCFT using

a tangent stiffness approach, but tested the model only against a shear panel, under static load cases.

The group from the University of Houston, also has been developing concrete models based on the smeared crack approach. Their models are commonly based on the experimental data obtained from the experiments carried out in the universal panel tester, which is located at the University of Houston. The conceptual model proposed by Hsu [53] in 1988, is the first attempt done in the University of Houston. This model was based on the same equilibrium equations and compatibility equations as the CFT. The conceptual model was used to analyze elements subjected to torsion and shear. The first official constitutive model was the Rotating-Angle, Softened Truss Model (RA-STM) ([17, 55, 110]). This model used the following assumptions:

- The principal directions of stress and strain are equal.
- The tension in the concrete after cracking is taken into account.
- The stress-strain relation can be represented by average stress-strain.
- The constitutive model for concrete in compression can be represented with a uniaxial model with the two principal strain components.
- Steel was consider also smeared and only acts in its orientation. The constitutive model of the steel was based on the averaged stress-strain relation of steel bars embedded in concrete.
- The Poisson ratio is neglected after cracking.

With these assumptions, this model was able to correctly use the equilibrium and compatibility equations based on continuous materials. The use of a new average stress-strain relation for steel was introduced because in the experimental data done by Tamai et al. [130] in 1988, it was observed that the behavior of reinforcing steel inside the concrete presented some different behavior compared to bare steel. This was corroborated later by Belarbi and Hsu [17] in 1995. This RA-STM showed good agreement with the experimental data done in the universal panel tester.

In 1996, Pang and Hsu [111], and in 1997, Hsu and Zhang [57] developed the Fixed-Angle Softened Truss Model (FA-STM). This model emerged from the concern that the rotating-angle model did not represent the shear contribution of the concrete on the orientation of the crack. Inclusion of this effect requires that a fixed angle needed to be used, because after a crack is formed the principal axis of stresses needs to be maintained fixed. Representation of the shear contribution of concrete at the crack orientation requires a complex relation. In this model the constitutive relationship of concrete is represented in terms of the principal direction of stress over the element. The equilibrium and compatibility equations are then used to iterate until convergence is found. In 2001, Zhu et al. [160] extended the FA-STM by simply incorporating a rational derivation of the shear modulus that simplified the equation proposed previously. The new model was implemented by Wang and Hsu [146] in 2001, and the result of this model agreed well with the experimental results of beams, framed shear walls and panels. In addition, FA-STM assumes that the crack is oriented perpendicular to the principal direction of tensile stress in the element [157].

The RA-STM and the FA-STM represented correctly the peak behavior of the elements considered. However, these models were not able to represent the post-peak behavior of the element, because the Poisson effect was ignored after cracking of the concrete [157]. To study the effect of Poisson Ratio on the two principal normal directions, a series of 12 panels were tested. This study showed that the Poisson effect can be represented by two Hsu/Zhu ratios defined as “the Poisson ratios of cracked reinforced concrete based on the smeared crack concept,” this mean, the Hsu/Zhu ratios are the Poisson ratios of concrete after cracking. These ratios were expressed as $\nu_{12} = 0.2 + 850\varepsilon_{sf}$ if $\varepsilon_{sf} \leq 0.002$ and 1.9 otherwise. This case is needed to calculate the tensile strain produced by a perpendicular strain in compression. A value of zero to calculate the strain in compression produced by a perpendicular tensile strain is recomended [158, 159]. This was used to modify the FA-STM, and in 2002, Hsu and Zhu [58] develop the Softened Membrane Model (SMM). This model was able to reproduce the complete monotonic behavior of the experimental data.

In 2005, Mansour and Hsu ([86], [87]) developed an extension of the SMM to incorporate in the model the cycling constitutive laws. This model is known as the Cyclic Softened Membrane Model (CSMM). This model was based on the same assumptions of the SMM, but the value of the Hsu/Zhu ratio was modified from 1.9 to 1. This model is able to accurately represent the behavior of a panel in monotonic and reversal loading behavior. This model was able to represent the peak load capacity of the section , and the post-peak behavior. In addition, it is able to incorporate the softening of concrete, the tension stiffening and the effect of poison ratio in the constitutive model of the concrete. In the next section, a detailed review of this model will be done. In 2005 Zhong [157] and

in 2008, Mo et al. [97] presented the implementation of the CSMM model in the OpenSees Framework [82], using a tangent stiffness approach.

Other researchers have also attempted to represent the behavior of concrete using biaxial stresses for monotonic and cycling loading cases. This was summarized by Zhong [157] in 2005. A resume of these other models and additional models and information found in the literature is presented next.

Cervenka [25] in 1985 proposed a smeared cracked model using the fixed-angle formulation, where the cracks form perpendicular to the direction of the principal direction of tension stress, and after the crack is formed the compression resistance of the concrete is in the direction parallel to the cracks, also included was the tension stiffening in the direction normal to the cracks, and the shear stiffness at the orientation of the cracks, to account for the dowel action effects and aggregate interlocking. This model was tested against the experimental panels done in the University of Toronto by Vecchio and Collins [139].

Balakrishnan and Murray [8] in 1988, used a rotating angle orthotropic model to predict monotonic behavior of shear panels and deep beams. This model used a new constitutive law at the principal axis of orthotropy and the Poisson ratio was assumed to be zero after cracking. In 1991, Shin et al. [124] used a smeared concrete model to predict the behavior of wall elements, cyclic behavior was included in the material behavior. In 1994, Park [112] developed an orthotropic crack model to represent the behavior of planar structures for monotonic and cyclic load cases. The model consists of a two dimensional tension stiffening curve that considers the evaluation of the cracking process, and a tension and compression damage surfaces in two-dimensional strain field.

This defines the boundary between loading and unloading, and an equivalent uniaxial stress-strain curve in concrete was used for compression and tension.

In 1995, Sittipunt and Wood [126] developed a FEM based on a 4 node plane stress element and a smeared, fixed crack model. This included hysteresis behavior, tension stiffening, degradation of the concrete, compression softening for the concrete, and a truss element to model the reinforced steel bars. A smeared fixed angle was used to consider aggregate interlock, dowel effects and degradation for cycling loads.

In 1998, Ayoub and Filippou [7] used an othotropic rotating angle model to predict the behavior of concrete in biaxial state of stress, using a combination of the model proposed by Vecchio [136] in 1992 and the model by Balakrishnan and Murray [8] in 1988. The Poisson ratio was assumed to be zero in the direction of tension after cracking and the Poisson ratio in the principal direction of compression strain follows an equation that is a function of the compression strain. This model gave good results compared with the experimental data. In 1998, Kaufmann [69] proposed the cracked membrane model (CMM); this model was a combination between the MCFT [140] and a new stress-strain relation for the tension behavior of the concrete. This tension model incorporates stiffening with the use of a stepped, rigid-perfectly plastic concrete-steel bond-slip model.

Ile and Reymouard [61] in 2000 developed a smeared fixed crack model to represent the cyclic behavior of reinforced concrete structures subjected to biaxial stress. Experiments done with wall elements were used to verify the model Zhong [157]. In 2001, Belletti et al. [18] developed a fixed crack model with a stress-strain relation that takes into account the softening coefficient proposed by Pang and Hsu [110] in 1995, and the effect of aggregate interlock, dowel effects and concrete-steel bond. It was used with the results of the panels

tested at the University of Toronto and the University of Houston to evaluate the new material model. The result of the new model agreed well with the experimental data.

Powanusorn [118] in 2003 developed a smeared rotating crack model from the combination of the MCFT [139] and the RA-STM [17]. It was assumed that the directions of principal stress and strain coincide, principal stresses can be represented as a function of the principal strains, the steel is perfectly bonded to the concrete, and the effect of Poisson ratio after cracking was used. In addition, the new model incorporated the effect of confinement with the use of the Willam and Warnke [148] failure criterion. This new constitutive model was used to study RC Bent Caps. This model presented some discrepancies with experimental data.

In 2003, Foster and Marti [49] extended the CMM model [69] to eliminate the assumption that the principal axis of stress coincided with the principal axis of strains, and also incorporated the cyclic behavior of concrete. The tension stiffening effect was modeled using a stepped, rigid steel bond relationship, and a trilinear constitutive model was used for the steel. This constitutive model was used with a 4-node plane stress element. To verify the results, a set of experiments done on shear wall elements were used. The element gave good results compared with the experimental data.

4.1.2 Formulation of the Concrete Constitutive Model

A constitutive model to represent the plane stress behavior of concrete, which will be used to model the behavior of each concrete layer in the formulation developed in the last chapter, is proposed. This plane stress concrete material is based on a smeared crack approach using the orthotropic model with the axes of orthotropy represented by the

equivalent uniaxial average stress-strain relation. The axes of orthotropy are assumed to coincide with the principal axes of total strain, and using a tangent stiffness-based approach for nonlinear finite element implementation. In addition, this concrete model incorporates characteristics from the models of the University of Houston's Group (CSMM presented by Zhong [157] in 2005), the models from the University of Toronto's Group, (expanded MCFT developed by Palermo [105] in 2002, and Palermo and Vecchio [106] in 2003 and the concrete model by Vecchio [136] in 1992), and other additional models to consider the influence of biaxial compression or tension-compression (softening) in the axes of orthotropy. Also included was the enhancement due to confinement, and accounting for damage in the material during cycling loads.

The approach selected for the model is the known rotating crack model. This was selected because this type of model produced excellent agreement with the experimental data as is mentioned by Ayoub and Filippou [7] in 1998. In addition, the selection of the different features for the model presented here are selected to be able to use a layered section approach developed in the last chapter, and also to obtain a numerically stable, reliable and efficient constitutive material. The basic assumption used to formulate the concrete material were the following:

- The principal directions of strain and stress coincide.
- The stress-strain relation can be represented by the average stress-strain.
- The constitutive model for concrete in each of the the principal directions of stress can be represented with a uniaxial concrete model.
- The Poisson ratio is neglected after cracking.

Using these assumptions, and the derivations given in Appendix A, which shows the complete derivation of the transformation of the strain and stress between coordinate system and the derivation of the principal direction of strain, the biaxial strain (ε_{11} and ε_{22}) in the principal directions of strain can be determine as:

$$\varepsilon_{11} = \frac{1}{2} (\varepsilon_{xx} + \varepsilon_{yy}) + \frac{1}{2} \sqrt{(\varepsilon_{xx} - \varepsilon_{yy})^2 + (\gamma_{xy})^2} \quad (4.1a)$$

$$\varepsilon_{22} = \frac{1}{2} (\varepsilon_{xx} + \varepsilon_{yy}) - \frac{1}{2} \sqrt{(\varepsilon_{xx} - \varepsilon_{yy})^2 + (\gamma_{xy})^2} \quad (4.1b)$$

or in matrix form

$$\begin{Bmatrix} \varepsilon_{11} \\ \varepsilon_{22} \\ \gamma_{12} \end{Bmatrix} = [T_{strain}(\theta_{pd})] \begin{Bmatrix} \varepsilon_{xx} \\ \varepsilon_{yy} \\ \gamma_{xy} \end{Bmatrix} \quad (4.2)$$

using the strain transformation matrix, and recalling that for principal strain $\gamma_{12} = 0$:

$$[T_{strain}(\theta)] = \begin{bmatrix} \cos^2(\theta) & \sin^2(\theta) & \sin(\theta) \cos(\theta) \\ \sin^2(\theta) & \cos^2(\theta) & -\sin(\theta) \cos(\theta) \\ -2 \sin(\theta) \cos(\theta) & 2 \sin(\theta) \cos(\theta) & \cos^2(\theta) - \sin^2(\theta) \end{bmatrix} \quad (4.3)$$

and the angle of the principal direction of strain is defined by

$$\theta_{pd} = \frac{1}{2} \arctan \left(\frac{\gamma_{xy}}{(\varepsilon_{xx} - \varepsilon_{yy})} \right) \quad (4.4)$$

where $(\{\varepsilon_{x-y}\}) = \begin{Bmatrix} \varepsilon_{xx} & \varepsilon_{yy} & \gamma_{xy} \end{Bmatrix}^T$ are the strain components in the local coordinate system ($x - y$) of the concrete layer.

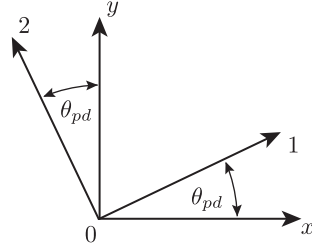


Figure 4.3: Principal Direction of Strain

Now, it is required to transform from biaxial to uniaxial strains to be able to use this result in the uniaxial stress-strain relation for each axes of orthotropy, and the poison ratio (ν_{12}, ν_{21}) is used for this. This transformation has been studied and discussed extensively by the University of Houston's Group and the University of Toronto's Group in the references reviewed before. The reader is referred to these for more information. Using the transformation presented in Zhong [157] in 2005, but with the Poisson ratio proposed by Vecchio [136] in 1992, the relation of the biaxial strain and uniaxial strain result in the following set of equations

$$\bar{\varepsilon}_1 = \frac{1}{1 - \nu_{12}\nu_{21}}\varepsilon_1 + \frac{\nu_{12}}{1 - \nu_{12}\nu_{21}}\varepsilon_2 \quad (4.5a)$$

$$\bar{\varepsilon}_2 = \frac{\nu_{21}}{1 - \nu_{12}\nu_{21}}\varepsilon_1 + \frac{1}{1 - \nu_{12}\nu_{21}}\varepsilon_2 \quad (4.5b)$$

or writing the equations in matrix form

$$\begin{Bmatrix} \bar{\varepsilon}_{11} \\ \bar{\varepsilon}_{22} \\ \bar{\gamma}_{12} \end{Bmatrix} = [V] \begin{Bmatrix} \varepsilon_{11} \\ \varepsilon_{22} \\ \gamma_{12} \end{Bmatrix} \quad (4.6)$$

where

$$[V] = \begin{bmatrix} \frac{1}{1-\nu_{12}\nu_{21}} & \frac{\nu_{12}}{1-\nu_{12}\nu_{21}} & 0 \\ \frac{\nu_{21}}{1-\nu_{12}\nu_{21}} & \frac{1}{1-\nu_{12}\nu_{21}} & 0 \\ 0 & 0 & 1 \end{bmatrix} \quad (4.7)$$

and

$$\nu_{ij} = \begin{cases} 0.2 & \text{if } \varepsilon_j > \frac{\varepsilon_{c0}}{2} \\ 0.2 \left(1 + 1.5 \left(\frac{2\varepsilon_j}{\varepsilon_{c0}} - 1 \right)^2 \right) > 0.5 & \text{if } \frac{\varepsilon_{c0}}{2} \geq \varepsilon_j \end{cases} \quad (4.8)$$

in addition, to obtain a stable solution, the values of Poisson ratios (ν_{12}, ν_{21}) after cracking are neglected (consider equal to zero).

Using the uniaxial strain $\bar{\varepsilon}_{11}$ and $\bar{\varepsilon}_{22}$ and recalling that $\bar{\gamma}_{12} = \gamma_{12} = 0$, the stress in the concrete in the direction of orthotropy or principal direction of stress can be defined as a function of this uniaxial strains as $\sigma_{11}(\bar{\varepsilon}_{11}, \bar{\varepsilon}_{22})$ and $\sigma_{22}(\bar{\varepsilon}_{11}, \bar{\varepsilon}_{22})$, and due to the assumption that the principal direction of strain and stress coincide, it is possible to determine the stress in the local coordinate $x - y$ using the transformation (Appendix A) defined by the angle θ_{pd} , as:

$$\begin{Bmatrix} \sigma_{xx}^c \\ \sigma_{yy}^c \\ \tau_{xy}^c \end{Bmatrix} = [T_{stress}(-\theta_{pd})] \begin{Bmatrix} \sigma_{11}^c \\ \sigma_{22}^c \\ 0 \end{Bmatrix} = [T_{strain}(\theta_{pd})]^T \begin{Bmatrix} \sigma_{11}^c \\ \sigma_{22}^c \\ 0 \end{Bmatrix} \quad (4.9)$$

with the stress transformation matrix

$$[T_{stress}(\theta)] = \begin{bmatrix} \cos^2(\theta) & \sin^2(\theta) & 2\sin(\theta)\cos(\theta) \\ \sin^2(\theta) & \cos^2(\theta) & -2\sin(\theta)\cos(\theta) \\ -\sin(\theta)\cos(\theta) & \sin(\theta)\cos(\theta) & \cos^2(\theta) - \sin^2(\theta) \end{bmatrix} \quad (4.10)$$

Now, using the definitions for strain and stress presented before, the tangent material constitutive matrix for the concrete layer in the local coordinate system ($x - y$) can be defined as:

$$[D_{x-y}^c] = \frac{\partial \sigma_{x-y}}{\partial \varepsilon_{x-y}} = \frac{\partial \begin{Bmatrix} \sigma_{xx} \\ \sigma_{yy} \\ \tau_{xy} \end{Bmatrix}}{\partial \begin{Bmatrix} \varepsilon_{xx} \\ \varepsilon_{yy} \\ \gamma_{xy} \end{Bmatrix}} = [T_{strain}(\theta_{pd})]^T [D_{1-2}^c] [V] [T_{strain}(\theta_{pd})] \quad (4.11)$$

where $[D_{1-2}^c]$ is the material tangent matrix for the concrete layer in the principal direction of strain (or stress), and can be defined as proposed by Crisfield and Wills [36] in 1989:

$$[D_{1-2}^c] = \begin{bmatrix} \frac{\partial \sigma_{11}}{\partial \varepsilon_{11}} & \frac{\partial \sigma_{11}}{\partial \varepsilon_{22}} & 0 \\ \frac{\partial \sigma_{22}}{\partial \varepsilon_{11}} & \frac{\partial \sigma_{22}}{\partial \varepsilon_{22}} & 0 \\ 0 & 0 & \frac{\sigma_{11} - \sigma_{22}}{2(\varepsilon_{11} - \varepsilon_{22})} \end{bmatrix} \quad (4.12)$$

For simplicity and stability $\frac{\partial\sigma_{11}}{\partial\varepsilon_{22}}$ and $\frac{\partial\sigma_{22}}{\partial\varepsilon_{11}}$, will be neglected which reduces Eq. 4.12 to:

$$[D_{1-2}^c] = \begin{bmatrix} \frac{\partial\sigma_{11}}{\partial\varepsilon_{11}} & 0 & 0 \\ 0 & \frac{\partial\sigma_{22}}{\partial\varepsilon_{22}} & 0 \\ 0 & 0 & \frac{\sigma_{11}-\sigma_{22}}{2(\varepsilon_{11}-\varepsilon_{22})} \end{bmatrix} \quad (4.13)$$

As was mentioned in the assumptions, the behavior of the concrete in the principal directions of stress, which coincide with the principal directions of strain, are defined by average uniaxial stress-strain relations. In this study the average uniaxial stress-strain relations are represented by uniaxial concrete material models, which will be reviewed next. Two uniaxial concrete materials were selected to represent the average uniaxial stress-strain relations for the principal directions of stress for this smeared rotating angle model. These two material models are those proposed by Massone [90] in 2006 for static load and after extended to include hysteretic rules, also developed by Massone on OpenSees [82], as the uniaxial concrete material “*Concrete06*” in OpenSees [82], and the second model is a simplified Chang-Mander model proposed by Waugh [147] in 2009. In addition, in the next chapters, it will be referred to as “the smeared plane stress concrete model with Thorenfeldt’s curve” when a plane stress concrete model using the uniaxial material model proposed by Massone [90] in 2006 is used, and it will be referred to as “the smeared plane stress concrete model with Chang-Mander Model” when a plane stress concrete model using the simplified Chang Mander Model proposed by Waugh [147] in 2009 is used.

4.1.2.1 Uniaxial Concrete Models using Thorenfeldt Curve

This uniaxial concrete model was proposed by Massone [90] in 2006 for static load and after extended to include hysteretic rules, also done by Massone and developed on OpenSees [82], under the name of “*Concrete06*”. The following is a representation of the main characteristic, rules and equations that define the Model proposed by Massone [82, 90]. The envelope of the model is composed for two different equations, one used for the compression envelope, see Fig. 4.4, and the other for the tension envelope, see Fig. 4.5.

The compression envelope is defined by the curve proposed by Thorenfeldt et al. [133] in 1987, which is similar to the equation defined by Popovics [117] in 1973. The Thorenfeldt base curve was later calibrated for Collins and Porasz [33] in 1989, see Fig. 4.4, and has been used for shell and membranes by Polak and Vecchio [115] in 1993, and Vecchio and Collins [141] in 1993, and in MVLM by Orakcal et al. [103] and Massone [90] in 2006. It can be defined as:

$$\sigma_c(\varepsilon_c) = f'_c \frac{n \left(\frac{\varepsilon_c}{\varepsilon_{c_0}} \right)}{n - 1 + \left(\frac{\varepsilon_c}{\varepsilon_{c_0}} \right)^{nk}} \quad (4.14)$$

where f'_c is the peak resistant stress of the concrete in compression, ε_{c_0} is the strain at the peak resistant stress of the concrete in compression, and n and k are the parameters calibrated by Collins and Porasz [33] in 1989 for the use with high-strength concrete:

$$n = 0.8 + \frac{f'_c (\text{MPa})}{17} = 0.8 + 0.41 f'_c (\text{ksi}) \quad (4.15a)$$

$$k = \begin{cases} 1 & \text{if } 0 \leq \varepsilon_c \leq \varepsilon_{c_0} \\ 0.67 + \frac{f'_c (\text{MPa})}{62} = 0.67 + \frac{f'_c (\text{ksi})}{9} & \text{if } \varepsilon_c > \varepsilon_{c_0} \end{cases} \quad (4.15b)$$

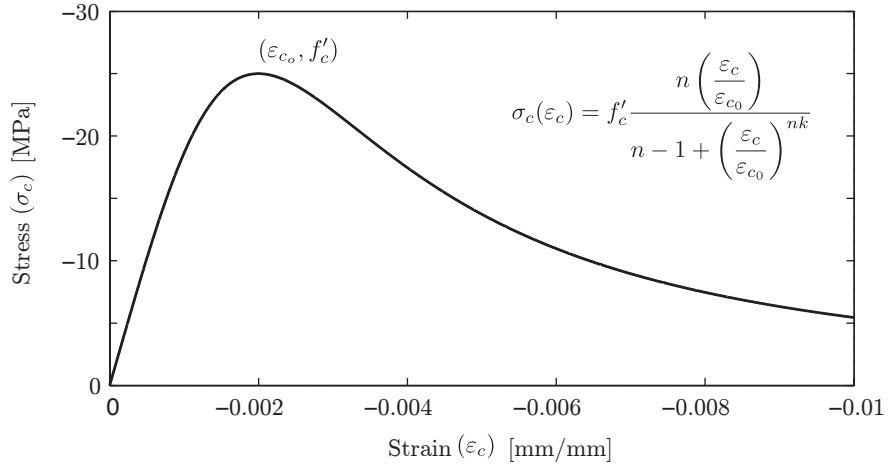


Figure 4.4: Constitutive Model for Concrete in Compression using Thorenfeldt base curve

Carreira and Kuang-Han [23] in 1985, proposed the calibration for the parameters for concrete with lower compressive resistant stress as:

$$n = 1.55 + \left(\frac{f'_c (MPa)}{32.4} \right)^3 = 1.55 + \left(\frac{f'_c (ksi)}{4.7} \right)^3 (ksi) \quad (4.16a)$$

$$k = 1 \quad (4.16b)$$

The tension envelope used by Massone [90] is the one proposed by Belarbi and Hsu [16] in 1994, which is based on the equation used by Tamai et al. [130] in 1988. Belarbi and Hsu [16] proposed this model from the results of testing 17 reinforced concrete panels under pure tension. The tension envelope is divided in two section (Eq. 4.17), see Fig. 4.5, pre-peak or pre-cracking and post-peak or post-cracking. Before the cracking a linear interpolation is selected, and for post cracking, a descending branch is selected to include

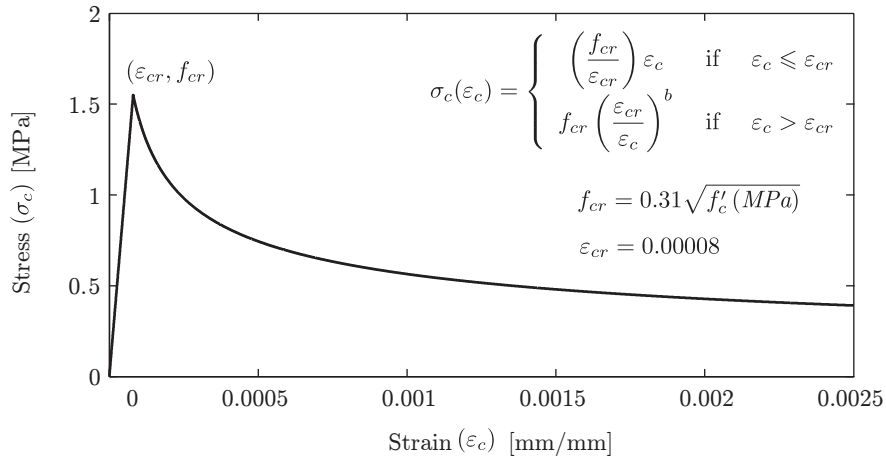


Figure 4.5: Constitutive Model for Concrete in Tension using the Belarbi and Hsu [16] equation

the tension stiffening observed in the average stress-strain relation of the concrete in tension (Eq. 4.17).

$$\sigma_c(\varepsilon_c) = \begin{cases} \left(\frac{f_{cr}}{\varepsilon_{cr}}\right)\varepsilon_c & \text{if } \varepsilon_c \leq \varepsilon_{cr} \\ f_{cr}\left(\frac{\varepsilon_{cr}}{\varepsilon_c}\right)^b & \text{if } \varepsilon_c > \varepsilon_{cr} \end{cases} \quad (4.17)$$

where, b is a parameter that defines the descending branch of the envelope in tension, f_{cr} is the peak of resistant stress of the concrete in tension, and ε_{cr} is the strain at the peak of resistant stress of the concrete in tension. Belarbi and Hsu [16] in 1994 proposed the value of $b = 0.4$, and the other parameters as:

$$f_{cr} = 0.31\sqrt{f'_c(MPa)} \text{ [MPa]} \quad \text{or} \quad f_{cr} = 0.118\sqrt{f'_c(ksi)} \text{ [ksi]} \quad (4.18a)$$

$$\varepsilon_{cr} = 0.00008 \quad (4.18b)$$

Massone extended this model to include hysteretic rules, see Fig. 4.6, on OpenSees [82]. The hysteretic rules proposed used a linear representation of unloading and reloading in

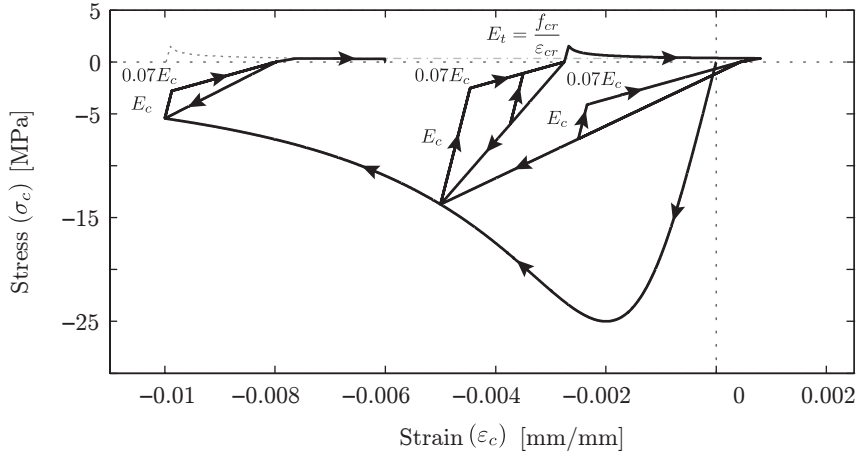


Figure 4.6: Hysteretic Rules for the Concrete Model

compression, connected between them, also, with a linear equation with the slope equal to the initial stiffness of the concrete (E_{c0}). The slope of the unloading path in the compression zone was selected to be $0.071E_{c0}$, which is the same value proposed by Palermo and Vecchio [106] in 2003. The expression in Eq. 4.19 was selected to determinate the plastic strain (ε_p^c) of the concrete at each full unloading, which is the unrecovered strain deformation in the material:

$$\varepsilon_p^c = \varepsilon_m^c \left(1 - e^{-\left(\frac{\varepsilon_m^c}{\varepsilon_{c0}}\right)\alpha_c} \right) \quad (4.19)$$

where ε_m^c is the maximum previous compression strain recorded in the material, and α_c is a parameter that determines the amount of plastic strain in the concrete, and a value of $\alpha_c = 0.32$ was used for the analysis in this study.

For the unloading and reloading rules in tension, linear paths that have the slope equal to the previous unloading stiffness of the concrete in tension, (Fig. 4.6), were selected and defined using a plastic strain determinate from:

$$\varepsilon_p^t = \varepsilon_m^t \left(1 - e^{-\left(\frac{\varepsilon_m^t}{\varepsilon_{cr}}\right) \alpha_t} \right) \quad (4.20)$$

where ε_m^c is the maximum previous tension strain recorded in the material, and α_t is a parameter that determines the amount of plastic strain in the concrete. A value of $\alpha_t = 0.08$ was used for the analysis in this study. In addition, Massone considered a shifting of the origin of the tension envelope, see Fig. 4.6, to produce a more accurate model, reduce pinching, and be able to model the gap closure with a linear path.

4.1.2.2 Uniaxial Concrete Model using a Simplified Chang-Mander Model

This second model is a simplified version done by Waugh [147] in 2009 of the Chang-Mander model proposed by Chang and Mander [27] in 1994 for the representation of the cyclic behavior of the unconfined and confined concrete. The simplifications introduced by Chang and Mander [27] to the model were done to produce a more efficient and stable model. However, this model, instead of the model using the Thorenfeldt curve, is based on the uniaxial behavior observed in concrete, and is typically used to represent the concrete stress-strain relationship for a fiber section in beams, columns and beam-columns. A review of the simplified Chang-Mander model presented by Waugh [147] in 2009, that was also implemented on OpenSees [82], under the name of “Concrete07 - Chang & Manders 1994 Concrete Model” by Waugh follows.

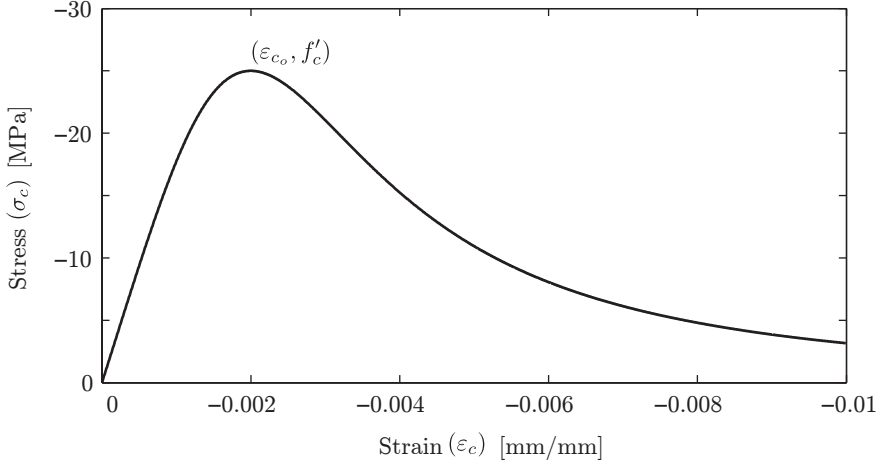


Figure 4.7: Compression Envelope Curves of the Simplified Chang-Mander Concrete Model

This uniaxial concrete model uses the same equation type for the representation of the envelope of the concrete in compression and in tension (Fig. 4.8). The envelope uses Tsai's equation that was defined in non-dimensional form and used by Waugh [147] as:

$$y(x) = \frac{nx}{D(x)} \quad (4.21)$$

$$z(x) = \frac{1 - x^r}{[D(x)]^2} \quad (4.22)$$

where

$$D(x) = \begin{cases} 1 + \left(n - \frac{r}{r-1}\right)x + \frac{x^r}{r-1} & \text{if } r \neq 1 \\ 1 + (n-1 + \ln(x))x & \text{if } r = 1 \end{cases} \quad (4.23)$$

and n and r are parameters that control the shape of the curve.

The non-dimensional parameters for compression are defined as:

$$x^- = \frac{\varepsilon_c}{\varepsilon_{c_0}} \quad (4.24a)$$

$$y^- = \frac{\sigma_c}{f'_c} \quad (4.24b)$$

$$n^- = \frac{E_c \varepsilon_{c_0}}{f'_c} \quad (4.24c)$$

and the non dimensional value of the spalling strain as

$$x_{sp}^- = x_{cr}^- - \frac{y(x_{cr}^-)}{n^- z(x_{cr}^-)} \quad (4.25)$$

where f'_c is the peak resistant stress of the concrete in compression, ε_{c_0} is the strain at the peak resistant stress of the concrete in compression, E_c is the initial Young's Modulus of the concrete, x_{cr}^- is the critical strain in non-dimensional form, and x_{sp}^- is the spalling strain in non-dimensional form. Using these parameters, the values σ_c and E_t that define the envelope curve in concrete can be calculated as

$$\sigma_c(x^-) = \begin{cases} f'_c y(x^-) & \text{if } x^- \leq x_{cr}^- \\ f'_c \left(y(x_{cr}^-) + n^- z(x_{cr}^-) (x^- - x_{cr}^-) \right) & \text{if } x_{cr}^- < x^- \leq x_{sp}^- \\ 0 & \text{if } x^- > x_{sp}^- \end{cases} \quad (4.26)$$

$$E_t^-(x^-) = \begin{cases} E_c z(x^-) & \text{if } x^- \leq x_{cr}^- \\ E_c z(x_{cr}^-) & \text{if } x_{cr}^- < x^- \leq x_{sp}^- \\ 0 & \text{if } x^- > x_{sp}^- \end{cases} \quad (4.27)$$

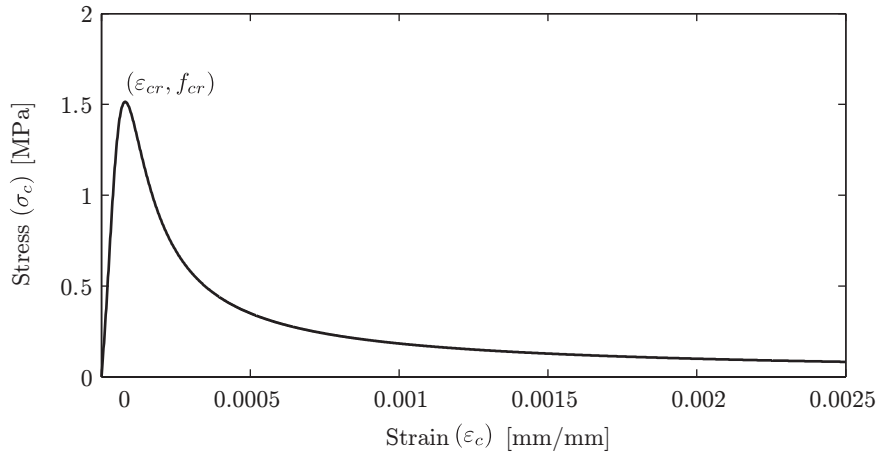


Figure 4.8: Tension Envelope Curves of the Simplified Chang-Mander Concrete Model

In tension, the non-dimensional parameters are defined as:

$$x^+ = \left| \frac{\varepsilon_c - \varepsilon_0}{\varepsilon_{cr}} \right| \quad (4.28a)$$

$$y^+ = \frac{\sigma_c}{f_{cr}} \quad (4.28b)$$

$$n^+ = \frac{E_c \varepsilon_{cr}}{f_{cr}} \quad (4.28c)$$

and the non dimensional value of the spalling strain as

$$x_{sp}^+ = x_{cr}^+ - \frac{y(x_{cr}^+)}{n^+ z(x_{cr}^+)} \quad (4.29)$$

where f_{cr} is the peak resistant stress of the concrete in tension, ε_{cr} is the strain at the peak resistant stress of the concrete in tension, E_c is the initial Young's Modulus of the concrete, x_{cr}^+ is the critical strain in non-dimensional form, and x_{sp}^+ is the spalling strain in non-dimensional form. Using this parameters the values of σ_c (stress in the concrete)

and E_t (tangent stiffness of the concrete) that define the envelope curve in concrete can be calculated as

$$\sigma_c(x^+) = \begin{cases} f_{cr}y(x^+) & \text{if } x^+ \leq x_{cr}^+ \\ f_{cr}\left(y(x_{cr}^+) + n^+z(x_{cr}^+)(x^+ - x_{cr}^+)\right) & \text{if } x_{cr}^+ < x^+ \leq x_{sp}^+ \\ 0 & \text{if } x^+ > x_{sp}^+ \end{cases} \quad (4.30)$$

$$E_t^+(x^+) = \begin{cases} E_c z(x^+) & \text{if } x^+ \leq x_{cr}^+ \\ E_c z(x_{cr}^+) & \text{if } x_{cr}^+ < x^+ \leq x_{sp}^+ \\ 0 & \text{if } x^+ > x_{sp}^+ \end{cases} \quad (4.31)$$

The parameter r defines the descending branch of the Tsai's curve, and can be defined for unconfined concrete as

$$r = \frac{f'_c(MPa)}{5.2} - 1.9 = \frac{f'_c(ksi)}{0.75} - 1.9 \quad (4.32)$$

and for confined concrete as

$$r = \frac{n}{n-1} \quad (4.33)$$

The simplified Chang-Mander model incorporates a number of 15 rules to represent the complete and partial loading, unloading and reloading behavior of the concrete for pre-cracking and post-cracking concrete behavior, see Fig. 4.9. These rules are extensively detailed and presented by Waugh [147] in 2009. In addition, the model focus is in the representation of the gap closing and opening due to the cracks [147]. In this study, this

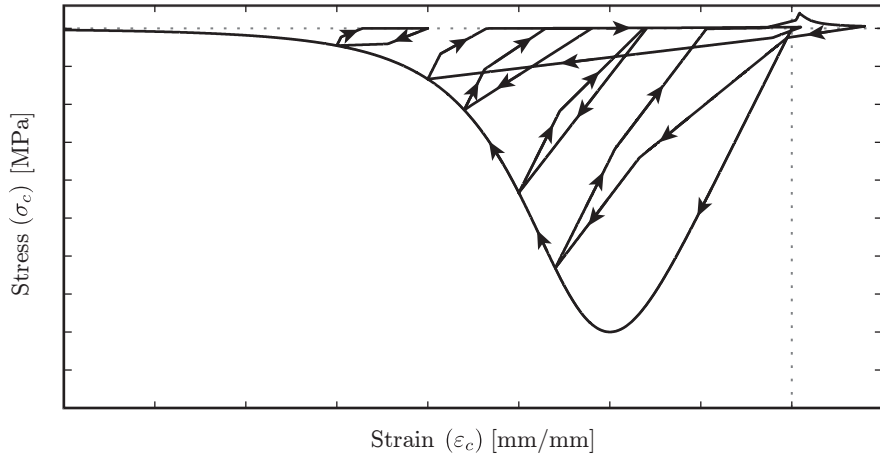


Figure 4.9: Hysteretic rules for the Simplified Chang-Mander Concrete Model proposed by Waugh [147] in 2009

model was only used for the analysis of monotonic load cases, due to some numerical instabilities produced when cycling or reversed loads where analyzed.

4.1.2.3 Biaxial Strength Coefficients

This section presents the functions of the coefficients that are used to account for compression softening, enhancement due to biaxial compression, and the damage due to cyclic or reversal load in a concrete material in a biaxial state of stress. This behavior has been extensively observed and mentioned in the literature (e.g, Vecchio and Collins [140] in 1986, Belarbi and Hsu [17] in 1995, Ayoub and Filippou [7] in 1998, Mansour et al. [88] in 2001, Powanusorn [118] in 2003, Palermo and Vecchio [106] in 2003 ,Zhong [157] in 2005, Massone [90] in 2006). Different equations to account for this behavior have been developed. Typically, these account for the behavior of the peak resistant stress of the concrete in compression (f'_c) which is modified by a factor, and also the strain at the peak resistant stress of the concrete in compression (ε_{c0}) which is modified sometimes. However, in this

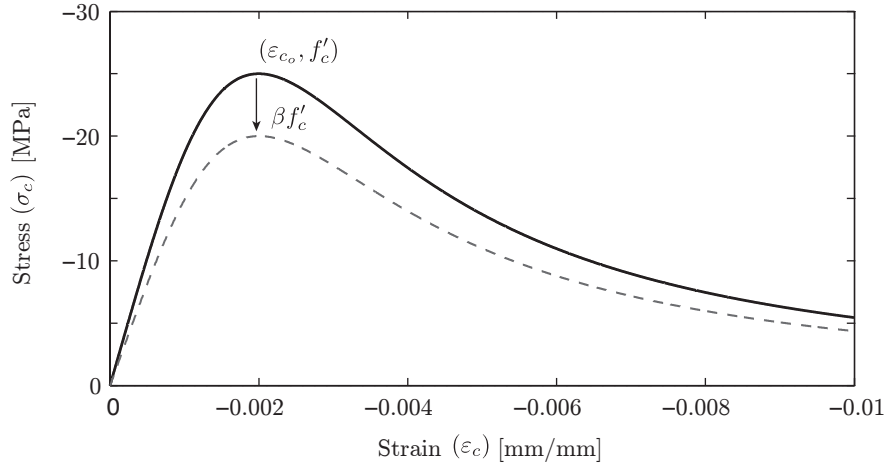


Figure 4.10: Compression Softening Effect

study only a modification to f'_c will be applied, as was suggested by Massone [90], and because Vecchio and Collins [141] in 1993 observed that more sophisticated models only result in marginally better solutions [90]. In addition, the modification of only the f'_c is selected to retain a stable and efficient numerical solution.

Compression softening effect ($\beta_s f'_c$) is the reduction of the compression resistance of the concrete in one direction due to tension strain in the perpendicular direction. It is modeled with the use of the coefficient proposed by Belarbi and Hsu [17] in 1995, and defined as

$$\beta_s = \frac{k}{\sqrt{1 + k_\sigma \varepsilon_{tension}}} \quad (4.34)$$

where $\varepsilon_{tension}$ is the tension strain in concrete, and k and k_σ are two parameters that define the reduction factor. The factor k_σ was defined as 250 for sequential loading and 400 for proportional loading [17], and k was defined as 0.9 by Belarbi and Hsu [17]. However, it was observed during this study that a value of 1 for k results in more stable solutions without much loss of accuracy.

Enhancement of the compression strength ($\beta_e f'_c$) is the increase of the peak resistant stress f'_c in the concrete which can be produced by the following two factors, biaxial compression stress state, as was mention by Kupfer et al. [75] in 1969 and Vecchio [136] in 1992, or by the confinement produced by stirrups, cross ties and hoops in the concrete, as is studied by Mander et al. [85] in 1988. The enhanced compression strength due to biaxial compression is considered using equation (Eq. 4.35) proposed by Vecchio [136] in 1992.

$$\beta_{eij} = 1 + 0.92 \left(\frac{\sigma_{cj}}{f'_c} \right) - 0.76 \left(\frac{\sigma_{cj}}{f'_c} \right)^2 \quad (4.35)$$

where i is the direction enhanced, j is the direction normal to i , σ_{cj} is the stress in the direction normal to i , and f'_c is the peak of resistant stress of the concrete in compression.

Damage due to cyclic or reversal load ($\beta_d f'_c$) is the deterioration of the compression strength of the concrete under the loading and unloading process in the cyclic load. This effect was studied by Palermo and Vecchio [106] in 2003, who proposed an equation for the deterioration in compression and in tension which is a function of the difference between the maximum and minimum strain that occurs during the reversed loading. In this study only the damage in compression is used. The equation proposed by Palermo and Vecchio [106] can be written as:

$$\beta_d = \frac{1}{1 + \alpha_1 \left(\frac{\varepsilon_{rec}}{\varepsilon_{c0}} \right)^{\alpha_2}} \quad (4.36)$$

where ε_{c0} is the strain at the the peak of resistant stress of the concrete in compression, the parameter α_1 is equal to 0.5 for pre-cracking and 0.6 for post-cracking in compression,

α_2 is equal to 0.1 for pre-cracking and 0.175 for post-cracking in compression, and ε_{rec} is defined as

$$\varepsilon_{rec} = \varepsilon_{max} - \varepsilon_{min} \quad (4.37)$$

with ε_{max} the maximum strain recorded in the cyclic loading, and ε_{min} the minimum strain recorded in the cyclic loading.

In addition, in this study an additional factor is used to account for the enhancement due to confinement (β_{conf}). This factor is applied over the compression peak strength of the concrete (f'_c) as $\beta_{conf} f'_c$ at the beginning of the analysis, and it is maintained constant during the rest of the analysis. This factor can be done using the sophisticated equation proposed by Mander et al. [85] in 1988 or a more simple coefficient like the use by Orakcal et al. [103] in 2006 and defined as

$$\beta_{conf} = 1 + \frac{\rho_s f_y}{f'_c} \quad (4.38)$$

where ρ_s is the ratio between the volume of transverse steel and the volume of core concrete measured from the outside of the stirrups, f_y is the yielding strength of the transverse steel, and f'_c is the peak resistant stress of the concrete in compression. In this study, Eq. 4.38 is mainly used to determinate the coefficient of enhancement due to confinement.

4.2 Constitutive Model for Steel

In this section, the smeared steel constitutive material used to represent the horizontal and vertical reinforcement steel layers in the membrane and shell element is presented. In this approach, it is assumed that the steel bars are consider as a layer of homogenous material

at certain positions inside the reinforced concrete element, and the variation stress due to the crack over an area can be modeled using the average stress-strain of steel in that zone, see Fig. 4.2. In addition, it is assumed that the smeared steel works only in the direction of the bar, since the bars are typically in a uniaxial state of stress, and this allows the use of a uniaxial constitutive model. This smeared steel material assumes:

- Steel was considered smeared and only acts in its orientation.
- The stress-strain relation can be represented by the average stress-strain relation of steel bars embedded in the concrete.
- Concrete and smeared steel are consider fully bonded.
- The Poisson ratio is neglected after cracking.

Using these assumptions and the assumption for concrete, and an approach similar to that proposed by Zhong [157] in 2005, the uniaxial strain in the orientation of steel can be represented by

$$\left\{ \varepsilon_s \right\} = [T_{strain}(\theta_s - \theta_{pd})] [V] [T_{strain}(\theta_{pd})] \begin{Bmatrix} \varepsilon_{xx} \\ \varepsilon_{yy} \\ \varepsilon_{xy} \end{Bmatrix} \quad (4.39)$$

where $[T_{strain}(\theta)]$ is the strain transformation defined by Eq. 4.3, θ_s is the angle that defines the orientation of the steel layer with respect to the local coordinate system ($x - y$), see Fig. 4.11, θ_{pd} is the orientation of the principal direction of strain defined by Eq. 4.4, and $[V]$ is the Poisson ratio matrix defined by Eq. 4.7. Since the steel is considered as a

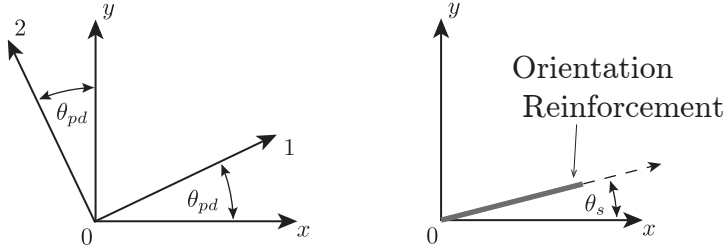


Figure 4.11: Steel Layer Orientation

uniaxial material, the only component needed is the strain for the direction of the steel, which is the component ε_{s_1} . This strain is used to determinate the stress ($f_s(\varepsilon_{s_1})$) and the stiffness tangent $\left(E_s(\varepsilon_{s_1}) = \frac{\partial f_s}{\partial \varepsilon_s}\right)$ in the direction of action of the smeared steel from the average uniaxial stress-strain relations, which will be presented later. Using these values the stiffness tangent of the layer in the plane stress state for the coordinate system ($x - y$) can be determinate as:

$$[D_{x-y}^s] = [T_{strain}(\theta_s)]^T [D_s] [T_{strain}(\theta_s - \theta_{pd})] [V] [T_{strain}(\theta_{pd})] \quad (4.40)$$

or for simplicity without consider the Poisson ratio as:

$$[D_{x-y}^s] = [T_{strain}(\theta_s)]^T [D_s] [T_{strain}(\theta_s)] \quad (4.41)$$

where

$$[D_s] = \begin{bmatrix} \rho E_t^s & 0 & 0 \\ 0 & 0 & 0 \\ 0 & 0 & 0 \end{bmatrix} \quad (4.42)$$

with ρ being the ratio of reinforced steel in the layer, and E_t^s is the tangent stiffness of the smeared steel.

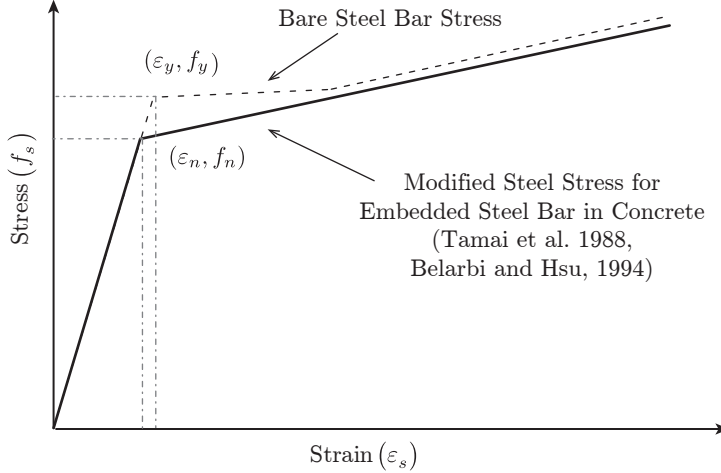


Figure 4.12: Stress-Strain relation of embedded steel bar in concrete and bare steel Bar

For the resistant stress of the smeared steel layer, the in-plane stress state for the coordinate system ($x - y$) can be determinate as:

$$\begin{Bmatrix} \sigma_{xx}^s \\ \sigma_{yy}^s \\ \tau_{xy}^s \end{Bmatrix} = [T_{stress}(-\theta_s)] \begin{Bmatrix} \rho f_s \\ 0 \\ 0 \end{Bmatrix} = [T_{strain}(\theta_s)]^T \begin{Bmatrix} \rho f_s \\ 0 \\ 0 \end{Bmatrix} \quad (4.43)$$

with the stress transformation matrix defined by Eq. 4.10.

In this study, as was mentioned before, the action of the smeared steel in its orientation is modeled using average uniaxial stress-strain relations. Different steel materials have been implemented to determinate the unaxial stress-strain relation of the steel bar inside of the concrete. Commonly, it is assumed in models that the behavior of the steel bar without concrete and with concrete are the same. However, Tamai et al. [130] in 1988 observed during a set of experimental data done over reinforced concrete prisms, that the behavior of reinforcing steel inside of the concrete presented some difference in behavior when compared to the bare steel. This was corroborated later by Belarbi and Hsu [17] in

1995. In Fig. 4.12, it is shown that the behavior of steel reinforcing bar embedded in the concrete is modified from the bare steel bar, with a reduction on the position of yielding point. This variation of the behavior in the steel is attributed to the consideration of the stress in the steel as a function of the average strain in concrete. This means that while in the crack the steel could already have started to yield, in between the cracks the stress of the steel will be less [16], see Fig. 4.2.

The average uniaxial stress-strain relations are represented by uniaxial steel material models with a reduction of the position of the yielding point to consider the effect observed and study by Belarbi and Hsu [17] in 1995. Two uniaxial steel materials were selected to model the behavior of the smeared steel in the orientation of the reinforcement. These two material model are the one proposed by Mansour et al. [88] in 2001, and the well known Menegotto and Pinto model in 1973 [94], and later modified by Filippou et al. [48] in 1983. The following is a review of these two models.

4.2.1 Uniaxial Mild Steel Bar Embedded in Concrete Model

This model was proposed by Mansour et al. [88] in 2001 to represent the cyclic behavior of the stress-strain relationships for steel bars embedded in concrete. It considers two main features; the envelope curve in tension can be expressed by a bilinear relation proposed by Belarbi and Hsu [16] in 1994, and the reloading and unloading portion of the curves can be modeled using a form of the Ramberg-Osgood equation. Mansour et al. [88] in 2001 found that the Ramberg-Osgood type of expression proposed by Yokko and Nakamura [153] in 1977 can be used to best describe the behavior of steel and includes the Bauschinger effects.

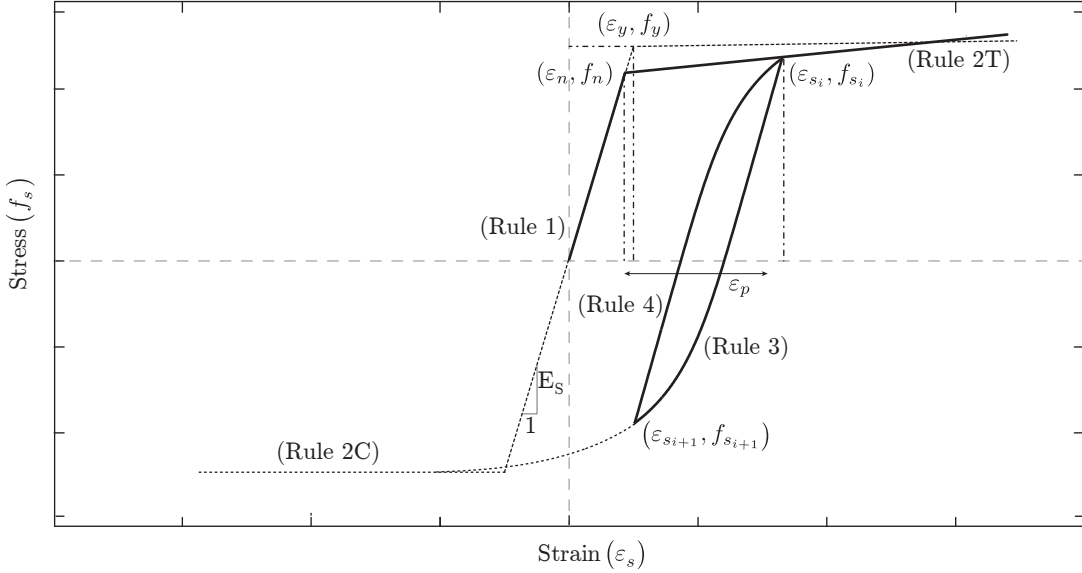


Figure 4.13: Constitutive Model for Embedded Steel Bars Model

The following is a review of the equations that define this cyclic stress-strain relationship of mild steel bars embedded in concrete proposed by Mansour et al. [88].

The model is divided in four rules, see Fig. 4.13. The two first rules define the envelope of the average stress-strain relationship, and are defined by a bilinear relation proposed by Belarbi and Hsu [16] in 1994. Rule 1 defines the elastic behavior of the steel prior to yielding as:

$$f_s(\varepsilon_s) = E_s \varepsilon_s \quad \text{if } -\varepsilon_y \leq \varepsilon_s \leq \varepsilon_n \quad (4.44)$$

and Rule 2 defines the yielding of the steel bar embedded in concrete as

$$f_s(\varepsilon_s) = \begin{cases} f_y \left((0.91 - 2B) + (0.02 + 0.25B) \frac{\varepsilon_s}{\varepsilon_y} \right) & \text{if } \varepsilon_s > \varepsilon_n \\ -f_y & \text{if } \varepsilon_s < -\varepsilon_y \end{cases} \quad (4.45)$$

where f_s is the average stress of the embedded steel bar, ε_s is the average strain of the embedded steel bar, f_y is the yielding strength of the bare steel bar, ε_y is the yielding strain of the bare steel bar, E_s is the initial Young's Modulus for the elastic steel bar, $\varepsilon_n = \left[\left(\frac{(0.91 - 2B)}{(0.98 - 0.25B)} \right) \varepsilon_y \right]$ is the average yielding strain of the embedded steel bar, and parameter B is defined as

$$B = \frac{1}{\rho} \left(\frac{f_{cr}}{f_y} \right)^{1.5} \quad (4.46)$$

where ρ is the ratio of reinforcement steel ($\rho_{min} = 0.25\%$), and f_{cr} is the peak resistant stress of the concrete in tension.

Rules 3 and 4 define the unloading and reloading of the embedded steel bars, and are represented by the Ramberg-Osgood type of equation defined as

$$\varepsilon_s - \varepsilon_i = \frac{f_s - f_i}{E_s} \left(1 + A^{-R} \left| \frac{f_s - f_i}{f_y} \right|^{R-1} \right) \quad (4.47)$$

where f_i and ε_i are the stress and strain of the steel bar at the load reversal point, the parameters A and R are represented by $A = 1.9k_p^{-0.1}$ and $R = 10k_p^{-0.2}$, which were determined from the experimental data by Mansour et al. [88] in 2001, and k_p is the ratio of plastic strain defined as $\frac{\varepsilon_p}{\varepsilon_n} = \frac{(\varepsilon_i - \varepsilon_n)}{\varepsilon_n}$ and ε_p is the plastic strain.

The difficulty of this Ramberg-Osgood type of equation is that the rules need to use an iterative approach to find the stress as a function of the strain. In this study a Newton-Raphson method was used to do the iterative procedure to determinate the stress in Rules 3 and 4. This iterative process can produce an increase in the computational time during the stress determination at each steel layer, for cyclic analysis.

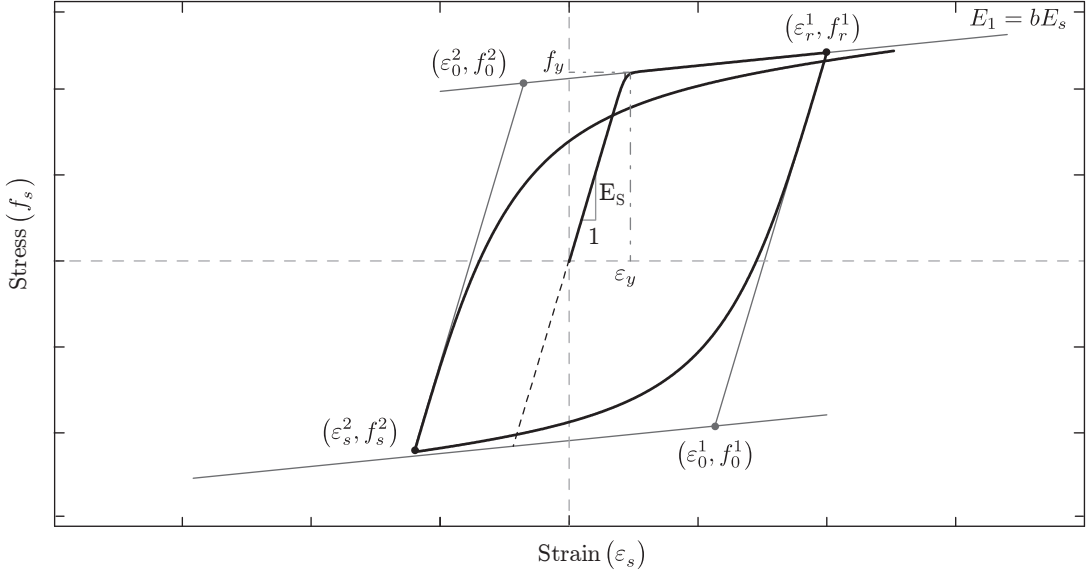


Figure 4.14: Constitutive Model for Menegotto and Pinto Steel model

4.2.2 Uniaxial Menegotto and Pinto Steel Model

This model corresponds to the well known Menegotto and Pinto model of 1973 [94], and afterwards was modified by Filippou et al. [48] in 1983 to include isotropic hardening, using a shifting of the yielding stress asymptote. This model is computationally efficient and can represent very well the behavior of the steel observed experimentally [103]. The following is a review of the model definition done by Filippou et al. [48] in 1983 and Orakcal et al. [103] in 2006.

The stress-strain relationship of this model is defined by Eq. 4.48 that represents a curve transition between two asymptotes defined by two straight line. The first line has a slope equal to E_s , which is the initial Young's Modulus for the elastic steel, and the other has a slope equal to $E_1 = bE_s$, where the b is the strain-hardening ratio (Fig. 4.14), and allows the incorporation of the Bauschinger effects in the material model.

$$f_s^*(\varepsilon_s^*) = b\varepsilon_s^* + \frac{(1-b)\varepsilon_s^*}{\left(1+(\varepsilon_s^*)^R\right)^{\frac{1}{R}}} \quad (4.48)$$

where

$$\varepsilon_s^* = \frac{\varepsilon_s - \varepsilon_r}{\varepsilon_0 - \varepsilon_r} \quad (4.49)$$

and

$$f_s^* = \frac{f_s - f_r}{f_0 - f_r} \quad (4.50)$$

with f_r and ε_r are the stress and strain at the last position of strain reversal, which is the origin for the straight line that defines the asymptote with slope E_s , and f_0 and ε_0 are the stress and strain point where the two asymptotes intercept, see Fig. 4.14. The R parameter defines the form of the transition curve, and can be expressed as:

$$R = R_0 - \frac{a_1\xi}{a_2 + \xi} \quad (4.51)$$

where R_0 is the value for the first loading or the monotonic loading and the parameters a_1 and a_2 define the variation of R during the cyclic loading. These parameters are determinated experimentally, and in this study are assumed to be $R_0 = 18$, $a_1 = 16.2$, and $a_2 = 0.15$. The parameter ξ is defined as

$$\xi = \left| \frac{\varepsilon_m - \varepsilon_0}{\varepsilon_y} \right| \quad (4.52)$$

where ε_y is the yielding strain of the bare steel, and ε_m is the minimum or maximum strain from the previous strain reversal, depending on whether the current strain is decreasing or increasing.

In order to use this uniaxial model in an average stress-strain relationships, the values of $f_y^{average}$ and $b_{average}$ need to be determined as

$$f_y^{average} = (0.91 - 2B) f_y \quad (4.53a)$$

$$b_{average} = (0.02 + 0.25B) b \quad (4.53b)$$

In these uniaxial models, it is assumed that the steel and the concrete are fully bonded, and the bond slippage is approximated by incorporation in the average stress-strain relationship. In addition, these models do not incorporate some of the characteristics observed for the embedded steel, such as the degradation, cycling fatigue, or buckling failure of the steel bars.

4.3 Summary

In this chapter, many published models for the material constitutive laws to represent the behavior of concrete were reviewed. Of the models available, the smeared cracked concrete model, which is based on the assumption that different cracks over an area can be modeled using the average stress-strain relation of concrete in that zone, are the preferable concrete models to use. Among the smeared cracked models, the orthotropic models stand out for their accuracy and simplicity, and they are robust enough to represent the material behavior of concrete.

In addition, it was concluded that in order to work with a layered section approach, a separate constitutive model for the smeared concrete layer and the smeared steel layer are necessary. These constitutive models are presented separately, which is different from the more advanced orthotropic model like the Softened Membrane Model (SMM) and Cyclic Softened Membrane Model (CSMM) [17, 55, 57, 58, 86, 87, 110, 157]. The constitutive model used to represent the plane stress behavior of concrete is based on the smeared crack approach using the orthotropic model with the equivalent uniaxial average stress-strain relations in the axes of orthotropy. The axes of orthotropy are assumed to coincide with the principal axes of total strain, and this model is developed in a tangent stiffness-based approach in order to be used in a general nonlinear finite element program. In addition, this concrete model incorporates characteristics from the models of the University of Houston's Group, like the CSMM presented by Zhong [157] in 2005 and the models from the University of Toronto's Group, like the expanded MCFT developed by Palermo [105] in 2002, and Palermo and Vecchio [106] in 2003 and the concrete model by Vecchio [136] in 1992, and other additional models to consider the influence of biaxial compression or tension-compression (softening) in the axes of orthotropy, and also to account for damage in the material during cycling loads and enhancement due to confinement. The selection of the different features for the model presented were done to be able to use the layered section approach developed in the last chapter, and also to obtain a numerically stable, reliable and efficient constitutive material.

The behavior of the concrete in the principal directions of stress, which coincide with the principal directions of strain, are defined by average uniaxial stress-strain relations. In this study the average uniaxial stress-strain relations are represented by uniaxial concrete

material models. Two uniaxial concrete materials were selected to represent the average uniaxial stress-strain relations for the principal directions of stress for this smeared rotating angle concrete model. The two material models are: the one proposed by Massone [90] in 2006 for static load and after extended to include hysteretic rules, also developed by Massone on OpenSees [82], as the uniaxial concrete material “*Concrete06*” in OpenSees [82]. The second model is a simplified Chang-Mander model proposed by Waugh [147] in 2009. In addition, in the next chapters, the first model is referred to as the proposed smeared plane stress concrete model with Thorenfeldt’s curve when the smeared rotating angle concrete model is used with the uniaxial material model proposed by Massone [90] in 2006. And it will be referred to as the proposed smeared plane plane stress concrete model with Chang-Mander Model when the smeared rotating angle concrete model using the simplify Chang Mander Model proposed by Waugh [147] in 2009 is used.

In addition, in this chapter the smeared steel constitutive material used to represent the horizontal and vertical reinforcement steel layers in the membrane and shell element was presented. In this approach, it is assumed that the steel bars are considered as a layer of homogenous material at certain positions inside the reinforced concrete element and the variation stress due to cracking over an area can be modeled using the average stress-strain of steel in that zone. In addition, it will be assumed that the smeared steel works only in the direction of the bar since to the bars are typically in a uniaxial state of stress, and this allows the use of a uniaxial constitutive model. Two uniaxial steel material models are used in this study, the one proposed by Mansour et al. [88] in 2001 knowns as the Mild Steel Bar Embedded in Concrete Model, and the well known Menegotto and Pinto Steel model proposed by Menegotto and Pinto [94] in 1973.

Chapter 5

Finite Element Implementation

The finite elements method is the most common approach used today to study the response of linear and nonlinear steel or reinforced concrete structures such as frames, walls, frame-wall buildings, or single elements. This is true not only in research, but also in design offices where the use of finite element software, like SAP2000 and ETABS [38], for the linear analysis of stresses and demands over structures due to static and dynamic loads are almost a standard. The finite element is a very powerful method because it allows one to take into account the geometric behavior and the nonlinear constitutive relationships of structures [122], and especially the complex behavior of the nonlinear constitutive relationship of concrete and the embedded steel bars in concrete [157]. Previously, nonlinear analysis of complex structures using finite elements was a very complex endeavor and computationally expensive. However, today it is becoming possible to use this analysis approach due to the recent advancements in computer capability and the application of more stable, and easier implementation of open source algorithms and finite element codes, as was also mentioned by Zhong [157].

The finite element analysis programs are typically structured in five steps: (1) building of the structural model (nodes, elements, loads, boundaries conditions), which are related to the geometry of the model, (2) definition of the constitutive material law that defines the behavior of each element, (3) assembly of the system of equations that define the type of analysis performed over the structure, (4) solving of the linear or nonlinear system of equations, and (5) recording of the results of the analysis or visualization of the results [122, 157].

Two type of approaches are used to develop finite elements programs, the procedural and the object-oriented approach [93, 122]. In the procedural approach the program is represented by the assemblage of a set of subroutines or functions that act over the variables stored globally, to solve the system of equations. This approach is difficult to modify or to reuse the code, because of the dependence of the functions on the global variables [122, 123], and a deep knowledge of the structure of the code are needed to be able to extend the libraries to new materials, elements, and algorithm [93]. In the literature, the majority of the available finite element softwares available use this type of approach because they are faster, and more straightforward to program, like DRAIN [143] and FEAP [131]. The Object-Oriented approach for finite elements involves the abstraction of the components used in the analysis, which where reviewed in the five steps above, and representing theses abstractions as a collections of objects communicating and interacting between them. This approach allows the maintainability and extensibility necessary for expansion of finite element packages [93]. In addition, this type of approach is one of the most used programming paradigms for the development of software, frameworks and operating systems, due to their main characteristics such as abstraction, polymorphism,

encapsulation, messaging, inheritance and modularity [78]. The most used and important implementation of this approach for nonlinear structural analysis is OpenSees [82]. From these two approaches, the object-oriented is the optimal to produce modular and reusable finite element software.

Typically, to perform nonlinear analysis of structures, researchers are limited to the use of some of the commercial finite element software or programs, like SAP2000 and Perform3D [38], that are limited to some type of nonlinear analysis, elements, or constitutive material laws. In addition, these programs are commonly black boxes, which cannot be modified or expanded by the user. Other options are the use of more flexible programs with extensive libraries of elements and materials like ADINA [3], or ABAQUS [51]. In addition, ABAQUS allows the incorporation of new material laws through the use of the UMAT subroutine. In non-commercial programs, the options are the use of open source programs like FEAP [131], and OpenSees [82], or other packages available in the literature by simply using the extensive libraries that are available in the precompiled binary of the programs. If the researchers need to modify or extend the packages, the user needs a more deep knowledge of various programming languages, due to the required compilations of different libraries used in the programs to perform the analysis. However, these are the more powerful and faster options for nonlinear analyses. In other cases, the researchers can use a more friendly but powerful programming environment like Python [50] or MATLAB [62] to develop their own routines to implement new algorithms, elements, and materials. However, these routines are specific for the problem being studied and may be difficult to reuse. An open source framework for the linear and nonlinear analysis of structures under static and dynamic loads that use the object-oriented approach in MATLAB [62], which

allows easy reuse of the code, and quick implementation and testing of new algorithms, solution strategies, elements, and material laws, has not been developed before. Only some approaches like FEDEASLab [46] that use procedural methodology and a structure-data approach for the management of the elements, nodes, loads, and results, or other libraries, in which the base of the program is an external package or software that is connected to MATLAB [62]. Other option is the use of more simple procedural functions for the finite element analysis that have been implemented and available in the literature.

In the next sections of this chapter an overview of the Object-Oriented approaches used for Finite Elements is presented, and in particular the approach proposed by McKenna [93], which has been extended to OpenSees [82]. Also, a review of the finite element toolbox available for MATLAB [62] is briefly discussed. The abstractions of the components for finite element and structural analysis proposed by McKenna [93] in 1997 and extended in OpenSees [82] are used to develop the proposed Object-Oriented Finite Element Toolbox for MATLAB [62]. This proposed toolbox uses the object oriented programming language under MATLAB [62]. In addition, the nonlinear analysis algorithm used in this study will be reviewed.

5.1 Object-Oriented Approaches for Finite Elements

The object-oriented approach for finite elements, as was mentioned before, involves the abstraction of the components used in the analysis, and representing these abstractions as a collection of objects communicating and interacting between them. In order to determinate these objects, as Fenves [44] mentioned in 1990, three steps need to be done: first, selection of the classes (identifying patterns and defining the different classes of

objects necessary to be used to represent the finite element method), second, specification of the classes (defining the methods or operations that each of the classes can perform to solve the finite element analysis), and third, implementation of the classes (selection of the properties or variables encapsulated by each object and the specific operations that are programmed in each method or member functions).

The object-oriented programming paradigm is a form of programming in which the programs are organized around the objects, and the program can be represented as a collection of these objects interacting between each other [78]. The object is composed of properties or variables that are typically private, which means only the object has access to them, and methods or functions that operate over the data or properties in the object. The methods or member functions are the preferred form of communication between the objects, and recovery of information from them. Classes are the implementation in a programming language of the objects with similar properties and methods [93], and a class can be thought of as the template for a type of object in a program.

The object-oriented programming style has been proven to produce a balance between maintainability, extensibility, and reusability necessary for software development. This is due to the characteristic of the object-oriented programming approach that are abstraction (separation of the implementation from the behavior), encapsulation (the data or variables, and specific algorithm are enclosed in the object definition only), messaging (the interface between different objects is through messages or calling of the methods or member functions defined in each object), inheritance (subclass inherited the properties and methods from the super classes) and modularity (each portion of a program can be grouped in a set of classes or a single classes, which allows that future modification can be

applied only to the necessary classes, or if a portion of the program that does something special, it can be reused easily in other implementations) [78, 93].

Implementations of finite elements using the object oriented representation have been developed and studied by different researches in the past years. A complete literature review of this topic was done by McKenna [93] in 1997, and also a brief review was done by Scott [122] in 2004. McKenna [93] in 1997 grouped the necessary classes to use in a finite element into four groups, and performed a review of the different implementations proposed in the literature using these groups. The groups are: (1) Modeling classes (classes used to create the model for an specific problem), (2) Finite Element Model classes (classes used to represent the model like nodes, elements, constraints, loads), (3) Analysis classes (classes used to perform the type of analysis, such as linear or nonlinear and static or dynamics, using different the solution algorithms, and iterative methods), (4) Numerical classes (classes used to manage the numerical calculations and operations in the solution strategies). McKenna [93] in 1997, extended the finite element model classes available in the literature and proposed a new abstraction of the analysis algorithm. McKenna [93] also proposed additional abstractions for the implementation of the finite element using parallel computing. The work of McKenna [93] in 1997 was used as the base for the development of the Open System for Earthquake Engineering Simulation called OpenSees [82] framework. This framework also includes additional extensions done by Scott [122] in 2004, to use geometric transformation in the beam-columns elements, some nonlinear uniaxial materials, and sensitivity analysis for beam-column elements. OpenSees [82] is the most well known open source implementation of the object-oriented approach for nonlinear structural analysis and simulation using finite elements used by structural and geotechnical

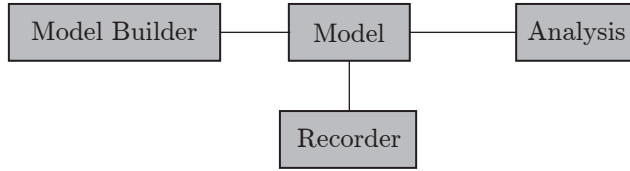


Figure 5.1: Main Abstractions in OpenSees [82] Framework

engineers in earthquake engineering. The following is an overview of the abstraction and class definitions done and presented by McKenna [93] in 1997 and extended and presented in OpenSees and it's user manuals [82].

OpenSees [82] is a framework developed primarily under the object-oriented programming language of C++, and has additional libraries written in C and Fortran [82]. OpenSees is defined with the concept that super classes, like elements, materials, constraints, loads, solutions algorithm, etc, are abstract classes that define the methods or member functions necessary to create the interface of the class in the framework, and the subclasses of these abstract classes define the implementation for each of the components [92]. This structure allows for the implementation of new elements and materials, solution algorithm, numerical solutions, and only needs to define the member function defined in the interface of their abstract classes, and with this, the new subclasses can be incorporated in the framework without any change in the existing code [157]. This promotes the interchangeability and modularity necessary in finite elements.

OpenSees [82] is divided into four main abstractions or types of objects, see Fig. 5.1, Model Builder, Domain, Analysis and Recorder. The Model Builder Class is responsible for the creation of the objects that represent the model (nodes, elements, constraints, load patterns, loads) of a specific problem, and adding them to the Domain Object. The

Domain Class is an object that stores the components of the model and provides the methods to add and remove, access, update the state, commit the state, and obtain information of the components in the Domain, and finally connect the model components with the Analysis and the Recorder object.

The components of the Domain defined by McKenna [93] in 1997 and OpenSees [82] are mainly: nodes, elements, constraints, and loads. Each of this components are subclasses of a domain component (DomainComponent) class, that is a subclass of a TaggedObject and MovableObject which provide part of the interface that allows the finite element analysis to occur in parallel or distributed computers or clusters [122]. The Element class is an abstract class that defines the interface of the different types of elements (subclasses) created in the framework. In addition, its provide the interface to obtain the stiffness, mass, damping, and resisting force of the element, and commits, updates the state of the element at the current step of the analysis. The element is typically composed by a section or material objects and in some cases of a geometric transformation objects. The Node class is the abstract representation of a point or node in the model of the structure, which stores the coordinates of the node, and the current values of the state of the node, like displacement, and unbalance loads. The Constraint class, is divided into single point constraints (SP_Constraint) and multi-point constraints (MP_Constraint), depending on whether the constraint involves only one node or multiple nodes. In OpenSees [82] the Constraint class does not enforce the constraints, it only stores the data with the information of the constraint and the state of the constraint at the current step. The Load Class is divided into NodeLoad and ElementLoad, depending on whether the load acts over a

Node or an Element Class, and also provides the interface to apply the load over the nodes and elements, and store the information necessary to apply the load at the current step.

The Analysis Class, proposed by McKenna [93] in 1997, is the abstract representation of the solution procedure for the finite element analysis that can be static or dynamic. This means, it is responsible to check the components of the analysis, create the necessary links between the objects, inform to the objects in the analysis that the model has changed, and perform the analysis. It is typically formed by the following classes: AnalysisModel, SolutionAlgorithm, Integrator, ConstraintHandler, DOF_Numberer, SystemOfEqn, and ConvergenceTest. The AnalysisModel class is a container class that permits storage of the objects that handle the Nodes and the Element objects during the analysis, DOF_Group and FE_Element, respectively. These objects are responsible for keeping the information of the DOF associated with their objects (Nodes, and Elements), enforce the constraints, and add the unbalance loads to the system of equation for the nodes and the stiffness, mass, and damping, and resisting force for the elements. The SolutionAlgorithm class is responsible for performing the specific solution procedure by invoking the methods of the other components of the analysis class. Examples of this in OpenSees [82] are, Newton-Raphson, Newton-Rahpson with Line Search, and Accelerated Newton. The Integrator Class is responsible to set, update, and add the contribution of the different components of the AnalysisModel to the System of Equation. Examples of this class in OpenSees [82] are the Load control, Displacement control or ArchLength for static analysis and the Wilson- θ , Newmark, Huilbert-Hugues-Taylor (HHT) methods for the dynamic analysis. The ConstraintHandler class is responsible for establishing the constraints, and creating the DOF_Group and FE_Element objects. The DOF_Numberer class is responsible for

defining the numbering of the DOF in the system of Equations. The SystemOfEqn class is responsible for storing the system of equation, and solve numerically the system of the equation with the specified Solver Class. The ConvergenceTest class is responsible for determining if the iterative solution algorithm selected has converged to a solution within the error desired.

The Recorder Class in OpenSees [82] is responsible for recording or storing in a text file, in the data bases, or other types of files, and also monitoring the state of each of the components in the Domain object during each step in the analysis.

5.2 Finite Elements Toolbox for MATLAB

MATLAB [62] is a user-friendly and very powerful software and programming environment that is extensively used in the research and academic community because it allows a quick development and testing of new algorithms, theories, data analyses, and visualization. In addition, it allows the use of the vast libraries of mathematical algorithm, functions and toolboxes, like linear algebra, optimization, digital signal processing, neural network, curve fitting, statistics, control system, and many other available in the software, without any difficulty during the development of routines or programs. In addition, MATLAB [62] can be classified as an interpretative or scripting language, that allows developing routines or programs using both procedural and object-oriented programming.

In the following section, the different options available for performing finite element analyses under MATLAB [62] and reviewed, and following that the proposed object oriented finite element toolbox for Matlab using the object oriented programing language

under MATLAB [62] and the abstraction for finite element proposed by McKenna [93] and extended in OpenSees [82] is presented.

5.2.1 Review of Finite Element Toolbox for MATLAB

A need for a powerful toolbox or framework that will be easy to use, extend, maintain, and modularize for the nonlinear structural analysis or finite element analysis under MATLAB is a constant issue in the research community. Typically, as was mentioned before, researchers develop their own routines to implement new algorithms, elements, and materials in a procedural programming approach. These routines typically are specific for the problem being studied and are difficult to reuse or modify due to the dependence on global data. Other options are the use of routines, typically focused on linear analysis, like the ones proposed in the books by Ferreira [45] in 2009 or Kattan [68] in 2008. Or use other noncommercial options, such as FEDEASLab toolbox [46] which is focused on nonlinear structural analysis. Among the options reviewed for structural analysis using MATLAB [62], FEDEASLab [46], which uses a procedural methodology, is the preferable option. FEDEASLab [46] is a toolbox developed mainly by Prof. Filippou and his students at the University of California, Berkeley, since 1998 and is inspired by FEAP [131], but adapted to MATLAB [46]. A brief review of the FEDEASLab toolbox presented by Filippou and Constantinides [47] in 2004 and in FEDEASLab's webpage [46] follows.

FEDEASLab toolbox ([46],[47]) is an intuitive, versatile and powerful toolbox used for the linear and nonlinear analysis of structures under static and dynamic loads, that was developed using a procedural programming style. Its structure is based on a series

of functions grouped by different categories, like general, geometry, utilities, output, element library, section library, material library, and solution library that works over a global data. This global data is divided into five basic data structure objects and one optional. The five data structures are: Model (keeps the model geometry and DOF numbers), El-
emData (represents the information with the properties of the each element, like type element, section, material, geometric transformation), Loading (stores the information of the loads over the nodes and elements and the load histories, and the enforced displacements that will be applied during the analysis), State (stores the response of the structure, like displacement, velocity, acceleration in the nodes, stiffness, mass, damping matrix, and response in the elements), SolStrat (stores the static or dynamic parameters used in the solution procedure), and the optional structure data is the Post (stores the information necessary for post-processing of the analysis). In addition, FEDEASLab allows the post-processing and visualization of the results of the analysis. It has mainly element libraries for beam-columns elements, with different approaches, like lumped plasticity, nonlinear hinges, spread plasticity, fiber sections, and different type of analysis, like second order, P- δ , and corotational. Also, FEDEASLab allows the use of different solution strategies, for static (load control, arc-length, and others) and dynamic analysis (Newmark, Wilson- θ , and others) [47]. Even though this is a procedural approach, it presents an easy structure that can be understood quickly, and allows an easy implementation of new elements of type beam-column if the users wants. However, this toolbox is distributed through p-code file type, this type of file distribution for MATLAB [62] does not allow review of the code in the functions, which is necessary for making modifications. In addition, an important

factor could be the computational cost used to pass the data structure to the different functions during the analysis for large models.

5.2.2 Proposed Object-Oriented Finite Elements Toolbox for MATLAB

Due to the options available for the finite element analysis using MATLAB [62], and the conclusions of past studies showing that the object-oriented programming paradigm is the most flexible, modular and easy to expand and maintain approach to develop finite elements frameworks, it was decided for this study to develop a Finite Element Toolbox using the object oriented programming language under MATLAB [62], without the need to couple MATLAB [62] to external software or libraries. This allows a seamless transportability of the framework or Toolbox between the version of MATLAB [62] for the different operative systems, which creates a user-friendly but powerful framework that is easy to use, expand, maintain, and understand by researchers with different levels of knowledge in programming languages.

First, it is important to present some of the symbolic notations and nomenclature used in the object oriented programming language under MATLAB (Fig. 5.2). The main nomenclature, mention in the references [62, 78], which are common to different object-oriented programming language are:

1. **is-a**: the is-a relationship indicates that a class is a subclass of another, which means the object or class is a decedent of a super class.
2. **has-a (aggregation)**: the has-a aggregation relationship indicates that a class has as property other objects, but they are not owned by the object and can live outside of the object.

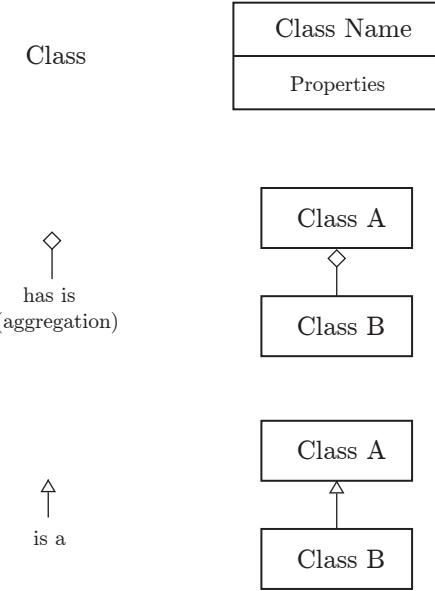


Figure 5.2: Class Diagram Notation used in MATLAB [62]

3. **has-a (composition)**: the has-a composition relationship indicates that a class has as property other objects that are owned by the object, and cannot live outside of the object.

The Classes in MATLAB are written in m-file type, following a certain structure, (heading of the class, properties, methods and events), see Fig. 5.3. The heading indicates that the file contains a class definition, and which is the type of class, and the attributes of the class, and if the new class is a subclass of others. The properties are the variables encapsulated by the object, and their attributes indicate if the variables are public, private, etc. The methods define the different functions that act over the properties in the object, and return the information requested to the objects or add data to the object. The class can be divided in value classes or handle classes. The difference is that the constructor of a value class returns an instance of the class and relates that instance with the variable, and

```

classdef (attribute - name = expression, ...) ClassName < SuperClass
    properties (attribute - name = expression, ...)
        ....
    end
    methods (attribute - name = expression, ...)
        ....
    end
    events (attribute - name = expression, ...)
        ....
    end
end

```

Figure 5.3: MATLAB's Class Definition structure

if the variable is reassigned the variable creates a copy of the original object, and if the object is passed to a function the function makes a copy of the variable, and the variable outside of the function is not modified by the code inside of the function. Instead, in the handle class, the constructor returns a handler of the object, this mean that when it is reassign or passed to a function the program is only passing the reference to the actual object and no copy of the object is done [62]. Due to this difference, in this study all the classes used are subclass of the handle class, this allows the data to maintain uniqueness, and the programs run faster because less information is sent between callings of methods and functions.

The Toolbox proposed here follows the abstractions of the components for finite element and structural analysis proposed by McKenna [93] in 1997 and extended in OpenSees [82]. Due to these abstractions produced a more flexible and modular, and reusable framework. However, some modifications are included to adapt the abstractions to MATLAB [62]. The following is a review of the final abstractions used in this proposed Toolbox to define the finite element analysis that was implemented and used for the analysis presented

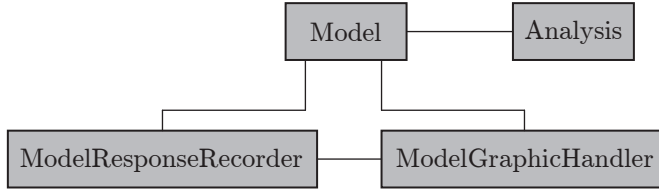


Figure 5.4: Main Abstractions in the proposed Toolbox

in the next chapter in this study. In addition, in this study the proposed Object-Oriented Finite Elements Toolbox will be referred to as either indistinguishable the Toolbox or Framework

This Toolbox is divided into four main abstractions or types of objects: Model, Analysis, ModelResponseRecorder and ModelGraphicHandler, see Fig. 5.4. The Model Class is a container object that holds the ModelComponent objects , like Node, Element, Constraints, LoadPatterns, and provides the methods to add, remove, access, update the state, commit the state, and obtain information of the components in the Model, and connect the ModelComponents objects with the Analysis, the ModelResponseRecorder and the ModelGraphicHandler object. This Model class is similar to the abstraction proposed by McKenna [93] in 1997 and extended in OpenSees [82] for the Domain Class, only with changes to some of the names and some methods or member functions, to include the ModelResponseRecorder and ModelGraphicHandler.

The components stored in the Model, see Fig. 5.5, as mentioned before, are: Nodes, Elements, Constrains, LoadPatterns, Loads. Each of these components are subclasses of a ModelComponent, that is a subclass of a TagObject and ClassTagObject. These model

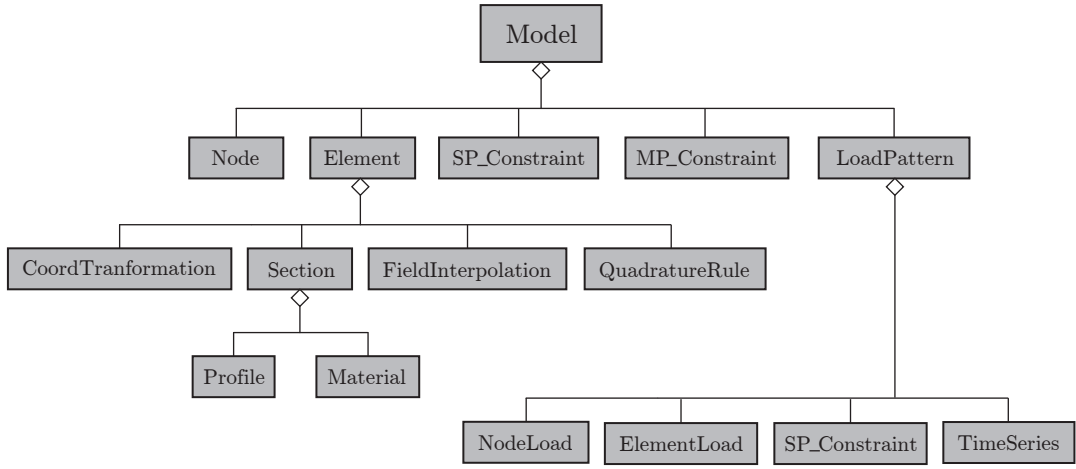


Figure 5.5: Model abstraction in the proposed Toolbox

component class are similar to the abstraction proposed by McKenna [93] in 1997 and extended in OpenSees [82] with minimal modifications.

The Element class is an abstract class that defines the interface of the different types of elements (subclasses) created in the framework, and provides the interface to obtain the stiffness, mass, damping, and resisting force of the element, commit, and update the state of the element at the current step of the analysis. The element is composed of a Section object, and has a set of Nodes that define the geometry of the element, in some cases it also has a geometric transformation object, see Fig. 5.5. Similar to the abstraction proposed by McKenna [93] in 1997 and extended in OpenSees [82] with minimal modifications. The Section object is also a subclass of the ModelComponent class, and is composed of a profile object and one or more Material Objects, which are also ModelComponent Objects.

The Node class is the abstract representation of a point or a node in the model of the structure, which stores the coordinates of the node, and the current values of the state of

the node such as displacement, and unbalanced loads. Similar to the abstraction proposed by McKenna [93] in 1997 with minimal modifications.

The Constraint class, can be classified in single point constraint (SP_Constraint) or multi point constraint (MP_Constraint) depending on whether only one node or multiple nodes are involved. Similar to OpenSees [82] the Constraint class does not enforce the constraint, and it only stores the data with the information of the constraint and the state at the current step of the constraint.

The LoadPatterns Class is the abstract representation of the load pattern applied to a structure in finite element, and it is implemented as a container class that stores the Load Objects, such as Node Loads, Element Loads, or Earthquake Loads. These objects are also subclasses of the ModelComponent class. In addition, as in OpenSees [82], this class also could store constraints if these depended on the load history, and also store the information necessary to apply the load at the current step (load histories), and provides the interface to apply the load over the nodes and elements.

The Analysis Class is the abstract representation of the solution procedure for the finite element analysis that can be static or dynamic, and is responsible to check the components of the analysis, create the necessary links between the objects, inform to the objects that the model change, and perform the analysis. Also, It is typically formed by the following classes: AnalysisModel, SolutionAlghorithm, Integrator, ConstraintHandler, DOFNumberer, SystemOfEq, and ConvergenceTest, see Fig. 5.6. Each of this components of the analysis are subclasses of a AnalysisComponent, that is a subclass of the ClassTagObject. The main subclasses of the Analysis class are the StaticAnalysis class and a DynamicAnalysis Class. The Analysis class and their components are similar to

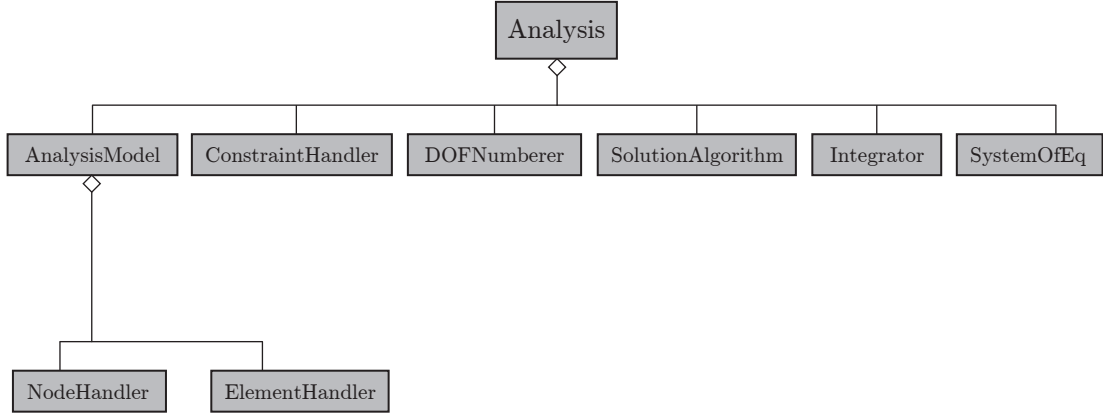


Figure 5.6: Analysis abstraction in the proposed Toolbox

the abstractions proposed by McKenna [93] in 1997 and extended in OpenSees [82], with minimal modification in the names and minimal changes in the methods in the classes to be able to adapt the classes to MATLAB [62]. These analysis components are reviewed next.

The AnalysisModel class is a container class that storage the object that handle the Nodes and the Element objects during the Analysis, NodeHandler and ElementHandler, respectively. These objects are subclasses of an AnalyisModelComponent class. The NodeHandler and ElementHandler are responsible for keeping the information of the DOF associated to the objects that these classes handle in the Model Object, and enforce the constraints, add the unbalance loads to the system of equation for the Nodes and the stiffness, mass, damping matrix, and resisting force vectors for the elements.

The SolutionAlgorithm class performs the specific solution procedure by invoking the methods of the other components of the analysis class. The Newton-Raphson, Modified Newton-Raphson, and Linear method have been implemented until now in this toolbox.

The Integrator Class is responsible to set, update, and add the contribution of the different components of the AnalysisModel to the System of Equation, which means it forms the system of equations of the analysis. The methods programmed so far in this toolbox are the Load control, Displacement control, and Arch Length for static analysis, and the Wilson- θ , Newmark, Huilbert-Hugues-Taylor (HHT) , Central Difference methods for dynamic analysis.

The ConstraintHandler is responsible to establish the constraints, and create the NodeHandler and ElementHandler objects.

The DOFNumberer class is responsible for defining the numbering of the DOF in the system of Equations.

The SystemOfEq class is responsible to store the system of equation, and solve numerically the system of the equation with the use of the mathematical libraries in MATLAB [62]. This toolbox includes until now a LinearSystemOfEq class that has as subclass the full general linear system of equation (FullGenLinearSystemOfEq), and Sparse General Linear system of equation (SparceGenLinearSystemOfEq).

The ConvergenceTest class is responsible to determinate if the iterative solution algorithm selected has converged to a solution below the error desired.

The ModelResponseRecorder Class is the abstract representation of the storage of the result and state of the different components in the Model Object. It is implemented as a container class that stores and saves to a file the response recorded from the model components, using the response recorder of the model components. It is also connected to ModelGraphicHandler objects to provide the recorded information for the visualization in

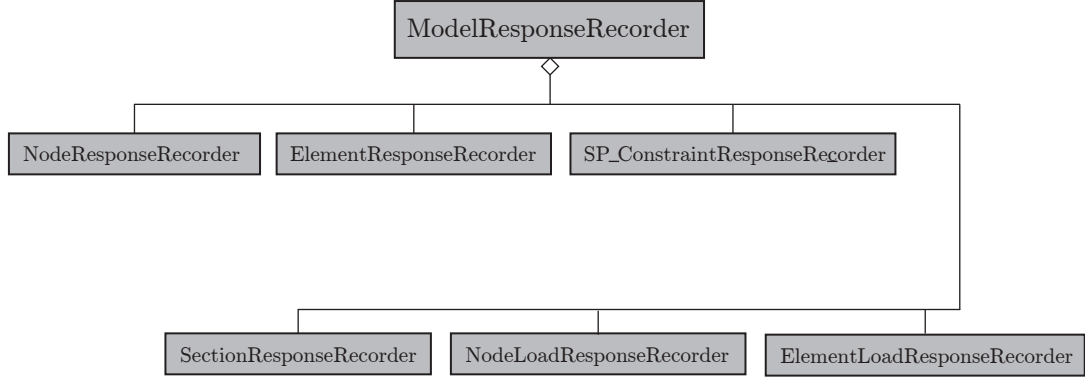


Figure 5.7: Model response recorder abstractions in the proposed Toolbox

the post-processing part. These response recorder components are subclasses of the ModelComponentResponseRecorder class, and each of this component is related with one component in the Model Objects. The components in the ModelResponseRecorder object are: NodeResponseRecorder, ElementResponseRecorder, ConstrainResponseRecorder, LoadResponseRecorder, SectionResponseRecorder, MaterialResponseRecorder, see Fig. 5.7. Each ModelComponentResponseRecorder object is responsible for the storing and recording the state of the corresponding ModelComponent.

The ModelGraphicHandler Class is the abstract representation of the visualization of the Model Object and their result during the analysis. The ModelGraphicHandler Class is implemented as a container class that stores the graphics handlers of the model components, and the axes handles, which are the canvas where the model are drawn or visualized. In addition, it is in charge of orchestrating the visualization or drawing of the model, their components and the results at each step of the analysis in the axes of a figure in MATLAB [62]. These components are subclass of the ModelComponentGraphicHandler class, and each of these components are related with one component in

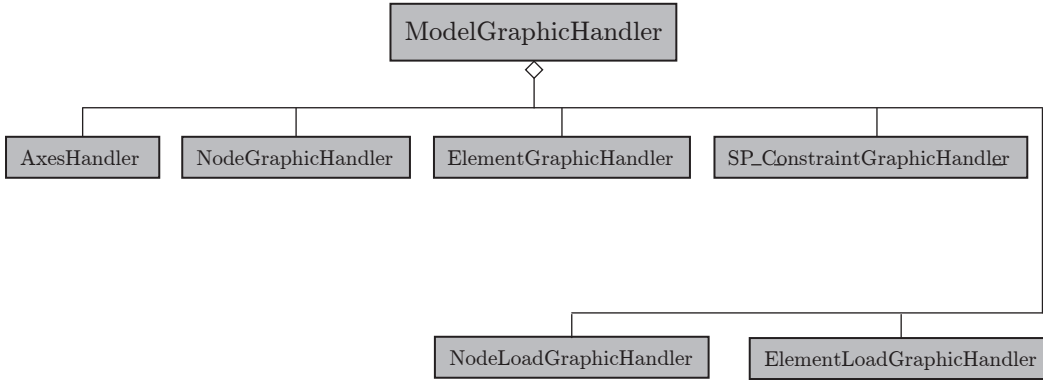


Figure 5.8: Model Graphics abstractions in the proposed Toolbox [92]

the Model Objects. These graphic handler components stored in the ModelGraphicHandler object are: NodeGraphicHandler, ElementGraphicHandler, ConstrainGraphicHandler, LoadGraphicHandler, LoadPatternGraphicHandler, see Fig. 5.8. Each of the ModelComponentGraphicHandler objects is responsible for the implementation of the visualization of the model component that handles graphically, and their resulting storage in the ModelResponseRecorder object. In addition, ModelComponentGraphicHandler has a different set of PencilGraphic objects that define the color and format used to draw the model components

5.3 Incremental Iterative Solution Algorithm

The nonlinear analysis of reinforced concrete wall structures is a highly nonlinear system. This type of analysis needs the implementation of an incremental iterative solution algorithm to solve the linearized nonlinear system of equations, which is created from the assembly of the current stiffness matrix and the unbalanced load in the structure. A simple incremental approach is not used because it may lead to an excessive accumulation of

errors [157]. Since the analysis in this study can be considered as quasi-static, incremental iterative solutions using a Newton-Raphson with load-control or a Newton-Raphson with displacement-control solution strategy can be used. A nonlinear quasi-static analysis for monotonic or cyclic load refers to the fact that the application of the loads do not produce any dynamic effects in the analysis, because the loading process is performed at a slow rate [103].

Different Newton-Raphson strategies can be used, like Full Newton-Raphson (the stiffness tangent of the system is updated at each iteration) or Modified Newton-Raphson (the stiffness matrix of the system is updated only at the beginning of each step). However, it was decided to use the Full Newton-Raphson because it produces a faster convergence rate (less number of iterations), but with a computational cost due to the continuous updating of the stiffness matrix for the structure. The main difference between a load control and a displacement control approach is that in the load control only the load value over the system is managed at each step, which means the load is considered as the independent variable. In the displacement control approach, a dominant displacement in the system is controlled, and at each step and during each iteration the force applied and the increment displacement in the rest of the system is controlled by a set of parameters until it converges on the equilibrium solution. The following section presents the Displacement Control Iterative Algorithm used in this study. The Load-Control Iterative Algorithm is presented for the sake of completeness of the presentation.

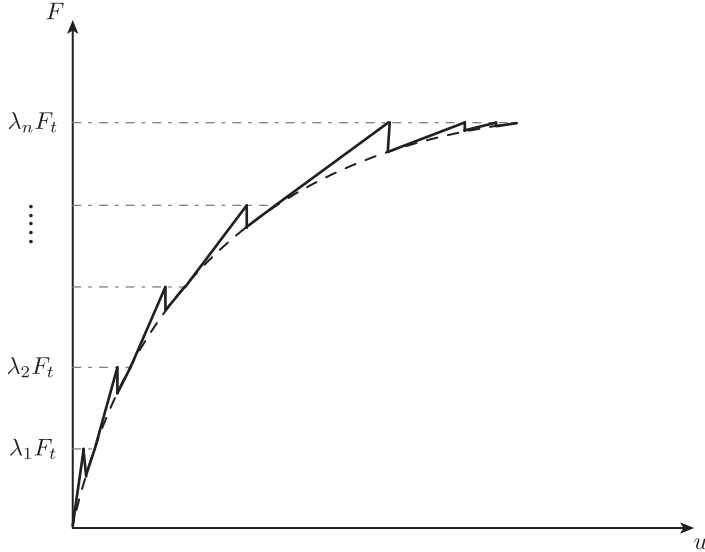


Figure 5.9: Full Newton-Raphson with Load-Control Iterative Algorithm

5.3.1 Load-Control Iterative Algorithm

This increment iterative algorithm is the most common solution used to perform nonlinear analysis, because it is obtained directly from the implementation of the Newton-Raphson methods. It is based on application of the load over the system in steps defined by a load parameter λ , as $\lambda = 0.1, \dots, 1$, and at every time step the new load step is applied in an iterative procedure is done until convergence is obtained, see Fig. 5.9. This method relies only on the stiffness tangent to continuously search for the equilibrium solution of the residual equation at each step [122].

This can be expressed in mathematical form using the residual equation obtained from virtual work for a structural system at each iteration as:

$$\text{Residual } (U^i) = \lambda F_{\text{external}} - R^i \quad (5.1)$$

where $F_{external}$ is the total final load that will be applied to the system, λ is the factor that controls the increment of the load in the system, and R^i is the resisting force of the structural system.

Linearizing the *Residual* $(U'^i + \Delta U'^i)$ using a Taylor expansion and excluding high order terms:

$$Residual(U'^i + \Delta U'^i) = Residual(U'^i) + \frac{\partial Residual(U'^i)}{\partial U'^i} \Delta U'^i \quad (5.2)$$

and performing the derivative over the *Residual* equation, one finds the stiffness tangent of the system:

$$\frac{\partial Residual(U'^i)}{\partial U'^i} = - \underbrace{\frac{\partial R^i}{\partial U'^i}}_{K_t^i} \quad (5.3)$$

and substituting Eq. 5.3 into Eq. 5.2, the iterative increment solution can be written as Eq. 5.4 because it is assumed that the residual $Residual(U'^i + \Delta U'^i)$ will be zero for the equilibrium solution

$$K_t^i \Delta U^i = \lambda F_{external} - R^i \quad (5.4)$$

A drawback of this incremental iterative algorithm is that it cannot be used and does not converge in the case of softening or snap-through or load limit point, or when the stiffness matrix become nearly to singular. This failure in the analysis does not indicate that the structure has collapsed, only that the solution method is not able to converge to a solution, as was mention by [7] in 1998 and Zhong [157] in 2005.

5.3.2 Displacement-Control Iterative Algorithm

Different researchers have proposed different methods, like arch-length by Riks [119] in 1972 or variations of this as was done by Crisfield [37] in 1981 or the Displacement Control Iterative Algorithm proposed by Batoz and Dhatt [10] in 1979, to overcome the disadvantages of the Load Control Iterative Algorithm. And these methods allow modelling of the complete load-displacement curve for complex nonlinear analysis that has softening, reduction of force due to cracking, snap-through, post-buckling, or local limits [157]. These methods typically control the displacement of one DOF over the structure, that is used as the independent variable [10], and iterate until convergence is reached. The following presents the algorithm proposed by Batoz and Dhatt [10] in 1979. In addition, here it is also followed the presentation of this iterative procedure done by Zhong [157] in 2005, with some modification and a constant displacement increment.

The increment displacement can be separated into two parts:

$$\Delta u = \Delta u_u + \Delta \lambda \Delta u_{ref} \quad (5.5)$$

where Δu_u is the increment displacement produced by the unbalanced load, Δu_{ref} is the increment displacement produced by a reference load, and $\Delta \lambda$ is the parameter that controls the load increment applied to the system.

Also, it is necessary to define a vector with only zeros, except the n^{th} DOF that will be used to control the displacement increment between steps, and it is used as the

independent variable. In the vector at the n^{th} DOF is assigned the value of 1 (Eq. 5.6), to be able to use a matrix approach to represent the algorithm.

$$\Gamma_n = \begin{Bmatrix} 0 & \dots & 0 & 1 & 0 & \dots & \dots & 0 \end{Bmatrix} \quad (5.6)$$

Now, it is possible to define the increment displacement using a first order approximation as:

$$\Delta u_u^i = (K_t^i)^{-1} P_u^i \quad (5.7a)$$

$$\Delta u_{ref}^i = (K_t^i)^{-1} P_{ref} \quad (5.7b)$$

where, K_t^i is the tangent stiffness at the i^{th} iteration, P_u^i is the unbalanced load at the i^{th} iteration, and P_{ref} is a reference load over the entire structure determinate at the beginning of the analysis, and that can be updated as the model changes.

Using the equations presented before the increment displacement for the n^{th} DOF can be expressed as:

$$\Gamma_n \cdot \Delta u = \Gamma_n \cdot \Delta u_u + \Delta \lambda \Gamma_n \cdot \Delta u_{ref} \quad (5.8)$$

For the first iteration a displacement of Δu_n for the n^{th} DOF is imposed, and assuming that a perfect convergence was achieved at the end of the last increment step, one obtains the $\Delta \lambda$ necessary at the initial iteration as:

$$\Delta \lambda^1 = \frac{\Delta u_n}{\Gamma_n \cdot \Delta u_{ref}} \quad (5.9)$$

which results in that the initial increment displacement for the system at the first iteration as:

$$\Delta u^1 = \Delta \lambda^1 \Delta u_{ref} \quad (5.10)$$

and the new load applied to the system is described by

$$\lambda_{NewStep}^1 = \lambda_{LastStep} + \Delta \lambda^1 \quad (5.11)$$

where $\lambda_{LastStep}$ is the load factor at the end of the iteration of the previous step and for the initial iteration of the current step the load in the system is:

$$P^1 = \lambda_{NewStep}^1 P_{ref} \quad (5.12)$$

Now for any other i^{th} iteration the displacement at the n^{th} DOF must be maintained constant, which results in Eq. 5.8 being rewritten as:

$$\Gamma_n \cdot \Delta u^i = \Gamma_n \cdot \Delta u_u^i + \Delta \lambda^i \Gamma_n \cdot \Delta u_{ref}^i = 0 \quad (5.13)$$

and using this one finds the next $\Delta \lambda$ (Eq. 5.12) necessary to proceed with the iteration as:

$$\Delta \lambda^i = - \frac{\Gamma_n \cdot \Delta u_u^i}{\Gamma_n \cdot \Delta u_{ref}^i} \quad (5.14)$$

where $\Delta u_u^i = \Delta u^{i-1}$, and this results in the next increment displacement for the whole system as:

$$\Delta u^i = \Delta u_u^i + \Delta \lambda \Delta u_{ref}^i \quad (5.15)$$

and the new load applied to the system is described by:

$$\lambda_{NewStep}^i = \lambda_{NewStep}^{i-1} + \Delta\lambda^i \quad (5.16)$$

and

$$P^i = \lambda_{NewStep}^i P_{ref} \quad (5.17)$$

This increment iterative algorithm just presented, a full Newton-Raphson with a incremental iterative displacement-control, is the selected solution strategy to perform the analysis in this study. It also allows modeling of the softening behavior of the concrete, and limit points that can occurs in analysis. This means the algorithm allows one to obtain the complete load-displacement curve for wall structures. In addition, this algorithm is selected because the experimental tests used to compare the accuracy of the proposed wall model are based typically on drift-controlled (monotonic and reversed or cyclic) experiments.

5.3.3 Convergence Criteria

Convergence criteria are necessary to determinate if an analysis has arrived at an equilibrium solution with the precision prescribed by the criteria tolerance. This is very important for iterative solution strategies, because these criteria determinate the end of the iteration process. Realistic criteria need to be used and evaluated at the end of each iteration to determine if the solution has converged or is diverging [9]. Different methods can be used to define the convergence criteria, this can be based on the nodal unbalanced

force, the displacement increment, the energy increment, or maximum component displacements. Typical convergence criteria that can be used in iterative solution algorithms for finite element can be found in different references or books on finite elements, such as [9, 103, 157].

Some example of the convergence criteria that can be used are:

$$\text{Force Criterion: } \frac{\|P_u^i\|}{\|P_u^0\|} < \text{Tolerance} \quad (5.18)$$

where P_u^i is the unbalance load at the i^{th} iteration, and P_u^0 is the unbalance load at the initial iteration for the current step.

$$\text{Increment Displacement Criterion: } \frac{\|\Delta U^i\|}{\|\Delta U^0\|} < \text{Tolerance} \quad (5.19)$$

where ΔU^i is the increment displacement at the i^{th} iteration, and ΔU^0 is the increment displacement at the initial iteration for the current step.

$$\text{Energy Criterion: } \frac{\|(\Delta U^i)^T P_u^i\|}{\|\Delta (\Delta U^0)^T P_u^0\|} < \text{Tolerance} \quad (5.20)$$

where ΔU^i is the increment displacement, and P_u^i is the unbalanced load at the i^{th} iteration, and ΔU^0 is the increment displacement and P_u^0 is the unbalanced load at the initial iteration

$$\text{Maximum Increment Displacement Criterion: } \max_k \left| \frac{\Delta U_k^i}{\Delta U_k^0} \right| < \text{Tolerance} \quad (5.21)$$

where ΔU_k^i is the increment displacement at the i^{th} iteration for the k^{th} DOF, and ΔU^0 is the increment displacement at the initial iteration for the k^{th} DOF for the current step.

In this study, the Increment Displacement Criteria and the Maximum Increment Displacement Criteria are used as the convergence criteria for determining when the iteration solution must stop.

5.4 Summary

The finite element programs are typically structured in five steps: (1) building of the structural model, which are related to the geometry of the model, (2) definition of the constitutive material laws that define the behavior of each element, (3) assembly of the system of equation that define the type of analysis performed on the structure, (4) solving of the linear or nonlinear system of the equation, and (5) recording of the results of the analysis or visualization of the results [122, 157]. With this basic conceptualization of the finite element (FE) in mind, two approaches can be used to develop FE programs , a procedural and the object-oriented approach. In the procedural approach the program is represented by the assembling of a set of subroutine or functions that act over the variables stored globally, to solve the system of equations. Instead, the Object-Oriented approach for finite elements involves the abstraction of the components used in the analysis, which were reviewed in the five steps above, and representing these abstractions as a collections of objects communicating and interacting between them. This approach allows a maintainability and extensibility necessary for finite element programs [93].

From the options for finite element using object oriented programming it was concluded that the abstractions proposed by McKenna [93] and which has been extend to

OpenSees [82], which is the most important framework used nowadays in the simulation of large models on earthquake engineering, are the best representation for developing a Object-Oriented Finite Element Toolbox for MATLAB [62]. This toolbox was done using the object oriented programing language under MATLAB [62]. The abstractions of the components for finite element and structural analysis proposed by McKenna [93] in 1997 and extended in OpenSees [82] were presented in this chapter, and also their extension for the developing of the proposed Finite Element Toolbox under MATLAB [62] used in this study.

MATLAB [62] was selected, because it is a user friendly, and very powerful software and programming environment, which is extensively used in the research and academic community, due to it allows a quick development and testing of new algorithms, theories, data analysis, and visualizations. Also, because there is a need for a powerful toolbox or framework in the research community that is easy to use, extend (developing of new elements, algorithms and analysis procedures, new materials), maintain, and modularize for the nonlinear structural analysis or finite element analysis under MATLAB [62] was required.

In addition, the nonlinear analysis algorithm, Full Newton-Raphson with an incremental iterative displacement-control, which is used to perform the analysis in this study, was reviewed. This solution strategy was selected, because it allows modelling of the softening behavior of concrete and limit points that can occur in the analysis. This mean, the algorithm allows to obtain the complete load-displacement curve for the wall structures.

Chapter 6

Evaluation and Verification of Analytical Results

Evaluation and verification of the new analytical model developed in this work against benchmarks or experimental results are a crucial step before the use of the model for numerical simulations of more complex structures in order to demonstrate the accuracy, applicability, limitations and usefulness of the new analytical models. In the case of reinforced concrete walls, which behave different under different load conditions and different configurations (single walls, coupled walls, wall sizes), a set of experiment results with different type of walls configurations and load conditions need to be used to verify the new analytical models.

The evaluation of the accuracy, applicability, and usefulness of the nonlinear layered quadrilateral membrane and shell element with drilling degrees of freedom proposed, and the constitutive model defined in the previous chapters in this study is presented in this chapter. In order to do this, a set of experimental results for reinforced concrete wall elements under monotonic and reversed load available in the literature, which are used as benchmarks for other models, are compared against the analytical model using the proposed elements.

The experiments results used in this dissertation are selected after a thorough revision of the available experimental results found in the literature. The experimental results can be divided into monotonic loading and reversed loading. For monotonic load this work uses one of the experimental results of the tests of a shear wall done by Cervenka and Gerstle and presented in Cervenka [24] in 1971, and the experiment results of the tests of two types of walls done by Lefas et al. [80] in 1990. For reversal or cyclic loading this work uses the experimental results of the tests of two rectangular single walls and two T-shaped cross section walls with slabs at four different levels done by Thomsen and Wallace [132] in 1995.

6.1 Monotonic Loading

The following section presents the evaluation and verification of nonlinear layered quadrilateral membrane elements with drilling degrees of freedom proposed using experimental test results under monotonic loads.

6.1.1 Reinforced Concrete Shear Wall - Cervenka and Gerstle

Cervenka [24] in 1970 presented the results for a series of tests using reinforced concrete shear panels. These panels were built and loaded in groups of two bounded by thickened ribs at each side of the panel that form a deep beam (Fig. 6.1). The loading was done at the middle of the deep beam specimen (center rib), which was simply supported at the end, as is shown in Fig. 6.1. The panel were 760 [mm] (30 [in]) height and 760 [mm] (30 [in]) wide with a thickness of 51 [mm] (2 [in]) or 76 [mm] (3 [in]), and also, the panels were reinforced with orthogonal reinforcement (Horizontal and Vertical) at the center of

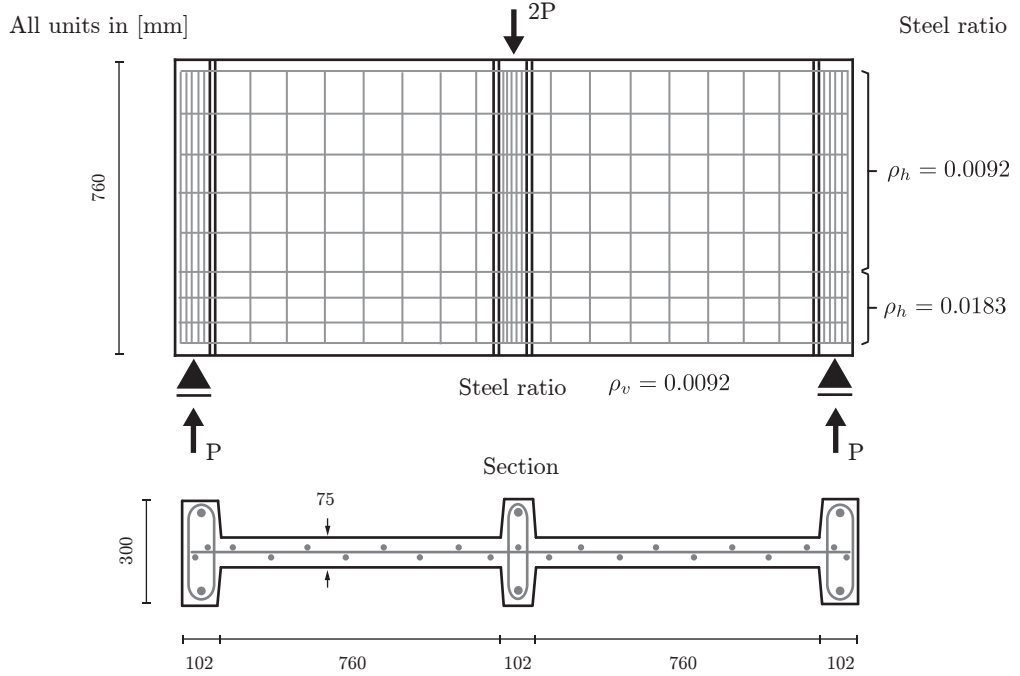


Figure 6.1: Geometry and Reinforcement Details of the RC Shear Panel W2

section of each panel (Fig. 6.1). Beside the difference in the thickness of the specimens, the panels were built with different amounts of steel assigned at each direction, some with lightly reinforced ratios and other with more heavily reinforced ratios and with variation of steel ratios in the orthogonal directions.

For the validation of the proposed analytical model, the reinforced concrete shear panel W2 was selected, which has been used as benchmarks before by other authors ([40], [135], [7]). This test was selected, because the specimen has a variation of ratio of horizontal steel over the height of the model, and constant ratio of steel in the vertical direction (Fig. 6.1), which make the model an interesting case study.

The geometry of the panel W2 is 76 [mm] (3 [in]) thick, and 760 [mm] (30 [in]) wide by 760 [mm] (30 [in]) height, and has a thickened ribs of 300 [mm] (11.75 [in]) by 102

[mm] (4 [in]), as is shown in Fig. 6.1. The horizontal reinforcement ratio in the panel is 0.92% in the top portion of the panel and 1.83% in the lower 150 [mm] of the panel, and the vertical reinforcement is constant over the length of the panel and is equal to 0.92%. For the horizontal and vertical reinforcement bars N°3 were used, with a cross section area of 70 [mm²] (0.11 [in²]) and a yielding strength of $f_y = 353$ [MPa] (51.2 [ksi]) and a young modulus of $E_s = 190000$ [MPa] (27300 [ksi]) found from tensile tests of bare bars [24]. The concrete used in the specimens was specified to have a compression strength of (4 [ksi]) at the 28-day using cylinder test. The concrete used in the panel W2 return a compression strength of $f'_c = 26.8$ [MPa] (3.88 [ksi]) at the 15-day, and a compression strain (ε_{c0}) between -0.002 and -0.003 [mm/mm] [24]. The tension strength of the concrete (f_{cr}) in the model was consider equal to $0.31\sqrt{f'_c[\text{MPa}]}$ (0.118 $\sqrt{f'_c[\text{ksi}]}$), and the tension strain ε_{cr} at the maximum tension strength equal to 0.00008 [mm/mm]. In addition, for the Simplify Chang-Mander model, the initial young modulus for the concrete E_c equal to $8200|f'_c[\text{MPa}]|^{\frac{3}{8}}$ was used.

The analytical model of the panel was represented using only half of the specimen (only one panel), due to the symmetry of the specimen in geometry and loading. In addition, the test was model using a mesh of 150 [mm] by 150 [mm] (Fig. 6.2). and it was used a 3 by 3 gauss integration in each element for the analysis of the panel, and a layered section, in order to model the concrete and the steel over the thickness of the panel. For the modeling of steel the smeared steel approach defined in the previous chapter was used with the use of the uniaxial mild steel bar embedded in concrete model. The other uniaxial steel model was not used for the analysis of the panel W2, because the uniaxial Menegotto-Pinto steel model was adjusted to return the same envelope that the model used here. This is, the

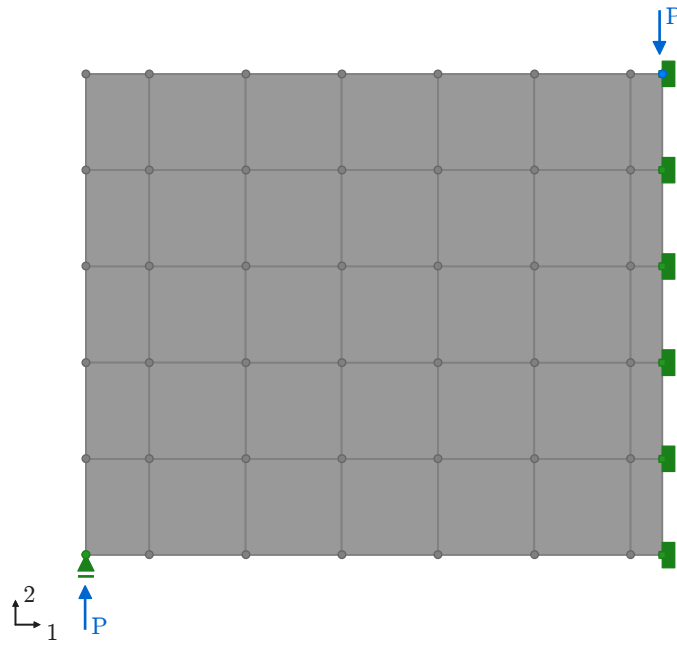


Figure 6.2: Analytical Model of the RC Shear Panel W2

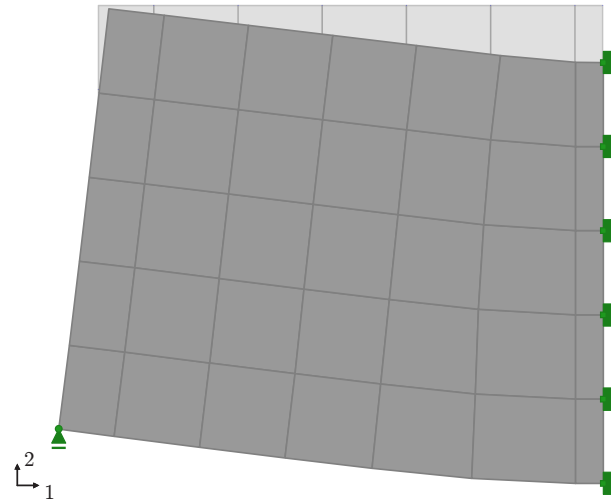
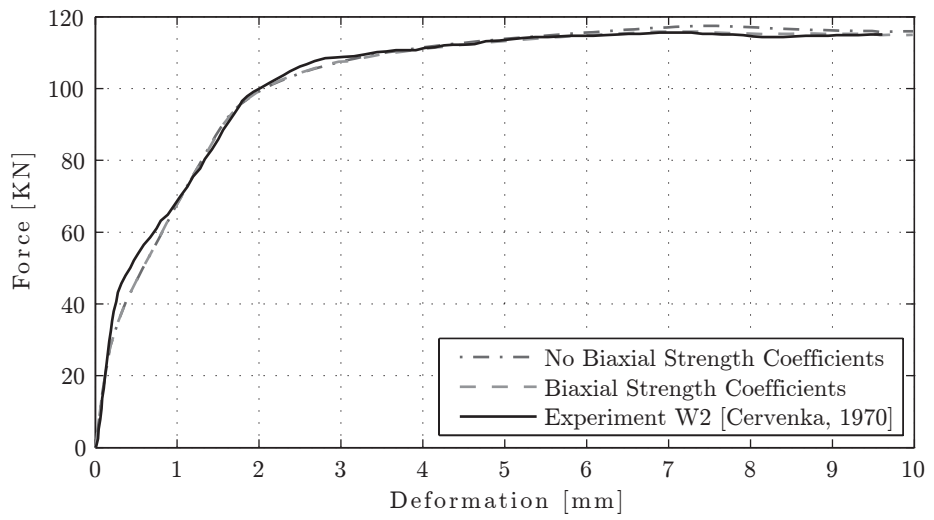
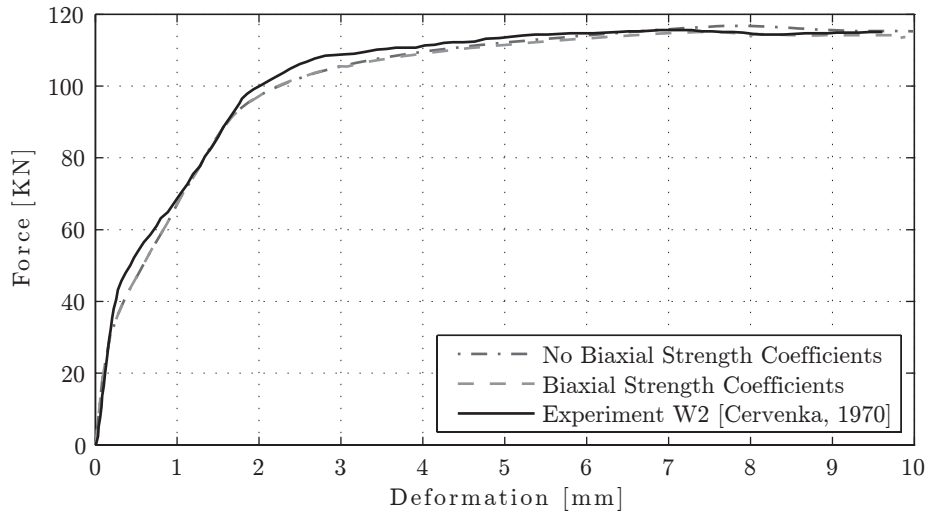


Figure 6.3: Deformation of the Analytical Model of the RC Shear Panel W2 at $P \approx 114$ [KN] (Scale Factor of 10)

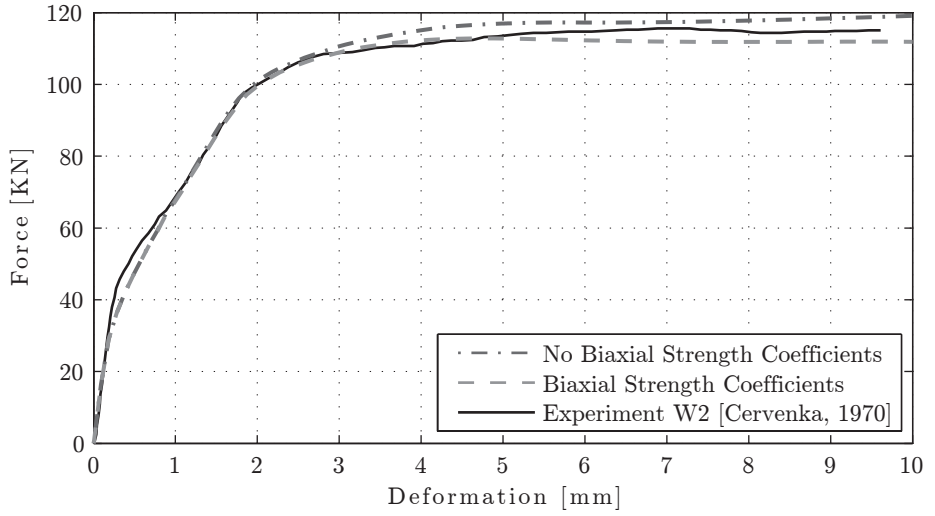


(a) Using the Uniaxial Concrete Models with Thorenfeldt Curve



(b) Using the Uniaxial Concrete Models with Simplified Chang-Mander Model

Figure 6.4: Load-Deformation of the Response of the RC Shear Panel W2



(a) Smeared Steel model using the uniaxial mild steel bar embedded in concrete model

Figure 6.5: Load-Deformation of the Response of the RC Shear Panel W2 with the plane stress concrete model with Thorenfeldt's curve and the smeared steel model using the uniaxial mild steel bar embedded in concrete model and a quadrilateral layered membrane element without drilling degrees of freedom

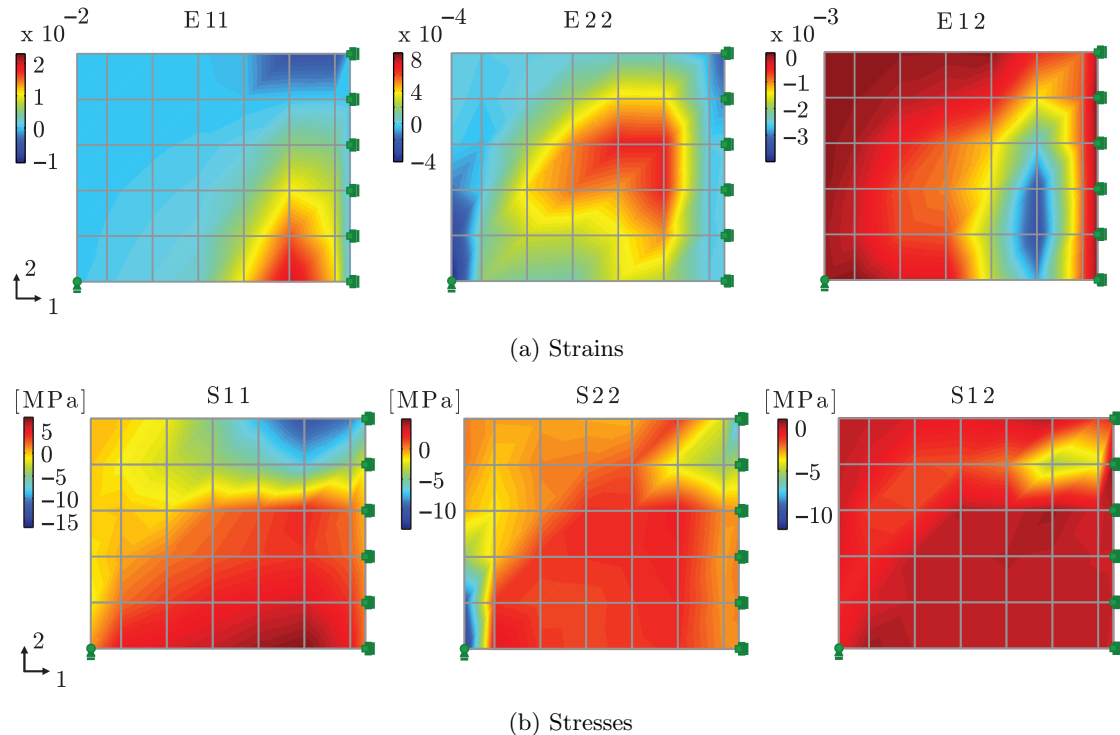


Figure 6.6: Strains and Stresses in the Model of the RC Shear Panel W2 at $P \approx 114$ [kN]

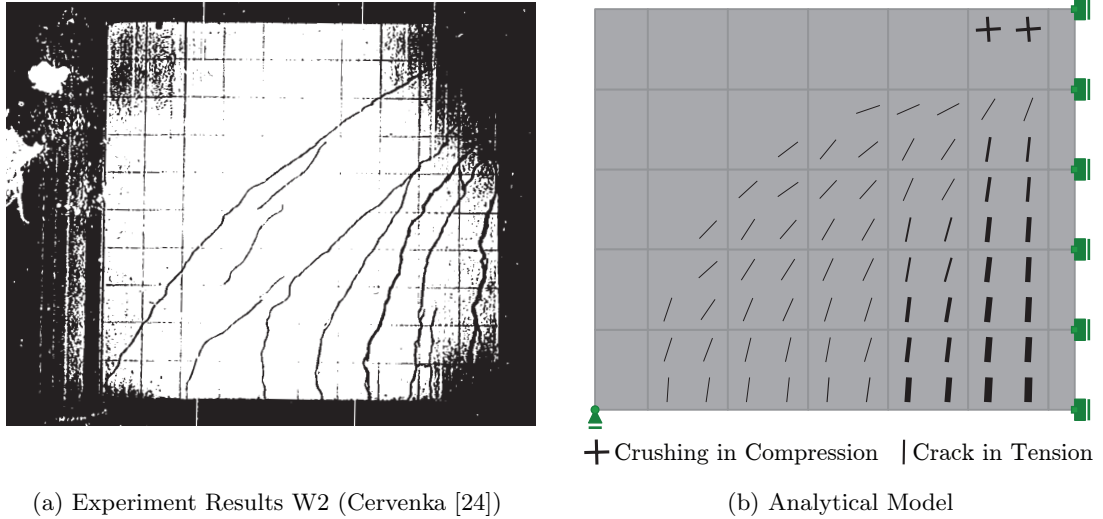


Figure 6.7: Crack Patterns observed in the RC Shear Panel W2 at $P \approx 114$ [KN]

two models will produce very similar results without significant variation. For concrete the plane stress concrete model with Thorenfeldt's curve and the plane stress concrete model with Chang-Mander model proposed before were both used in order to compare the results of the proposed quadrilateral membrane element.

In addition, the analytical model was analyzed without considering any biaxial strength coefficients and again considering the biaxial strength coefficients (softening, and enhancement) to investigate the influence of these factors, and these are compared against the Load-Displacement response obtained from the experimental results, see Fig. 6.4. In the figures, it is observed that the biaxial strength coefficients allow a closer representation of the response of the analytical model when it is compared to the experimental results of the deformation of the right bottom corner of the specimen. Also it is observed that the envelope using the Thorenfeldt Curve better represents the results of the experimental results than the model using the Simplified Chang-Mander Model. In Figure 6.5 is shown the response of the analytical model with the use of quadrilateral membrane elements without

drilling degrees of freedom and the same factors and parameters used in the model with drilling degrees of freedom, if it is compared this figure with Fig. 6.4 is observed that the element without drilling degrees of freedom underestimate the response of the panel when the biaxial strength coefficients are used. The deformation obtained for the model using the biaxial strength coefficients and the plane stress concrete model with Thorenfeldt's curve for a load value of $P \approx 114$ [KN] with a scale factor of 10 are shown in Figure 6.3.

In addition, Figure 6.6 shows the stress and strain distribution for the same analytical model for a load equal to $P = 114$ [KN], which is the model that better represents the experiments results. Also, in Figure 6.7 the crack patterns obtained in the analytical model and during the experiment are compared, which shows an excellent agreement.

6.1.2 Reinforced Concrete Walls - Lefas, Kotsovov and Ambraseys

Lefas et al. [80] in 1990 presented the results for a series of thirteen walls submitted to constant vertical load and monotonic load applied horizontally at the top of the wall specimen until failure of the wall was reached. The test program was done with the purpose of studying the influence of the axial load, height-to-width ratio, concrete strength and ratio of steel in the response of the walls with rectangular cross section [80]. The wall specimens were divided in two types, Type-I Wall and Type-II Wall, depending of their geometry (height-to-width ratio). The Type-I Walls correspond to specimens with a height-to-width ratio of $h/l = 1$ (750 [mm] wide x 750 [mm] high) and a thickness of 70 [mm] for the rectangular cross section (Fig. 6.8). The Type-II Walls correspond to specimens with a height-to-width ratio of $h/l = 2$ (650 [mm] wide x 1300 [mm] high) and a thickness of 65 [mm] for the rectangular cross section (Fig. 6.8). In addition, all the

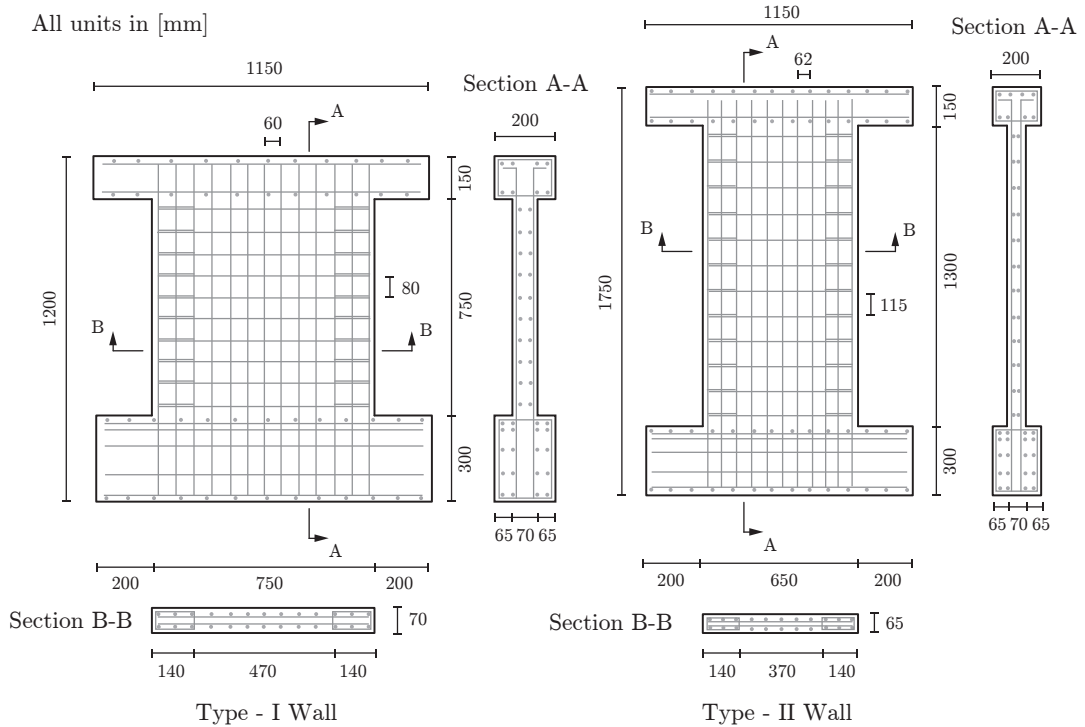


Figure 6.8: Geometry and Reinforcement Details of Type-I and Type-II Walls tested by Lefas et al. [80] in 1990

walls were built with a thicker beam at the top and bottom of the walls, to allow the transfer of the loads and anchor the vertical bars at the top of the wall, to act as a rigid foundation, and provide anchorage of the vertical bars at the bottom of the wall. These beams were cast complete with the walls.

Almost all the specimens of the both type of walls were designed following the ACI318-83 [2], with the exception of two specimens. Three different sizes of steel bar were used as reinforcement in the walls, see Table 6.1 for values provided in the article by Lefas et al. [80] in 1990. Two of these bars were high-tensile deformed steel bar with a diameter of 8 and 6 [mm]. The bar of 8 [mm] diameter was used for the vertical reinforcement, which was spaced every 60 [mm] for the Type-I wall, and 62 [mm] for the Type-II wall. The bar

Table 6.1: Properties of the Reinforcement Steel Bars

Type	Yield Strength (f_y) [MPa]	Ultimate Strength (f_u) [MPa]
8 [mm] High-Tensile Bar	470	565
6 [mm] High-Tensile Bar	520	610
4 [mm] Mild Steel Bar	420	490

of 6 [mm] diameter was used for the horizontal reinforcement, which was spaced every 80 [mm] for the Type-I wall, and 115 [mm] for the Type-II wall. The third size of bar, a mild steel bar with a diameter of 4 [mm], was used to build the stirrups, which provided the necessary confinement to the boundary elements or ends of the walls.

The ratio of reinforcement steel for each orientation of the specimens used in this study to compare the results are presented in Table 6.2, as it was reported by Lefas et al. [80].

In this study 3 specimens for the Type-I wall and 3 specimens for the Type-II wall are used to compare the analytical results against the experimental results, and only the information with respect to these groups of specimens will be mentioned here. The concrete used in the different wall specimens were prepared to obtain two target levels of concrete strength ,45 [MPa] (6.53[ksi]) and 30 [MPa] (4.35 [ksi]), however, different values of concrete strength were obtained. In Table 6.2 the cube strength of the concrete and the ratio of reinforcement steel at each orientation for the specimens used in this study and provided by [80] in 1990 are presented. These values are used to generate the model, but using a transformation of cube strength to cylinder strength, which typically is defined as $f'_c = \alpha f'_{c_cube}$ with α a factor determinate from experimental data. This value is between 0.77 for low strength concrete to 0.95 for high strength concrete [96]. Also, the tension strength of the concrete (f_{cr}) defined as $0.31\sqrt{f'_c[\text{MPa}]}$ ($0.118\sqrt{f'_c[\text{ksi}]}$), and the tension

Table 6.2: Properties of the Wall Specimens

Type	Specimen	Steel Ratio				Cube Strength f'_{c_cube} [MPa]	Axial Load	
		ρ_{hor} [%]	ρ_{ver} [%]	ρ_{flex} [%]	ρ_s [%]		F_v [KN]	$\nu = \frac{F_v}{blf'_c}$
I	SW11	1.10	2.40	3.10	1.20	52.3	0	0.0
	SW12	1.10	2.40	3.10	1.20	53.6	230	0.1
	SW16	1.10	2.40	3.10	1.20	51.7	460	0.2
II	SW22	0.80	2.50	3.30	0.90	50.6	182	0.1
	SW23	0.80	2.50	3.30	0.90	47.8	343	0.2
	SW24	01.80	2.50	3.30	0.90	48.3	0	0.0

strain ε_{cr} at the maximum tension strength equal to 0.00008 [mm/mm] were used in the model. To match the results, it was necessary to use a value of strain for the peak resistant strength of concrete between -0.003 to -0.0055 [mm/mm] for the different specimens. In addition, for the Simplify Chang-Mander model, the initial young modulus for concrete E_c equal to $\alpha_c \sqrt{f'_c}$ [MPa] with α_c equal to 3875, as is used by [56], for modeling unconfined concrete and confined concrete was also used in this model. And for steel, a value of 1% for the hardening ratio and a value of $E_s = 200000$ [MPa] for the young modulus of the steel were used.

The test program follows the protocol described next. Each wall was first loaded vertically until it reached the level of axial load assigned ($\nu = \frac{F_v}{blf'_c} = 0$ or 0.1 or 0.2) to the specimens tested. After that the value of the vertical load was held constant until the end of the testing. The next step was the application of the horizontal load at the top of the wall, and the load was applied incrementally and monotonically at a speed of 0.04 [KN/sec]. In Figure 6.9 is shown the testing setting used by Lefas et al. [80] in 1990.

The analytical model of the Type-I and Type-II walls were performed using a mesh between 120 [mm] to 150 [mm] (Fig. 6.10), and a 3 by 3 gauss integration in each element

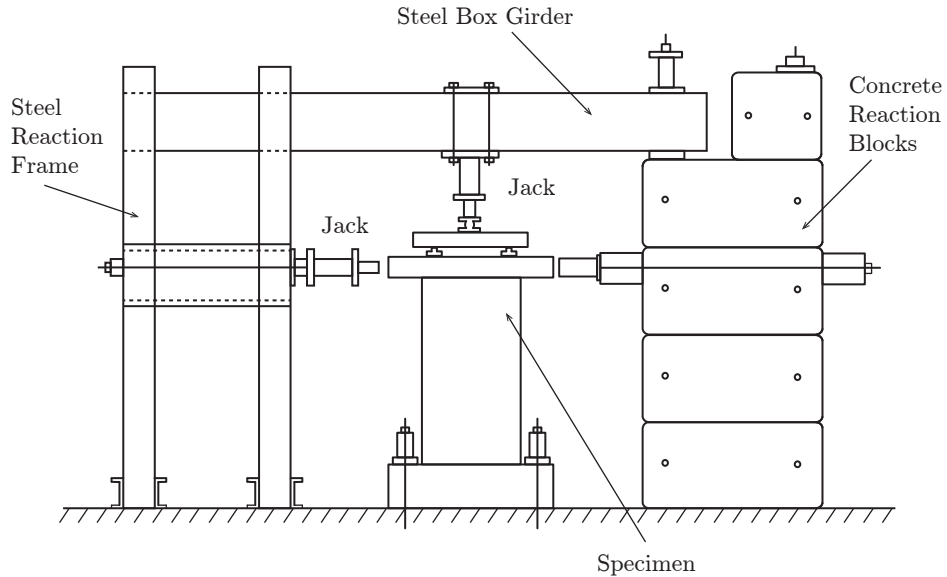


Figure 6.9: Schematic of Testing Setting used by Lefas et al. [80] in 1990

for the analysis of the walls and a layered section was used, in order to model the concrete and the steel over the thickness of the panel. For the modeling of steel the smeared steel approach defined in the previous chapter was used with the use of the uniaxial mild steel bar embedded in concrete model, and the uniaxial Menegotto-Pinto steel model. These two models were used to demonstrate that both models produce very similar results without significant variation. For concrete the plane stress concrete model with Thorenfeldt's curve and the plane stress concrete model with Chang-Mander model proposed before were both used for the Type-I walls. However, due to some numerical instability produced during the analysis of the Type-II walls using the plane stress concrete model with the simplify uniaxial Chang and Mander concrete model, the plane stress concrete model with Thorenfeldt's curve was the only model used for the Type-II walls.

In addition, as for the previous analysis, the analytical model was analyzed without considering any biaxial strength coefficients but using the enhanced coefficient due to

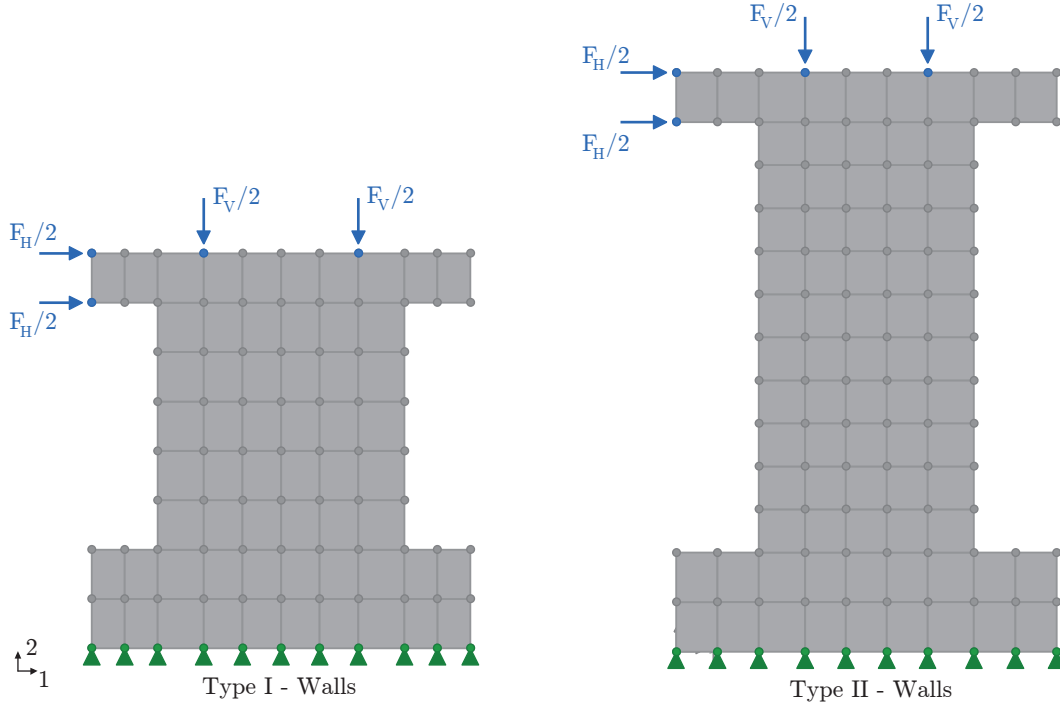


Figure 6.10: Analytical Model for Type-I and Type-II Walls

confinement at the boundary elements of the wall. Another analysis was performed considering the biaxial strength coefficients (softening, and enhancement) and the enhanced coefficient due to confinement at the boundary elements of the wall. This was done in order to investigate the influence of these factors, and these are compared against the Load-Displacement response of the top of the wall obtained from the experimental results, see Fig. 6.11, Fig. 6.12, Fig. 6.13, and Fig. 6.14. In these figures, it is observed that the biaxial strength coefficients allow a better representation of the response of the analytical model when it is compared to the experimental results of the Top deformation of the wall, and the model without the biaxial strength overestimates the resistance of the wall, which is expected due to the fact that softening of the concrete is not considered.

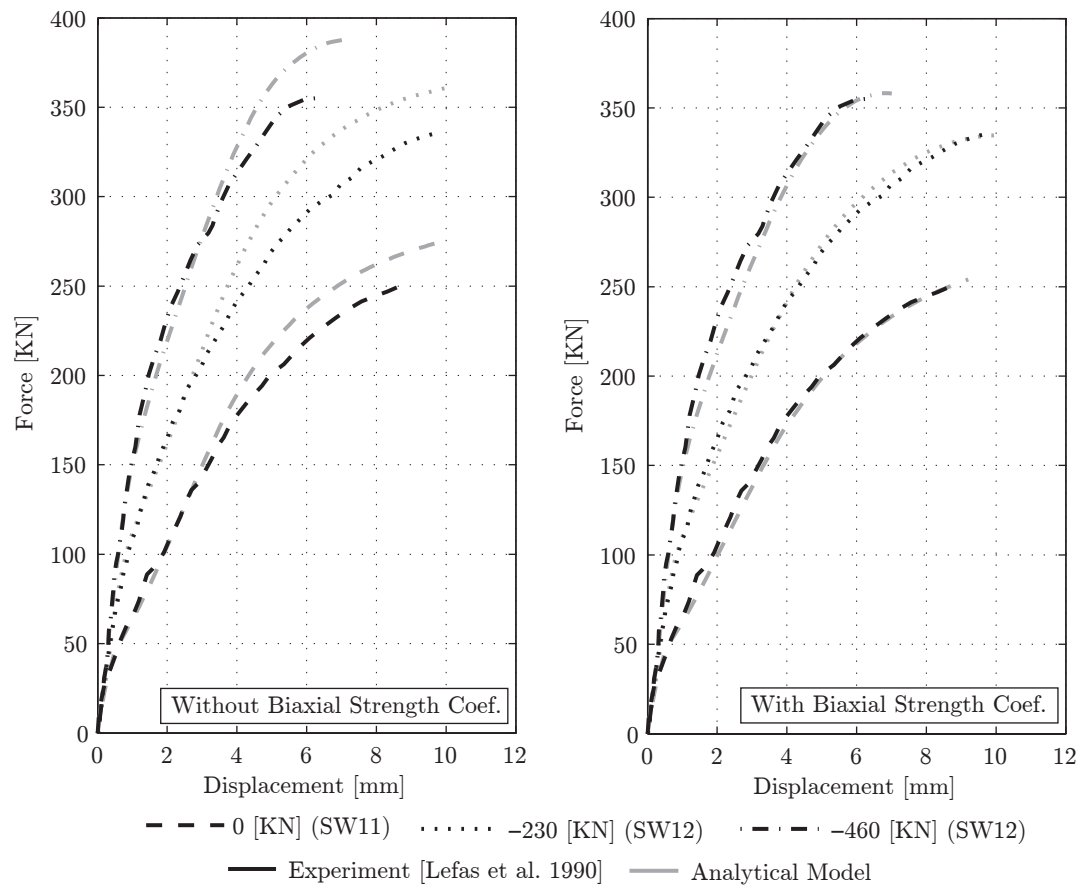


Figure 6.11: Load-Displacement Curve of Analytical Model with the plane stress concrete model with Thorenfeldt's curve and the smeared steel model using the uniaxial mild steel bar embedded in concrete model versus Experiment Results for Type-I Walls

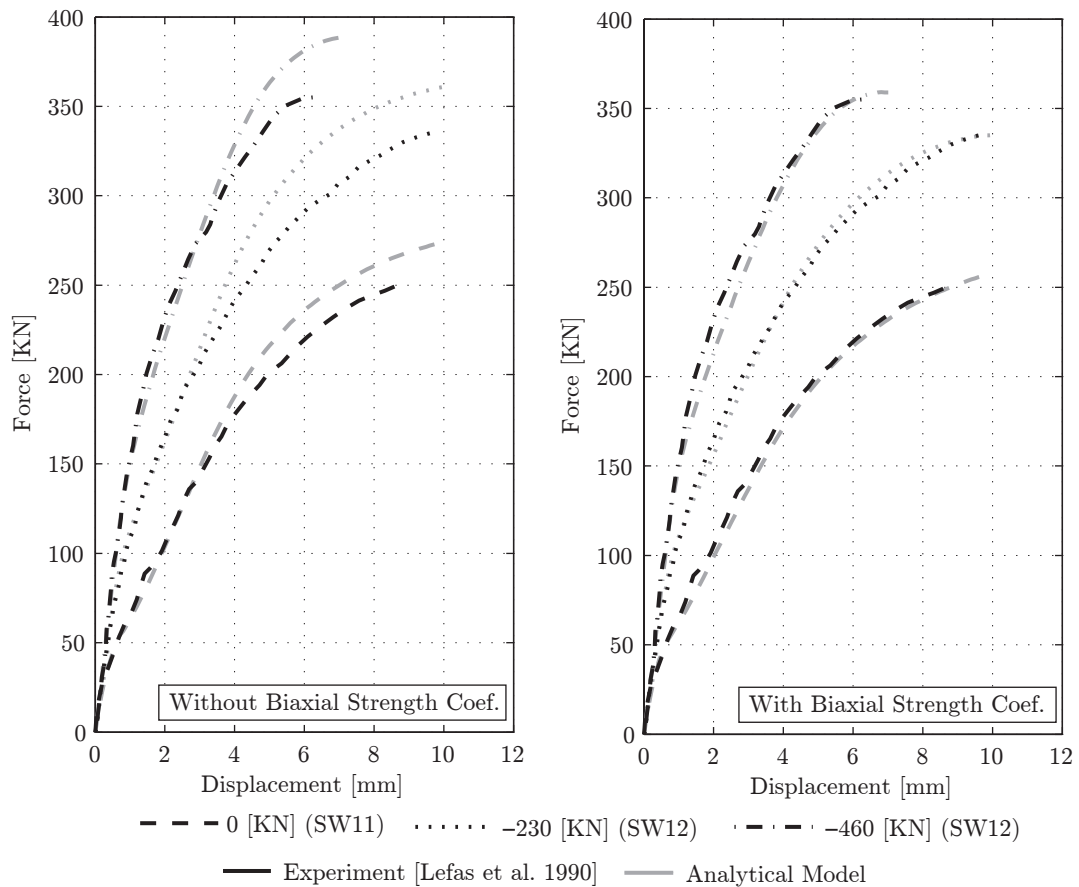


Figure 6.12: Load-Displacement Curve of Analytical Model with the plane stress concrete model with Thorenfeldt's curve and the smeared steel model using the uniaxial Menegotto-Pinto steel model versus Experiment Results for Type-I Walls

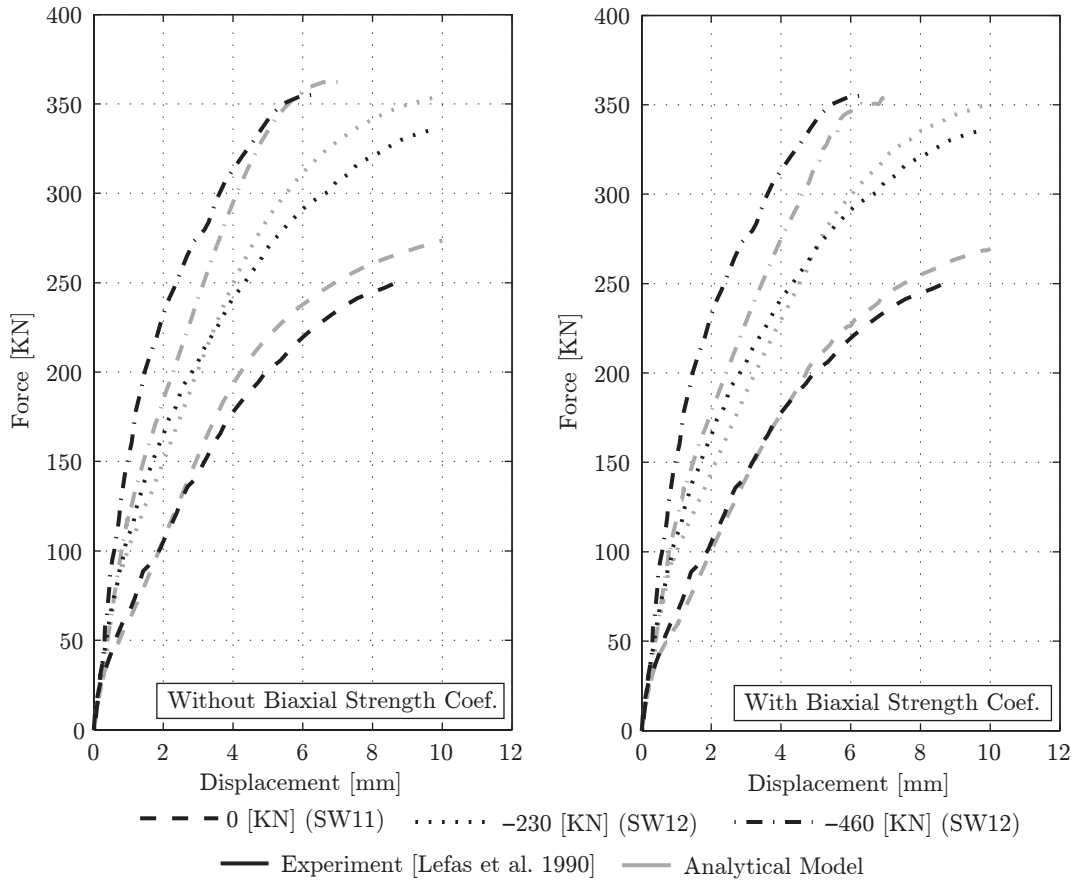


Figure 6.13: Load-Displacement Curve of Analytical Model with the plane stress concrete model with Chang-Mander Model and the smeared steel model using the uniaxial mild steel bar embedded in concrete model versus Experiment Results for Type-I Walls

Also, it is observed a closer representation of the experimental results with the model using the quadrilateral layered membrane element with drilling degrees of freedom than the model with quadrilateral layered membrane elements without drilling degrees of freedom. The models do not present significant difference for the two different types of steels for monotonic loading, which was expected. Also, it is observed that the envelope using the Thorenfeldt Curve represents the results of the experiments much better than the model using the Simplified Chang-Mander Model for the Type-I wall.

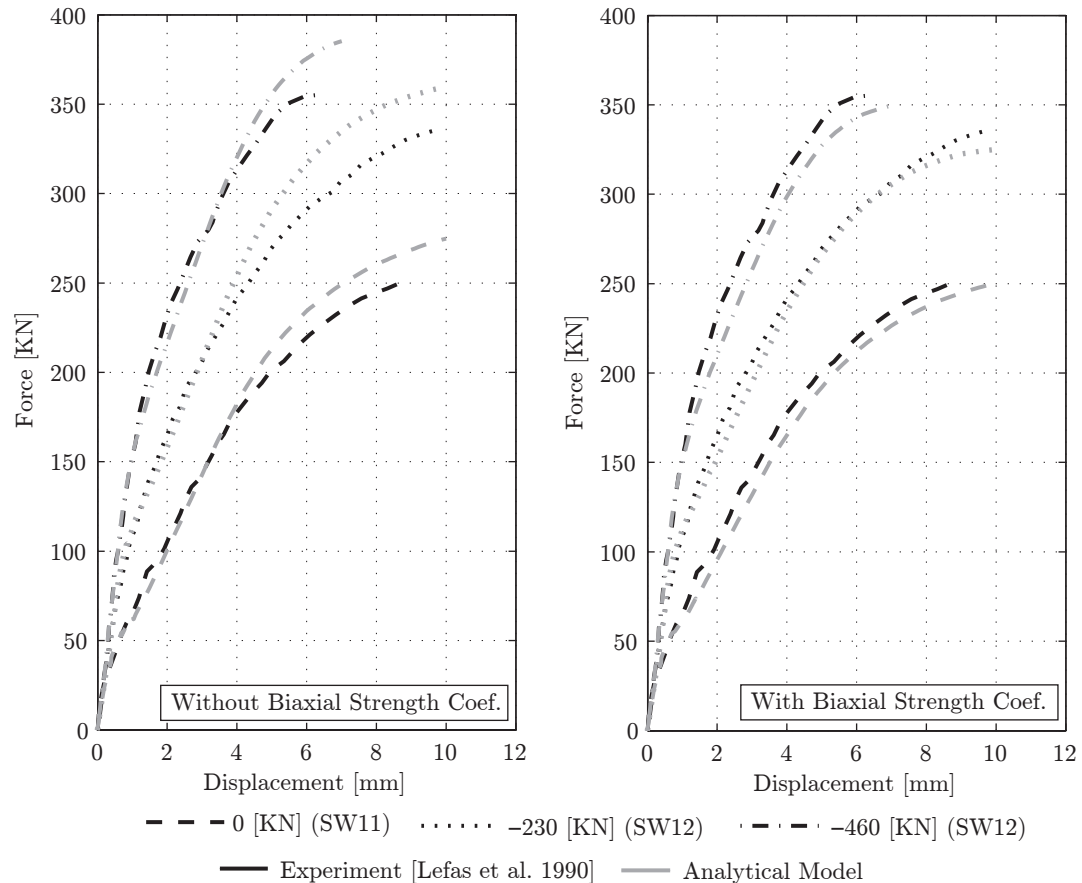


Figure 6.14: Load-Displacement Curve of Analytical Model with the plane stress concrete model with Thorenfeldt's curve and the smeared steel model using the uniaxial mild steel bar embedded in concrete modelversus Experiment Results for Type-I Walls and a quadrilateral layered membrane element without drilling degrees of freedom

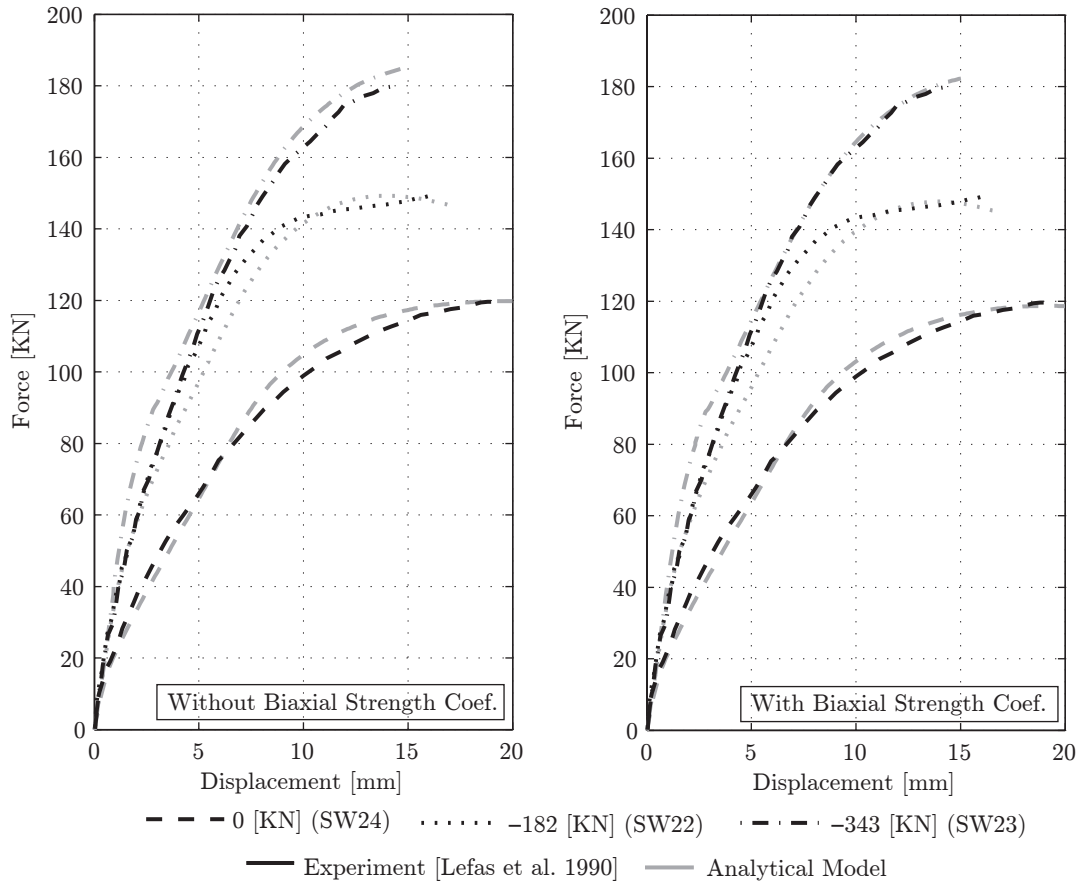


Figure 6.15: Load-Displacement Curve of Analytical Model with the plane stress concrete model with Thorenfeldt's curve and the smeared steel model using the uniaxial mild steel bar embedded in concrete model versus Experiment Results for Type-II Walls

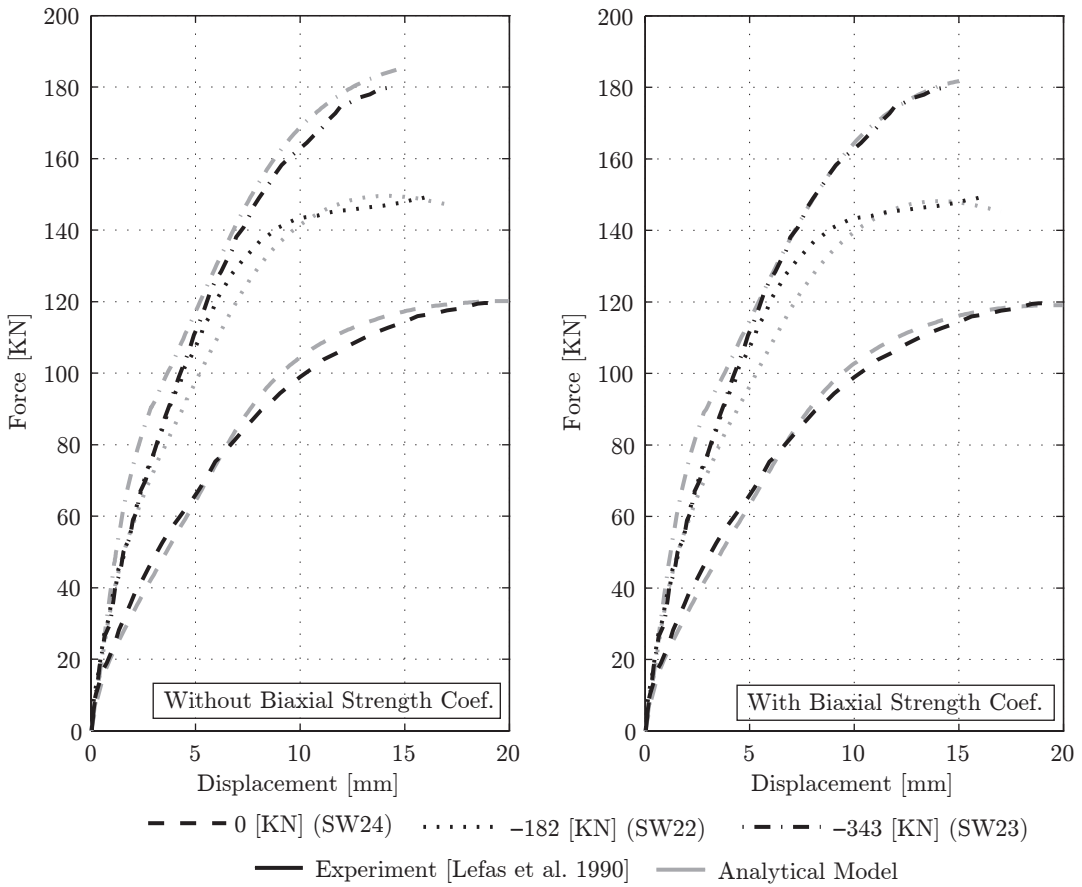


Figure 6.16: Load-Displacement Curve of Analytical Model with the plane stress concrete model with Thorenfeldt's curve and the smeared steel model using the uniaxial Menegotto-Pinto steel model versus Experiment Results for Type-II Walls

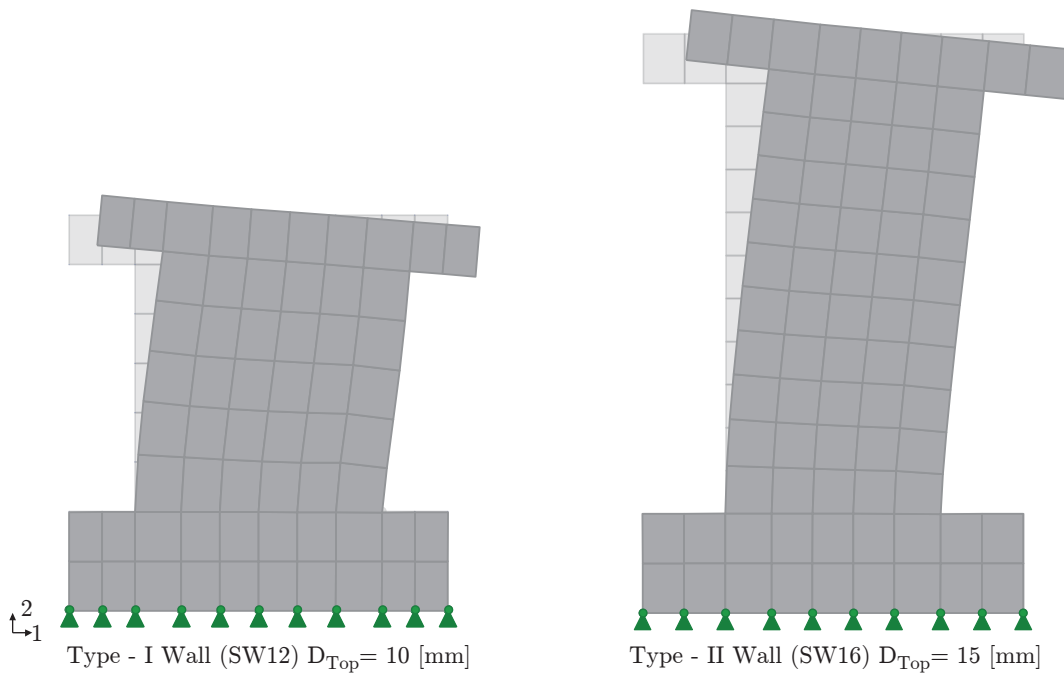
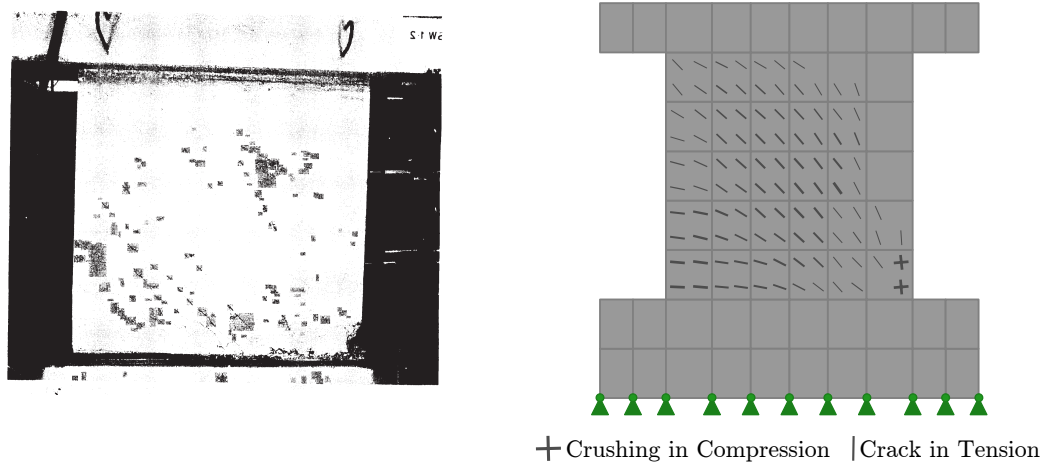


Figure 6.17: Deformation of the Analytical Model of the Type-I and Type-II Walls (Scale Factor of 10)



(a) Experiment Results SW12 (Mirror Image) [80]

(b) Analytical Model

Figure 6.18: Crack Patterns observed in the Specimen SW12 of the Type-I wall at the end of the analysis vs the observed at the end of the experimental testing

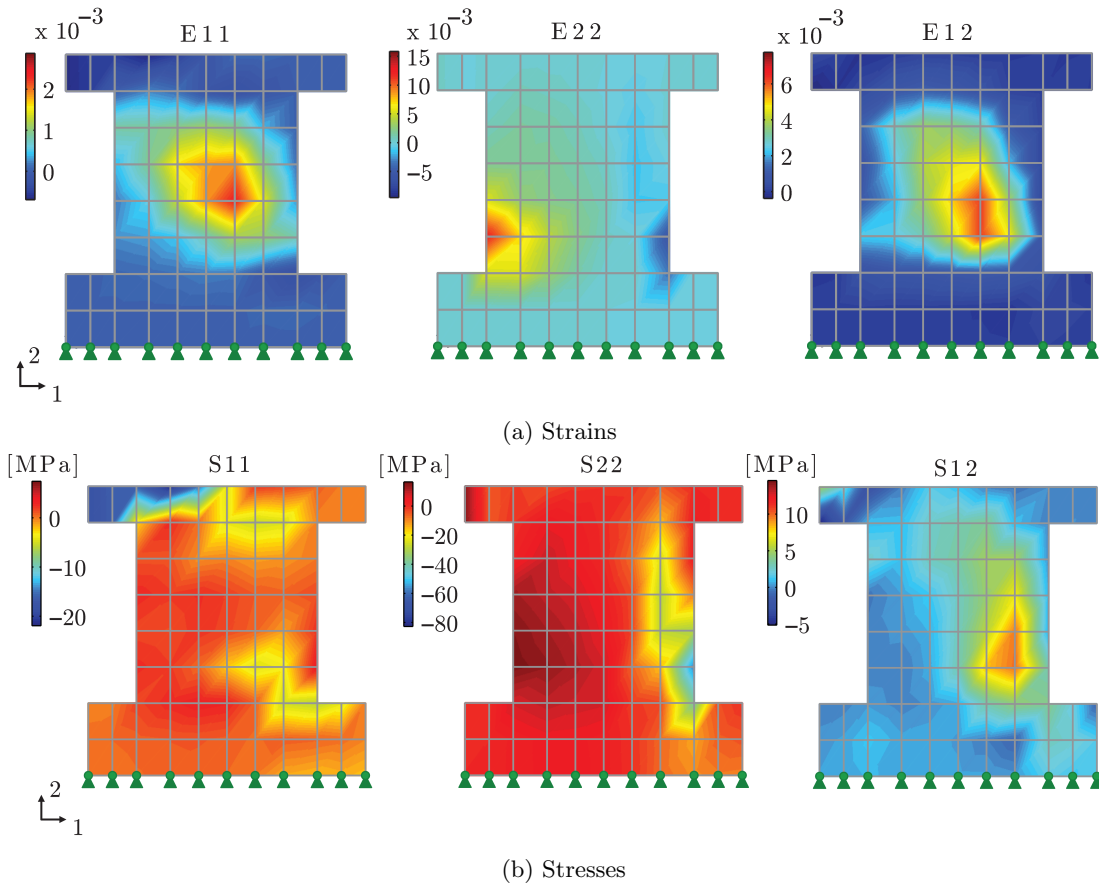
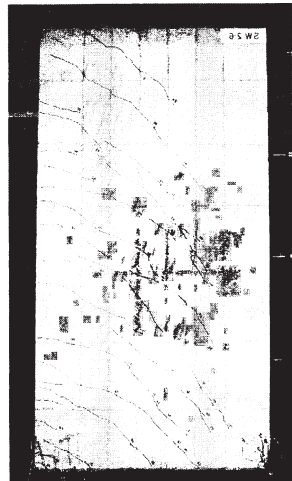
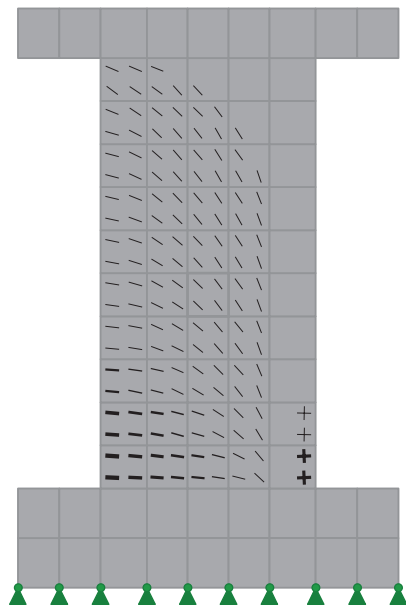


Figure 6.19: Strains and Stresses in the Model of the Specimen SW12 of the Type-I Wall at the maximum displacement



(a) Experiment SW26 ($\nu = 0.0$) (Mirror Image) [80]



(b) Analytical Model SW24
+ Crushing in Compression | Crack in Tension

Figure 6.20: Crack Patterns observed in the Specimen SW24 of the Type-I wall at the end of the analysis vs the observed at the end of the experimental testing for the SW26 that represent the failure observed by Lefas et al. [80] in 1990 for the Type-II Walls

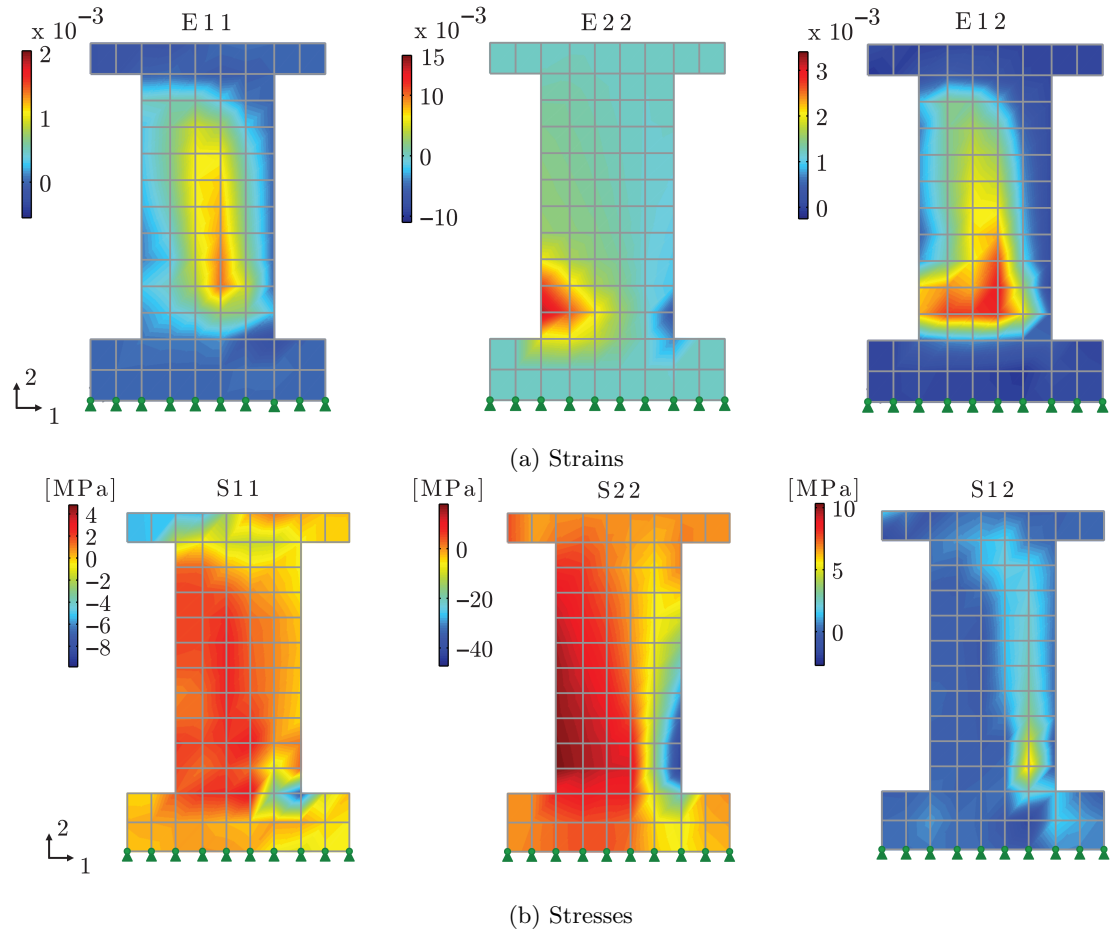


Figure 6.21: Strains and Stresses in the Model of the Specimen SW24 of the Type-II Wall at the maximum displacement

In Figure 6.17 the maximum deformation obtained for the analytical models, Type-I wall Specimen SW12 and Type-II wall Specimen SW23, is shown using the biaxial strength coefficients and the plane stress concrete model with Thorenfeldt's curve with a scale factor of 10. Also, in Figure 6.18 the crack patterns obtained in the analytical model and during the experiment are compared for the specimen SW12 of the Type-I wall, which shows an excellent agreement. Also, Figure 6.19 shows the strain and stress for the specimen SW12 of the Type-I wall at the point of maximum deformation. In addition, for completeness the crack patterns for a specimen of the Type-II walls (SW24) is shown in Fig. 6.20, and the strain and stress for the specimen SW24 is shown in Fig. 6.21

6.2 Reversal or Cyclic Loading

In this section the evaluation and verification of the proposed nonlinear layered quadrilateral membrane and shell elements with drilling degrees of freedom using experimental results of tests under reversal loads is presented. The test selected corresponds to the test program done by Thomsen and Wallace [132], and from this program two rectangular wall specimen (RW1 and RW2) of 1219 [mm] (48 [in]) long and two other specimens with T-shaped cross sections (TW1 and TW2) with a web of 1120 [mm] (44 [in]) and a flange of 1219 [mm] (48 [in]) will be used. These specimens were designed to represent approximately a one quarter-scale experimental model of a real wall designed by the Uniform Building Code of 1994 (UBC) [63] with additional boundary detailing in the reinforcement for the bottom part of the wall (the last 1220 mm or 48 [in] of the wall). The specimen walls were 3658 [mm] (144 [in]) tall with a thickness of 102 [mm] (4 [in]) over the entire cross section for the four specimens. In addition, T shaped walls had slabs at the level of

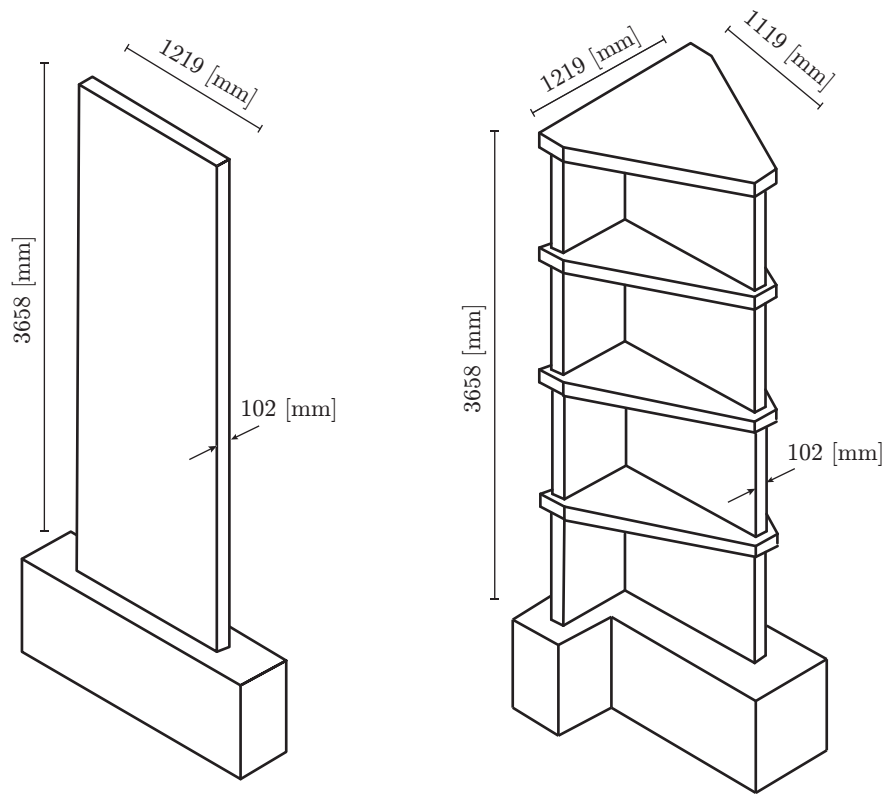


Figure 6.22: Three-Dimensional View of the Rectangular and T-Shaped Wall Specimen used by Thomsen and Wallace [132] in 1995

each floor (914.5 [mm] or 36 in). These specimens were built with a thicker and heavily reinforced pedestal or bottom beam to provide anchorage to the vertical bars at the bottom of the wall and act as a rigid foundation. The pedestal for the rectangular walls were 690 [mm] (27 [in]) deep and 410 [mm] wide and 1930 [mm] (76 [in]) long and for the T-Shaped wall the pedestal was also 690 [mm] (27 [in]) deep, but the web portion of the wall was 610 [mm] wide and 1677 [mm] long and the flange portion of the pedestal was 410 [mm] (16 [in]) wide and 1524 [mm] long. The specimens where built in five steps, each of the steps correspond to a level of the specimen (Pedesta or foundation, Level 1, 2, 3, and 4) as was reported by Thomsen and Wallace [132].

Table 6.3: Properties of the Reinforcement Steel Bars

Type	Yield Strength (f_y) [MPa]	Area b [mm 2]
No 3 - 9.53 [mm] Bar	414	71
No 2 - 6.35 [mm] Bar	448	32
3/16 in - 4.75 [mm] smooth wire	~448	17.72

The specimens used three sizes of steel reinforced. A deformed No. 3 bar ($d_b = 9.53$ [mm]) was used as longitudinal bars at the boundary elements in the walls. The other was a deformed No. 2 bar ($d_b = 6.35$ [mm]) used for the two curtains of distributed horizontal and vertical bars. The third bar used was a 3/16 in or 4.75 mm smooth wire, which was annealed to reduce its yielding strength from its original level to the that required for the specimens. This wire steel was used to build the transverse reinforcement or stirrups at the boundary portions of the walls.

In Table 6.3 the properties for the steel bars provided in the report by Thomsen and Wallace [132] are presented.

The concrete used in the different wall specimens and at different levels of the wall were mixed to obtain a target value of concrete strength of 27.6 [MPa] (4 [ksi]). However, a different values of concrete strength were obtained for the different cylindrical tests performed to the concrete mixed at the day of the specimen was tested. The value range between 28.7 to 58.4 [MPa] (4.16 to 8.46 [ksi]) with an average value for the concrete resistant strength of 37.7 [Mpa] (5.47ksi) for the concrete used in the first level of the difference specimens, as it was reported by Thomsen and Wallace [132] or more detailed value of an average of 32.8 [MPa] (4.76 [ksi]) for the specimen RW1 and TW1 and of 42.8 [MPa] (6.2 [ksi]) for the RW2 and TW2 [103].

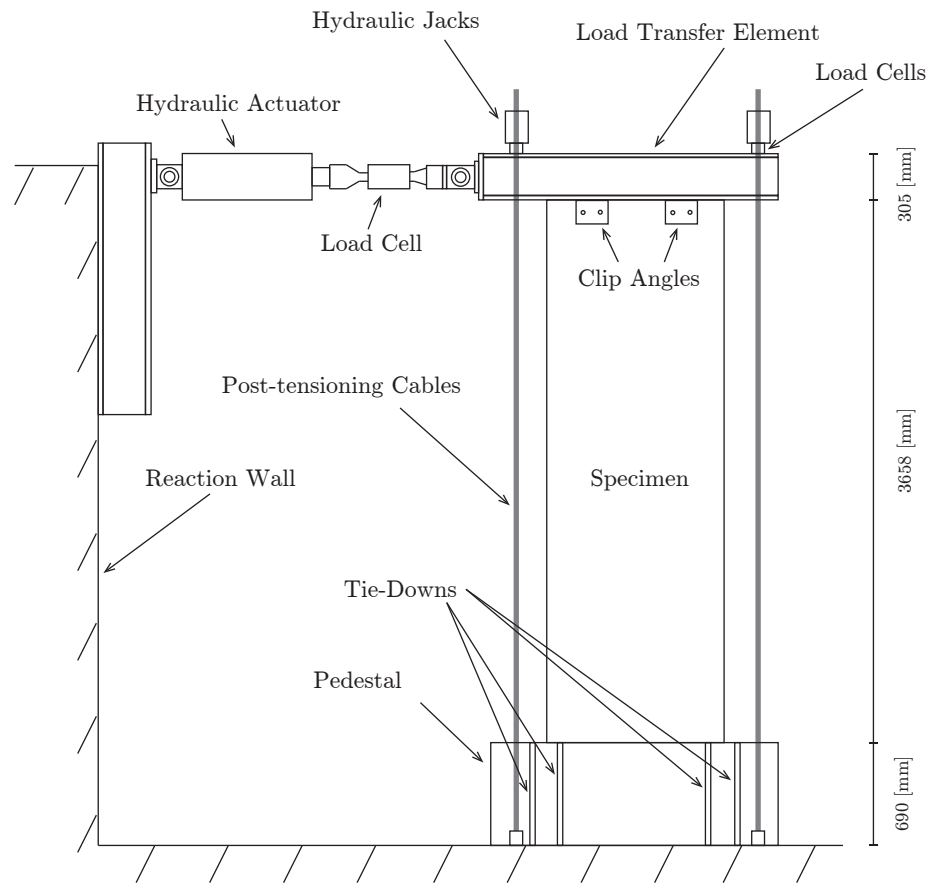


Figure 6.23: Schematic of Testing Setting used by Thomsen and Wallace [132] in 1995

The wall specimens were tested at the Structural Engineering Research Laboratory (SERL) at Clarkson University (Fig. 6.23, each wall was mounted over the testing position and held firmly in position using eight high-strength steel tie-down, which passed through the entire height of the pedestal. For the transfer of the vertical load and the horizontal load to the wall specimens, a steel element built with two back to back channel section (C-12x68) was used. The load transfer element was connected to the wall using clip angles and threaded rods of 25 [mm] (1 [in]) (6 for the rectangular walls, and 9 for the T-Walls), these rods were cast directly into the wall at the building stage of the specimens. The axial load was applied using hydraulic jacks mounted at the top of the steel element using post-tensioning cables connected to the pedestal at the bottom of the walls. The post-tensioning cable were tensioned monotonically until the axial load over the wall was equal to $\sim 0.10A_g f'_c$, after which the value of axial load was maintained constant for the rest of the test. The Horizontal cyclic loads were applied using hydraulic actuators of 556 KN (125 [Kips]) mounted against a reaction walls, and located at 4600 [mm] (180 [in]) from the strong floor. The actuator was connected to the steel load transfer using a ping connection. In addition, the testing set up used an out of plane support to avoid twisting of the wall and out-of-plane restraint, this support was a steel truss located at the top of the wall as was reported by Thomsen and Wallace [132]. A diverse number of instruments were used to measure loads, deformation and strain over the difference portions (Steel, Concrete) of the specimens. For a complete description of this the reader is referred to the report done by Thomsen and Wallace [132] in 1995.

After the axial load was applied monotonically over the specimen, a cycling procedure was used. This cycling was done using displacement control, and two complete cycles of

each level of drift were performed. The initial drift level was approximately 0.1%, and after reaching 0.25%. In the next step the displacement was incremented progressively until it reached 1.0% of deformation, using an increment of 0.25%. After reaching 1.0% drift the level was incremented using steps of 0.5% until failure. However for the specimens RW2 and TW2 after reachind 1.5% of drift, two additioned levels of 1.0% and 1.5% were performed again, see Fig. 6.27 and Fig. 6.33, and afterwards was continued with increments of 0.5% until it reached a 2.5% or 3% of lateral drift.

In this study the analysis to the two rectangular walls (RW1 and RW2) was performed, as well as the two T-Shaped Walls (Tw1 and TW2) and the analytical results were compared agaisns the experimental results. The values of peak strength of concrete provided by Thomsen and Wallace [132] are used to generate the model. Also, the model uses the tension strength of the concrete (f_{cr}) defined as $0.31\sqrt{f'_c[\text{MPa}]}$ ($0.118\sqrt{f'_c[\text{Ksi}]}$), and the tension strain ε_{cr} at the maximum tension strength equal to 0.00008 [mm/mm]. In addition, in order to match the results it was necessary to use a value of strain for the peak resistant strength at concrete between -0.0055 to -0.0065 [mm/mm] for the different specimens. And for steel a value of 1% was used for the hardening ratio and a value of $E_s = 200000$ [MPa] for the Young's modulus of the steel.

The analytical model of the specimen walls were developed using a mesh of 170 [mm] (Fig. 6.26), and a 3 by 3 gauss integration was used in each element for the analysis of the walls and a layered section, in order to model the concrete and the steel over the thickness of the panel. For the modeling of steel the smeared steel approach defined in the previous chapter was used with the use of the uniaxial mild steel bar embedded in concrete model, and the uniaxial Menegotto-Pinto steel model. These two models were

used to compared the variation between the Menegotto-Pinto and the Ramberg-Osgood equation models under reversal loads. For concrete the plane stress concrete model with Thorenfeldt's curve only was used, due to some numerical instability produced during the analysis of the specimens walls using the plane stress concrete model with the simplified uniaxial Chang and Mander concrete model. In addition, in the model is included the bi-axial strength coefficient for damage due to cycling in the material,

The following are the analytical results for the rectangular wall and the walls with T-Shaped cross section, under reversed loads.

6.2.1 Reinforced Concrete Rectangular Wall - Thomsen and Wallace

The RW1 and RW2 specimen walls are modeled using the proposed layered quadrilateral membrane element with drilling degrees of freedom. The steel ratio used in each location in the wall was calculated from the reinforcement details provided in the report by Thomsen and Wallace [132] in 1995. In Figure 6.24 and Figure 6.25 are shown the reinforcement details of the rectangular wall specimen.

The mesh used for the two models are the same as shown in Figure 6.26. The model was analyzed using the displacement control solution algorithm, with pseudo constant incremental step, which means, if the analysis has not reached convergence for an increment of displacement, the increment is reduced until the initial increment has passed, and after this the analysis continues with the increment displacement defined at the beginning, until the solution does not converge for a certain number of iterations or reaches the end of the testing procedure.

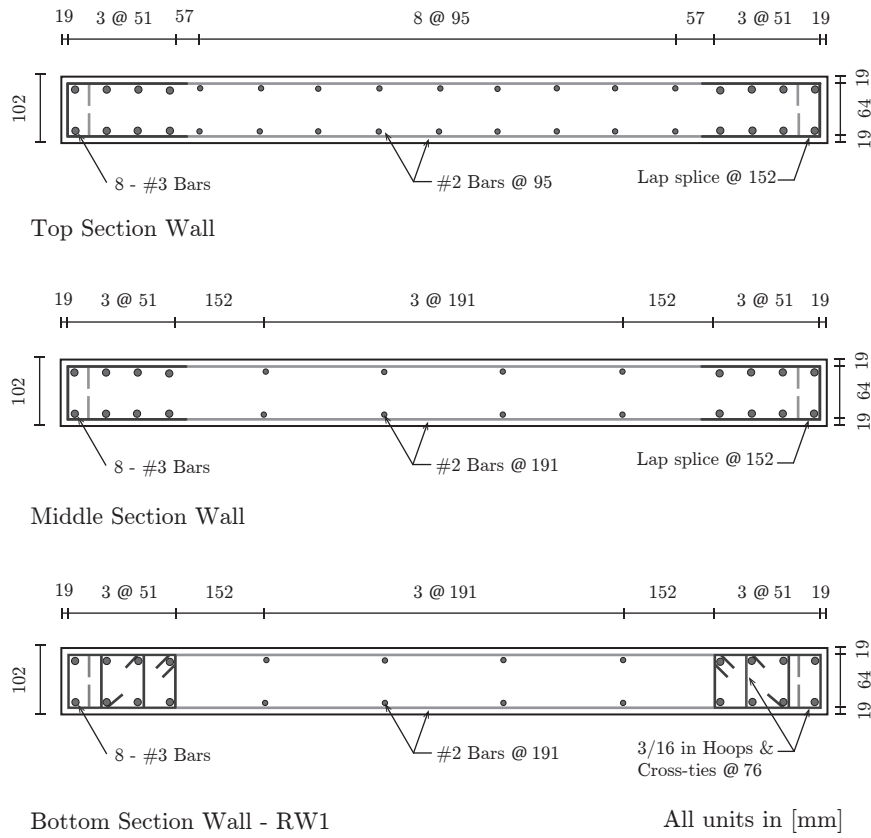


Figure 6.24: Reinforcement Details for Specimen Wall RW1 used by Thomsen and Wallace [132] in 1995

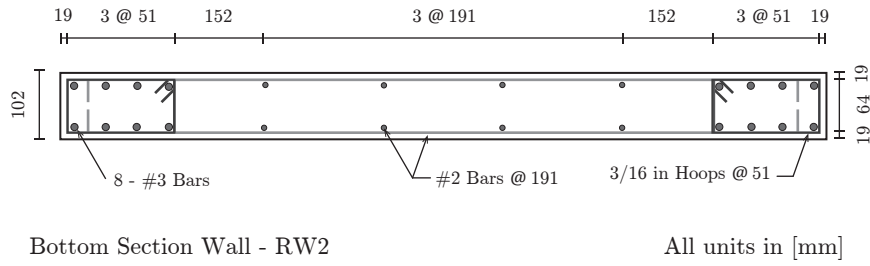


Figure 6.25: Reinforcement Details for Specimen Wall RW2 used by Thomsen and Wallace [132] in 1995

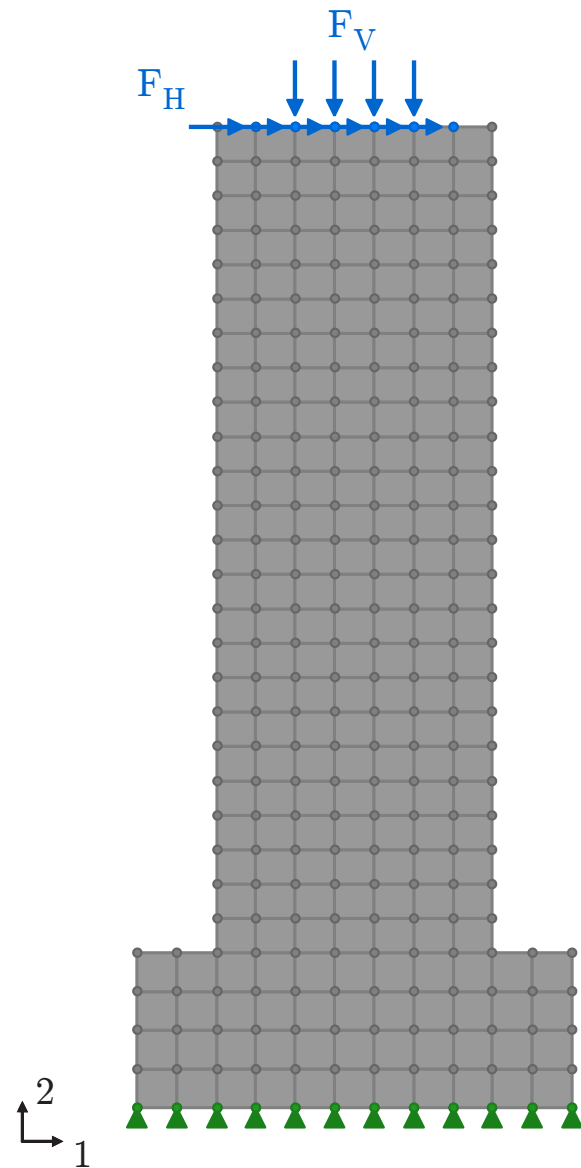
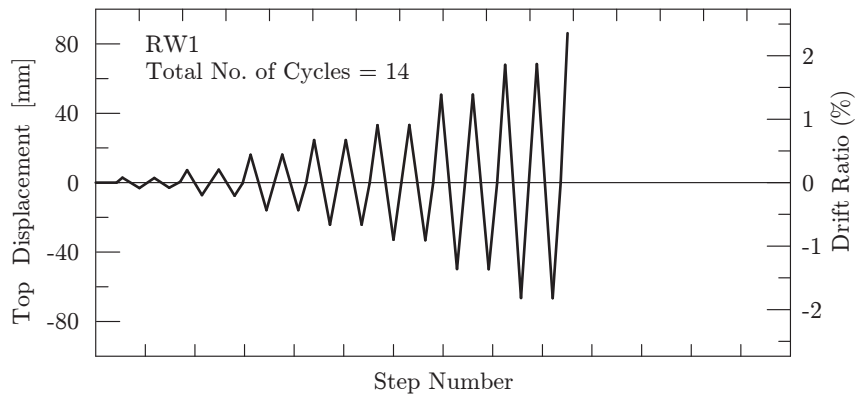
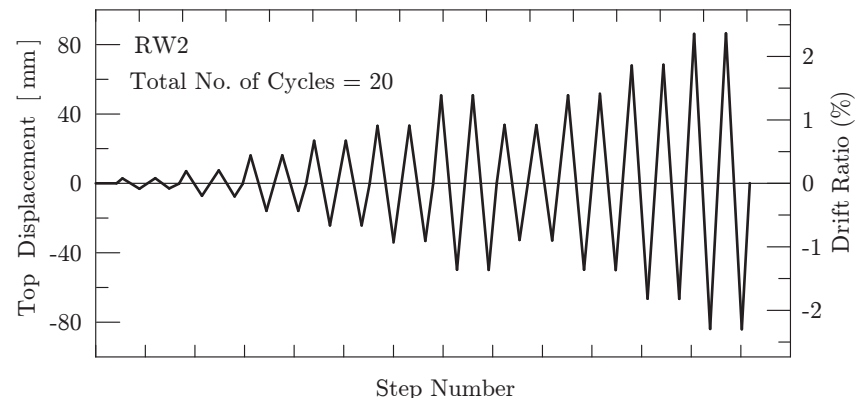


Figure 6.26: Analytical Model for Rectangular Walls Specimens (RW)

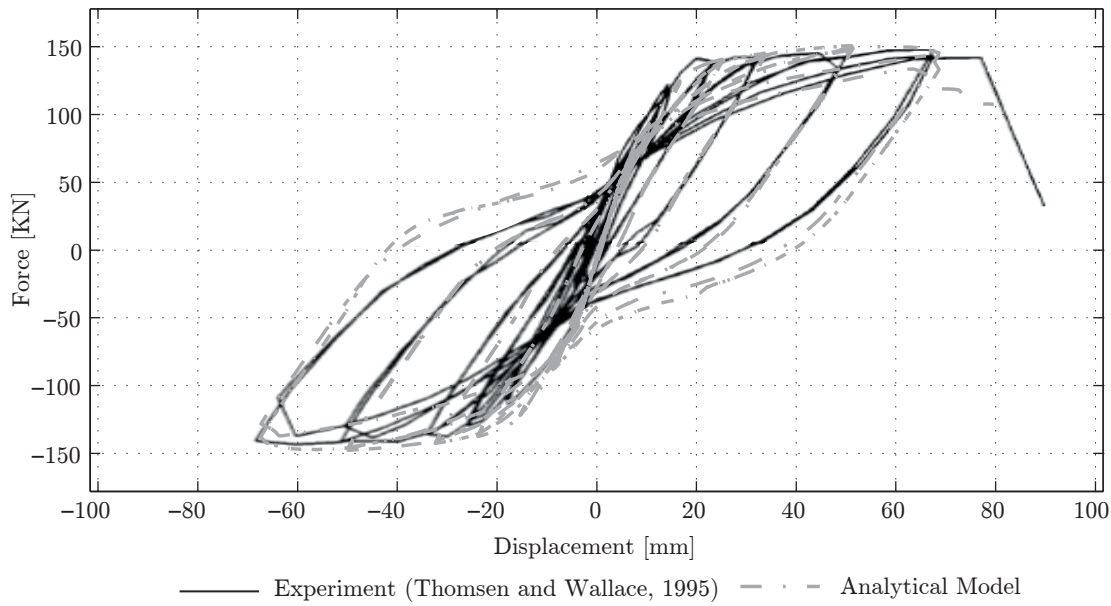


(a) RW1

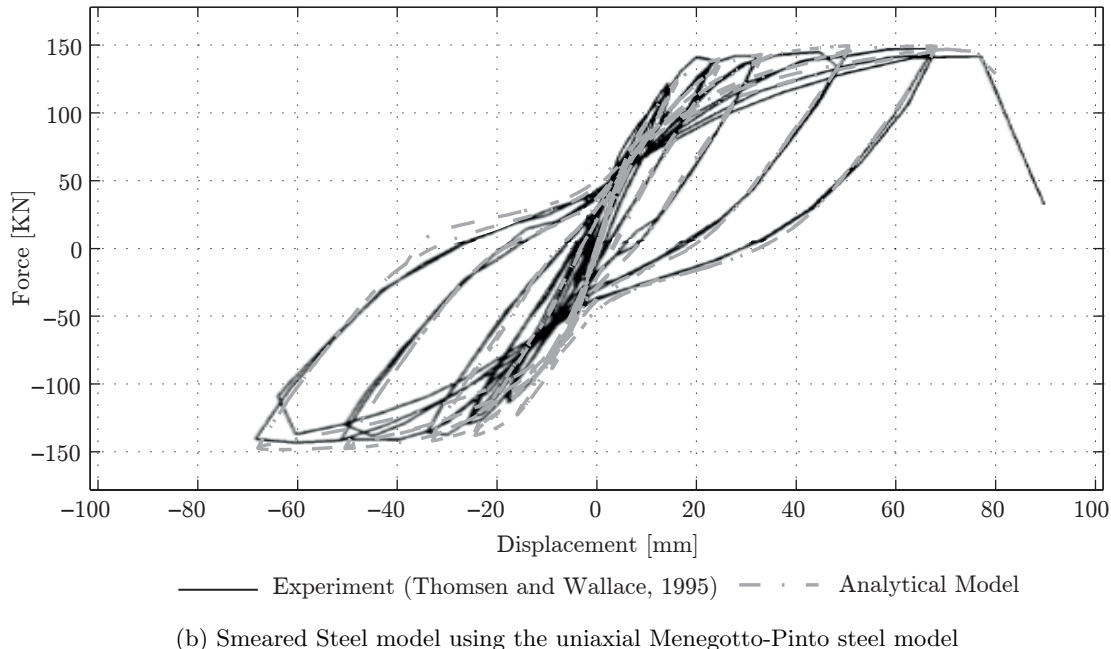


(b) RW2

Figure 6.27: Lateral Drift Procedure used by Thomsen and Wallace [132] in 1995 for Wall Specimens: RW1 and RW2

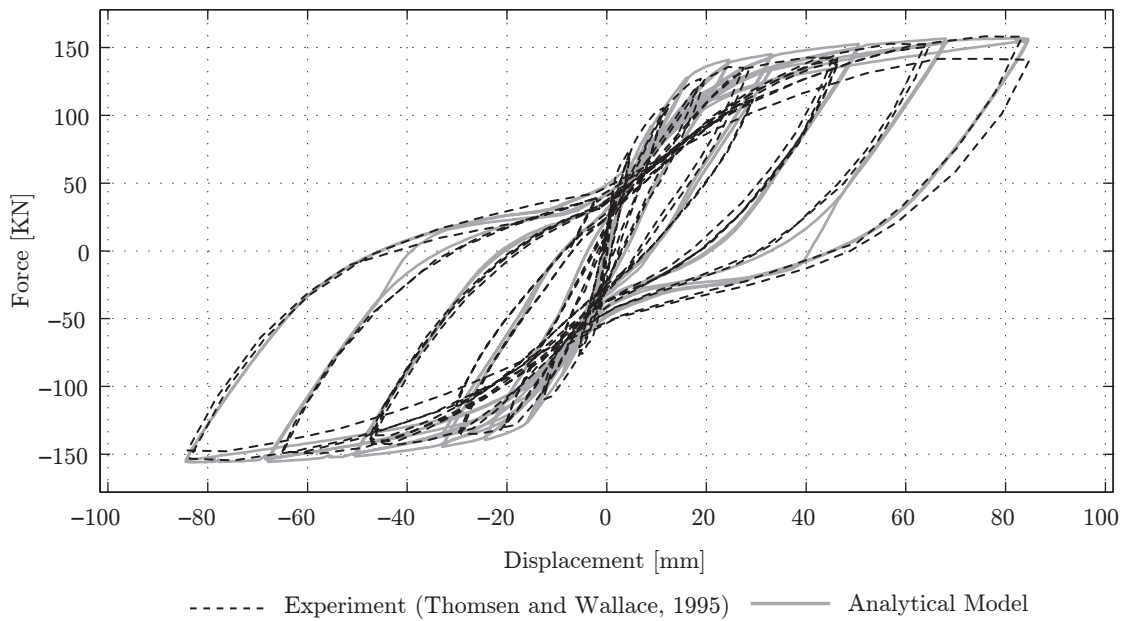


(a) Smeared Steel model using the uniaxial mild steel bar embedded in concrete model

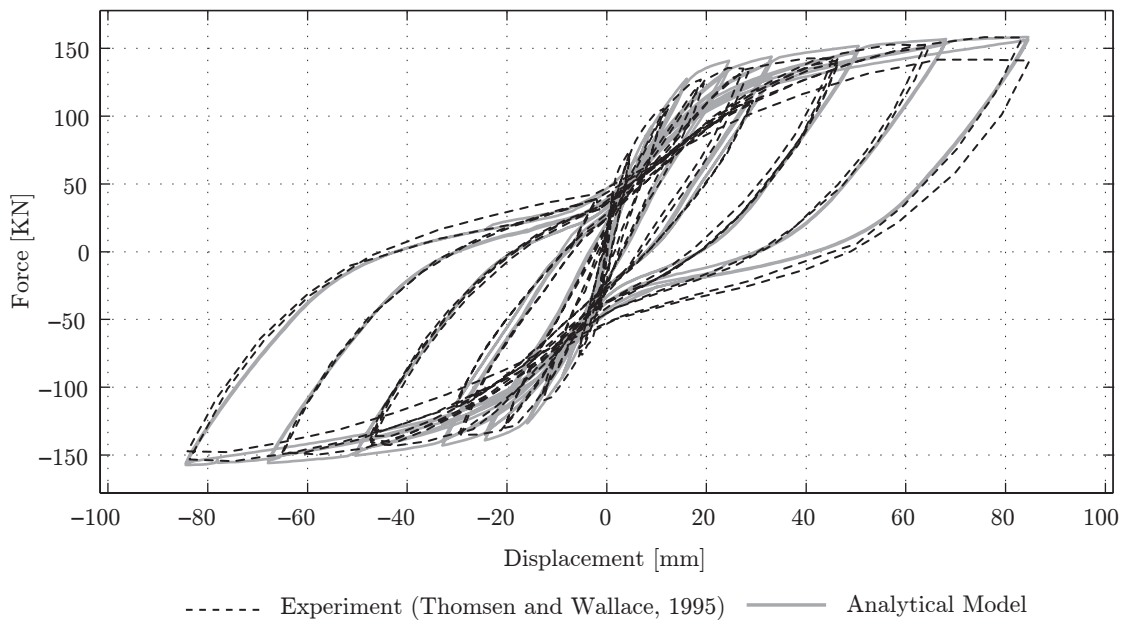


(b) Smeared Steel model using the uniaxial Menegotto-Pinto steel model

Figure 6.28: Load-Displacement Curve of Analytical Model with the plane stress concrete model with Thorenfeldt's curve vs Experiment Results for RW1



(a) Smeared Steel model using the uniaxial mild steel bar embedded in concrete model



(b) Smeared Steel model using the uniaxial Menegotto-Pinto steel model

Figure 6.29: Load-Displacement Curve of Analytical Model with the plane stress concrete model with Thorenfeldt's curve vs Experiment Results for RW2

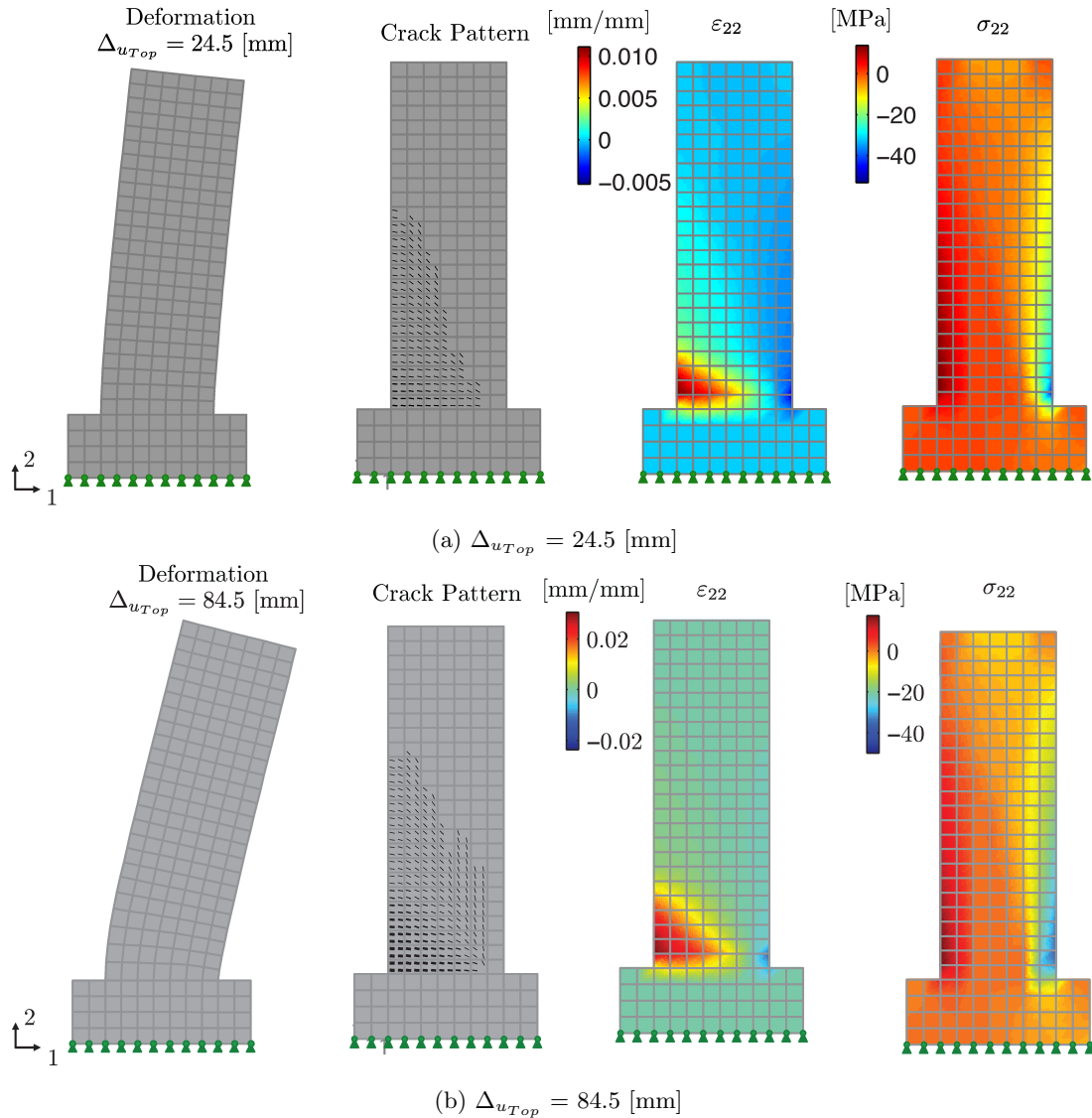


Figure 6.30: Deformation, Crack Pattern, Strain and Stress of the RW2 Analytical Model with the plane stress concrete model with Thorenfeldt's curve and the smeared steel model using the uniaxial Menegotto-Pinto steel model

In Figure 6.28 and Figure 6.29 are shown the comparison of the response for the analytical model against the experimental results of the load applied to the wall versus the deformation of the top of the wall for the two wall RW1 and RW2 using a damage coefficient (α_1) of 0.15 in Eq. 4.36. It is observed that for both models the use of the Smeared Steel model using the uniaxial Menegotto-Pinto steel model returns the better agreement with the experimental data. Also, it is shown in Fig. 6.28 that the analytical model is able to capture the failure of the experimental model for the case RW1, at the maximum displacement of approximately 80 [mm].

6.2.2 Reinforced Concrete Wall with T-Shaped Cross Section - Thomsen and Wallace

The TW1 and TW2 specimen walls are modeled using the proposed layered quadrilateral shell element with drilling degrees of freedom. These two wall specimens are very good benchmarks for the use of Reinforced Concrete Shell elements, because they combine interaction between walls in different directions and interaction with the slabs. The steel ratio used in each location in the wall was calculated from the reinforcement details provided in the report by Thomsen and Wallace [132] in 1995. In Figure 6.31 and Figure 6.32 are shown the reinforcement details of the rectangular wall specimen. In addition, due to the lack of information in the slabs reinforcement and dimension, the slabs in this analysis were modeled using elastic material, but with a reduced section to account for cracking in these elements.

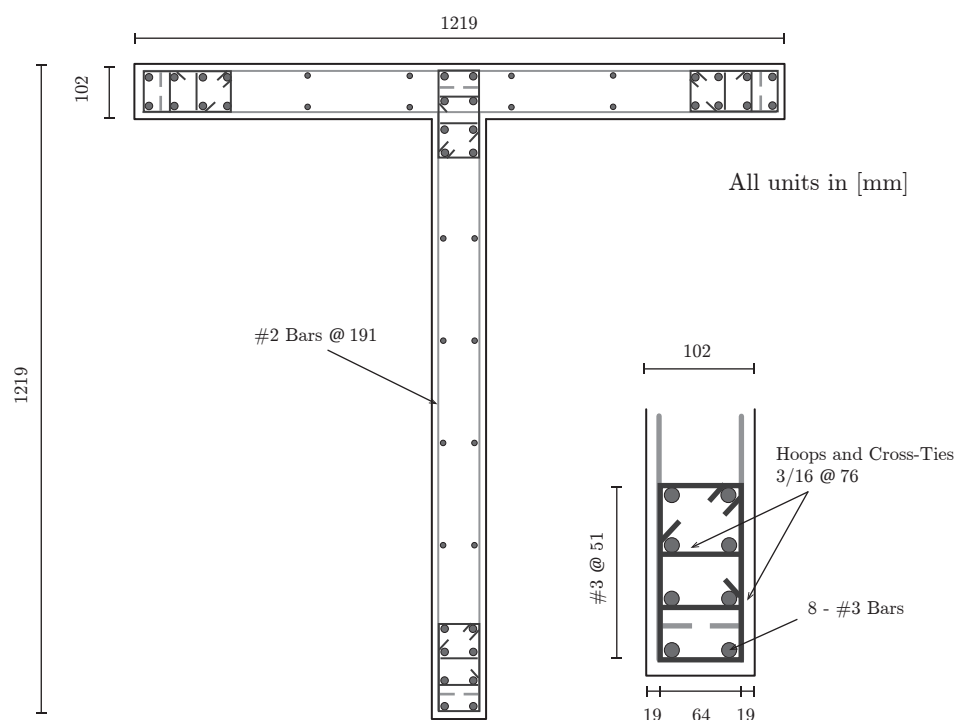


Figure 6.31: Reinforcement Details for Specimen Wall TW1 used by Thomsen and Wallace [132] in 1995

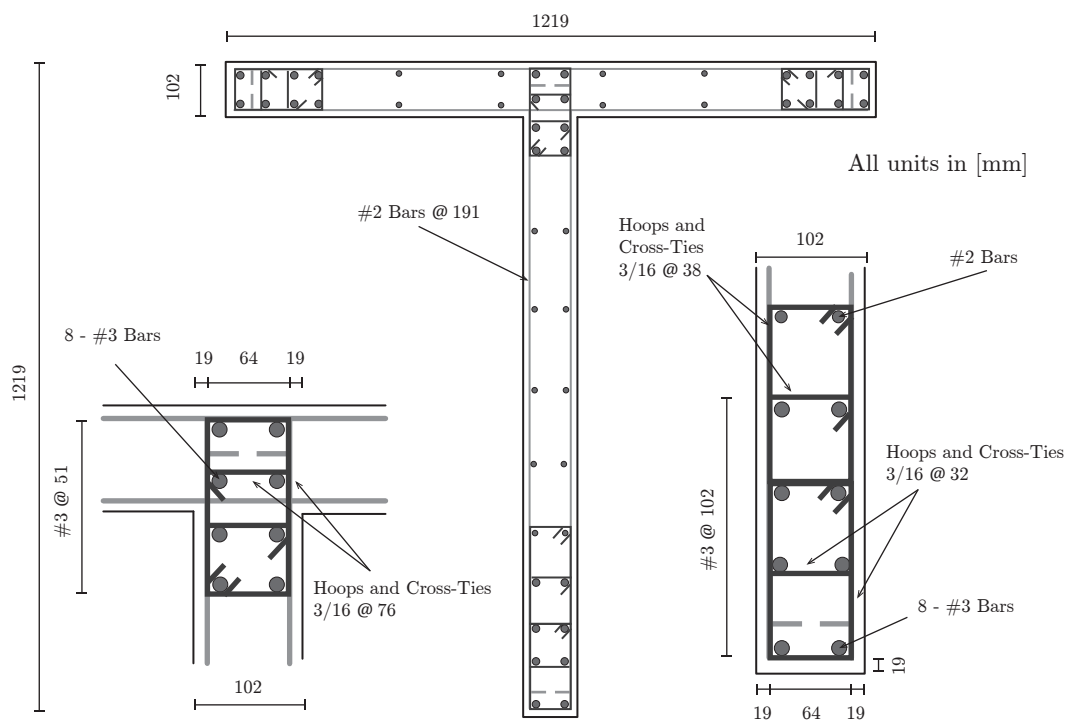


Figure 6.32: Reinforcement Details for Specimen Wall TW2 used by Thomsen and Wallace [132] in 1995

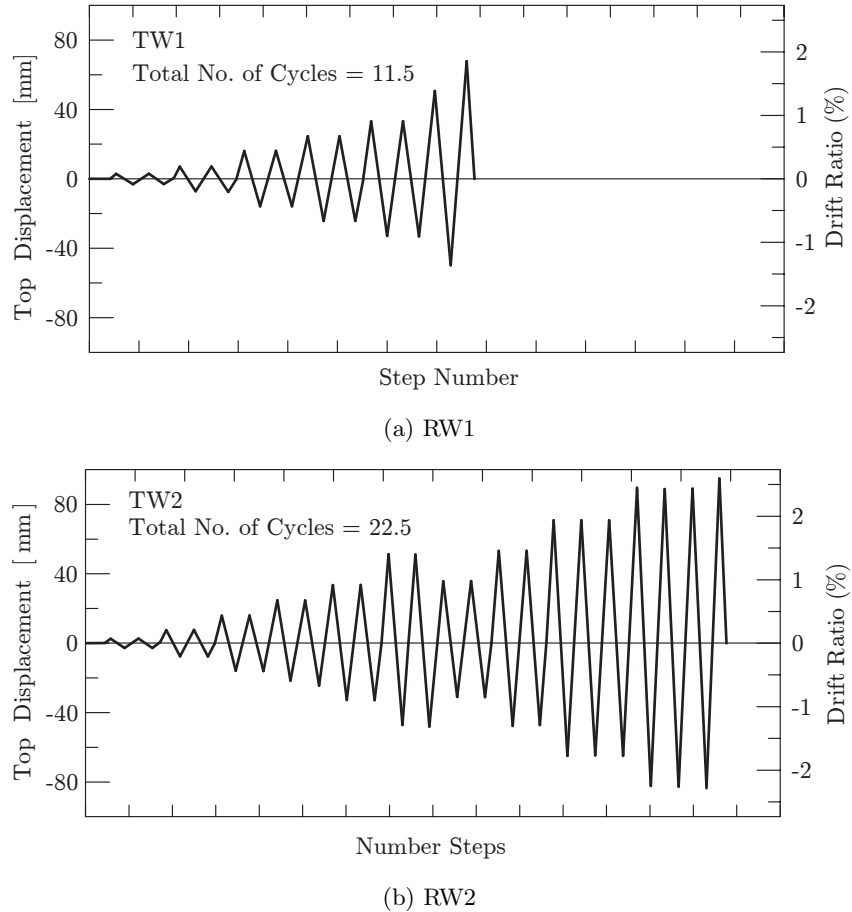


Figure 6.33: Lateral Drift Procedure used by Thomsen and Wallace [132] in 1995 for Wall Specimens: TW1 and TW2

The mesh used for the two models are the same as shown in Figure 6.34. The model was analyzed using the displacement control solution algorithm, with pseudo constant increment step, which means that, if the analysis has not reach convergence for an increment displacement, the increment is reduced until the initial increment is passed, and after this the analysis continues with the increment displacement defined at the beginning, until the solution does not converge for a certain number of iterations or reaches the end of the testing procedure.

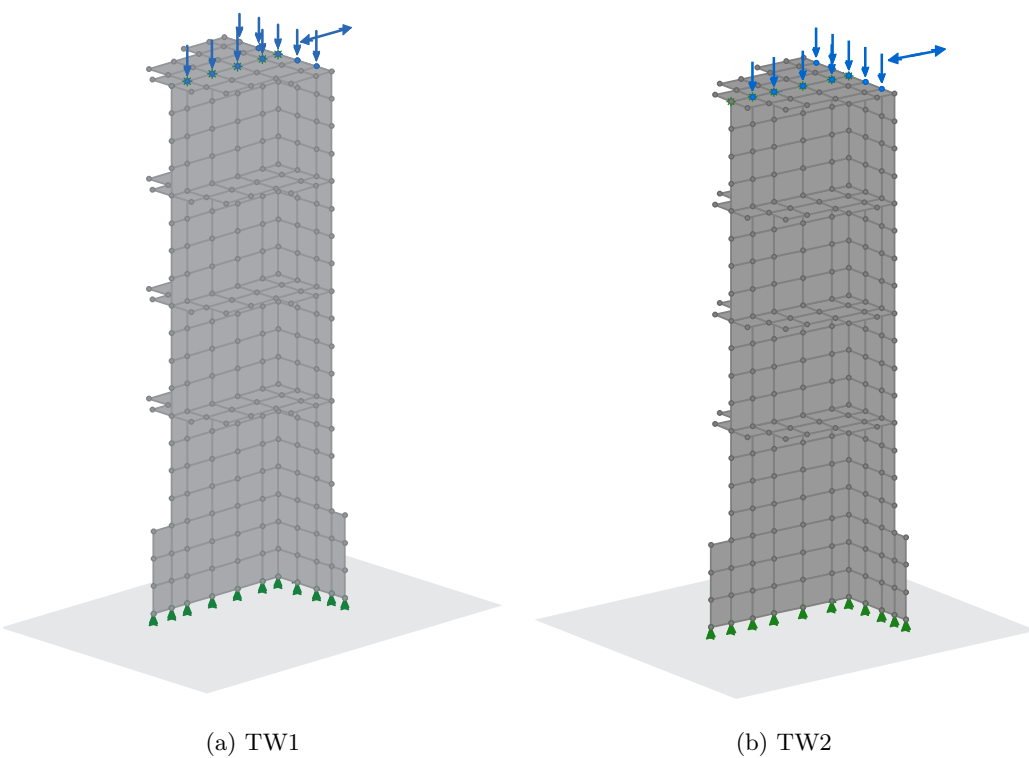
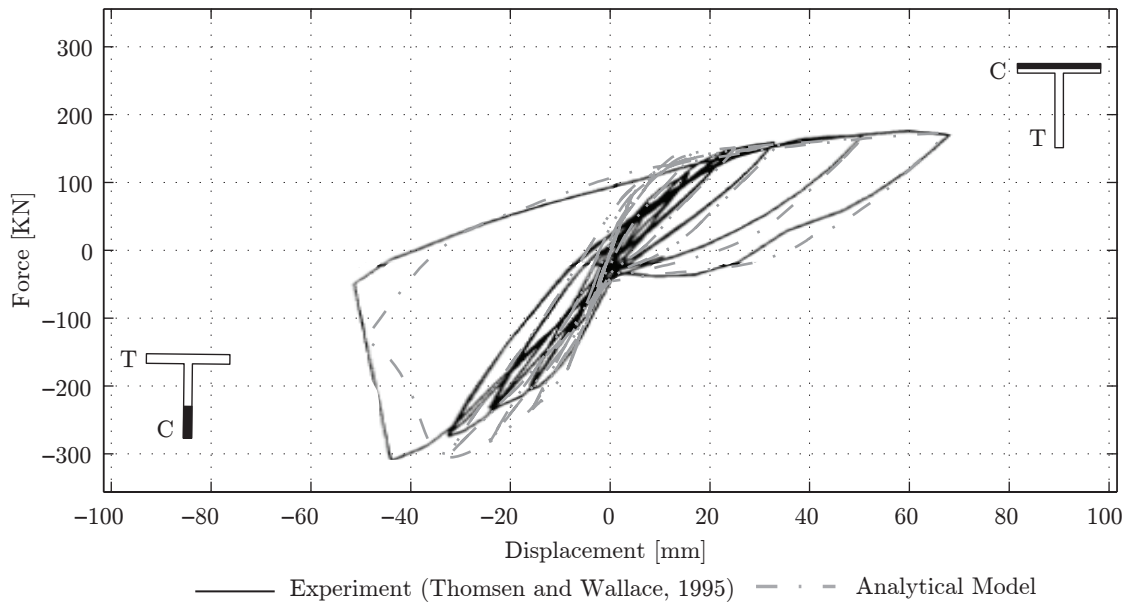
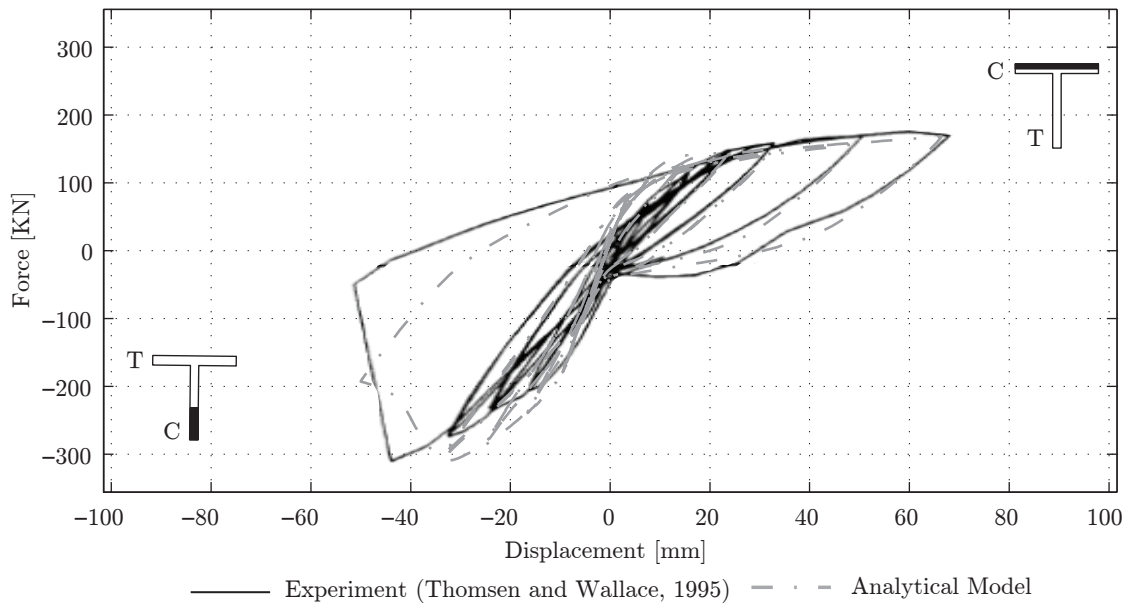


Figure 6.34: Analytical Model for T-Shaped Walls Specimens (TW)

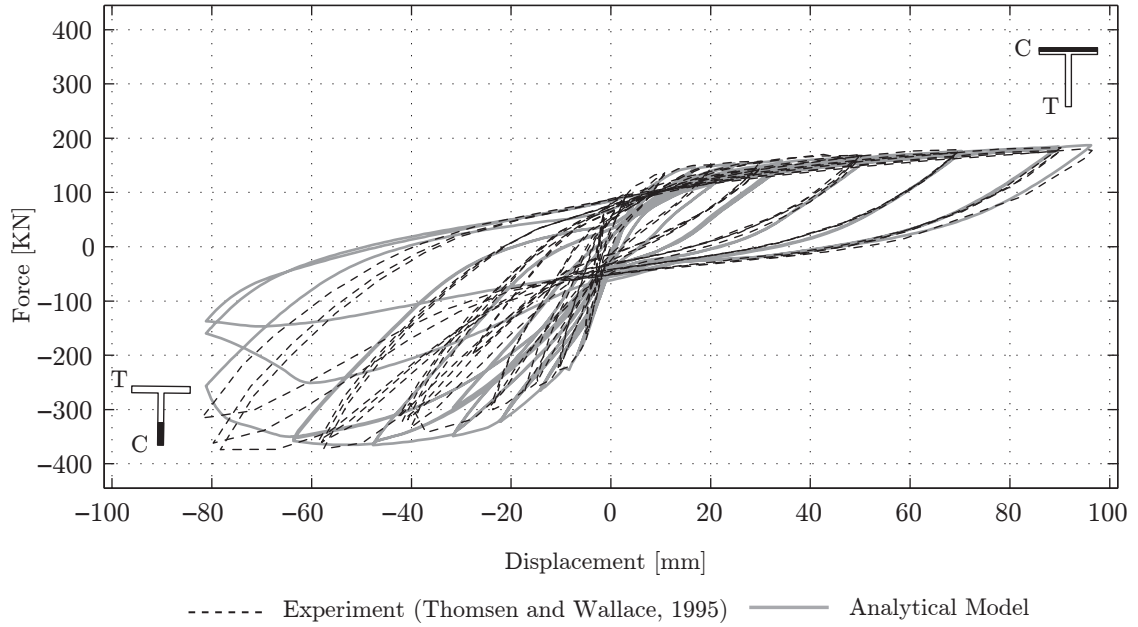


(a) Smeared Steel model using the uniaxial mild steel bar embedded in concrete model

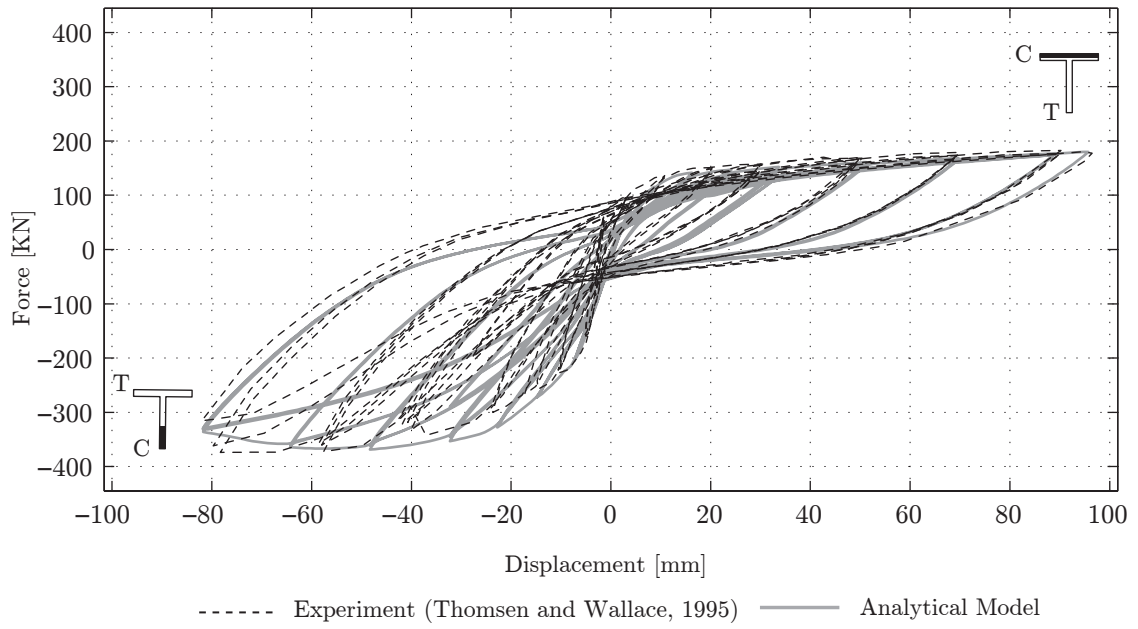


(b) Smeared Steel model using the uniaxial Menegotto-Pinto steel model

Figure 6.35: Load-Displacement Curve of Analytical Model with the plane stress concrete model with Thorenfeldt's curve vs Experiment Results for TW1



(a) Smeared Steel model using the uniaxial mild steel bar embedded in concrete model



(b) Smeared Steel model using the uniaxial Menegotto-Pinto steel model

Figure 6.36: Load-Displacement Curve of Analytical Model with the plane stress concrete model with Thorenfeldt's curve vs Experiment Results for TW2

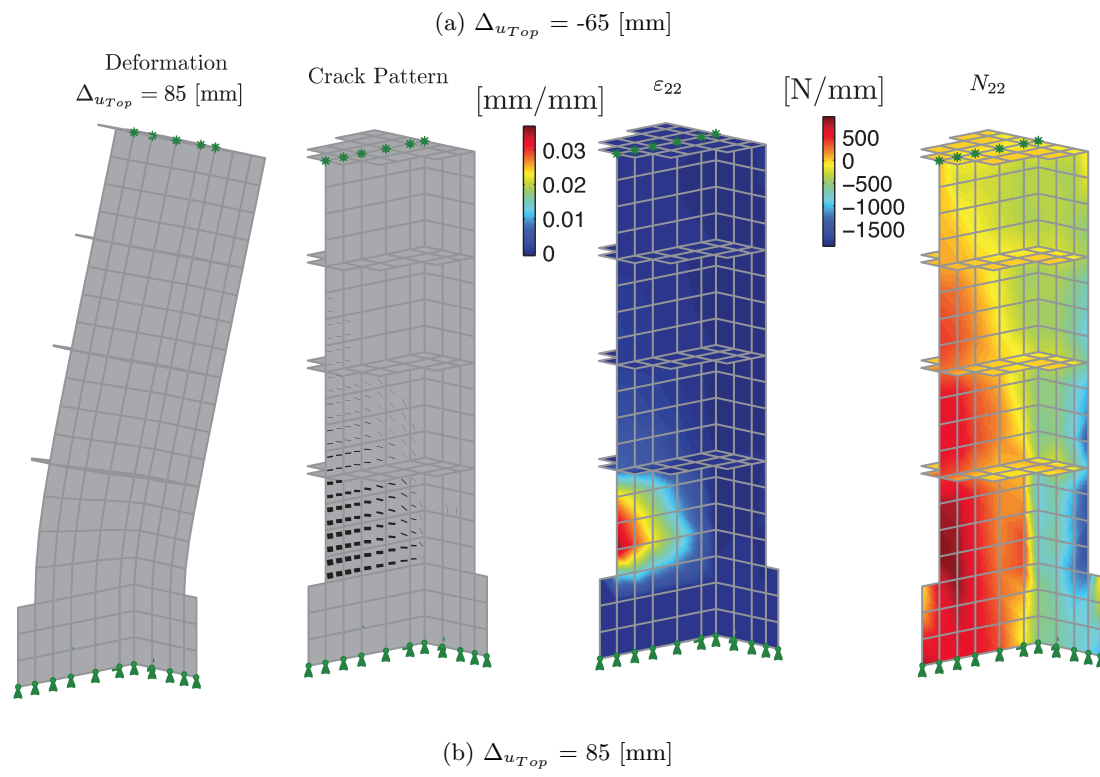
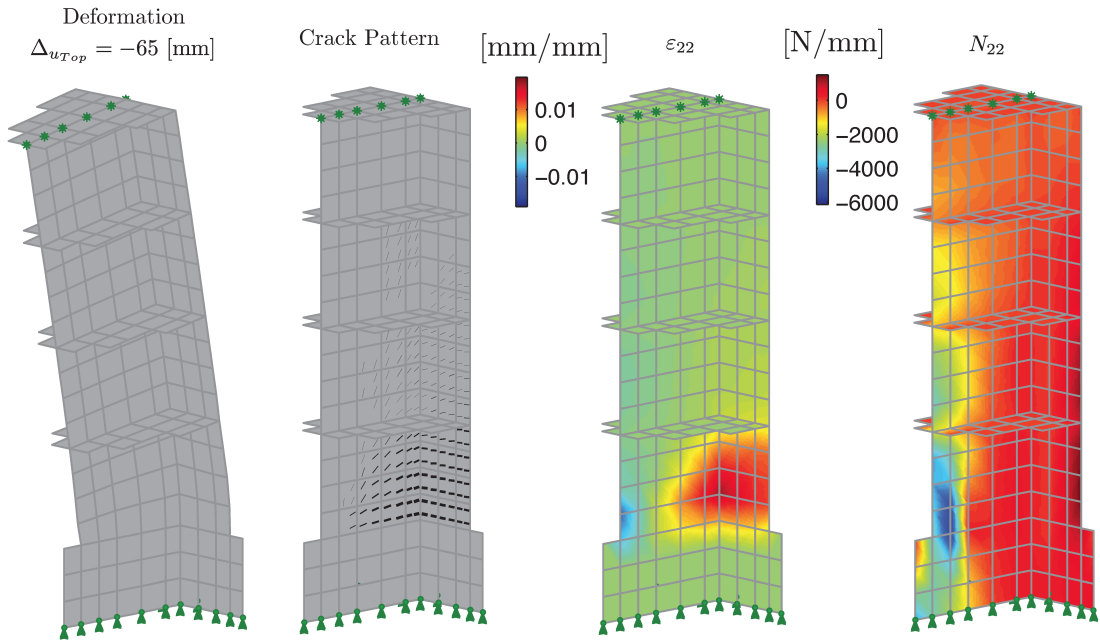


Figure 6.37: Deformation, Crack Pattern, Strain and Stress of the TW2 Analytical Model with the plane stress concrete model with Thorenfeldt's curve and the smeared steel model using the uniaxial Menegotto-Pinto steel model

In Figure 6.35 and Figure 6.36 are shown the comparison of the response for the analytical model against the experimental results of load applied to the wall versus the deformation of the top of the wall for the two walls TW1 and TW2 using a damage coefficient (α_1) of 0.12 in Eq. 4.36. It is observed that for both models the use of the Smeared Steel model using the uniaxial Menegotto-Pinto steel model returns a better agreement with the experimental data. For the TW2 which has a more ductile behavior the model is able to capture the maximum capacity of the wall, however some difference is observed in the portion of the curve, when the flange is in tension, see Figure 6.36. Also, it is shown in Fig. 6.35 that the model is able to capture the failure of the model for the case of TW1, but fails in the capture of the maximum displacement, this could be due to the holding of the wall specimens in the testing setting. In addition, in Fig. 6.37 is shown the deformation observed in the model, the crack pattern, and strains in the model, from this figure is observed the variation of strains through the flange of the model.

6.3 Summary

This chapter considers the evaluation of the accuracy, applicability, and usefulness of the proposed nonlinear layered quadrilateral membrane and shell elements with drilling degrees of freedom using the constitutive model defined in the previous chapters. For the verification of the analytical model a set of experiment results for reinforced concrete wall elements under monotonic and reversed load, that are available in the literature, are compared against the analytical model using the proposed element. Some of the selected test results have also been used as benchmarks by other authors.

The experimental results can be divided into monotonic loading, and reversed loading. For monotonic loading, two different experiments were used. The first set of experiments used considered one of the experimental results from the shear wall tests conducted by Cervenka and Gerstle and presented in Cervenka [24] in 1970. The second set of tests considered the experimental results from tests of two types of walls done by Lefas et al. [80] in 1990. For reversal or cyclic loading results of the tests of two rectangular single walls and two T-shaped cross section walls with slabs at four different levels done by Thomsen and Wallace [132] in 1995 are considered.

In the comparison, it is observed that the analytical model, using the nonlinear layered quadrilateral membrane element with drilling degrees of freedom proposed, is able to predict shear behavior in the wall elements, bending and axial coupling behavior for the slender walls, and shear type behavior (Axial Shear coupling) for the squat walls. Also, the model accurately represents the crack patterns observed in the experiments, and predicts the failure modes of the walls. For reversed load in the rectangular walls, the analytical model using the Menegotto-Pinto model, is the model that best predicts the results of the experimental test. It is able to match the failure type observed for the RW1 wall, and the ductile behavior for the better confined rectangular wall RW2.

The nonlinear layered thin flat quadrilateral shell element with drilling degrees of freedom proposed in this study only used for the modeling of reversed load for two wall specimens with T-Shaped cross sections, tested by Thomsen and Wallace [132]. It is observed from the results that this model provides a close match to the behavior of the T-Wall when the flange is in compression and the web is in tension. For the portion when the flange is in tension and the web is in compression the model only gives a good

representation of representing the behavior and capacity of the T-Shaped wall (TW1 and TW2). However, this model returns better agreement than the proposed analytical models using the MVLM [102, 103], which is the standard model used today to analyze wall elements. In addition, the analytical model for TW1 is able to represent the failure type and capacity of the wall for a T-shaped wall with the same boundary element at the end of the web and the flanges.

Chapter 7

Summary and Conclusions

The main objective of this study was to develop and test a new nonlinear quadrilateral layered membrane element with drilling degrees of freedom and a quadrilateral thin flat layered shell element. These elements were selected because they incorporate the coupling of in-plane flexural, axial and shear behavior for two dimensional wall systems, and the flexural, axial and shear behavior of complex three dimensional reinforced concrete wall systems. The drilling degrees of freedom refer to the incorporation of a degree of freedom that represents the rotation in the plane of the element. In order to develop these elements, this study was divided into five areas, a review of literature of wall element models, a finite element formulation of the proposed elements, a review and definitions of the constitutive material laws to be used in the analysis, the finite element implementation, and the validation and verification of the new proposed elements, which were analysis in each of the chapters of this dissertation. The following is a summary of each of these areas.

In Chapter 2, the standard models used to study the nonlinear behavior of shear wall structures are reviewed. For simplicity and computational cost the macro models stand

out. These are based on predicting the overall behavior of a wall element with the use of simplified assumptions and idealizations [144]. However, this tends to be limited to the cases or problems from which the experimental data was used to create the model. The other type of model, the microscopic model, presented a more theoretical background and then was shown to be more flexible for modeling different structures. Considering this microscopic model, the membrane element used with the smeared orthotropic constitutive material laws is the most commonly used for the modeling of two dimensional structures. However, these models only include the in-plane effects over the walls, and are typically used with 2 degrees of freedom per node. Due to these limitations, they are difficult to connect with other elements such as beams. In the case of three dimensional structures the shell elements stand out over the rest, because, they permit the modeling of the complete interrelation of simple and complex wall structures and buildings. It was also concluded that layered shells should be the best option to model complex three dimensional walls, and the quadrilateral membrane element with drilling degrees of freedom to model two dimensional modes. The shell takes the advantage of incorporating the interrelation of all the different elements in a building in a simple and robust manner, and also incorporates all the coupling effect of the deformation inside of each wall. This allows the modeling of complex behavior of the wall structures and buildings.

In Chapter 3, the finite element formulation for the proposed elements are presented. First the finite element formulation for a nonlinear layered membrane element with drilling degrees of freedom was studied, and for the field interpolation the extension proposed in this dissertation of the 4-node membrane element with drilling degrees of freedom proposed by Xia et al. [151] was used. The proposed field interpolation, to be used in a general

finite element framework using natural coordinates, called blended interpolation, used a cubic interpolation in y and a linear interpolation in x for the horizontal displacement, and for the vertical displacement direction it used a cubic interpolation in x and a linear interpolation in y . The DKQ formulated by Batoz and Tahar [11], to model plate bending elements is also described. These two elements were combined to represent the theoretical framework for developing the formulation of a quadrilateral thin flat layered shell element with 24 DOF (6 DOF per node) which will be used to model the response of structure walls using the finite element method. These selected models balance accuracy, simplicity and computational cost.

In Chapter 4, the large amount of literature available for the material constitutive laws to represent the behavior of concrete was reviewed. Of the models available, it was determined that the smeared cracked concrete model, which is based in the assumption that different cracks over an area can be modeled using the average stress-strain relation of concrete in that zone, are the preferable concrete models to use. Between the smeared cracked models, the orthotropic models stand out for their accuracy and simplicity, and which are robust enough to represent the material behavior of concrete. Also, it was concluded that in order to work with a layered section approach, separate constitutive models for smeared concrete layer and smeared steel layer are necessary. The constitutive model used to represent the plane stress behavior of concrete is based on the smeared crack approach using the orthotropic model with the equivalent uniaxial average stress-strain relations in the axes of orthotropy. The axes of orthotropy are assumed to coincide with the principal axes of total strain, and this model is developed in a tangent stiffness-based approach for nonlinear finite elements. In addition, this concrete model incorporates

biaxial strength coefficients to consider the influence of biaxial compression or tension-compression (softening) in the axes of orthotropy, and also to account for damage in the material during cyclic loading and enhancement due to confinement. The selection of the different features for the model presented before were done to be able to use a layered section approach developed in the last chapter, and also to obtain a numerically stable, reliable and efficient constitutive material behavior.

The behavior of the concrete in the principal direction of stress, which coincides with the principal direction of strain, is defined by average uniaxial stress-strain relations. Two uniaxial concrete materials were selected to represent the average uniaxial stress-strain relations over the principal direction of stress for this smeared rotating angle concrete model. These two material models are: the one proposed by Massone [90] in 2006 for static load and later expanded to include hysteretic rules, also developed by Massone on OpenSees [82]. The second model is a simplified Chang-Mander model proposed by Waugh [147] in 2009. However, the second uniaxial concrete model was only used to model monotonic tests, because some numerical instability was reached during the analysis of cyclic loads.

In addition, in Chapter 4 the smeared steel constitutive material used to represent the horizontal and vertical reinforcement steel layer in the membrane and shell element was presented. In this approach, it is assumed that the steel bars are considered as a layer of homogenous material at certain positions inside of the reinforced concrete element and the variation in stress due to the crack over an area can be modeled using the average stress-strain of steel in that zone. In addition, it was considered that the smeared steel works only in the direction of the bar, due to the fact that the bars are typically in a uniaxial

state of stress, and this allows the use of a uniaxial constitutive model. Two uniaxial steel material models were used in this study, the one proposed by Mansour et al. [88] in 2001, the Mild Steel Bar Embedded in Concrete Model, and the well known Menegotto and Pinto Steel models proposed by [94] in 1973.

In Chapter 5, a summary of the finite implementation used in this study is presented. For this study, it was decided to develop an Object Oriented Finite Element Toolbox under MATLAB using the object oriented programming language in MATLAB [62]. Because of a need for a powerful toolbox or framework that will be easy to use, extend, maintain for the Nonlinear Structural Analysis or Finite Element Analysis under MATLAB [62] was required. The abstractions of the components for finite element and structural analysis proposed by McKenna [93] in 1997 and extended in OpenSees [82] are used to develop the proposed Object-Oriented Finite Element Toolbox for MATLAB [62], and some modification and extension to the abstraction proposed by McKenna [93] in 1997 were done in order to implement the toolbox.

In addition, in Chapter 5 the nonlinear analysis algorithms were reviewed and the Full Newton-Raphson with an incremental iterative displacement-control was the selected solution strategy to perform the analysis in this study.

In Chapter 6 an evaluation of the accuracy, applicability, and usefulness of the proposed nonlinear quadrilateral layered membrane with drilling degrees of freedom and the nonlinear quadrilateral thin flat layered shell element, and the constitutive model defined in the previous chapters in this study was performed. For the verification of the analytical model a set of experimental results for reinforced concrete wall elements under monotonic

and reversed load that are available in the literature, and which have been used as benchmarks for other models, were compared against the analytical model using the proposed element. For monotonic loading, two different result of experiments were used. The first comparison used the experimental results of one of the shear wall tests done by Cervenka and Gerstle and presented in Cervenka [24] in 1970. The second set of comparison considered the experimental results of the test program of two types of walls done by Lefas et al. [80] in 1990. For reversal or cyclic loading, results of the tests of two rectangular single walls and two T-shaped cross section walls with slabs at four different levels done by Thomsen and Wallace [132] in 1995 were used. Excellent agreement was obtained between the analytical model and the experiment results.

It is important to mention again that the Object Oriented Finite Element Toolbox under MATLAB was used integrally to analysis the models, and produce the different figures of the results of the models presented in this dissertation. This toolbox, as was expected, allows a fast programming and debugging of the new elements and material definitions presented in the chapters before, and also present a extensibility to include difference type of analysis, procedures and post processing views within the timing necessaries in academic and research applications. All the analysis were running in a regular personal computer, with a Intel Core i5 of 2.8 GHz and 12 Gb in RAM. For the monotonic loading test cases, the model need only a few minutes to finish the analysis. However for the cyclic loading test cases, the analysis took a day for the RW1 case and a day and a half for RW2 case. For the T-Shaped walls the model took around two days for the TW1 case and three days for the TW2 case. A more detailed comparison between the running time of a model

using this toolbox and a procedural approach or other compiled program need to be done to evaluate the speed of the program.

The nonlinear quadrilateral layered membrane element with drilling degrees of freedom, presents a good agreement with the test results, allowing it to model the different types of failure and behavior of the different type of walls (squat and slender), as shear behavior, axial bending coupling, influence of the multi axial load conditions, and the cycling behavior of rectangular walls with different ratios of steel. For monotonic load and reversed load the smeared plane stress concrete model with the Thorenfeldt's curve returns the better and more stable results for the analytical model. However a value of average strain (ε_{c_o}) for the peak strength of concrete (f'_c) of around 0.035 to 0.055 [mm/mm] was needed to use with this model to match the experimental results. This value could be attributed to the use of an average stress-strain relations instead of the uniaxial relationship. In addition, the other model using the simplified Chang Mander Model produces some instability for reversed loads, a possible reason of the instability could be due to the complex rules used to define the unloading and reloading paths in the material model, which were defined to model the behavior of uniaxial concrete and no biaxial behavior of concrete.

For the monotonic load tests, both smeared steel material with different uniaxial steel model return very similar results without any significant difference. This was expected, because the two models were calibrated to have the same envelope at tension, which accounts for the behavior of steel bars embedded in concrete. Also, the model using the biaxial strength return a better correlation with the experimental data. An overestimation of the response of the walls is obtained if the softening due to tension-compression is

not considerer. This is the case for the model without biaxial strength coefficients. The difference is more apparent between the model with and without biaxial strength coefficients for models that undergo larger values of biaxial tension and compression, like for squat walls.

In the model RW1 and RW2, it was observed that the model using the smeared plane stress concrete model with Thorenfeldt's curve including a damage factor for cycling and the use of the Menegotto and Pinto model are in excellent agreement with the experimental results. And for the model RW1, the analytical analysis determine the exact failure load and displacement as the experiment. For the analytical model using the other type of steel, the mild steel bar embedded in concrete model, it was only obtained good and adequate agreement with the experimental results. This could be attributed to how the steel pass from the unloading and reloading zone to the bilinear envelops of the material.

The nonlinear quadrilateral layered thin flat shell element with drilling degrees of freedom proposed in this study, was only used for the modeling of reversed load, for two walls specimens with T-Shaped cross sections, tested by Thomsen and Wallace [132]. It is observed from the results that the model perfectly predicts the behavior of the T-Wall when the flange is in compression and the web is in tension. Instead, for the portion when the flange is in tension and the web is in compression the model is able to adequately represent the behavior and capacity of the T-Shaped wall. However this model return better agreement than the proposed analytical models used and calibrated with this test by Orakcal et al. [103] and Orakcal and Wallace [102] in 2006, which use the standard type of element (MVLM) used today for the modeling of walls. Even so, the model did not capture perfectly the behavior of the T-Shaped wall when the flange is in compression,

the model is able to determine for test TW1 the failure type, capacity and the cycling level where failure happens. As mentioned this new model allows the modeling of the distribution and variation of strain over the length of the web and the flange, and it could allow to study the movement of the neutral axis and the real stress distribution over the elements. This is because there is no restriction of plane sections remaining plane for models like beams or MVLM or fiber elements. In addition, the model takes into consideration the interrelation of the different components in the wall without the necessity of coming up with fictitious springs or effective areas in the flange.

7.1 Future work and Recommendations

The quadrilateral membrane element with drilling degrees of freedom to large deformation will be extended. This is already undergoing. For this purpose the use of the Total Lagrangian approach was selected.

A more detailed hysteretic rule for the average stress-strain concrete will be proposed, but retaining the envelope defined by the Thorenfeldt's curve.

Walls under earthquake load to study the behavior of the proposed element and concrete and steel materials will be analyzed.

The analysis of more complex structures or small buildings under monotonic, cycling and earthquake load using the nonlinear quadrilateral thin flat shell element with drilling degrees of freedom need to be performed to study its applicability to complete real buildings.

The strain (ε_{c_o}) for the peak resistant stress of concrete under compression necessary to use in plane stress concrete materials need to be studied in more detailed.

Curve of fragilities using this model to compare the result to real walls and extend the fragilities curves available today to different type or dimension of walls will be developed.

The damage coefficients in the concrete to include cyclic fatigue will be studied better.

The inclusion of more complex constitutive laws for the steel that account for cycling fatigue and buckling of the bars need to be studied.

References

- [1] B. N. Abu Ghazaleh. *Analysis of Plate Type Prismatic Structures*. Phd dissertation, University of California, Berkeley, Berkeley, California, 1966.
- [2] *Building Code Requirements for Reinforced Concrete (ACI 318-83)*. ACI Committee 318, Detroit, 1983.
- [3] *ADINA Version 6.1.4*. ADINA R&D, Inc, Watertwon, M. A., 1995.
- [4] D. J. Allman. A compatible triangular element including vertex rotations for plane elasticity analysis. *Computers & Structures*, 19(1-2):1 – 8, 1984.
- [5] W. Aquino and I. Erdem. Implementation of the modified compression field theory in a tangent stiffness-based finite element formulation. *International Journal of Steel and Composite Structures*, 7(4):263–278, 2007.
- [6] J. D. Ariatizabal-Ochoa. Cracking and shear effects of structural walls. *Journal of Structural Engineering*, 109(5):1267–1275, May 1983.
- [7] A. Ayoub and F. C. Filippou. Nonlinear finite-element analysis of rc shear panels and walls. *Journal of Structural Engineering*, 124(3):298–308, 1998.
- [8] S. Balakrishnan and D. W. Murray. Concrete constitutive model for nlee analysis of structures. *Journal of Structural Engineering*, 114(7):1449–1466, July 1988.
- [9] K. J. Bathe. *Finite Elements Procedures*. Prentice Hall, Inc., Upper Saddle River, New Jersey 07458, 1996.
- [10] J. L. Batoz and G. Dhatt. Incremental displacement algorithms for nonlinear problems. *International Journal for Numerical Methods in Engineering*, 14(8):1262–1267, 1979.
- [11] J. L. Batoz and M. Tahar. Evaluation of a new quadrilateral thin plate bending element. *International Journal for Numerical Methods in Engineering*, 18(11):1655–1677, 1982.
- [12] Z. P. Bazant and F. C. Caner. Microplane model m5 with kinematic and static constraints for concrete fracture and anelasticity. i: Theory. *Journal of Engineering Mechanics*, 131(1):31–40, 2005.
- [13] Z. P. Bazant and B. H. Oh. Microplane model for progressive fracture of concrete. *Journal of Engineering Mechanics, ASCE*, 111(4):559–581, 1985.

- [14] Z. P. Bazant, Y. Xiang, and P. C. Prat. Microplane model for concrete. i: Stress-strain boundaries and finite strain. *Journal of Engineering Mechanics*, 122(3):245–254, 1996.
- [15] Z. P. Bazant, F. C. Caner, I. Carol, M. D. Adley, and S. A. Akers. Microplane model m4 for concrete. i: Formulation with work-conjugate deviatoric stress. *Journal of Engineering Mechanics*, 126(9):944–953, 2000.
- [16] A. Belarbi and T. T. C. Hsu. Constitutive laws of concrete in tension and reinforcing bars stiffened by concrete. *ACI Structural Journal*, 91(4):465–474, 1994.
- [17] A. Belarbi and T. T. C. Hsu. Constitutive laws of softened concrete in biaxial tension compression. *ACI Structural Journal*, 92(5):562–573, 1995.
- [18] B. Belletti, R. Cerioni, and I. Iori. Physical approach for reinforced-concrete (parc) membrane elements. *Journal of Structural Engineering, ASCE*, 127(12):1412–1426, December 2001.
- [19] P. G. Bergan and C. A. Felippa. A triangular membrane element with rotational degrees of freedom. *Computer Methods in Applied Mechanics and Engineering*, 50 (1):25–69, July 1985.
- [20] V. V. Bertero. Seismic behaviors of rc wall structural system. In *7th World Conference on Earthquake Engineering*, volume 6, pages 323–330, Instalbul, Turkey, September 1980 1980.
- [21] J. J. Bolander and J. K. Wight. Finite element modeling of shear-wall-dominant buildings. *Journal of Structural Engineering*, 117(6):1719–1739, 1991.
- [22] L. D. Carpenter, F. Naeim, M. Lew, N. F. Youssef, F. Rojas, G. R. Saragoni, and M. Schachter. Performance of tall buildings in viña del mar in the 27 february 2010 offshore maule, chile earthquake. *The Structural Design of Tall and Special Buildings*, 20(1):17–36, 2011.
- [23] D. J. Carreira and C. Kuang-Han. Stress-strain relationship for plain concrete in compression. *ACI Structural Journal*, 82(6):797–804, 1985.
- [24] V. Cervenka. *Inelastic Finite Element Analysis of Reinforced Concrete Panels under In-plane Loads*. Phd thesis, University of Colorado, Boulder, Colorado, 1970.
- [25] V. Cervenka. Constitutive model for cracked reinforced concrete. *ACI Journal*, 82 (6):877–882, November-December 1985.
- [26] M. Cervera, E. Hinton, and O. Hassan. Nonlinear analysis of reinforced concrete plate and shell structures using 20-noded isoparametric brick elements. *Computers & Structures*, 25(6):845–869, 1987.
- [27] G. A. Chang and J.B. Mander. Seismic energy based fatigue damage analysis of bridge columns: Part 1 evaluation of seismic capacity. Technical report no. nceer-94-0006, State University of New York, Buffalo, NY, 1974.

- [28] F. A. Charney. *Correlation of the Analytical and Experimental Seismic Response of a 1/5th-Scale Seven-Story Reinforced Concrete Frame-Wall Structure*. Phd dissertation, University of California, Berkeley, 1987.
- [29] W. F. Chen. *Plasticity in Reinforced Concrete*. J Ross Publishing Classic, 5765 N Andrews way, Fort Lauderdale, reprint edition, 2007.
- [30] Y. K. Cheung. *Handbook of Structural Concrete*, chapter 38: Tall Buildings 2, pages 38–1 to 38–51. Pitman Books Limited, London, England, 1983.
- [31] U. Cicekli, G. Z. Voyiadjis, and R. K. Abu Al-Rub. A plasticity and anisotropic damage model for plain concrete. *International Journal of Plasticity*, 23(10-11):1874 – 1900, 2007.
- [32] M. P. Collins. Towards a rational theory for rc members in shear. *Journal of Structural Engineering, ASCE*, 104(4):649–666, April 1978.
- [33] M. P. Collins and A. Porasz. *Bulletin D'Information No. 193 - Design Aspects of High Strength Concrete*, chapter Shear Strength for High Strength Concrete, pages 75–83. Paris, France, 1989.
- [34] R. D. Cook. On the allman triangle and a related quadrilateral element. *Computers & Structures*, 22(6):1065 – 1067, 1986.
- [35] R. D. Cook, D. S. Malkus, M. E. Plesha, and R. J. Witt. *Concepts and Applications of Finite Element Analysis*. John Wiley & Sons, Inc, 4th edition, 2002.
- [36] M. A. Crisfield and J. Wills. Analysis of r/c panels using different concrete models. *Journal of Engineering Mechanics, ASCE*, 115(3):578–597, March 1989.
- [37] M.A. Crisfield. A fast incremental/iterative solution procedure that handles 'snap through'. *Computers & Structures*, 13(1-3):55 – 62, 1981.
- [38] CSI. Computer & structures, inc, developer of sap2000, etabs, perform3d. <http://www.csiberkeley.com>, 2010.
- [39] D. Darwin and D. A. Pecknold. Analysis of cyclic loading of plane structures. *Computers & Structures*, 7(1):137 – 147, 1977.
- [40] D. Darwin and D. A. W. Pecknold. Inelastic model for cyclic biaxial loading of reinforced concrete. Civil Engineering Studies, Structural Research Series 409, University of Illinois at Urbana-Champaign, Urbana, Illinois, United States, July 1974.
- [41] T. Eimani. *Analytical Model for Reinforced Concrete Shear Wall Structures*. Phd dissertation, University of Southern California, Los Angeles, California, May 1997.
- [42] R. J. Evans and K. S. Pister. Constitutive equations for a class of nonlinear elastic solids. *International Journal of Solids Structures*, 2(3):427–445, 1966.
- [43] P. Fajfar and M. Fischinger. Mathematical modeling of rc structural walls for non-linear seismic analysis. In *European Conference on Structural Dynamics.*, Bochum, Germany, 1990.

- [44] G. L. Fenves. Object-oriented programming for engineering software development. *Engineering with Computers*, 6:1–15, 1990.
- [45] A. J. M.. Ferreira. *MATLAB Codes for Finite Element Analysis, Solids and Structures*. Solid Mechanics and Its Applications, Vol. 157. Springer, 2009.
- [46] F. C. Filippou. FedelasLab: Finite Elements in Design, Evaluation and Analysis of Structures, <http://fedeaslab.berkeley.edu/>, Getting Started Guide: <http://fedeaslab.berkeley.edu/NEESgrid-TR22.pdf>, University of California, Berkeley, 2004.
- [47] F. C. Filippou and M. Constantinides. Fedelaslab, getting started guide and simulation examples. NEESgrid 2004-22, NEESgrid, 2004. URL <http://fedeaslab.berkeley.edu/NEESgrid-TR22.pdf>.
- [48] F. C. Filippou, E. G. Popov, and V. V. Bertero. Effects of bond deterioration on hysteretic behavior of reinforced concrete joints. UCB/EERC 83/19, Earthquake Engineering Research Center, University of California, Berkeley, 1983.
- [49] S. J. Foster and P. Marti. Cracked membrane model: Finite element implementation. *Journal of Structural Engineering*, 129(9):1155–1163, 2003.
- [50] Python Software Foundation. Python: www.python.org, Documentation: <http://www.python.org/doc/>, 1990-2012.
- [51] *Abaqus Standard, Version 6.5.1*. Hibbit, Karlsson & Sorenson, Inc, Pawtucket, R. I., 2004.
- [52] H. Hiraishi. Evaluation of shear and flexural deformations of flexural type shear wall. In *4th Joint Technical Coordinating Committe, U.S.-Japan Cooperative Earthquake Research Program*. Building Research Institute , Tsukuba, Japan, 1983.
- [53] T. T. C. Hsu. Softened truss model theory for shear and torsion. *ACI Structural Journal*, 85(6):624–635, 1988.
- [54] T. T. C. Hsu. Nonlinear analysis of concrete membrane elements. *ACI Structural Journal*, 88(5):552–561, 1991.
- [55] T. T. C. Hsu. *Unified theory of Reinforced Concrete*. CRC Press Inc., Boca Raton, Fl, 1992.
- [56] T. T. C. Hsu and Y. L. Mo. *Unified theory of Reinforced Concrete Structure*. John Wiley & Sons, Ltd, 2010.
- [57] T. T. C. Hsu and L. X. Zhang. Nonlinear analysis of membrane elements by fixed-angle softened-truss model. *ACI Structural Journal*, 94(5):483–492, 1997.
- [58] T. T. C. Hsu and R. R. H. Zhu. Softened membrane model for reinforced concrete elements in shear. *ACI Structural Journal*, 99(4):460–469, 2002.

- [59] T. J. R. Hughes and F. Brezzi. On drilling degrees of freedom. *Computer Methods in Applied Mechanics and Engineering*, 72(1):105–121, January 1989.
- [60] A. Ibrahimovic, R. Taylor, and E. Wilson. A robust quadrilateral membrane finite element with drilling degrees of freedom. *International Journal for Numerical Methods in Engineering*, 30(3):445–457, 1990.
- [61] N. Ile and J. M. Reymouard. Nonlinear analysis of reinforced concrete wall under earthquake loading. *Journal of Earthquake Engineering*, 4(2):183–213, 2000.
- [62] The MathWorks Inc. MATLAB R2012: <http://www.mathworks.com/products/matlab/>, Documentation: Programing Fundamentals; Object-Oriented Programming, <http://www.mathworks.com/help/techdoc/>, 1994-2012.
- [63] *Uniform Building Code (1994)*. International Conference of Building Officials, Whittier, California, 1994.
- [64] J. Izumo, H. Shin, K. Maekawa, and H. Okamura. An analytical model for rc panels subjected to in-plane stresses. In *International Workshop on Concrete Shear Earthquake*, pages 206–215, Houston, Jan 14-16 1991. Elsevier Science Publishers, Inc.
- [65] T. Kabeyasawa and J. I. Milev. Modeling of reinforced concrete shear walls under varying axial load. In *14th International Conference on Structural Mechanics*, August 17-22 1997.
- [66] T. H. Kabeyasawa, S. Shiohara, S. Otani, and H. Aoyama. Analysis of the full-scale 7-story r.c. test structure. In *3rd Joint Technical Coordinating Committee, U.S Japan Cooperative Earthquake Research Program*. Building Research Institute, Tsukuba, 1982.
- [67] I. D. Karsan and J. O. Jirsa. Behavior of concrete under compressive loadings. *Journal of Structural Division*, 95:2535–2563, 1969.
- [68] P. I. Kattan. *MATLAB Guide to Finite Elements: An Interactive Approach*. Springer, 2nd edition, 2008.
- [69] W. Kaufmann. Structural concrete: Cracked membrane model. *Journal of Structural Engineering, ASCE*, 124(12):1467–1475, December 1998.
- [70] C. Kerem Gulec and A. S. Whittaker. Performance-based assessment and design of squat reinforced concrete shear walls. Technical Report MCEER 09-0010, Earthquake Engineering to Extreme Events, MCEER, University at Buffalo, State University of New York, September 15 2009.
- [71] M. Keshavarzian and W. C. Schnobrich. Computed nonlinear response of reinforced concrete wall-frame structures. Technical report, University of Illinois. Urbana, Champaign, SRS 515.
- [72] D. Khatri. *Nonlinear Analysis of Reinforced Concrete Shear Wall Structures*. Phd dissertation, University of Southern California, Los Angeles, California, May 1998.

- [73] T. Kim, J. Choi, and W. Kim. Nonlinear analysis of reinforced and prestressed concrete shells using layered elements with drilling dof. *Journal of the Korea Concrete Institute*, 17(4):645–654, August 2005.
- [74] S. K. Kunnath, Y. Heo, and J. F. Mohle. Nonlinear uniaxial material model for reinforcing steel bars. *Journal of Structural Engineering*, 135(4):335–343, 2009.
- [75] H. Kupfer, H.K. Hilsdorf, and H. Rusch. Behavior of concrete under biaxial stresses. *ACI Journal*, 66(8):656–666, 1969.
- [76] A. K. H. Kwan. Mixed finite element method for analysis of coupled shear/core walls. *Journal of Structural Engineering*, 119(5):1388–1401, May 1993.
- [77] A. K. H. Kwan and Y. K. Cheung. Analysis of coupled shear/core walls using a beam-type finite element. *Engineering Structures*, 16(2):111 – 118, 1994.
- [78] R. Lafore. *Object-Oriented Programming in C++*. Sams Publishing, 800 East 96th St., Indianapolis, Indiana 46240 USA, 4th edition, 2002.
- [79] J. Lee and G. L. Fenves. A return-mapping algorithm for plastic-damage models: 3-d and plane stress formulation. *International Journal for Numerical Methods in Engineering*, 50(2):487–506, 2001.
- [80] I. D. Lefas, M. D. Kotsovos, and N. N. Ambraseys. Behavior of reinforced concrete structural walls: Strength, deformation characteristic, and failure mechanism. *ACI Structural Journal*, 87(1):23–31, 1990.
- [81] Y. C. Loo and H. Guan. Cracking and punching shear failure analysis of rc flat plates. *Journal of Structural Engineering*, 123(10):1321–1330, October 1997.
- [82] F. MacKenna and G. L. Fenves. OpenSees: Open System for Earthquake Engineering Simulation. <http://opensees.berkeley.edu/index.php>, User Documentation: http://opensees.berkeley.edu/wiki/index.php/OpenSees_User, Command Manuals: http://opensees.berkeley.edu/wiki/index.php/Command_Manual, University of California, Berkeley, 2006.
- [83] R. H. Macneal and R. L. Harder. A refined four-noded membrane element with rotational degrees of freedom. *Computers & Structures*, 28(1):75 – 84, 1988.
- [84] K. Maekawa, A. Pimanmas, and H. Okamura. *Nonlinear Mechanics of Reinforced Concrete*. Spon Press, Taylor & Francis Group, 29 West 35th Street, New York, NY 10001, first edition edition, 2003.
- [85] J. B. Mander, J. N. Priestley, and R. Park. Theoretical stress-strain model for confined concrete. *Journal of Structural Engineering*, 114(8):1804–1826, 1988.
- [86] M. Mansour and T. T. C. Hsu. Behavior of reinforced concrete elements under cyclic shear. i: Experiments. *Journal of Structural Engineering*, 131(1):44–53, 2005.
- [87] M. Mansour and T. T. C. Hsu. Behavior of reinforced concrete elements under cyclic shear. ii: Theoretical model. *Journal of Structural Engineering*, 131(1):54–65, 2005.

- [88] M. Mansour, J. Y. Lee, and T. T. C. Hsu. Cyclic stress-strain curves of concrete and steel bars in membrane elements. *Journal of Structural Engineering*, 127(12): 1402–1411, 2001.
- [89] P. Martinelli and F. C. Filippou. Simulation of the shaking table test of a seven-story shear wall building. *Earthquake Engineering & Structural Dynamics*, 38(5): 587–607, 2009.
- [90] L. M. Massone. *RC Wall Shear - Flexure Interaction: Analytical and Experimental Responses*. Phd dissertation, University of California, Los Angeles, California, 2006.
- [91] L. M. Massone and J. W. Wallace. Load-deformation responses of slender reinforced concrete walls. *ACI Structural Journal*, 101(1):103–113, January–February 2004.
- [92] F Mckenna. Getting started with opensees: Introduction to opensees and tcl/tk. In *OpenSees Days 2011: A two-day workshop on OpenSees*, University of California, Richmond Field Station, 2011. NEES/PEER, University of California, Berkeley. URL <http://opensees.berkeley.edu/OpenSees/workshops/OpenSeesDays2011>.
- [93] F. T. McKenna. *Object-Oriented Finite Element Programming: Frameworks for Analysis, Algorithms and Parallel Computing*. Phd dissertation, University of California, Berkeley, Berkeley, California, 1997.
- [94] M. Menegotto and P. E. Pinto. Method of analysis of cyclically loaded reinforced concrete plane frames including changes in geometry and non-elastic behavior of elements under combined normal force and bending. In *IABSE Symposium on the Resistance and Ultimate Deformability of Structures Acted on by Well-Defined Repeated Loads*, Lisbon, 1973.
- [95] Z. W. Miao, X. Z. Lu, J. J. Jiang, and L. P. Ye. Nonlinear fe model for rc shear walls based on multi-layer shell element and microplane constitutive model. In *Computational Methods in Engineering and Science, EPMESC X*, Sanya, Hainan, China, Aug. 21-23 2006.
- [96] S. Mindess, J. F. Young, and D. Darwin. *Concrete*. Prentice Hall, Pearson Education, Inc., Upper Saddle River, NJ 07458, second edition edition, 2003.
- [97] Y. L. Mo, J. Zhong, and T. T. C. Hsu. Seismic simulation of rc wall-type structures. *Engineering Structures*, 30(11):3167 – 3175, 2008.
- [98] J. Moehle, J. W. Wallace, J. Maffei, C. Sempere, A. Celestino, J. J. Besa, J. Dragovich, B. Westenenk, A. Millan, C. Frings, and J. P. Herranz. February 27, 2010 chile earthquake reconnaissance team investigation: Reinforced concrete buildings. Reconnaissance report, EERI, 2010.
- [99] F. Naeim, M. Lew, L. D. Carpenter, N. F. Youssef, F. Rojas, G. R. Saragoni, and M. Schachter. Performance of tall buildings in santiago, chile during the 27 february 2010 offshore maule, chile earthquake. *The Structural Design of Tall and Special Buildings*, 20(1):1–16, 2011.

- [100] H. Nguyen-Van, N. Mai-Duy, and T. Tran-Cong. An improved quadrilateral flat element with drilling degrees of freedom for shell structural analysis. *CMES: Computer Modeling in Engineering & Sciences*, 49(2):81–110, 2009.
- [101] E. Oñate. *CISM Course and Lectures No. 328. International Centre for Mechanical Sciences: Nonlinear Analysis of Shells by Finite Elements*, chapter Nonlinear Finite element Analysis of Concrete, pages 195–256. Springer-Verlag-Wien, 1992.
- [102] K. Orakcal and J. W. Wallace. Flexural modeling of reinforced concrete walls - experimental verification. *ACI Structural Journal*, 103(2):196–206, March-April 2006.
- [103] K. Orakcal, L. M. Massone, and J. W. Wallace. Analytical modeling of reinforced concrete walls for predicting flexural and coupled-shear-flexural responses. PEER Report 2006/07, Pacific Earthquake Engineering Research Center. University of California, Los Angeles, October 2006.
- [104] S. Otani, T. H. Kabayesawa, S. Shiohara, and H. Aoyama. Analysis of the full-scale 7-story r.c. test structure. *ACI Special Publication SP-84*, 1985.
- [105] D. Palermo. *Behavior and Analysis of Reinforced Concrete Walls Subjected to Reversed Cycling Loading*. Phd thesis, Department of Civil Engineering, University of Toronto, Toronto, Canada, May 2002.
- [106] D. Palermo and F. J. Vecchio. Compression field modeling of reinforced concrete subjected to reversed loading: Formulation. *ACI Structural Journal*, 100(5):616–625, 2003.
- [107] D. Palermo and F. J. Vecchio. Compression field modeling of reinforced concrete subjected to revered loading: Verification. *ACI Structural Journal*, 101(2):155–164, 2004.
- [108] M. Panagiotou. *Seismic Design, Testing and Analysis of Reinforced Concrete Wall Buildings*. Phd dissertation, University of California, San Diego, San Diego, California, 2008.
- [109] M. Panagiotou, J. I. Restrepo, M. Schoettler, and G. Kim. Nonlinear cyclic truss model for reinforced concrete walls. *ACI Structural Journal*, 109(2):205–214, 2012.
- [110] X. B. D. Pang and T. T. C. Hsu. Behavior of reinforced concrete membrane elements in shear. *ACI Structural Journal*, 92(6):665–679, 1995.
- [111] X. B. D. Pang and T. T. C. Hsu. Fixed angle softened truss model for reinforced concrete. *ACI Structural Journal*, 93(2):196–208, 1996.
- [112] H. Park. *Nonlinear Finite Element Analysis of Reinforced Concrete Planar Structures*. Phd dissertation, Department of Civil Engineering, University of Texas at Austin, Texas, United States, May 1994.
- [113] H. Park. *Nonlinear Finite Element Analysis of Reinforced Concrete Planar Structures*. Phd dissertation, University of Texas at Austin, Austin, Texas, 1994.

- [114] T. Paulay and M. J. N. Priestley. *Seismic Design of Reinforced Concrete and Masonry Buildings*. John Wiley and Sons, Inc, 1992.
- [115] M. A. Polak and F. J. Vecchio. Nonlinear analysis of reinforced-concrete shells. *Journal of Structural Engineering*, 119(12):3439–3462, 1993.
- [116] M. A. Polak and F. J. Vecchio. Reinforced concrete shell elements subjected to bending and membrane loads. *ACI Structural Journal*, 91(3):261–268, 1994.
- [117] S. Popovics. A numerical approach to the complete stress-strain curve of concrete. *Cement and Concrete Research*, 3(5):583–599, 1973.
- [118] Suraphong Powanusorn. *Effect of Confinement on Shear Dominated Reinforced Concrete Elements*. PhD thesis, Texas A&M University, Texas, December 2003.
- [119] E. Riks. The application of newton’s method to the problem of elastic stability. *Journal of Applied Mechanics*, 39(4):1060–1065, 1972.
- [120] F. Rojas, F. Naeim, M. Lew, L.n D. Carpenter, N. F. Youssef, G. R. Saragoni, and M. Schachter. Performance of tall buildings in concepción during the 27 february 2010 moment magnitude 8.8 offshore maule, chile earthquake. *The Structural Design of Tall and Special Buildings*, 20(1):37–64, 2011.
- [121] M. S. Roufael and M. C. Meyer. Analytical modeling of hysteretic behavior of r. c. frames. *Journal of Structural Engineering*, 113(3):429–444, March 1987.
- [122] M. H. Scott. *Software Frameworks for the Computational Simulation of Structural Systems*. Phd dissertation, University of California, Berkeley, Berkeley, California, 2004.
- [123] M. H. Scott, G. L. Fenves, F. McKenna, and F. C. Filippou. Software patterns for nonlinear beam-column models. *Journal of Structural Engineering*, 134(4):562–571, 2008.
- [124] H. Shin, K. Maekawa, and H. Okamura. Analytical models for reinforced concrete shear walls under reversal cyclic loading. In *International Workshop on Concrete Shear Earthquake*, pages 289–298, Houston, Jan 14-16 1991. Elsevier Science Publishers, Inc.
- [125] R. G. Sisodiya and Y. K. Cheung. *Developments in Bridge Design and Construction*, chapter A Higer Order In-Plane Paralleloram Element and Its Application to Skewed Girder Bridges, pages 304–317. Crosby Lockwood, London, England, 1971.
- [126] C. Sittipunt and S. L. Wood. Influence of web reinforcement on the cyclic response of structural walls. *ACI Structural Journal*, 92(6):745–756, November 1995.
- [127] D. Soleimani, E. P. Popov, and V. V. Bertero. Nonlinear beam model for r.c. frame analysis. In *7th Conference on Elec. Comput., St. Louis, Missouri, ASCE, New York*, 1979.

- [128] R. Szilard. *Theories and Applications of Plates Analysis: Classical, Numerical and Engineering Methods*. John Wiley & Sons, Inc, Hoboken, New Jersey, 2004.
- [129] T. Takayanagi and W. C. Schnobrich. Computed behavior of reinforced concrete coupled shear walls. Report SRS 434, University of Illinois at Urbana, Champaign, 1976.
- [130] S. Tamai, H. Shima, J. Izumo, and H. Okamura. Average stress-strain relationship in post-yield range of steel bar in concrete. In *Concrete Library of JSCE, Translation of Proceedings of JSCE*, volume 378(6), pages 117–129, June 1988.
- [131] R. L. Taylor. FEAP: Finite Element Analysis Program. Version 8.3 User Manual. <http://www.ce.berkeley.edu/projects/feap/>, User Manual: <http://www.ce.berkeley.edu/projects/feap/manual.pdf>, University of California, Berkeley, 2011.
- [132] IV Thomsen, J. H. and J. W. Wallace. Displacement-based design of reinforced concrete structural walls: An experimental investigation of walls with rectangular and t-shaped cross sections. Report No. CU/CE-95-06, Clarkson University, 1995.
- [133] E. Thorenfeldt, A. Tomaszewicz, and J. J. Jensen. Mechanical properties of high-strength concrete and application in design. In *Symposium Utilization of High-Strength Concrete*, Stavanger, Norway, 1987.
- [134] C. Truesdell. Hipoelasticity. *Journal of Rational Mech. Anal.*, 4(1):83, 133 1955.
- [135] F. J. Vecchio. Reinforced concrete membrane element formulations. *Journal of Structural Engineering*, 116(3):730–750, 1990.
- [136] F. J. Vecchio. Finite element modeling of concrete expansion and confinement. *Journal of Structural Engineering*, 118(9):2390–2406, September 1992.
- [137] F. J. Vecchio. Disturbed stress field model for reinforced concrete: Formulation. *Journal of Structural Engineering*, 126(9):1070–1077, 2000.
- [138] F. J. Vecchio. Disturbed stress field model for reinforced concrete: Implementation. *Journal of Structural Engineering*, 127(1):12–20, 2001.
- [139] F. J. Vecchio and M. P. Collins. Response of reinforced concrete to in-plane shear and normal stresses. Report No. 82-03, University of Toronto, Toronto, Canada, 1982.
- [140] F. J. Vecchio and M. P. Collins. The modified compression-field theory for reinforced concrete elements subjected to shear. *ACI Journal Proceedings*, 83(2):219–231, 1986.
- [141] F. J. Vecchio and M. P. Collins. Compression response of cracked reinforced concrete. *Journal of Structural Engineering*, 119(12):3590–3610, December 1993.
- [142] F. J. Vecchio and R. G. Selby. Towards compression field analysis of reinforced concrete solids. *Journal of Structural Engineering*, 117(6):1740–1758, June 1991.

- [143] P. Vipul and G. H. Powell. Drain-2dx, drain-3dx and drain-building: Base program design documentation. UCB/SEMM 1993/16, Earthquake Engineering Research Center, University of California, Berkeley, 1983.
- [144] A. Vulcano and V. V. Bertero. Analytical models for predicting the lateral response of rc shear walls: Evaluation of their reliability. UCB/EERC 87/19, Earthquake Engineering Research Center. University of California, Berkeley, November 1987.
- [145] A. Vulcano, V. V. Bertero, and V. Colotti. Analytical modeling of rc structural walls. In *9th World Conference on Earthquake Engineering, Tokyo-Kyoto, Japan*, 1988.
- [146] T. Wang and T. T. C. Hsu. Nonlinear finite element analysis of concrete structures using new constitutive models. *Computers & Structures*, 79(32):2781 – 2791, 2001.
- [147] J. D. Waugh. *Nonlinear Analysis of T-shaped Concrete Walls Subjected to Multi-Directional Displacements*. Phd dissertation, Iowa State University, Ames, Iowa, 2009.
- [148] K. J. Willam and E. P. Warnke. Constitutive model for the triaxial behavior of concrete. In *Concrete Structures Subjected to Triaxial Stresses*, volume 19 (Paper III-1), pages 1–31, Bergamo, Italy, 1974. International Association of Bridge and Structural Engineers Seminar.
- [149] K. J. Willam, E. Pramono, and S. Sture. Fundamental issues of smeared crack models. In *Proceedings of the SEM/RILEM International Conference on Fracture of Concrete and Rock*, pages 192–207, Houston, Texas, 1987.
- [150] J. A. Wolf. *A Plasticity Model to Predict the Effects of Confinement on Concrete*. Phd dissertation, California Institute of Technology, Pasadena, California, 2008.
- [151] G. Xia, M. Yu, C. Li, and J. Zhang. Rectangular membrane element with rotational degree of freedom. In *Computational Structural Engineering, Procedings of the International Symposium on Computational Structural Engineering*, pages 1051–1058, Shanghai, China, June 22-24 2009.
- [152] H. Xiaolei, C. Xuewei, J. Cheang, G. Mao, and W. Peifeng. Numerical analysis of cyclic loading test of shear walls based on opensees. In *14th World Conference on Earthquake Engineering, Beijing, China*, October 12-17 2008.
- [153] Y. Yokko and T. Nakamura. Nonstationary hysteretic uniaxial stress-strain relations of a steel bar. *Trans. Arch Inst. of Japan, Tokyo*, 260:71–80, 1977.
- [154] N. F. Youssef, D. Tunick, F. Naeim, M. Lew, L. D. Carpenter, F. Rojas, G. R. Saragoni, and M. Schachter. Performance of the torre bosquemar and olas buildings in san pedro de la paz and the pedro de valdivia building in concepción in the 27 february 2010 offshore maule, chile earthquake. *The Structural Design of Tall and Special Buildings*, 20(1):65–82, 2011. ISSN 1541-7808. doi: 10.1002/tal.670. URL <http://dx.doi.org/10.1002/tal.670>.

- [155] Y. X. Zhang, M. A. Bradford, and R. I. Gilbert. A layered shear-flexural plate/shell element using timoshenko beam functions for nonlinear analysis of reinforced concrete plates. *Finite Elements in Analysis and Design*, 43(11-12):888 – 900, 2007.
- [156] Y. X. Zhang, M. A. Bradford, and R. I. Gilbert. A layered cylindrical quadrilateral shell element for nonlinear analysis of rc plate structures. *Advances in Engineering Software*, 38(7):488 – 500, 2007.
- [157] J. Zhong. *Model-Based Simulation of Reinforced Concrete Plane Stress Structures*. Phd dissertation, Department of Civil and Environmental Engineering, University of Houston, Houston, United States, August 2005.
- [158] R. Zhu. *Softened-Membrane Model of Cracked Reinforced Concrete Considering Poisson Effect*. Phd dissertation, Department of Civil and Environmental Engineering, University of Houston, Houston, United States, August 2000.
- [159] R. R. H. Zhu and T. T. C. Hsu. Poisson effect in reinforced concrete membrane elements. *ACI Structural Journal*, 99(5):631–640, 2002.
- [160] R. R. H. Zhu, T. T. C. Hsu, and J. Y. Lee. Rational shear modulus for smeared-crack analysis of reinforced concrete. *ACI Structural Journal*, 98(4):443–450, 2001.

Appendix A

Tensor Transformation

A continuation is reviewed the transformation for strain and stress components from one coordinate system to another.

A.1 Strain Transformation

The strain components ($\{\varepsilon_{1-2}\} = \left\{ \varepsilon_{11} \quad \varepsilon_{22} \quad \frac{1}{2}\gamma_{12} \right\}^T$) under plane stress state are a second order tensor, due to this the transformation from the global coordinate system ($x - y$) to a local coordinate system ($1 - 2$) rotated by an angle θ can be defined by the transformation

$$[\varepsilon_{1-2}] = [R(\theta)] [\varepsilon_{x-y}] [R(\theta)]^T \quad (\text{A.1})$$

where

$$[R(\theta)] = \begin{bmatrix} \cos(\theta) & \sin(\theta) \\ -\sin(\theta) & \cos(\theta) \end{bmatrix} \quad (\text{A.2})$$

and

$$[\varepsilon_{1-2}] = \begin{bmatrix} \varepsilon_{11} & \frac{1}{2}\gamma_{12} \\ \frac{1}{2}\gamma_{21} & \varepsilon_{22} \end{bmatrix} \quad \text{and} \quad [\varepsilon_{x-y}] = \begin{bmatrix} \varepsilon_{xx} & \frac{1}{2}\gamma_{xy} \\ \frac{1}{2}\gamma_{yx} & \varepsilon_{yy} \end{bmatrix} \quad (\text{A.3})$$

but, $\varepsilon_{12} = \varepsilon_{21}$ and $\gamma_{xy} = \gamma_{yx}$, which allows the transformation to be written as

$$\begin{Bmatrix} \varepsilon_{11} \\ \varepsilon_{22} \\ \frac{1}{2}\gamma_{12} \end{Bmatrix} = \begin{bmatrix} \cos^2(\theta) & \sin^2(\theta) & 2\sin(\theta)\cos(\theta) \\ \sin^2(\theta) & \cos^2(\theta) & -2\sin(\theta)\cos(\theta) \\ -\sin(\theta)\cos(\theta) & \sin(\theta)\cos(\theta) & \cos^2(\theta) - \sin^2(\theta) \end{bmatrix} \begin{Bmatrix} \varepsilon_{xx} \\ \varepsilon_{yy} \\ \frac{1}{2}\gamma_{xy} \end{Bmatrix} \quad (\text{A.4})$$

However, to use this transformation inside of a finite element approach, it is convenient to rewrite the relation as

$$\begin{aligned} \begin{Bmatrix} \varepsilon_{11} \\ \varepsilon_{22} \\ \gamma_{12} \end{Bmatrix} &= \begin{bmatrix} 1 & 0 & 0 \\ 0 & 1 & 0 \\ 0 & 0 & 2 \end{bmatrix} \begin{bmatrix} \cos^2(\theta) & \sin^2(\theta) & 2\sin(\theta)\cos(\theta) \\ \sin^2(\theta) & \cos^2(\theta) & -2\sin(\theta)\cos(\theta) \\ -\sin(\theta)\cos(\theta) & \sin(\theta)\cos(\theta) & \cos^2(\theta) - \sin^2(\theta) \end{bmatrix} \begin{bmatrix} 1 & 0 & 0 \\ 0 & 1 & 0 \\ 0 & 0 & \frac{1}{2} \end{bmatrix} \begin{Bmatrix} \varepsilon_{xx} \\ \varepsilon_{yy} \\ \gamma_{xy} \end{Bmatrix} \\ &= \underbrace{\begin{bmatrix} \cos^2(\theta) & \sin^2(\theta) & \sin(\theta)\cos(\theta) \\ \sin^2(\theta) & \cos^2(\theta) & -\sin(\theta)\cos(\theta) \\ -2\sin(\theta)\cos(\theta) & 2\sin(\theta)\cos(\theta) & \cos^2(\theta) - \sin^2(\theta) \end{bmatrix}}_{[T_{strain}(\theta)]} \begin{Bmatrix} \varepsilon_{xx} \\ \varepsilon_{yy} \\ \gamma_{xy} \end{Bmatrix} \quad (\text{A.5}) \end{aligned}$$

This result in the strain transformation matrix

$$[T_{strain}(\theta)] = \begin{bmatrix} \cos^2(\theta) & \sin^2(\theta) & \sin(\theta) \cos(\theta) \\ \sin^2(\theta) & \cos^2(\theta) & -\sin(\theta) \cos(\theta) \\ -2\sin(\theta) \cos(\theta) & 2\sin(\theta) \cos(\theta) & \cos^2(\theta) - \sin^2(\theta) \end{bmatrix} \quad (\text{A.6})$$

and it can be prove directly that $[T_{strain}(\theta)]^{-1} = [T_{strain}(-\theta)]$. Using this relation, the transformation from the principal direction of strain, defined by the angle θ_{pd} , to the system of coordinate $x - y$ can be defined as:

$$\begin{Bmatrix} \varepsilon_{xx} \\ \varepsilon_{yy} \\ \gamma_{xy} \end{Bmatrix} = \begin{bmatrix} \cos^2(\theta_{pd}) & \sin^2(\theta_{pd}) & \\ \sin^2(\theta_{pd}) & \cos^2(\theta_{pd}) & \\ 2\sin(\theta_{pd}) \cos(\theta_{pd}) & -2\sin(\theta_{pd}) \cos(\theta_{pd}) & \end{bmatrix} \begin{Bmatrix} \varepsilon_{11} \\ \varepsilon_{22} \\ 0 \end{Bmatrix} \quad (\text{A.7})$$

A.1.1 Principal Direction of Strains

Using the Eq. A.5 , and knowing that principal direction of strain happens when $\varepsilon_{12} = 0$, we can obtain the transformation from the system of coordinates $x - y$ to the principal direction system defined by the angle θ_{pd} :

$$\begin{Bmatrix} \varepsilon_{11} \\ \varepsilon_{22} \\ 0 \end{Bmatrix} = [T_{strain}(\theta_{pd})] \begin{Bmatrix} \varepsilon_{xx} \\ \varepsilon_{yy} \\ \gamma_{xy} \end{Bmatrix} \quad (\text{A.8})$$

and using the trigonometric relations:

$$\cos^2(\theta) = \frac{1}{2} (1 + \cos(2\theta)) \quad (\text{A.9a})$$

$$\sin^2(\theta) = \frac{1}{2} (1 - \cos(2\theta)) \quad (\text{A.9b})$$

$$\sin(\theta) \cos(\theta) = \frac{1}{2} \sin(2\theta) \quad (\text{A.9c})$$

the last equation of the system of equation in Eq. A.8 can be rewrite as

$$0 = (\varepsilon_{xx} - \varepsilon_{yy}) \sin(2\theta) + \gamma_{xy} \cos(2\theta) \quad (\text{A.10})$$

that result in:

$$\tan(2\theta_{pd}) = \frac{\sin(2\theta)}{\cos(2\theta)} = \frac{\gamma_{xy}}{(\varepsilon_{xx} - \varepsilon_{yy})} \quad (\text{A.11})$$

Eq. A.11 is used to calculate $\theta_{pd} = \frac{1}{2} \arctan \left(\frac{\gamma_{xy}}{(\varepsilon_{xx} - \varepsilon_{yy})} \right)$, which is the angle that define the direction of the principal directions of strain. Now, defining the relations:

$$\cos(2\theta) = \frac{(\varepsilon_{xx} - \varepsilon_{yy})}{\sqrt{(\varepsilon_{xx} - \varepsilon_{yy})^2 + (\gamma_{xy})^2}} \quad (\text{A.12a})$$

$$\sin(2\theta) = \frac{\gamma_{xy}}{\sqrt{(\varepsilon_{xx} - \varepsilon_{yy})^2 + (\gamma_{xy})^2}} \quad (\text{A.12b})$$

The two Equation that define ε_{11} and ε_{22} from Eq. A.8 can be reduced to:

$$\varepsilon_{11} = \frac{1}{2} (\varepsilon_{xx} + \varepsilon_{yy}) + \frac{1}{2} \sqrt{(\varepsilon_{xx} - \varepsilon_{yy})^2 + (\gamma_{xy})^2} \quad (\text{A.13a})$$

$$\varepsilon_{22} = \frac{1}{2} (\varepsilon_{xx} + \varepsilon_{yy}) - \frac{1}{2} \sqrt{(\varepsilon_{xx} - \varepsilon_{yy})^2 + (\gamma_{xy})^2} \quad (\text{A.13b})$$

A.2 Stress Transformation

The stress components ($\{\sigma_{1-2}\} = \begin{Bmatrix} \sigma_{11} & \sigma_{22} & \tau_{12} \end{Bmatrix}^T$) under a plane stress state are a second order tensor, due to this the transformation from the global coordinate system ($x - y$) to a local coordinate system (1 – 2) rotated by an angle θ can be defined by the transformation

$$[\sigma_{1-2}] = [R(\theta)] [\sigma_{x-y}] [R(\theta)]^T \quad (\text{A.14})$$

where

$$[R(\theta)] = \begin{bmatrix} \cos(\theta) & \sin(\theta) \\ -\sin(\theta) & \cos(\theta) \end{bmatrix} \quad (\text{A.15})$$

and

$$[\sigma_{1-2}] = \begin{bmatrix} \sigma_{11} & \tau_{12} \\ \tau_{21} & \sigma_{22} \end{bmatrix} \quad \text{and} \quad [\sigma_{x-y}] = \begin{bmatrix} \sigma_{xx} & \tau_{xy} \\ \tau_{yx} & \sigma_{yy} \end{bmatrix} \quad (\text{A.16})$$

but, $\tau_{12} = \tau_{21}$ and $\tau_{xy} = \tau_{yx}$, which allows the transformation to be written as

$$\begin{Bmatrix} \sigma_{11} \\ \sigma_{22} \\ \tau_{12} \end{Bmatrix} = \underbrace{\begin{bmatrix} \cos^2(\theta) & \sin^2(\theta) & 2\sin(\theta)\cos(\theta) \\ \sin^2(\theta) & \cos^2(\theta) & -2\sin(\theta)\cos(\theta) \\ -\sin(\theta)\cos(\theta) & \sin(\theta)\cos(\theta) & \cos^2(\theta) - \sin^2(\theta) \end{bmatrix}}_{[T_{stress}(\theta)]} \begin{Bmatrix} \sigma_{xx} \\ \sigma_{yy} \\ \tau_{xy} \end{Bmatrix} \quad (\text{A.17})$$

This result in the stress transformation matrix

$$[T_{stress}(\theta)] = \begin{bmatrix} \cos^2(\theta) & \sin^2(\theta) & 2\sin(\theta)\cos(\theta) \\ \sin^2(\theta) & \cos^2(\theta) & -2\sin(\theta)\cos(\theta) \\ -\sin(\theta)\cos(\theta) & \sin(\theta)\cos(\theta) & \cos^2(\theta) - \sin^2(\theta) \end{bmatrix} \quad (\text{A.18})$$

and it can be prove directly that $[T_{stress}(\theta)]^{-1} = [T_{stress}(-\theta)] = [T_{strain}(\theta)]^T$. Using these relation, the transformation from the principal direction of stress, defined by the angle θ_{pd} , to the system of coordinate $x - y$ can be defined as:

$$\begin{Bmatrix} \sigma_{xx} \\ \sigma_{yy} \\ \tau_{xy} \end{Bmatrix} = \begin{bmatrix} \cos^2(\theta_{pd}) & \sin^2(\theta_{pd}) & 0 \\ \sin^2(\theta_{pd}) & \cos^2(\theta_{pd}) & 0 \\ \sin(\theta_{pd})\cos(\theta_{pd}) & -\sin(\theta_{pd})\cos(\theta_{pd}) & 0 \end{bmatrix} \begin{Bmatrix} \sigma_{11} \\ \sigma_{22} \\ 0 \end{Bmatrix} \quad (\text{A.19})$$